The Cell Wall as a Barrier Against Water Loss and Plant Pathogens

A Thesis Submitted to the College of
Graduate and Postdoctoral Studies
in Partial Fulfillment of the Requirements
for the Degree of Master of Science
in the Department of Plant Sciences
University of Saskatchewan
Saskatoon

By
Ariana Dylis Forand
2021

PERMISSION TO USE

In presenting this thesis/dissertation in partial fulfillment of the requirements for a Postgraduate degree from the University of Saskatchewan, I agree that the Libraries of this University may make it freely available for inspection. I further agree that permission for copying of this thesis/dissertation in any manner, in whole or in part, for scholarly purposes may be granted by the professor or professors who supervised my thesis/dissertation work or, in their absence, by the Head of the Department or the Dean of the College in which my thesis work was done. It is understood that any copying or publication or use of this thesis/dissertation or parts thereof for financial gain shall not be allowed without my written permission. It is also understood that due recognition shall be given to me and to the University of Saskatchewan in any scholarly use which may be made of any material in my thesis/dissertation.

Requests for permission to copy or to make other uses of materials in this thesis/dissertation in whole or part should be addressed to:

Head of the Department of Plant Sciences
College of Agriculture and Bioresources
University of Saskatchewan
51 Campus Drive
Saskatoon, Saskatchewan S7N 5A8, Canada

OR

Dean
College of Graduate and Postdoctoral Studies
University of Saskatchewan
116 Thorvaldson Building, 110 Science Place
Saskatoon, Saskatchewan S7N 5C9, Canada

ABSTRACT

The ability to survive a range of stresses is crucial to the survival of plants. Structural modifications in the cell wall through pectin cross linkages may be key to mitigating damage caused by stress. Pectin reduces cell wall permeability and increases rigidity through calcium ion crosslinks to carboxylate ions in galacturonic acid residues in homogalacturonan, and boron crosslinks to apiosyl residues in rhamnogalacturonan II side chains. The objective of this research was to understand the influence of calcium and boron *in vitro*, and how changes in viscosity and rigidity may translate to resistance to dehydration and fungal pathogens in *Allium spp*. and *Arabidopsis* pectin methylesterase/boron mutant genotypes. *Allium spp*. served as an ideal model to study dehydration stress as the cells are large and a single layer of epidermal cells can be easily separated. *Arabidopsis* was useful given the availability of mutant genotypes. $CaCl_2$ and H_3BO_3 were both found to significantly ($p<0.05$) increase the viscosity of pure pectin standards, in addition to reducing percent water loss in the same standards. However, the impact of these compounds on improving dehydration stress resistance in the plant species of interest was less clear. The efficacy of calcium in enhancing dehydration stress resistance in *Allium spp*. was highly variable, in certain instances improving resistance and in others decreasing it. Nevertheless, calcium increased the force required to shear *Allium fistulosum* by ~63.39 N g^{-1}, suggesting it did cause structural modifications. Furthermore, *Allium fistulosum* (drought resistant) lost significantly less water ($p<0.05$) over 16-18hr compared to *Allium cepa* (drought sensitive) and had a lower limit of damage based on protoplasmic streaming, suggesting a link between resistance to dehydration stress and freezing stress. There also appears to be a link between boron and resistance to both dehydration stress and fungal pathogen stress. A boron transporter mutant *(bor1*) showed a greater susceptibility to dehydration stress ($p>0.05$) and *Colletotrichum higginsianum* infection ($p<0.05$). Because of the mechanism of infection, the rapid rate of *Colletotrichum higginsianum* infection in *bor1* is indicative of a weak cell wall. While the response to stress is highly complex, collectively this thesis indicates calcium, boron, pectin and the cell wall in general may play important but relatively under researched roles in plant resistance to both abiotic and biotic stress.

ACKNOWLEDGEMENTS

Throughout every stage of this process, I have received an unimaginable amount of support, encouragement and assistance. I would like first to express my deepest gratitude for my supervisor Dr. Karen Tanino. Without her endless support and encouragement from day one none of this would have been possible. I'm forever grateful for her excitement towards the project even throughout the most challenging moments when I struggled to see its full potential. I would also like to thank the members of my advisory committee- Dr. Curtis Pozniak, Dr. Supratim Ghosh, Dr. Martin Reaney and Dr. Yangdou Wei for all their thoughtful criticism, advice and hands on help with the project. My thanks are also extended to my external examiner Dr. Sylvie Renault (University of Manitoba).

I would also like to thank Rensong Liu and Gowri Valsala for all their help within the lab and for never failing to put a smile on my face. Thank you as well to Dr. Sheng Wang for genotyping Arabidopsis accessions and to Dr. Prakash Venglat for his assistance in the early days with microscopy, an instrumental part of this project.

I was extremely grateful to receive help from numerous other individuals. In particular, I would also like to extend my sincere appreciation towards, Dr. Phyllis Shand, Dr. Fatemeh Keivaninahr, Dr. Chi Diem Doan, Barry Goetz, Dr. Li Qin, Dr. Jarvis Stobbs, Dr. Chithra Karunakaran, Dr. Lucia Zuin, Dr. David Wang, Dr. Zou Finfrock, Miranda Lavier, Dr. Na Liu, Eldon Siemens, Jackie Bantle, Justin Schaeffer, Katie Sommerfield, Dr. John Lawrence, George Swerhone, Dr. Hong Wang and Dr. Eric Lamb. All these amazing individuals have helped contribute to the quality of this thesis.

Finally, I would also like to acknowledge the funding support I have received through various scholarships including the Roderick Alan McLean Memorial Bursary, the Alexander Graham Bell Canadian Graduate Scholarship-Masters ((CGS-M) NSERC Graduate Student Award), the Devolved Scholarship, the Harris & Lauretta and Raymond Earl Parr Memorial Scholarship, the Education Enhancement Grant and the University of Saskatchewan Travel Award. The financial

support provided by these families, funding agencies, and The University of Saskatchewan took a huge weight off my shoulders.

DEDICATION

I would like to start off by dedicating this thesis to my parents, Debra and Terry Vanderaar, and my brothers, Benoit and Merrik Forand. Despite being halfway across the country you were always there cheering me on during the best of times and raising me up when it would have been easier to quit. I love you all so much.

To my best friend and Opa, Leonardus "Dick" Vanderaar, our daily phone calls during the first few weeks of my program meant the world to me as I struggled to find my footing. Thank you for being one of my biggest supporters. I wish you could still be here, but I feel your presence every day and I know how proud you are.

To my lab mates, Eric Rae and Dr. Ian Willick, who became my friends and so much more. Thank you for being so supportive. I could always count on you to lend a hand, give valuable advice and keep me sane.

To all of my friends I met during my time at the University of Saskatchewan, you played an integral role in making my experience so memorable. In particular, Matthew Wengler, Amanda Fedorchuk and Denys Solskyi. You guys became so much more than my friends, you were my family. You three will truly never know how much your friendship means to me.

Finally, to Dr. Charu Kaushic (Department of Medicine, McMaster University). You have been my inspiration from the start. You are my role model for what it means to be a strong female leader in science. From visiting you in the Department of Pathology and Molecular Medicine as a child to growing up and seeing the impact you have on your field; I'm constantly looking up to you and in awe of your brilliantness. Because of you I continue to strive every day to be a strong woman in science, thank you for everything.

Table of Contents

LIST OF TABLES

LIST OF FIGURES

LIST OF ABBREVIATIONS AND DEFINITIONS

ACC: Cold Acclimation.

ACC12-4: Cold Acclimation with a 12ºC /4ºC (day/night) temperature.

ACC4-4: Cold Acclimation with a 4ºC/4ºC (day/night) temperature.

AIC Score: Akaike Information Criterion (AIC). Used to select the optimal generalized additive model. A lower value indicates a more optimal model.

APS: Advanced Photon Source (Lemont, IL, USA).

B: Boron. Used in replacement of "boron" and for boron species in general.

BOR1: Boric acid channel, part of the BOR family.

bor1: *Arabidopsis thaliana* genotype with mutation in BOR1 transporter**.**

Ca: Calcium.

CA: Calcium Applied/ Calcium Treatment.

Cell Wall: Within the context of this thesis, this term also incorporates the middle lamella.

Col-0: Wild-type *Arabidopsis thaliana*

EDF: Empirical Distribution Factor. Distribution of a function, where a value of one is indicative of a linear relationship, while a value above one is indicative of a non-linear relationship.

FDA: Fluorescein Diacetate.

GAM: Generalized Additive Model. A generalized linear model where the effect of predictive variables is captured using smoothing functions.

GB: GENU BETA Pectin (Sugar Beet Pectin).

HG: Homogalacturonan.

HM: High Methylated Citrus Pectin.

ICP-MS: Inductively Coupled Plasma Mass Spectrometry.

Limit of Damage: Level of damage following dehydration stress, based either on protoplasmic streaming and FDA (for *Allium*) or electrolyte leakage (for *Arabidopsis*). A lower limit of damage is indicative of a greater level of resistance to stress.

LM: Low Methylated Citrus Pectin.

LT-50: Temperature at which 50% of the population did not survive a freezing temperature based on viability measurements.

N: Nitrogen.

NACC: No Cold Acclimation.

NCA: No Calcium Applied/ No Calcium Treatment.

NIP5-1: Boric acid channel, part of the NIP family.

nip5-1: *Arabidopsis thaliana* genotype with mutation in NIP5-1 transporter**.**

NIP6-1: Boric acid channel, part of the NIP family.

nip6-1: *Arabidopsis thaliana* genotype with mutation in NIP6-1 transporter**.**

PBS: Phosphate Buffered Saline.

PMEI5: Pectin methylesterase inhibitor five, part of the PMEI family.

p35S::PMEI5: *Arabidopsis thaliana* genotype over-expressing of PMEI5**.** Over-expression of the PMEI5 gene is under the control of the Cauliflower mosaic virus (CaMV) 35S promoter.

RG-II: Rhamnogalacturonan II.

ROS: Reactive Oxygen Species.

VLS-PGM: Variable Line Spacing Plan Grating Monochromator.

XAS: X-ray Absorption Spectroscopy (XAS).

1.0 INTRODUCTION

1.1 Background

The cell wall is a key distinguishing feature between plants and animals. Within plant cells, the role of the cell wall is extremely diverse (Houston et al., 2016). Not only does the cell wall provide structural and mechanical support to the cell, it also supports plant growth, and acts as a physical barrier to abiotic and biotic stress (Houston et al., 2016; Keegstra, 2010). Within the cell wall and the plasma membrane, there are a wide range of receptors, pores and channels that help to regulate a range of functions (Houston et al., 2016). There are also variations among the cell wall structures found in different tissue types and plant species. Primary cell walls, which are synthesized during plant growth, must be thin, flexible and highly hydrated (Cosgrove & Jarvis, 2012; Alberts et al., 2002). The primary cell wall must be strong, extensible and capable of performing functions such as linking new polymers (Hamant & Traas, 2010). In contrast, secondary cell walls provide strength and rigidity to plant tissues that have stopped growing and are typically found in tall terrestrial plants (ie. Tree species) with stems that must resist bending and/or have water-conducting tissues that can withstand negative pressures (Speck & Burgert, 2011; Koch et al., 2004).

Plant cell walls are composed of cellulose, hemicellulose, proteins, pectins, and/or lignin. Moreover, primary cell walls are produced during cytokinesis and continue to undergo modifications during cell expansion, are generally comprised of 15-40% cellulose, 30-50% pectin polysaccharides, and 20-30% xyloglucans (Cosgrove & Jarvis, 2012). Secondary cell walls are typically composed of cellulose, lignin, and hemicellulose (xylan, glucuronoxylan, arabinoxylan, or glucomannan) (Cosgrove & Jarvis, 2012; Plant Cell Wall Basics, n.d.). Please note, within the context of this thesis use of the word “cell wall” includes the middle lamella.

In nature, pectin is the most structurally complex polysaccharide and within the cell wall it serves numerous functions (Mohnen, 2008). There are 5 members of the pectin family: 1) homogalacturonan (HG); 2) rhamnogalacturonan I (RG-I); 3) rhamnogalacturonan II (RG-II); 4) xylogalacturonan (XGA); and 5) apiogalacturonan (AP) (Mohnen, 2008). This thesis is focused on HG and RG-II since they are some of the most predominant forms of cell wall pectin. HG is

the most abundant form of pectin making up ~65% of all pectin, while RG-II accounts for ~10% (Mohnen, 2008).

As previously mentioned, pectin serves many key roles within the cell wall such as providing defense against stress (Sasidharan et al., 2011). One key characteristic of pectin enabling this role is its ability to form cross-linkages and bonds that influence both the rigidity and stability of the cell wall (Braccini & Pé Rez, 2001; Ravanat and Rinaudo, 1980). Calcium ions form cross-linkages with HG that have been demethylesterified by pectin methylesterases (PMEs) in a block-wise manner (Wormit & Usadel, 2018; Braccini & Pé Rez, 2001; Ravanat and Rinaudo, 1980). The formation of these cross-linkages creates "egg-box" structures (Braccini & Pé Rez, 2001; Ravanat and Rinaudo, 1980). In comparison, boron is capable of binding to RG-II to create RG-II dimers (O'Neill et al., 2004). The formation of "egg-box" structures and RG-II dimers have been found to influence cell wall integrity (Wormit & Usadel, 2018; O'Neill et al., 2004; Ravanat and Rinaudo, 1980).

While the cell wall is known to act as a barrier against abiotic and biotic stress, the mechanisms utilized by the cell wall are variable depending on the form of stress. There has been limited research focused on one common mechanism of defense for both abiotic and biotic stresses despite how prevalent and devastating these stresses can be on plants and the predicted increase in frequency and severity of both abiotic and biotic stress (Wu et al., 2018; Zhu, 2016; Underwood, 2012; Sasidharan et al., 2011). This project seeks to understand how the cell wall and more specifically, how calcium and boron and the resulting structural changes in pectin can influence the permeability of the cell wall, which may be key to its ability to act as a barrier against both abiotic and biotic stresses.

1.2 Objectives and Hypotheses

This research addresses the overarching hypothesis, "the application of calcium and/or boron results in cell wall structural changes which translate into increased resistance to both abiotic and biotic stress in *Allium* species and *Arabidopsis thaliana*". More specifically, the experiments outlined below address the following sub-hypotheses:

1. Calcium and boron independently increase the viscosity of pectin, in a dose- and temperature- dependent manner.
2. Calcium application and cold acclimation will increase the force required to shear through *Allium fistulosum*, and a combined application will further increase resistance to shear force in an additive manner.
3. Percent water loss in pure pectin standards will decrease as the concentration of pectin increases (4% to 8%), while the addition of $CaCl_2$ or H_3BO_3 will further decrease percent water loss. Moreover, boron will have a greater influence on reducing water loss in sugar beet pectin, while calcium will have a larger effect on citrus pectin.
4. The exogenous application of $CaCl_2$ reduces percent water loss in *Allium fistulosum* and *Allium cepa*.
5. $CaCl_2$ applied exogenously to *Allium fistulosum* (*A. fistulosum*) will localize to the apoplast of epidermal cells.
6. The stress sensitive *Allium cepa* has greater percent water loss compared to stress resistant *Allium fistulosum.*
7. *Arabidopsis thaliana* (*A. thaliana*) lines with mutations in boron transporters or a pectin methylesterase inhibitor over-expressing line (*p35S::PMEI5*) will lose water at a faster rate compared to the wild-type line.
8. *Arabidopsis thaliana* lines with mutations in boron transporters and pectin methylesterase inhibitor 5 (*p35S::PMEI5*) will have a faster rate of *Botrytis cinerea* and *Colletotrichum higginsianum* infection.
9. Mutations in boron transporters and PMEI5 within *Arabidopsis thaliana* will result in different boron species being present within the above ground biomass and soil collected from the pots used to grow the plants.

The above hypotheses were explored through the following objectives to:

1. Investigate the independent roles of calcium and boron, in both a dose dependent and temperature dependent manner, with respect to the viscosity of pectin (high methylated (HM) pectin and sugar beet (SB) pectin) *in vitro*.
2. Investigate how the application of calcium, in addition to cold acclimation, influences the force required to shear through *Allium fistulosum*.

3. Analyze how calcium and boron concentration, influences the rate of water loss in pure pectin solutions over 6 hr.
4. Investigate the influence of calcium on water loss in *Allium fistulosum*, *Allium cepa* and various *Arabidopsis thaliana* mutant genotypes over short (15minutes) and long periods (16hr and 24hr).
5. Investigate the influence of boron transporter and *p35S::PMEI5* mutations on *Botrytis cinerea* and *Colletotrichum higginsianum* infections in *Arabidopsis thaliana* by assessing lesion sizes.

2.0 LITERATURE REVIEW

2.1 The Cell Wall

One key distinguishing feature between plants and their animal counterparts is the presence of a cell wall that encases cells. The complexity of the cell wall with respect to the composition varies between the primary and secondary plant cell wall (Figure 4.1). In addition, the role of the cell wall is extremely diverse (Houston et al., 2016; Keegstra, 2010). It not only provides structural and mechanical support to the cell, acting in part like an exoskeleton in terms of defining cell shape, but it also supports plant growth and acts as a physical barrier to abiotic and biotic stress (Houston et al., 2016). This group also described the cell wall as having a wide range of receptors, pores and channels within the cell wall that regulate molecular movement and responses to both local and long-range elicitors such as sugars, hormones, proteins and RNA. The role of the cell wall is also variable between tissue types and plant species. Primary cell walls are synthesized during plant growth and are characterized as being thin, flexible and highly hydrated (Cosgrove & Jarvis, 2012). Ultimately, the primary cell wall must be strong to withstand tensile pressure, extensible to allow the cell wall to relax which promotes functions such as cell water uptake, and capable of preforming actions such as linking new polymers into the load-bearing structures in the cell wall (Hamant & Traas, 2010). In contrast, secondary cell walls provide strength and rigidity to plant tissues that have stopped growing and are typically found in tall terrestrial plants such as various species of trees (Alberts et al., 2002). While primary cell walls are found within all plant cells, secondary cell walls are typically only found in woody tissues and grasses, and more specifically only within specialized cells in those plants such as tracheids in seedless vascular plants and gymnosperms (Zhong & Ye, 2015; Cosgrove & Jarvis, 2012; Alberts et al., 2002). Outside of the plant, the cell wall also has numerous applications in human life including providing major dietary fibers for human consumption and the raw materials for various textiles, lumber, pulping and biofuels.

2.1.1 Cell Wall Composition- Type I vs Type II Cell Walls

Generally, plant cell walls are composed of cellulose, hemicellulose, proteins, pectins, and/or lignin. Primary cell walls are produced during cytokinesis and continue to undergo modifications during cell expansion and are comprised of 15-40% cellulose, 30-50% pectin polysaccharides, and 20-30% xyloglucans (Figure 2.1) (Cosgrove & Jarvis, 2012). Cosgrove and Jarvis (2012) also outlined that lesser amounts of arabinoxylans and structural proteins are in the lamella in primary cell walls. They also described how pectins serve many important roles including wall hydration, which is important for the slippage and separation of cellulose microfibrils during expansive growth. Variation also exists within the composition of primary cell walls. Such as in grass species, which contain between 10-20% arabinoxylans and mixed-linkage glucans within their cell walls (Gibeaut et al., 2005; Carpita et al., 2001). The parenchyma of celery (*Apium graveolens*) and sugar beet (*Beta vulgaris*) are also an exception as their primary cell walls are rich in cellulose and pectin, but they have little hemicellulose (Zykwinska et al., 2007; Thimm et al., 2002). The cell wall of *Allium cepa* (common onion) contains 93.7% uronic acid, indicating that the pectin found within the cell wall of onions is primarily composed of homogalacturonan (HG) (Mankarios et al., 1980). Only 0.6% rhamnose, a key component of rhamnogalacturonan I (RG-I) and rhamnogalacturonan II (RG-II) was found in the monosaccharide composition of pectin found within the cell wall of *A. cepa* (Mankarios et al., 1980). Similar to onions, citrus pectins are also primarily composed of HG (Yapo et al., 2007). In comparison to the onion, rhamnose was found to make up 5% of the monosaccharides that comprise the pectins found in sugar beet (Zhemerichkin & Ptitchkina, 1995). In general, RG-II accounts for ~4% of pectin found within the cell wall of dicots and less than 1% in monocots (Mohnen, 1999).

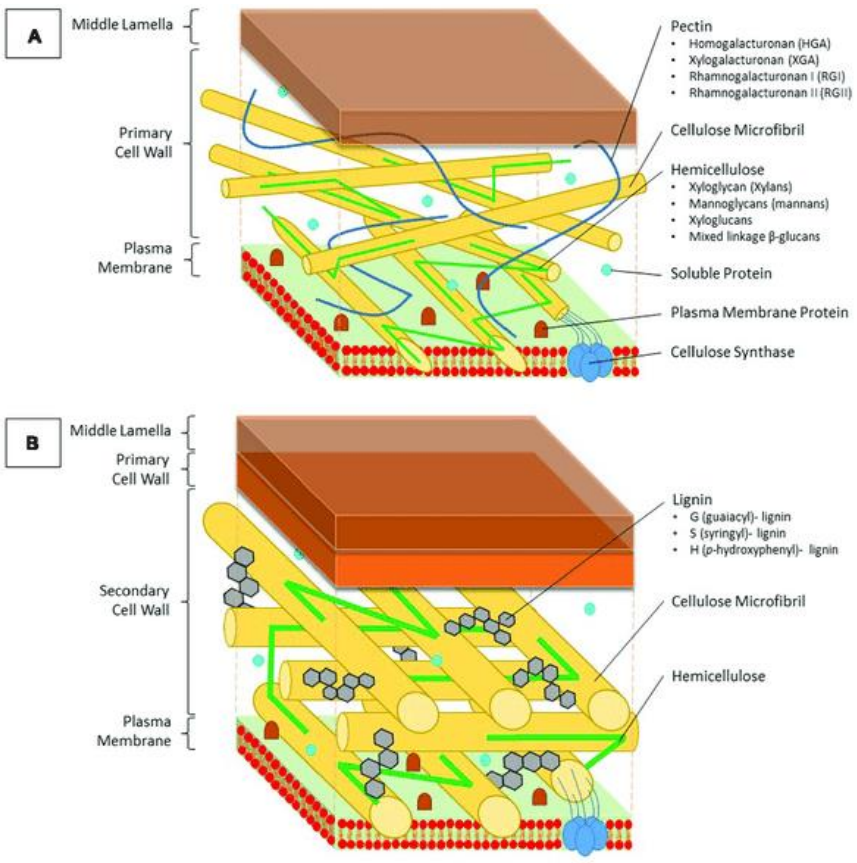

Figure 2.1 Schematic of the primary and secondary cell wall

The primary and secondary cell wall vary in composition as they serve different roles within the plant. **(A)** The primary cell wall is predominantly composed of the polysaccharide's cellulose, hemicellulose and pectin and to a lesser extent structural glycoprotein, phenolic esters, ionically and covalently bound minerals such as calcium and boron and enzymes. **(B)** The secondary cell wall also contains cellulose, hemicellulose and pectin however, to a much lesser proportion. The major component that distinguishes the secondary cell wall from the primary cell wall is the presence of lignin in the secondary cell wall. Image from Loix et al. (2017). Used under Creative Commons Attribution 4.0 International (https://creativecommons.org/licenses/by/4.0/).

2.1.2 The Cell Wall as a Barrier to Stress

The cell wall is a key determinant of plant response to environmental stresses (Sasidharan et al., 2011). The cell wall can undergo modifications that can both modulate growth or transform it into an impregnable physical barrier; these modifications are accomplished by various proteins. Pectin methylesterases (PMEs) are one form of protein that is found within the cell wall that plays a role in these modifications (Underwood, 2012). The way in which PMEs and its substrate pectins play a role in these cell wall modifications will be discussed in Section 2.2.3. While the cell wall

provides plants protection against abiotic and biotic stress, the way in which it does so is often variable depending on the stress.

Biotic stressors are the result of damage to an organism by another living organism. In the context of this project, biotic stress is therefore defined as damage to a plant by another organism such as a virus, bacteria, fungi or insects among other forms of biotic stress. The cell wall can act either as a passive structural barrier or as an active defense barrier against biotic stress (Underwood, 2012). As a passive structural barrier, organisms such as fungi and bacteria must have appropriate host recognition strategies and the development of suitable infection structures and/or chemical tools in order to circumvent the cell wall and other preformed barriers and establish a relationship with the host plant. Alternatively, the plant cell wall can act as an active defense barrier for organisms. An active response is characterized by a signal cascade that occurs during an infection (Houston et al., 2016; Zhu, 2016).

The cell wall can also act as a barrier to abiotic stress. Abiotic stress is a result of non-living factors such as extreme temperatures, drought, salt, flooding and heavy metal contaminants. When a plant is exposed to abiotic stress, there is an accumulation in ROS (reactive oxygen species) (Zhu, 2016). The accumulation of ROS can induce crosslinking phenolics and cell-wall glycoproteins such as expansins, and in turn the cell wall becomes increasingly rigid (Zhu, 2016). Stress also upregulates the expression of expansins and xyloglucan-modifying enzymes resulting in cell wall remodeling (Sasidharan et al., 2011). In addition, pectins which are particularly abundant in the primary plant cell wall, are of key interest to our proposed research as they modify the structure of the cell wall (Wu et al., 2018). Previous research into the role of pectins in mitigating the effects of various abiotic stresses has found pectins play a key role in modulating the structure of the cell wall in response to drought stress (Le Gall et al., 2015). Pectins also appear to play a key role in the response of plants to cold stress as an increase in PMEs has been observed in cold-acclimated plants including *A. fistulosum* and oil-seed rapeseed plants, which is correlated to an increase in the rigidity of the cell wall (Liu 2015; Solecka et al., 2008).

2.2 Pectin

Within the cell wall, pectin is a critical component in a diverse range of areas including growth, morphology, development and defense (Mohnen, 2008). Pectin is typically abundant in the walls of cells that are growing and dividing, cells in portions of the plant that are softer, within the middle lamella and the corners of the cells (Mohnen, 2008). Pectin can also be found in the junction zone between cells with secondary cell walls such as xylem and fiber in woody plants (Tan et al., 2013; Mohnen, 2008; Albersheim et al., 1996).

2.2.1 The Chemical Structure and Forms of Pectin

Pectin is a family of polysaccharides whose base-structure is composed of covalently linked galacturonic acid-rich plant cell wall polysaccharides (Mohnen, 2008). Pectin is an umbrella term for a family of polysaccharides, the structure is also variable depending on the form of pectin. There are five members of the pectin family: 1) homogalacturonan (HG); 2) rhamnogalacturnon I (RG-I); 3) rhamnogalacturnon II (RG-II); 4) xylogalacturonan (XGA); and 5) apiogalacturonan (AP) (Mohnen, 2008). The structure of these five members is illustrated in Figure 2.2. These various forms of pectic polysaccharides are believed to be covalently crosslinked, as mentioned above. Furthermore, HG, RG-I and RG-II are believed to link via. their backbones (Coenen et al., 2007; Nakamura et al., 2002; Ishii et al., 2001).

HG is the most abundant form of pectin, comprising approximately 65% of all pectins (Mohnen, 2008). HG is characterized by a linear polymer of α-1,4-linked galacturonic acid, partially methylesterified at the C-6 carboxyl and may be *O*-acetylated at *O*-2 or *O*-5 (Jackson et al., 2007; MacKinnon et al., 2002). HG chains are typically 100 GalA residues in length, however shorter HG regions have been previously found interspersed between other forms of pectic polysaccharides (Yapo et al., 2007; Nakamura et al., 2002). Compared to the other members of the pectin family, HG is the least structurally complex (Mohnen, 2008).

The second most abundant form of pectin is RG-I, which comprises 20-35% of pectins (Mohnen, 2008). RG-I is characterized by a high degree of cell type and development-dependent expression in the number and form of components such as sugars and oligosaccharides attached to its

backbone of an -α-D-GalA-1,2- α -L-Rha-1-4-disaccharide repeat (Guillemin et al., 2005; Ridley et al., 2001; Willats et al., 2001a). Structural changes in RG-I have been associated with numerous things within the plant such as tissue type and ripening of fruit (Mikshina et al., 2015).

Unlike HG, RG-II is the most structurally complex member of the pectin family, accounting for approximately 10% of pectins (Mohnen, 2008). Despite the structural complexity of RG-II, the structure is largely conserved across plant species (Mohnen, 2008). The structure of RG-II is characterized by an HG backbone that has at least eight 1,4-linked a-D-GalA residues with branched side chains containing 12 different types of sugars in over 20 different linkages (Mohnen, 2008). In plant cell walls, RG-II usually exists as RG-II dimers crosslinked by a 1:2 borate diol ester between the apiosyl residues in side chain A of two RG-II monomers (O'Neill et al., 2004). RG-II dimers have the ability to cross-link HG domains to create a pectin network (Matsunaga et al., 2004). Despite not being the most abundant form of pectin, RG-II is critical to proper plant development and structure. For example, minor modifications have been found to reduce the formation of RG-II dimers, in turn causing dwarfism (Mohnen, 2008).

The expression of the remaining two pectin varieties, XGA and AP, are more restricted. XGA has an HG backbone with a substitution at *O*-3 of a β-linked xylose, and this substitution sometimes occurs at *O*-4 as well (Mohnen, 2008; Zandleven et al., 2006). The final member of the pectin family, AP, is found in aquatic monocots and is a form of HG substituted at *O*-2 or *O*-3 with a D-apiofuranose (Mohnen, 2008).

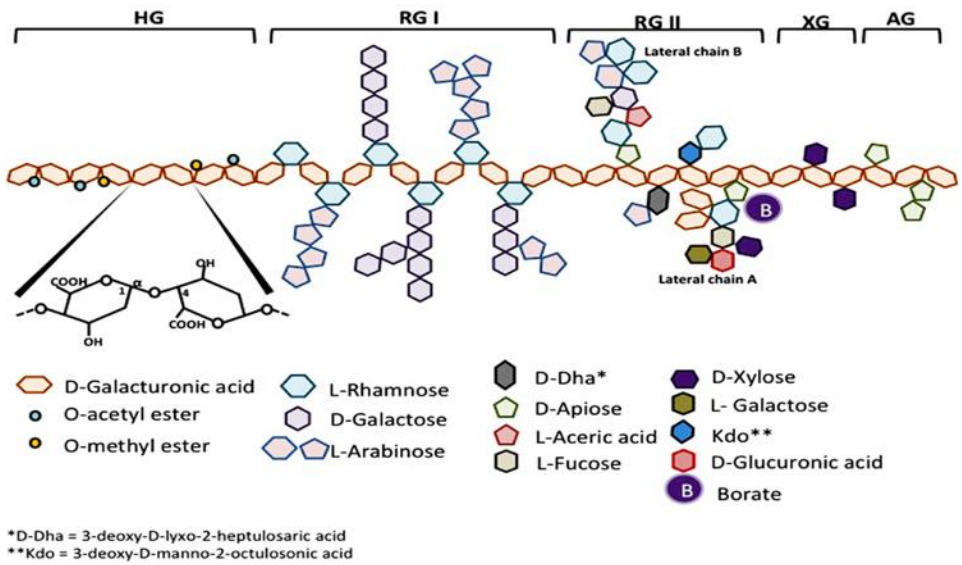

Figure 2.2 Chemical structures of the five types of pectin

The above figure is an illustration of the chemical structure of the different forms of pectin that comprise the pectin family. Image from Leclere et al., 2013. Used under Creative Commons Attribution 3.0 Unported (https://creativecommons.org/licenses/by/3.0/).

2.2.2 Pectin Biosynthesis

Pectin biosynthesis begins in the Golgi, where synthesis occurs simultaneously in numerous Golgi stacks in the cell (Mohnen, 2008). More specifically, Mohnen (2008) outlined that within the Golgi stacks, pectin is synthesized within the Golgi lumen by Golgi-localized glycosyltransferases (GTs). GTs act by transferring glycosyl residues from nucleotide-sugars onto oligosaccharide or polysaccharide acceptors (Nebenführ & Staehelin, 2001). During this process there is compartmentalization of specific biosynthetic enzymes which allows for increasingly complex pectin polysaccharides to be produced through the *cis*, medial, and *trans* Golgi cisternae (Nebenführ & Staehelin, 2001). A total of 67 glycosyltransferase, methyltransferase and acetyltransferase activities are predicted to be required in the process of pectin biosynthesis (Mohnen, 2008). Following pectin biosynthesis in the Golgi, pectin is then targeted to the cell wall by the movement of Golgi vesicles along actin filaments with myosin motors (Nebenführ et al., 1999). HG is then inserted into the cell wall as a highly methylesterified polymer (Pelloux et al., 2008).

2.2.3 Pectin Methyl Esterification

Following the insertion of HG into the cell wall, modifications occur to the structure of HG which affect pectin hydrolysis and other properties such as pH, charge and crosslinking (Wormit and Usadel, 2018). Demethylesterification catalyzed by PMEs is one of the modifications that occurs to HG following insertion into the cell wall. The process of demethylesterification creates negative carboxyl groups on the HG as methanol and protons are released (Wormit & Usadel, 2018). Demethylesterification can occur in either a block-wise or non-block-wise manner, the differences between these two patterns plays a critical role in the structure of the cell wall (Braccini & Pé Rez, 2001). The differences between both patterns of demethylesterification is illustrated in Figure 2.3. When block-wise demethylesterification occurs, meaning several GalA residues right next to each other are demethylesterified, the negatively charged carboxyl groups can form calcium bonds with other HGs (Braccini & Pé Rez, 2001). Braccini & Pé Rez (2001) refer to the structures these bonds created as "egg-box" structures. They form the underlying basis for pectin gels. These structures are also known to increase the amount of bound water, helping to maintain the hydration of the cell wall, consequently increasing cell wall rigidity (White et al., 2014; Ha et al., 1997). In this instance, increased cell wall rigidity is a result of turgor pressure exerted on the cell wall (Alberts et al., 2002). In contrast, non-block-wise demethylesterification (partial or random demethylesterification) results in pectin that becomes targeted by pectin-degrading enzymes (Wormit & Usadel, 2018). This paper reported the degradation of pectin by enzymes such as pectate or pectin lyases can hinder the structural integrity of the cell wall.

Demethylesterification of HG by PMEs is highly regulated at 4 levels: 1) transcriptional, 2) protein processing and degradation, 3) pH of the cell wall environment and 4) PMEI's (Levesque-Tremblay et al., 2015; Sénéchal et al., 2014; Voiniciuc et al., 2013; Wolf et al., 2009; Pelloux et al., 2007; Juge, 2006). PMEIs are members of large multigene families, with 71 PMEI genes having been identified in *Arabidopsis* and 97 PMEI genes in *Brassica rapa* (Tan et al., 2018; Wang et al., 2013). The regulation of PMEs by PMEIS is critical in controlling the demethylesterification of HG, and in turn the structural consequences of demethylesterification. Failure to regulate this process could have detrimental consequences to the structure of the cell wall (Wormit & Usadel, 2018; Hong et al., 2010).

PMEIs and PMEs are also capable of responding to both abiotic and biotic stresses and regulate the demethylesterification of pectin accordingly (Wormit & Usadel, 2018). During biotic stress, the role of PMEIs is characterized as a dynamic modulation of the PMEs activity with the degree of methylesterification determining the susceptibility of pectins within the cell wall to targeting by pectin degrading enzymes (Lionetti et al., 2012). With respect to the role of PMEIs in response to abiotic stress, one example of changes in PMEI expression occurs during cold acclimation. In cold acclimated plants such as oil-seed rape leaves and *A. fistulosum*, enhanced PME activity has been observed (Liu, 2015; Solecka et al. 2008). Increased PME likely results in increased rigidity which may be beneficial to plants under cold stress (Le Gall et al., 2015).

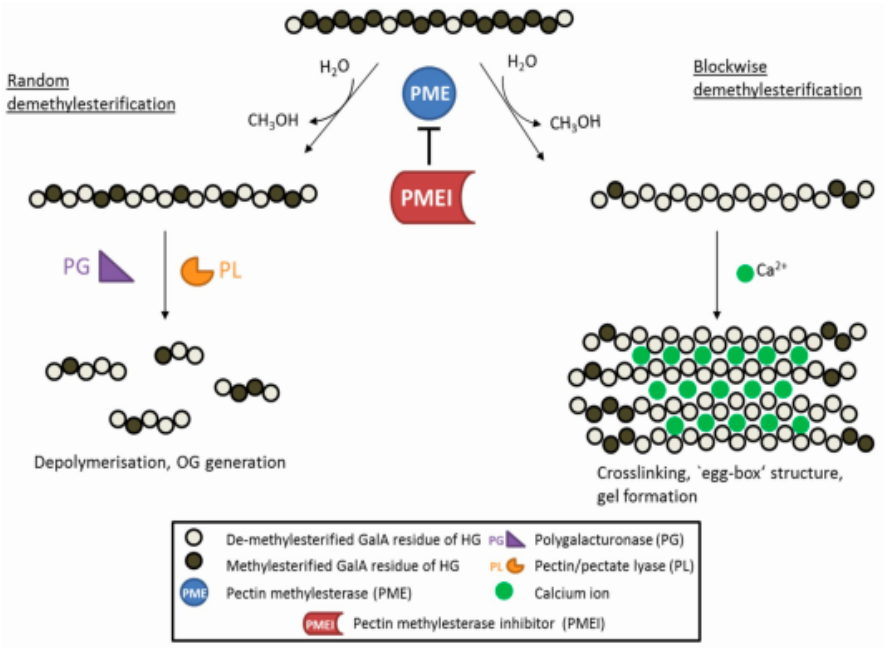

Figure 2.3 Demethylesterification of homogalacturonan by pectin methylesterase

PMEs influence the rigidity of the cell wall through the demethylesterification of homogalacturonan (HG). Random demethylesterification, also known as non-blockwise demethylesterification results in cell wall loosening, with methyl groups interspersed with GalA residues. As a result, low-methylesterified (LM) HG is depolymerized by polygalacturonase (PG) and pectin lyase (PL) resulting in the formation of oligogalacturonides (OG). Blockwise demethylesterification results in several consecutive GalA residues without methyl groups. The string of GalA residues, (the HG backbone), carries a negative charge. Calcium, a cation, can then crosslink with the GalA and form "egg-box" structures which increases cell wall rigidity as the pectin forms a gel. PMEI inhibits PME. Image from Wormit and Usadel (2018). Used under Creative Commons Attribution 4.0 International (https://creativecommons.org/licenses/by/4.0/).

2.3 Calcium

Calcium is an essential macronutrient in plants, making up between 0.1-5% of the dry weight of a shoot (White & Broadley, 2003; Marschner, 1995). In general, as a divalent cation, Ca^{2+} has a structural role within the cell wall and membranes, a role as a counter-cation in the vacuole, in addition to one as a secondary messenger in the cytosol (White & Broadley, 2003; Burstrom, 1968). Given the role of calcium in numerous functions within the plant, it is crucial to ensure that calcium is present at an adequate concentration within the plant. Like the majority of nutrients, calcium is taken up from the soil by the roots and delivered to the shoots via. the xylem (White & Broadley, 2003). More specifically, this paper outlines that calcium enters plant cells through Ca^{2+} permeable ion channels found within the plasma membrane.

The uptake of calcium is highly regulated in order to prevent the accumulation of toxic cations (Thor, 2019). Following uptake from the roots, one common and widely accepted model outlines that Ca^{2+} moves in the apoplast from the epidermis through the cortex and finally through to the casparian strip of the endodermis (White, 2001). Previously, Schreiber et al. (1999) have outlined that the casparian strip forms a barrier around endodermal cells. As the barrier is mainly composed of suberin and lignin, Ca^{2+} is required to enter the cytosol of the endodermal cells through protein channels before it can be exported to the apoplast (Thor, 2019; Schreiber et al., 1999).

While highly regulated, rapid influxes of Ca^{2+} ions through their respective cation channels do occur in order to initiate cellular processes in response to a range of developmental cues and environmental stresses. One example of this is the influx of Ca^{2+} that occurs as a result of abscisic acid, thus inducing stomatal closure (MacRobbie, 1992). As previously mentioned, calcium influxes are also tied to environmental stresses, and there is a lot of evidence of Ca^{2+} influxes in response to salt stress. Increased calcium has been closely tied to salt stress resistance (Etehadnia et al., 2010; Etehadnia et al., 2008; Shaterian et al., 2005). Calcium also plays an important role as a signalling molecule in drought stress resistance, with Knight et al. (1997) observing changes in the Ca^{2+} during drought stress.

In *Arabidopsis* there are estimated to be over 250 calcium sensors (Day et al., 2002). The three main families of calcium sensors are: 1) calcineurin B-like protein (CBLs), 2) calmodulin (CaM),

and calmodulin-like proteins (CMLs) and 3) calcium-dependent protein kinases (CPKs) and the calcium and calmodulin-dependent protein kinase (CCaMK) (Wang et al., 2015; Bender & Snedden, 2013; Luan, 2009; Yang & Poovaiah, 2003; Cheng et al., 2002). In general, the role of these sensors is to transduce Ca^{2+} signals which in turn cause the downstream target to be phosphorylated, triggering a response to the drought stress (Hepler, 2005; Burstrom, 1968; Jones & Lunt, 1967). This is a general overview of the importance and role of Ca^{2+} as a signalling molecule. While this role of calcium should not be disregarded, this thesis focuses on the structural role of calcium.

2.3.1 The Structural Role of Calcium

Calcium plays a key role in the structure of cells, as it is well known to influence the rigidity of the cell wall through the formation of cross-linkages to deesterified pectin in the middle lamella (Thor, 2019). In addition to providing structure to the cell wall, Marschner (1995) and Hepler (2005) have both described the role of Ca^{2+} in stabilizing cell membranes through interactions with phospholipids. Based on these principles, it is well understood that a reduced calcium content weakens the cell wall (Thor, 2019).

2.3.2 The Influence of Calcium on Homogalacturonan- The Egg-Box Model

The interaction between calcium ions and blocks of galacturonic acid has been well characterized, and the gelatinization of pectin has been found to result from the formation of these strong bonds (Ravanat & Rinaudo, 1980). Previous research by that group found when these bonds occur within pectin, calcium induces chain-chain associations which constitute the formation of junctions that are responsible for pectin gel formation. These junction zones form “egg-box” structures as described by the “egg-box model” and are characterized as two helical chains of galacturonic acids with calcium ions in between (Figure 2.4) (Braccini & Pé Rez, 2001; Ravanat & Rinaudo, 1980). These calcium cross-linkages are well known to influence the rigidity of the cell wall, and in general help maintain the structure of the cell wall (Thor, 2019; Alberts et al., 2002).

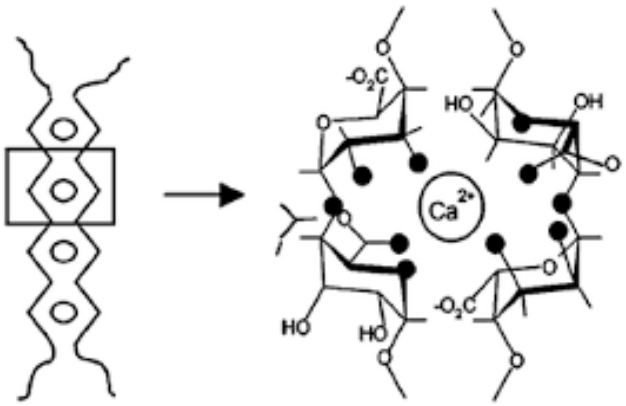

Figure 2.4 Formation of "egg-box" structures

Homogalacturonan that is demethylesterified in a blockwise manner results in a string of GalA residues. These blocks of GalA are capable of crosslinking with calcium and forming junction zones referred to as "egg-box" structures as indicated by the box in the image on the left. Image from Fu et al., 2011. Copyright permission obtained from Springer Nature.

2.4 Boron

Unlike calcium, boron is considered an essential micronutrient, however boron still plays a critical role in the proper physiological functioning of higher plants (Brown et al., 2002). Boron is required for optimum growth, development, yield and overall quality of crops (Shireen et al., 2018). Boron is similar to calcium in terms of its importance in the structural integrity of plant cells (Matoh, 1997). Hu and Brown (1994) demonstrated the importance of boron in the plant cell wall through their findings showing that in tobacco and squash, 95-98% of boron present within the plant is found in the cell wall. The structural role of boron is further outlined in Section 2.4.1.

In addition to boron's role in maintaining structural integrity, boron also influences ion activity within plants (Goldbach & Wimmer, 2007). While adequate levels of B enhance plasma membrane hyperpolarization, limited B alters membrane potential and reduces H^+ -ATPase activity and this direct influence of B on plasma membrane-bound proton-pumping ATPases influences ion fluxes (Goldbach & Wimmer, 2007; Lawrence et al., 1995). This change in ion flux as a result of boron was demonstrated in *Vicia faba* as a variety of ions fluctuated including H^+, K^+, Rb^+ and Ca^{2+} as a result of B-deficient conditions (Robertson & Loughman, 1973). Boron also plays an important role in cell division and elongation, as well as numerous other functions outside the scope of this project (Dell & Huang, 1997).

2.4.1 The Structural Role of Boron and RG-II Dimers

As previously mentioned, boron plays an important role in maintaining the structural integrity of plant cells. Within the cell wall, boron is cross-linked with pectin assembly, glycosylinositol phosphorylceramides (GIPCs) and RG-II (Voxeur & Fry, 2014).

These cross-linkages are known to control the tensile strength and the porosity of the cell wall (Ryden et al., 2003; Fleischer et al. 1999). O'Neill et al. (2004) further confirmed that in plants, the main role of boron is structural as a result of borate-diol ester cross-links to RG-II. These borate-diol ester cross-links are known to link RG-II monomers, thus creating RG-II dimers (O'Neill et al., 2004). More specifically, RG-II dimers form as a result of ester bonds between a boron atom and the apiosyl residue of side chain A in RG-II (Ishii et al., 1999). Furthermore, due to the nature of pectin, RG-II dimers cross-linked with boric acid has the added benefit of covalently cross-linking the two HG chains in which the RG-II molecules are attached (Ishii & Matsunaga, 2001). This series of linkages, in addition to the previously described cross-links between HG and Ca^{2+} results in the formation of a 3D pectin network (O'Neill et al., 2004).

While the general understanding behind the formation of RG-II dimers is well founded, many questions remain regarding dimer biosynthesis. For example, the timing and location for the formation of RG-II dimers is unknown. Funakawa and Miwa (2015) explored various locations where these structures may form. They first outlined that since RG-II is known to be synthesized in the Golgi, the most plausible explanation is that RG-II dimers form in either the Golgi or the apoplast However, that hypothesis posed by them raises more questions. Initially this group explored the idea that RG-II dimers form within the Golgi, prior to RG-II being secreted into the apoplast. The drawback with that hypothesis is it remains unclear how the complex structure of RG-II is then incorporated into HG chains. Alternatively, if RG-II dimers are formed within the apoplast, it is unknown how RG-II monomers would be able to find each other (Funakawa & Miwa, 2015). In boron sufficient conditions, more than 90% of RG-II exists in dimers confirming, their importance, however it is unclear how this level of dimer formation could be reached if the dimers form within the apoplast (Funakawa & Miwa, 2015).

In addition, while numerous studies have identified enzymes responsible for the formation of RG-II monomers, there are no currently known enzymes that are responsible for catalyzing the formation of RG-II dimers (Funakawa & Miwa, 2015). An experiment by O'Neill et al. (1996) has also observed that borate cross-linking can occur only with isolated RG-II and boric acid if divalent cations are present, thus supporting the notion that no enzymes are required for the formation of RG-II dimers. However, this study was conducted *in vitro* (O'Neill et al., 1996). Despite the questions that remain regarding fine details behind the formation of RG-II dimers, its critical role in the structure of the cell wall has been confirmed through a range of experiments. In plants deficient in B, 80-90% of the total amount of RG-II was found as a monomer (in contrast to the normal 80% of RG-II chains in dimer form) and cell wall swelling was observed in addition to the formation of small and irregular shaped cells (Ishii et al., 2001). This group also found that the formation of RG-II dimers determines cell wall thickness in pumpkin tissue.

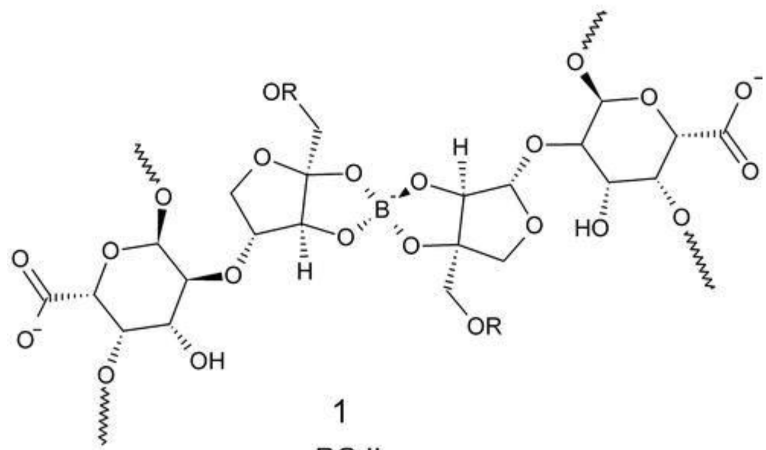

1

RG II

Figure 2.5 Formation of RG-II dimers

Boron plays a critical role in cell structure. Boron forms cross-links with the polysaccharide rhamnogalacturonan II (RG-II). RG-II, a 5-10kDa polysaccharide composed of D-galactose along with 11 other glycosyl residues has been found to exist as a dimer through a covalent crosslinking with a borate diester. Cross-linking of RG-II is critical for plant development as it is required for the formation of a 3D pectin network in the cell wall. Image from Breydo, 2013. Copyright permission obtained from Springer Nature.

2.5 Abiotic Stress

Abiotic stresses are characterized by environmental stresses and include drought, cold stress and other extreme temperatures, salinity and heavy metals. The need to gain further understanding into how plants respond to abiotic stresses is critical to ensure the demand for food is met in the face of climate change. Weather events such as increased occurrence and intensity of drought and heat waves are just two examples of weather events resulting from climate change that affect plant growth and yield, and in turn are of critical importance as global climate change is already having a large impact on not only temperature but also on rainfall and extreme weather scenarios (Food and Agriculture Organization of the United Nations, 2009).

2.5.1 Drought Stress

As a result of growing population, the expansion of agriculture and growth in the energy and industrial sectors, the demand for water has increased (Food and Agriculture Organization of the United Nations, 2009). These factors paired with climate change and contamination of water supplies have further contributed to water scarcity (Dai, 2013; Mishra & Singh, 2010). As a result, the severity and frequency of droughts has increased. While over one half of the earth's terrestrial space is vulnerable to droughts, within Canada, the Prairies are at an increased risk of drought due to the high variability in precipitation both in time and space within the region. At least 40 long-duration droughts have occurred in Western Canada over the past two-hundred years (Dotto et al., 2010). In the 1890's, 1910's, 1930's, 1960's and the 1980's multi-year droughts occurred in southern regions of Alberta, Manitoba and Saskatchewan (Hanesiak et al., 2011). One of the most severe droughts experienced in the Prairies occurred in 2001 and 2002, with a weather station in Saskatoon, SK, showing a 46% decrease in the average annual precipitation (Wittrock et al., 2002). While drought stress also occurs in Eastern Canada, the droughts in regions such as southern Ontario and Quebec, are usually shorter, smaller in area, less frequent and less intense (Bonsal et al., 2011).

The impact of drought stress on plant function is primarily related to reduced carbon fixation that occurs during a period of drought, this can affect plant growth depending on other variables such as the length of the drought (Alizadeh et al., 2014). In addition, this paper explained that during drought stress, plants will close their stomata, leading to increased resistance to CO_2 diffusion

from the leaves and reduced water loss. While there is an understanding of some of physiological mechanisms employed by plants to adapt to drought such as cuticular waxes, the role of the cell wall as a physical barrier to water loss has been relatively unexplored (Rahman et al., 2021).

2.5.1.1 Calcium and Drought Stress Tolerance

While the role of calcium in drought stress tolerance is well outlined, the vast majority of the literature has focused only on the role of calcium in physiological and cellular processes, as well as its role as a signalling molecule. There are few papers exploring the structural role of calcium in relation to drought stress tolerance. One example of the structural role of calcium in drought stress tolerance is the relationship between Ca^{2+} and polyamines (Ma et al., 2005). Along with pectin, polyamines play an important role in the structure of the cell wall, as they help to maintain the thickness of the cell wall through the strengthening of bonds (Berta et al., 1997). Ma et al. (2005) found that exogenous Ca^{2+} may have modified endogenous polyamine levels during drought stress in bread wheat, contributing to increased drought stress resistance. Calcium application has also been found to help stabilize the structure and function of chloroplasts, mitochondria and the endomembrane system in mesophyll cells (Hu et al., 2018).

While these papers are evidence that calcium plays a structural role in improving resistance to drought stress, the link between pectin, calcium cross-linkages and how the resulting structural changes influence drought stress does not appear to have been well explored. A handful of papers have shown that pectin, and the side chains present do influence tolerance to drought stress in wheat cultivars (Konno et al., 2008; Leucci et al., 2008; Piro et al., 2003). HG has also been shown to play an important role in increasing resistance to desiccation in a green algae species (Herburger et al., 2019). In addition, the degree of pectin methylation has been shown to influence water holding capacity, with reduced methylation (which is required for "egg-box" structure formation) being shown to increase water holding capacity (Willats et al., 2001b). They also showed the addition of calcium to pectin gels influences the water holding capacity. However, there is a need to explore these concepts in a whole plant system.

2.5.1.2 Boron and Drought Stress Tolerance

While even more limited than the current body of literature exploring the role of calcium in mitigating drought stress, boron has also been implicated in current literature for its role in enhancing drought stress tolerance in a range of crops. However, as observed with calcium, there is an absence of research examining the impact of the structural role of boron on the cell wall and the influence this may have on tolerance to drought stress.

With that being said, one of the roles in which boron has been implicated to increase tolerance to drought stress is through enhanced gene expression and antioxidant enzyme activity (Aydin et al., 2019). Aydin et al. (2019) found that in drought stressed tomatoes, boron in combination with polyethylene glycol (PEG) increased the transcription of stress related genes. They also found that chlorophyll content increased in plants that received boron and PEG. The antioxidant defence system has also been shown to benefit from the application of boron when plants are under drought stress (Naeem et al., 2018). This group observed that an up-regulation of the antioxidative defense-system in drought stress maize that had received boron. The application of boron in drought stress maize was also found to improve the water status within the plant, photosynthetic capacity and tissue-B concentration (Naeem et al., 2018). Both wheat and winter wheat have been found to have enhanced drought stress tolerance as a result of boron application (Abdel-Motagally & El-Zohri, 2018; Karim et al., 2012). RG-II, as well as RG-I, has also been shown to be important in drought stress resistance. Leucci et al. (2008) compared wheat cultivars with varying tolerances to drought and they found that cultivars with increased drought stress tolerance had a larger quantity of RG-I and RG-II side chains. They proposed this is likely the result of the pectin forming hydrated gels, which in turn limited damage to cells during drought stress.

In addition, in *Arabidopsis*, the MUR1 gene has been associated with the fucosylation of side chain A in RG-II, which is critical to the proper formation of RG-II dimers (Reiter et al., 1993). The proportion of RG-II dimers in the *mur1* genotypes was also found to decrease by approximately 50%, in comparison to the wild-type line where RG-II dimers accounted for around 95% of RG-II within the cell walls (Reuhs et al., 2004). In addition, Panter et al. (2019) found that the *mur1* genotype was sensitive to freezing stress, however the application of boric acid improved resistance to freezing stress. The increased ability for *mur1* to tolerate freezing stress following

supplementation with boric acid is suggestive of the importance of RG-II dimer formation in tolerance to this stress (Panter et al., 2019). Prior studies had also confirmed *mur1* was associated with reduced RG-II borate cross-linkages, as the *mur1* phenotype was restored with boron application (Feng et al., 2018; Sechet et al., 2018; Voxeur et al., 2017; Ryden et al., 2003; O'Neill et al., 2001). While Panter et al. (2019) examined freezing stress, dehydration stress and freezing stress share overlapping characteristics in relation to cellular water loss. Thus, RG-II dimer formation does likely also play an important role in dehydration stress tolerance. However, further studies should be done exploring the role of boron, RG-II and dehydration stress tolerance.

2.5.1.3 PME/ PMEI and Drought Stress

While seemingly convoluted, the over-expression of both PME's and the corresponding inhibitors such as PMEI's have been found to enhance drought stress tolerance in various crops. Focusing first on PME, proper stomatal functioning has been closely tied to de-methylesterification of pectin (Amsbury et al., 2016). They observed PME6 was highly expressed in *Arabidopsis* guard cells and was essential for the proper functioning of the stomata. Furthermore, Amsbury et al. (2016) showed in *pme6-1* mutants, the ability for stomata to adequately function was decreased as a result of higher levels of methylated pectin and the resulting smaller dynamic range in movement caused decreased growth under drought stress condition. Similarly, Yang et al. (2020) found the over-expression of PtoPME35 in *Arabidopsis*, a PME gene from poplar trees, decreased water loss during drought stress through the inhibition of stomatal opening.

In contrast to these results, An et al. (2008) found over-expression of CaPMEI1 in *Arabidopsis*, a PMEI found in pepper, enhanced drought stress tolerance. These findings are interesting when compared to those outlined above as PMEI's inhibit PME. While the results from Amsbury et al. (2016) and Yang et al. (2020) found that increased de-methylation of pectin enhanced drought stress tolerance, the over-expression of CaPMEI1 in *Arabidopsis* which likely has increased pectin methylation, was also found to enhance drought stress tolerance (An et al., 2008). The contradictions may be indicative of functional variation within the wide range of PME's and PMEI's (Wormit & Usadel, 2018; Wang et al., 2013).

2.6 Biotic Stress

Biotic stress is a category of stress caused by living organisms such as fungi, bacteria and viruses. Biotic stresses can affect plants through multiple different means such as through the release of toxin enzymes or nutrient deprivation. The release of these enzymes and/or nutrient deprivation can lead to reduced plant vigor, yield and/or death (Gimenez et al., 2018) There is a wide range of biotic stresses that can affect plants that are significant in the agriculture industry, however this section will focus on *Botrytis cinerea* and *Colletotrichum higginsianum.*

2.6.1 Botrytis cinerea

Botrytis cinerea (*B. cinerea*), an ascomycete fungus, is an extremely destructive fungal pathogen (Boddy, 2016). Boddy (2016) further expanded on the catastrophic nature of *B. cinerea*, outlining this pathogen is capable of infecting over 200 plants species and causing losses of $10 to $100 billion (USD) annually. Furthermore, *B. cinerea* is able to persist in greenhouses as conidia, mycelia or sclerotia, as well as year-round outdoors on living or dead plants. Both sclerotia and conidia can also survive in soil (Gleason & Helland, 2003). Conidia (a type of spore) can also easily travel through the air, allowing for widespread distribution (Gleason & Helland, 2003). Given the wide-spread nature of *B. cinerea*, it is one of the most commonly studied nectrotrophic plant pathogens (Boddy, 2016).

The necrotrophic nature of *B. cinerea* further contributes to its devastating consequences since unlike biotrophs, necrotrophic pathogens do not rely on the host being alive to complete their lifecycle. A *B. cinerea* infection begins when asexual spores land on a plant surface (Boddy, 2016). The conidia will form a germ tube within 2-4hr post-inoculation, while the appressoria along with the penetration peg will form within 8hr post-inoculation (Figure 2.6) (Chakraborty, 2015). The formation of the appressoria and penetration peg will allow for entrance to the cuticle (Williamson et al., 2007; Boddy, 2016). However, unlike the appressoria formed in *Colletotrichum* species or *Magnaporthe*, the appressoria produced by *B. cinerea* do not have a wall that seals the appressorium from the germ tube (Boddy, 2016; van Kan, 2006; De Jong, 1997). The lack of this wall means that while appressoria produced by *Magnaporthe* species for example can penetrate the host by physical pressure alone through the generation of high amounts of osmotic pressure, *B. cinerea* does not have this ability (van Kan, 2006). In order to compensate, *B. cinerea* release a

range of enzymes such as cutinases and lipases, while the tip of the penetration peg produces H_2O_2 (Boddy, 2016).

Alternatively, a B. cinerea infection can also occur via. mycelium. Infection from mycelium is different because as opposed to conidia landing on the surface and forming an appressoria, penetration occurs in a different manner (Choquer et al., 2007). Penetration via. mycelium occurs as a result of hyphae growing and becoming aggregated together (Choquer et al., 2007). These aggregates have been described as "claw-like" and similar to "infection cushions" and "complex appressoria" which occur as a result of a *Sclerotinia sclerotiorum* infection (Jurick & Rollins, 2007; Kunz et al., 2006; Hegedus & Rimmer, 2005). Toxins will still be released to facilitate the infection and cell death, as outlined in the above paragraph.

Once *B. cinerea* breaches the cuticle, the penetration peg will search for an epidermal cell and from there grow into the pectin-rich cell wall of the epidermal cell (Boddy, 2016). This typically occurs 16-24hr post-inoculation (Figure 2.6) (Chakraborty, 2015). While pectin is an important component in the structure and function of the cell wall, ironically plant species with high pectin contents are more susceptible to *B. cinerea* infections (Boddy, 2016). They go onto explain that *B. cinerea* has a well-established and effective pectinolytic machinery, thus plant species with low pectin contents in their cell walls are poor hosts for *B. cinerea.* Despite this drawback, *B. cinerea* is highly resourceful with the ability to establish infections in incompatible hosts (Petrasch et al., 2019). While in compatible hosts, *B. cinerea* is able to induce a rapid death in the host, in non-compatible hosts *B. cinerea* will establish a quiescent infection (Petrasch et al., 2019). *B. cinerea* can then begin to turn a non-compatible host into a compatible one through the suppression of the immune system (Boddy, 2016).

As *B. cinerea* is a necrotroph, the fungal pathogen seeks to kill the host plant. *B. cinerea* has a large arsenal of various chemicals that it utilizes to cause cell death in the host and in compatible hosts, *B. cinerea* begins to kill the host during cuticle penetration and the formation of the primary lesion (Boddy, 2016). During this time, *B. cinerea* triggers an oxidative burst in the host resulting in an accumulation of free radicals and ultimately cell death in the host (Petrasch et al., 2019; Boddy, 2016). As previously mentioned, in non-compatible hosts, the immune system is

suppressed through the production of small RNA (sRNA) molecules which will silence genes in the host (Boddy, 2016). Around 24-48hr post-inoculation, the H_2O_2 concentration in the mesophyll cell layers will increase as a result of the ROS released from the pathogen in order to help kill the host plant (Figure 2.6) (Chakraborty, 2015). During *B. cinerea* infections, the fungus will also obtain nutrition through the plant cell wall, releasing cellulases and hemicellulases to first decompose it (Romanazzi & Feliziani, 2014).

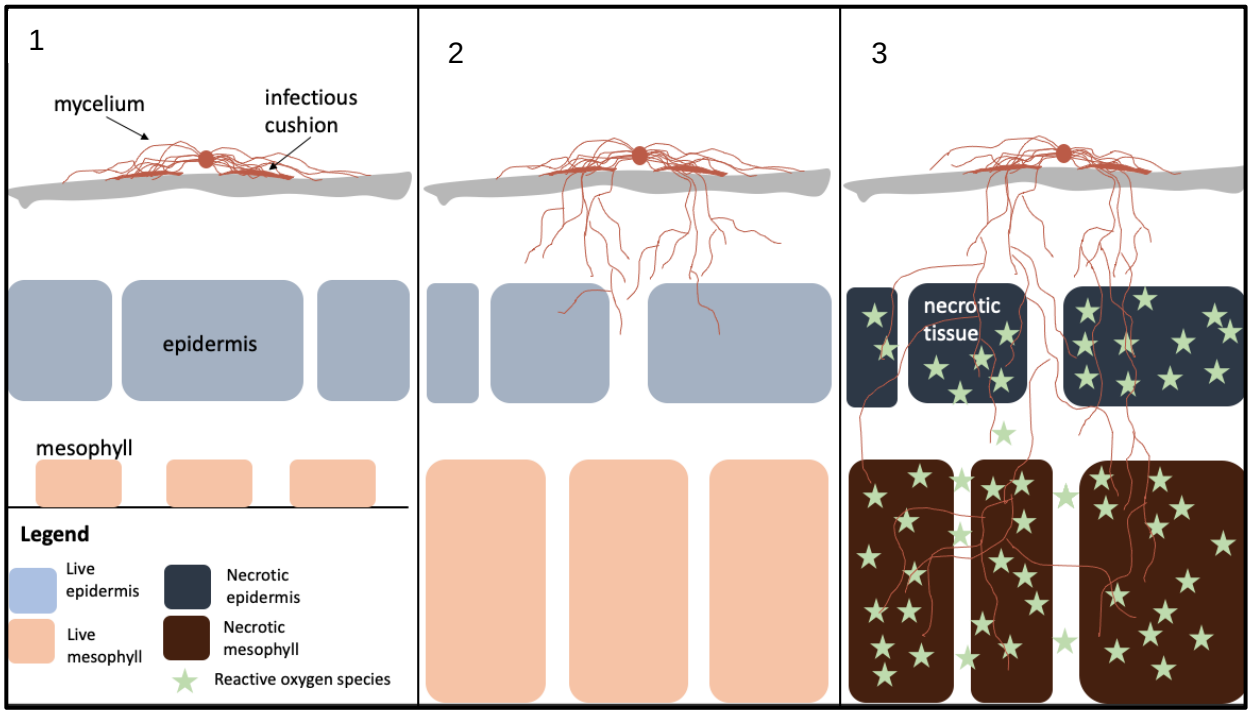

Figure 2.6 Developmental stages of *Botrytis cinerea* infection

Developmental stages of a *Botrytis cinerea* infection occurring from mycelium. **1)** Hyphae grow on the surface of the host plant. Hyphae growing on the surface of the plant will also begin to aggregate, forming "claw-like" structures, similar to infectious cushions from other pathogens. In this figure, those aggregates are labelled infectious cushions. These structures allow for penetration into the host. **2)** Hyphae continue to grow through plant tissues and begin to infect epidermal cells. **3)** Growth of hyphae continues, invading mesophyll cells. Reactive oxygen species begin to accumulate, contributing to the appearance of necrotic tissue. Figure based on information obtained from Peters, 2015 and Choquer et al., 2007.

2.6.1.1 Current Management Practices for Botrytis cinerea

Currently, the most common management practice to control *B. cinerea* infections is the use of synthetic fungicides throughout the growing cycle (Romanazzi & Feliziani, 2014). When selecting

a fungicide(s) to control *B. cinerea*, there are several families of synthetic fungicides that are effective in controlling *B. cinerea.* Fungicides effective in the management of *B. cinerea* can be classed into the following categories based on biochemical mode of action: fungicides affecting fungal respiration, microtubule function, osmoregulation methionine biosynthesis or sterol biosynthesis (Romanazzi & Feliziani, 2014). Despite the current reliance on synthetic fungicides, *B. cinerea* has been classified as a "high-risk" pathogen as a number of variants have popped up that are resistant to a range of fungicides used for *B. cinerea* management such as: fenexamide, boscalid and pyraclostrobin, carbendazim, pyrimethanil, cyprodinil, iprodione, procymidone, diethofencarb and fluazinam (Romanazzi & Feliziani, 2014). While synthetic fungicides are the most common approach, there has been a push to develop management practices outside of synthetic fungicides (Romanazzi & Feliziani, 2014). There are 4 main alternative management practices: 1) biological control agents (BCAs), 2) natural compounds, 3) compounds generally recognized as safe (GRAS), and 4) physical methods alone or in combination with the other alternative practices.

2.6.1.1.1 Boron and *Botrytis cinerea*

In general, there is little information available regarding the use of boron in controlling plant pathogens including *B. cinerea*. Even though boron-deficient plants are known to have a range of physiological and biochemical issues including changes in cell wall structure and membrane integrity (Marschner, 1995). Nevertheless, there are a few studies that have explored the use of boron, primarily as a foliar spray, in mitigating *B. cinerea*. Qin et al. (2010) found that in table grapes, the application of boron strongly inhibited not only the germination of *B. cinerea* spores but also reduced germ tube elongation and mycelial spread. Furthermore, this group found that the application of boron led to the leakage of cellular constituents from *B. cinerea* hyphae, allowing for the cytoplasmic materials to leak out from the hyphae, ultimately destroying the hyphae. It was proposed that the breakdown of hyphae as a result of boron application may be the result of the boron disrupting the cellular membrane of *B. cinerea* (Qin et al., 2010). Another horticulture crop that has been shown to benefit from boron application in relation to *B. cinerea* is strawberries (Wójcik & Lewandowski, 2003). Wójcik and Lewandowski (2003) found that when calcium and boron were applied together, strawberry plans were more resistant to rot from *Botrytis.*

2.6.1.1.2 PME/ PMEI and *Botrytis cinerea*

Numerous papers have implicated the role of PMEI's in reducing susceptibility against *B. cinerea*. For example, Lionetti et al. (2007) observed that in *Arabidopsis* plants over-expressing PMEI-1 and PMEI-2, there are increased resistance to *B. cinerea*. They found increased resistance to *B. cinerea* in AtPMEI-1 and AtPMEI-2 was found to be the result of *B. cinerea*'s impaired ability to grow on methylesterified pectin. Collectively in AtPMEI-1 and AtPMEI-2, the degree of pectin methylesterfication was increased by approximately 16% (Lionetti et al., 2007). PMEI-10, PMEI-11 and PMEI-12 have also been identified as PMEI's that are induced in *Arabidopsis* infected with *B. cinerea* and are suggested to play a role in maintaining the structural integrity of the cell wall during an immune response (Lionetti et al., 2017). This group observed that in *pmei10*, *pmei11* and *pmei12* mutants, when pectin methylesterification decreased, susceptibility to *B. cinerea* was increased.

Both PMEI's and PME's appear to play a role in disease resistance despite the opposing effects of the two on methylation in pectin. Del Corpo et al. (2020) found that in *Arabidopsis*, PME-17 plays a critical role in the response to *B. cinerea*. They established that PME-17 plays a role in immune protection against *B. cinerea* through both its contribution to pathogen-induced PME activity and its ability to trigger jasmonic acid-ethylene-dependant PDF1.2 expression. After 48hr, the lesion size in the wild-type line were approximately 3mm^2, while lesions in *pme17-2* and *pme17-3* were around 6mm^2 (Del Corpo et al. 2020). This group emphasized the importance of PME-17 for an adequate immune response during a *B. cinerea* infection. Del Corpo et al. (2020) also identified that PME-17 demethylesterify HG in a block-wise manner thus allowing for the formation of "egg-box" structures. Despite this, they did not specifically investigate the role of these structures and their influence on cell wall integrity in relation to their results. Nevertheless, this paper suggested that AtPME-17 may mechanically reinforce the cell wall and in turn counteract the ability for *B. cinerea* to breach the cell wall (Del Corpo et al., 2020). However, as *B. cinerea* is known to heavily rely on pectinolytic machinery to penetrate the cell wall as it lacks the ability to penetrate with physical pressure alone, this proposed idea raises some questions (Boddy, 2016).

In contrast, Raiola et al. (2011) found that PME-3 is important to the ability of *B. cinerea* to successfully colonize its host. PME-3 was found to be rapidly expressed during *B. cinerea*

infections in *Arabidopsis*, thus acting as a susceptibility factor for the plant (Raiola et al., 2011). Overall, the opposing findings with regards to the role of PME and PMEI in *B. cinerea* infections is suggestive that while on the surface the role of PME and PMEI appear well understood, the relationship between these two and their effect on *B. cinerea* infections is complex and more research in this area is required.

2.6.2 *Colletotrichum higginsianum*

Unlike *B. cinerea*, *Colletotrichum higginsianum* (*C. higginsianum*) is a hemibiotroph, meaning it combines strategies characteristic of biotrophs and necrotrophs (Yan et al., 2018). As a hemibiotroph, the initial phase of a *C. higginsianum* infection is similar to a biotroph in the sense that the invading pathogen will suppress both the immune system and induce cell death in the host to allow for the spread of hyphae (Figure 2.7) (Yan et al., 2018; De Silva et al., 2017). Once *C. higginsianum* has successfully spread its hyphae, there is a switch to a necrotrophic phase (Figure 2.7) (Yan et al., 2018). These previous papers further outlined that the necrotrophic phase is characterized by the release of toxins including enzymes that induce damage within the host and result in the death of the infected plant (Figure 2.7). More specifically, the hemibiotrophic portion of the *C. higginsianum* lifecycle begins when conidia land on the surface of the leaf, and in turn produce appressoria which penetrate the surface of the leaf (Yan et al., 2018). Following the breach of the leaf surface by the appressoria, they will begin to mature which is partially characterized by the appressoria becoming melanized while solutes accumulate in the cytoplasm, then, unlike *B. cinerea*, extremely high turgor pressure with the appressorium allows the peg to penetrate the cell wall by physical force alone (Yan et al., 2018).

Once the epidermal cell is breached, the hyphae continue to grow and remain biotrophic hyphae. Within 36-40hr of the infection, *C. higginsianum* establishes itself as a biotroph (Yan et al., 2018). As with all biotrophs, the host tissue is still alive and at this point in the infection, the infected cells of the host plant remain functional. 72hr after the infection began, as additional cells are colonized by the infection, there is a switch where the once biotrophic hyphae become necrotrophic (Yan et al., 2018). This is a classic characteristic of hemibiotrophic pathogens, a switch from a biotrophic infection to a necrotrophic infection. The growth of necrotrophic hyphae results in necrotic lesions with a “water-soaked” appearance approximately 84hr post infection (Münch et al., 2008). These

lesions play a critical role in allowing *C. higginsianum* to spread to other plants as an acervuli form on these lesions and begin producing conidia (Yan et al., 2018).

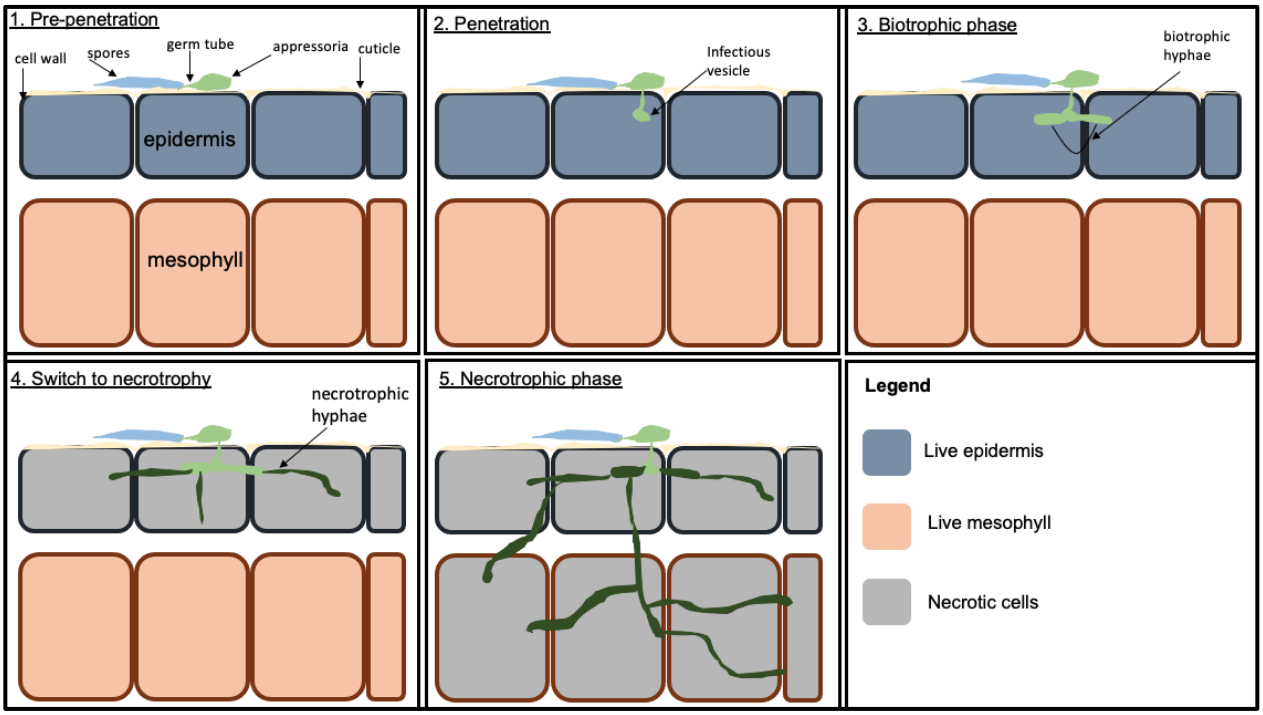

Figure 2.7 Developmental stages of *Colletotrichum higginsianum* infection

The process of a *Colletotrichum higginsianum* broken down into five steps. **1)** ~24hr post infection, the appressoria forms from spores that adhered to the cuticle of the host plant. A germ tube is also formed. This is the pre-penetration phase. **2)** Following pre-penetration, the penetration phase will occur. During this stage and infectious vesicle forms. The cells of the host plant remain alive at this stage. **3)** ~48hr post infection, biotrophic hyphae form. Effectors will be secreted. The host remains alive during this phase, while the pathogen obtains nutrients from the plant. **4)** ~60hr post infection, the necrotrophic phase begins to occur, and cells begin to die. 5) ~70hr post infection necrotrophic hyphae continue to spread into surrounding cells and directly penetrate the host cytoplasm. Additional host cells are killed during this phase. Figure based on information obtained from Jayawardena et al., 2021 and Yan et al., 2018.

2.6.2.1 Current Management Practices for Colletotrichum higginsianum

The *Colletotrichum* genus is similar to *B. cinerea* in the widespread and devastating consequences of its infections (Dowling et al., 2020). *Colletotrichum* has been described as one of the most economically important types of fungi given that it is capable of infection over 3,200 species of monocots and dicots (Nyombi, 2019). While typical losses due to *Colletotrichum* infections are known to cause post-harvest losses of up to 100% (Machado et al., 2014; Ademe, 2013).

Colletotrichum higginsianum is known to infect species in the Brassicaceae family which includes *Brassica napus* (*B. napus*, rapeseed), a crop that holds significant economic value (Dowling et al., 2020).

Despite the opportunity for wide scale devastation of rapeseed as a result of a *C. higginsianum* infection, literature regarding current management strategies specific to *C. higginsianum* is scarce. However, in general, *Colletotrichum* species, like *B. cinerea* are primarily managed by fungicides (Dowling et al., 2020). As a result of the heavy reliance on fungicides to manage this pathogen, *Colletotrichum* species have developed and are continuing to develop resistance to various fungicides that were once effective. In addition to relying on fungicides for the management of *Colletotrichum,* there are a number of other cultural and biological controls that have been used to control *Colletotrichum* with the general goal to decrease the production and spread of inoculum (Dowling et al., 2020). Examples of strategies that would aid in accomplishing this goal include adjusting soil nutrients, managing weeds and the use of resistant cultivars or cultivars with limited susceptibility to the *Colletotrichum* species of concern.

2.6.2.1.1 Boron and *Colletotrichum higginsianum*

Boron application and boron transporters do not appear to have been explored in relation to *C. higginsianum*, however there are a select number of papers that have explored the use of borate as an antifungal agent against *Colletotrichum gleosporioides* (*C. gleosporioides*). Both Shi et al. (2011) and Shi et al. (2012) observed that borate provides antifungal protection to mangos during *C. gleosporioides* infection. These studies found that borate treatment on mangos inhibited the germination of spores, in addition to aiding in the control of anthracnose on the fruit. One of the antifungal mechanisms that borate was observed to have on *C. gleosporioides* was mitochondrial degeneration (Shi et al., 2012; Shi et al., 2011).

2.6.2.1.2 PME/ PMEI and *Colletotrichum higginsianum*

While PMEI has been explored in its role in *C. higginsianum* infections, the body of research available regarding changes to the methylation of pectin and this fungal pathogen is small. One study conducted by Engelsdorf et al. (2017) found that *Arabidopsis pmei6-2* mutants had reduced susceptibility to *C. higginsianum*. This study also explored a range of other genotypes and while

they were not specifically PME or PMEI mutants, they did have altered amounts of pectin. Thus, there appears to be a connection between the biotrophic establishment of *C. higginsianum* and pectin content (Engelsdorf et al. 2017). This connection is possibly the result of the structural impact of pectin on the cell wall and in turn, the force required to penetrate the cell wall. The overall lack of studies exploring PME or PMEI in relation to *C. higginsianum* in comparison to *B. cinerea* may be due to the *B. cinerea* pectinolytic enzymes (Boddy, 2016). *B. cinerea* relies on this machinery and its ability to break down pectin in order to circumvent the cell wall in comparison to *C. higginsianum* which can breach the plant through physical pressure alone (Yan et al., 2018; Boddy, 2016). Thus, a more rigid, stronger cell wall may more effectively alleviate *C. higginsianum* infection compared to *B. cinerea.*

2.7 Interaction of Abiotic and Biotic Stress

While the impact of both abiotic and biotic stress on various aspects of plants have been, and continue to be investigated in lab settings, field conditions are drastically different. In addition, there is increasing evidence from both field and laboratory studies that plants respond to specific combinations of stresses in a non-additive manner (Figure 2.8) (Suzuki et al., 2014). These responses produce effects that could not have been predicted if each stress were studied individually. Different combinations of stresses have also been found to affect plants differently in relation to characteristics such as plant growth and yield (Rizhsky et al., 2004).

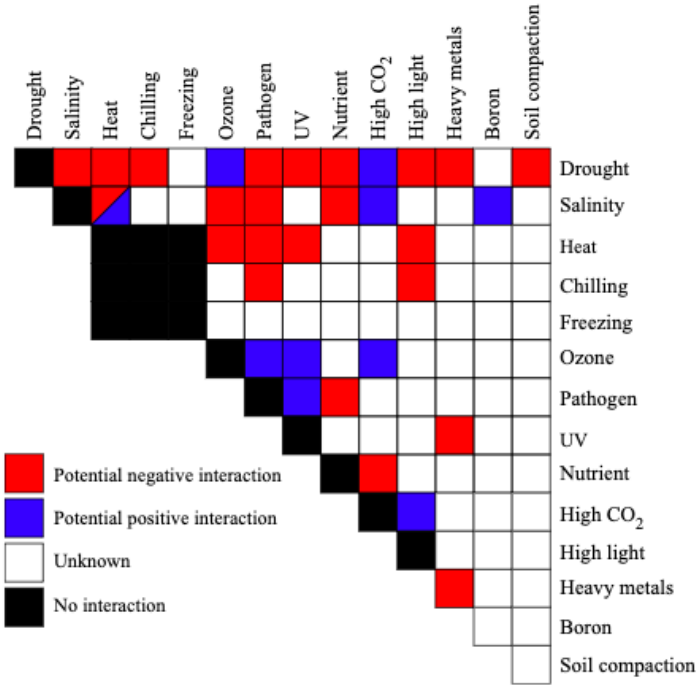

Figure 2.8 Impact of a combination of both abiotic and/or biotic stresses on a plant

The impact of a combination of both abiotic and/or biotic stresses on a plant can have numerous different effects on a plant with respect to plant growth and yield. While some combinations of stresses may result in a positive interaction (blue boxes) with the plant, some can result in negative interactions (red boxes). The effects of combinations of a variety of stresses are still unknown (white boxes). This matrix from Suzuki et al. shows a compilation of results from numerous studies that examined the effects of these stressors in combination with one another. Image from Suzuki et al. (2014). Copyright permission obtained from John Wiley and Sons.

Under natural conditions, plants experience multiple stresses at once. For example, dehydration stress and heat stress commonly occur together. Several studies have investigated the effect of these two stresses (Jagtap et al., 1998; Savin & Nicolas, 1996; Craufurd & Peacock, 1993; Heyne & Brunson, 1940). These previous studies found that when paired together the effect on growth and productivity of crops such as maize, barley and sorghum far exceed what would have happened if only dehydration or heat stress had occurred, as opposed to a combination of the two. This exaggerated response may be the result of the combined physiological consequences that occur during both stresses including high respiration, low photosynthesis, closed stomata and high leaf temperature (Mittler, 2006). Furthermore, a comparison of all major US weather events where the total losses exceeded 1 billion dollars from the period of 1980 and 2012 indicated weather events characterized by both drought and heat caused losses above $200 billion dollars, where events

characterized by drought alone caused $50 billion in damages (Suzuki, 2014). The impact of biotic stress on plants is also different in the field compared to what is simulated in the lab as plants not only face the threat of pathogenic infection in the field but are also attacked by herbivorous pests (Suzuki, 2014). While it may seem logical that when two stresses occur simultaneously, the respective signal transduction pathways would become activated and provide protection, these pathways may not have a synergistic effect (Mittler, 2006). Mittler (2006) further described that while these pathways may be synergistic, they may also be antagonistic. Thus, it is critical to find a solution that is effective against a combination of stresses, in order to try and circumvent the possible detrimental effects of multiple pathways being occurring at once.

2.8 *Allium fistulosum*

2.8.1 Taxonomy and Biology

Allium fistulosum (*A. fistulosum*), also commonly referred to as spring onion, Welsh onion, or Japanese bunching onion, is a perennial diploid plant that was discovered in 1735 near Lake Baikal in Russia by G.W. Steller and is believed to have been derived from *Allium altaicum* (Figure 2.9) (Friesen et al., 1999). *A. fistulosum* is also known to have the ability to tolerate both extreme drought and freezing conditions, as it can survive in the Canadian prairies during the winter months where temperatures can fall below -40ºC (Tanino et al., 2013). The hardy characteristics of *A. fistulosum* will be further discussed in Section 2.8.2.

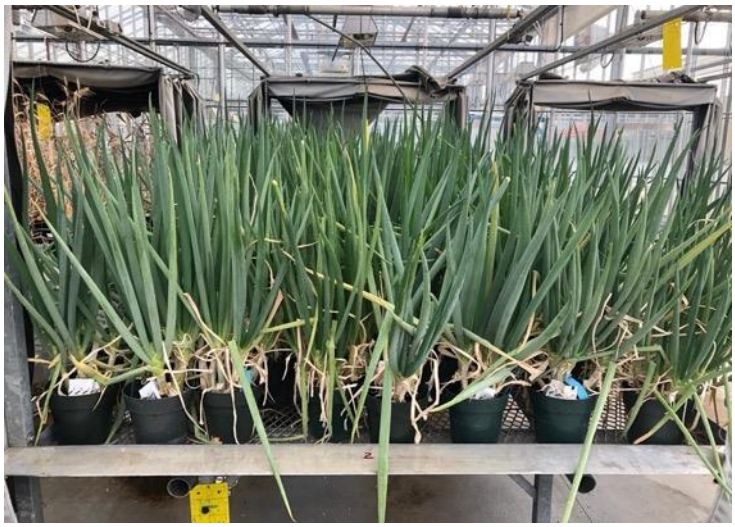

Figure 2.9 *Allium fistulosum* plants

Allium fistulosum also known as Japanese bunching onion or Welsh onion is a cold-hardy perennial onion.

2.8.2 Role in Abiotic Stress Research

A. fistulosum's ability to tolerate extreme weather, as outlined above, contributes to its success as a model species for experiments studying abiotic stress. Research conducted by Tanino et al. (2013) and Liu (2015) further demonstrated the functionality of *A. fistulosum* for this form of research since the freezing process can be observed directly. In addition, this model offers simplicity in obtaining epidermal cell layers as the average cell size is quite large, > 250 x 50 x 90 µm, and a single layer of epidermal cells can be peeled by hand (Tanino et al., 2013).

2.9 *Allium cepa*

2.9.1 Taxonomy and Biology

Allium cepa, known as the common onion, is a bulbous plant widely cultivated in almost every country in the world (Figure 2.10). Originally thought to belong to the Liliaceae family, recent advancements in the taxonomic schemes of the genus *Allium* have found that *A. cepa* belongs to the Amaryllidaceae family (Marrelli et al., 2018). The *Allium* genus is one of the largest, comprised of approximately 850 monocot species (Marrelli et al., 2018).

Figure 2.10 *Allium cepa* plant

Allium cepa also known as the common onion is a bulbous plant that is widely cultivated.

2.9.2 Role in Abiotic Stress Research

Allium cepa (*A. cepa*) has served as a common plant system for research as it is not only readily available, but it also has a large cell size, ranging from 250-400µm (Tanino et al., 2013). Similar to *A. fistulosum*, single epidermal cell layers can also be easily obtained from the plant by hand. *A. cepa* has been used to explore a range of abiotic stresses. Palta et al. (1977) and Arora and Palta (1998) utilized *A. cepa* to explore cold hardiness. To this point, *A. cepa* lacks the ability to cold acclimate and has a low tolerance to freezing with the minimum survival temperature of -11^{o}C (Palta et al., 1977) compared to below -35^{o}C for fully acclimated *A. fistulosum* (Tanino et al., 2013). This contrast between *A. fistulosuma and A. cepa* made it ideal for this thesis, allowing for the exploration of dehydration stress resistance in two species of the same Genus. *A. cepa* has also been used as a model to explore drought stress, and metal stress (Ghodke et al., 2020; El Balla et al., 2013; Achary et al., 2008).

2.10 *Arabidopsis thaliana*

2.10.1 Taxonomy and Biology

Arabidopsis thaliana is a common model organism characterized as a small flowering plant with a small genome size (TAIR, About Arabidopsis, n.d). *A. thaliana* belongs to the Brassicaceae family which also includes rapeseed (TAIR, About Arabidopsis, n.d).

2.10.2 Role in Research

The small genome of *A. thaliana* is just one characteristic that makes this a valuable plant species in plant science research. The genome has also been sequenced with extensive genetic maps of all 5 chromosomes (TAIR, About Arabidopsis, n.d). In addition, the short life-cycle of this plant makes it convenient with respect to efficiency in research (TAIR, About Arabidopsis, n.d). Finally, there are a large number of mutants available as a result of the sequenced genome (TAIR, About Arabidopsis, n.d). This large bank of mutants allows for a wide variety of topics to be investigated using *Arabidopsis*.

2.10.3 Genes of Interest

2.10.3.1 NIP5-1

NIP5-1 (AT4G10380.1) is a protein coding gene for a boric acid channel (TAIR, 2015). The NIP5-1 boric acid transporter is essential for efficiency boron uptake and the development of plants under boron-limited conditions (TAIR, 2015). This transporter also functions in the transport and tolerance of arsenite (TAIR, 2015). The NIP5-1 transporter is primarily localized in the outer membrane of root cells, specifically in the lateral root plasma membrane and the plasma membrane as a whole (TAIR, 2015).

2.10.3.2 NIP6-1

NIP6-1 (AT1G80760.1) is a protein coding gene for boron transporter activity (TAIR, 2013). The NIP6-1 protein helps to direct boron to developing tissues in the shoot such as immature leaves when the environment is low in boron (TAIR, 2013). Unlike the NIP5-1 boron transporter, the boron channel coded for by this gene is impermeable to water (TAIR, 2013). The NIP6-1 transport also transports glycol and urea and is located in the plasma membrane (TAIR, 2013).

2.10.3.3 BOR1

BOR1 (AT2G47160.2) is a protein coding gene for a transporter that is key when boron is limited in the soil (TAIR, 2021). When a plant is in a low boron environment, the BOR1 protein accumulates in the shoots and roots (TAIR, 2021). This protein is degraded when boron levels are restored to normal (TAIR, 2021). The BOR1 transporter is localized to the plasma membrane when a plant is in a boron deficient environment (TAIR, 2021). After boron levels are restored but prior to degradation, this protein is located in the cytoplasm (TAIR, 2021). When degradation occurs, the protein is transported to the endosomes via. the vacuoles. In an environment with high levels of boron, BOR1 is transported to the vacuole for degradation (TAIR, 2021). When BOR1 expression is required, the transporter is localized to the inner plasma membrane domain in the columella, lateral root cap and the epidermis/ endodermis in both the root tip and elongation zone and is also involved in detection of nutrients and ion homeostasis (TAIR, 2021).

2.10.3.4 PMEI5

PMEI5 (AT2G31430) is a pectin methylesterase inhibitor that targets PME from seeds (Müller at al., 2013). PMEI5 is expressed in seeds, buds and mature flowers (Müller at al., 2013). More specifically, within these tissues, PMEI5 is found within the apoplastic region of cells. Phenotypic differences between Col-0 and *Arabidopsis* plants over-expressing PMEI5 include decreased fertility, faster germination and larger seed size (Müller at al., 2013). In addition, previous research by Müller et al. (2013) found that in plants over-expressing PMEI5, the growth of the stem was altered in addition to defective separation of organs within the plant. The defective organ separation may be a result of the defective cuticle that was characterized in the *p35S::PMEI5* mutants as plants with defective cuticles often have defective organ fusion (Müller at al., 2013; Krolikowski et al., 2003).

In conclusion, all the aforementioned genes likely play a pivotal role in not only the overall health of *Arabidopsis* but also in the ability for *Arabidopsis* to withstand abiotic and biotic stress. This notion is supported through each of their descriptions provided above as well as the remainder of the literature review which outlined the importance of boron and PMEI's within the cell wall and the plant as a whole. Therefore, these four genes were selected for analysis of abiotic and biotic stress resistance within this thesis. More specifically, the three boron transporters of interest

(BOR1, NIP5-1 and NIP6-1) were selected based on the current availability of boron transporter mutants at the time of ordering. PMEI5 was selected as it has been previously used in other studies of abiotic stress within the Tanino lab, in addition to its availability.

3.0 INVESTIGATING THE INFLUENCE OF CALCIUM AND BORON ON TEXTURAL AND MECHANICAL PROPERTIES OF PECTIN AND ALLIUM FISTULOSUM

3.1 Introduction

3.1.1 Introduction to Rheology

Given that rheology is the study of the flow of matter, rheology serves as an important tool to gain insight into the viscosity of solutions. Viscosity is defined as the measure of how resistant a fluid is to flow (Abraham et al., 2017). Previous researchers have used rheology to analyze pectin obtained from the cell walls of various plants including Chinese quince fruits and apples (Qin et al., 2020; Mikshina et al., 2015). Nonetheless, the focus of this research has primarily been to improve pectin within plants to make commercial gains as pectin obtained from plants is utilized in the manufacturing process of various foods (Qin et al., 2020; Mikshina et al., 2015). Rheology has also been used in the analysis of pollen tube growth (Kroeger & Geitmann, 2012; Bosch et al., 2005; Parre & Geitmann, 2005; Geitmann, 1999). Research utilizing rheology to gain a greater understanding into the role of the cell wall as a barrier to stress is limited to a handful of papers including Sahaf & Sharon (2016) who studied rheological changes of growing *Nicotiana tabacum* leaves under stress and Hohl & Schopfer (1995) who analyzed changes in maize cell walls from osmotic stress.

Rheological properties of pectin were explored in order to gain an insight into the strength of the intermolecular interactions in pectin as reflected by viscosity and to examine how calcium and boron may regulate these interactions in relationship to low temperature. Calcium and boron, as well as cold acclimation to a lesser extent, are all treatments that are utilized in this research project. Therefore, given the focus of this project on pectin within the cell wall, it was of key importance to attempt to gain a better understanding of how the viscosity of pectin is altered. This *in vitro* study was conducted in order to try and mimic what may be occurring to pectin within the cell wall. While all attempts were made to utilize pectin samples similar to the pectin found within *A. fistulosum, A. cepa,* and *A. thaliana,* there were some limitations to this experiment and therefore the results should be interpreted with caution. The following experiment addresses the hypothesis: Calcium and boron independently increase the viscosity of pectin, in a dose- and temperature- dependent manner. The objective of the following experiment was to investigate the independent roles of calcium and boron, in both a dose dependent and temperature dependent

manner, with respect to the viscosity of pectin (high methylated (HM) pectin and sugar beet (SB) pectin) *in vitro.*

3.1.2 Introduction to Texture Analysis

Unlike rheology, which is often used to analyze viscosity, texture analysis is commonly used to measure the hardness and firmness of foods and is frequently used to study various meat products (Bao & Ertbjerg, 2015; Cavitt et al., 2004). In the context of this thesis, analyzing the force required to shear through *A. fistulosum* sheaths was critical to understanding how calcium application and cold acclimation influenced the shear strength of the samples. An increase in the force required to shear *A. fistulosum* sheaths translates to increased toughness in the sheaths. Toughness is a mechanical property that describes the ability for a material to resist fracture, furthermore the toughness of a material is influenced by both its strength and ductility (Polymer Solutions News Team, 2015; Ritchie, 2011). The analysis of shear force allowed for results obtained from the rheological analysis of pure pectin to be put into the context of a biological system as changes in the force required to shear *A. fisutlosum* may be partially attributable to structural changes in pectin. The basis for this experiment is founded in an abundance of literature outlining the structural influence of calcium and cold acclimation, by way of increasing PME, on the cell wall and the ability for these factors to increase cell wall rigidity (Thor, 2019; Wormit & Usadel, 2018; Alberts, 2002). Therefore, the use of a texture analyzer allowed for further understanding into the physical influence of calcium application and cold acclimation on a biological system. Precisely, the influence of these factors on the toughness of *A. fistulosum* sheaths. The experiment below addresses the hypothesis: Calcium application and cold acclimation will increase the force required to shear through *Allium fistulosum*, while a combined application will result in shear force increasing in an additive manner. The objective of the following experiment was to investigate how the application of calcium, in addition to cold acclimation, influences the force required to shear through *Allium fistulosum.*

3.2 Materials and Methods

3.2.1 Rheology

3.2.1.1 Pectin Powders and Pectin Solutions

Pectin samples were prepared using two different pectin powders prepared by TIC Gums (White Marsh, Maryland, United States) and CP Kelco (Atlanta, Georgia, United States); TIC Pretested Pectin HM (69-75% methylation) (Hutton, B. pers.comm. 2019) slow set (standardized with

dextrose) and GENU BETA pectin (55% methylation) (Meyers, D. pers.comm. 2019) (standardized with EU non-GM beet sucrose). The HM pectin is derived from citrus pectin which has a high HG content and a lower RG content, similar to the pectin found within the cell wall of *Allium* spp. (Yapo et al., 20007; Mankarios et al., 1980). While the GENU BETA pectin is produced using sugar beet pulp which contains more RG-II (~5% compared to 0.6%), and more closely resembles the pectin found within the cell wall of *Arabidopsis thaliana* (Ishii & Matsunaga, 1996; O'Neill et al., 1996; Zhemerichkin & Ptitchkina, 1995).

Initial attempts were also made to use a third type of pectin, TIC Pretested Pectin LM (30-32% methylation) Powder (standardized with dextrose), however the addition of calcium to this pectin resulted in a non-homogenous solution (Figure 4.1). In order to try and circumvent this issue solutions were prepared in which both the LM pectin and the HM pectin were combined to try and create a pectin solution with an intermediate methylation level, however the aforementioned problem persisted. Therefore, LM pectin was not included in the analysis.

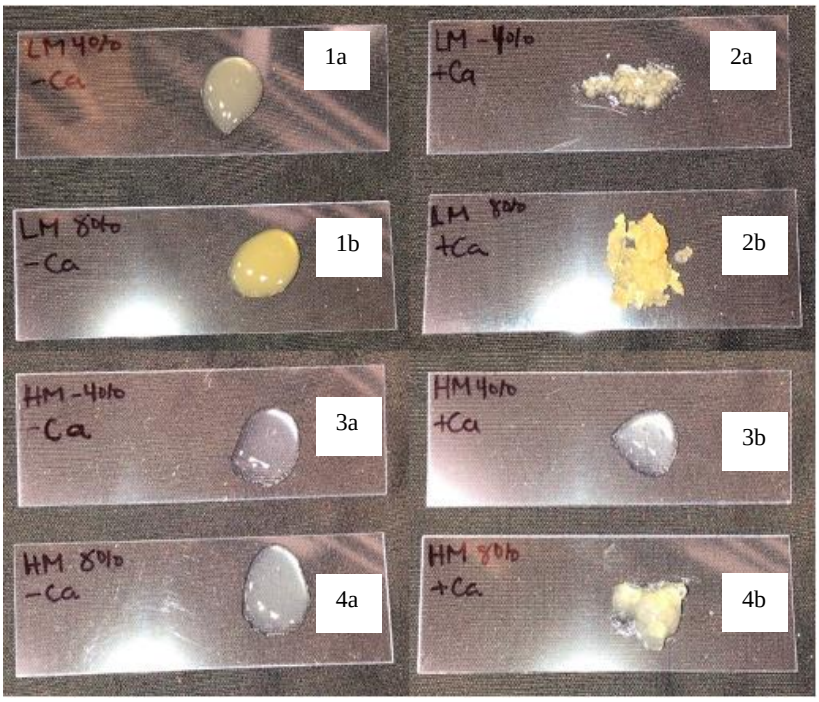

Figure 3.1 Pectin solutions used for rheology experiment

1a and 1b) Homogenous solutions (4% and 8%) of low methylated pectin without $CaCl_2$. (2a and 2b) Non-homogenous solutions (4% and 8%) of low methylated pectin with 0.05M of $CaCl_2$. (3a and 3b) Homogenous solutions (4% and 8%) of high methylated pectin without $CaCl_2$. (4a and 4b) Homogenous solutions (4% and 8%) of high methylated pectin with 0.05M of $CaCl_2$. Slides 2a and 2b show that when $CaCl_2$ is added to low methylated pectin, a non-homogenous mixture is formed.

Two concentrations of each pectin solution were examined: 4% and 8%. Through extrapolation, these concentrations were selected to gain an understanding of how pectin might behave at a 35% concentration, the average pectin concentration within the cell wall (Ridley et al., 2001; O'Neill et al., 1990). The initial experimental design had also included a 16% concentration, however at this concentration, the majority of the solutions became solid and therefore were not appropriate for use with the rheometer. At each concentration, both pectin powders were prepared with either calcium (0.05M $CaCl_2$) (Fisher Scientific, Waltham, MA, USA), boron (0.05M H_3BO_3) (Fisher Scientific, Waltham, MA, USA) or no additional additive. Table A1 outlines the 12 treatment combinations utilized in this analysis.

3.2.1.2 Rheology

Changes in pectin viscosity were measured using the AR G2 rheometer (TA Instruments, New Castle, Delaware, United States) with the 40mm smooth acrylic geometry (Figure A1). The rheometer functions by lowering the geometry to a 1000µm gap between the geometry and the plate. From there, torque is applied to the geometry as the sample in the middle of the geometry and the plate is put under stress. Viscosity measurements were then taken at three different temperatures; 20°C, 12°C and 4°C. Prior to taking measurements of viscosity at 20°C, the sample was first conditioned to 20°C with a soak time of $120.0s^{-1}$ and a duration of $60.0s^{-1}$. The sample was then held at 20°C for $300.0s^{-1}$ with a shear rate of $0.11s^{-1}$. The temperature was then ramped down to 12°C at a rate of 5.0°C/min. The sampling rate, in which measurements of viscosity were taken during the temperature rate, was $10s^{-1}$/pt. The shear rate was kept at constant at $0.11s^{-1}$ during the temperature ramp. Measurements of viscosity were then taken for $300.0s^{-1}$ with a shear rate of $0.11s^{-1}$. Finally, the temperature was ramped down to 4°C and measurements of viscosity were taken as previously described above. The experiment was repeated three independent times with four replicates of each treatment group per trial (n=12).

3.2.1.3 Statistical Analysis

Generalized additive models (GAMs) were used to analyze data. Viscosity was the response variable for the GAMs while temperature was the continuous explanatory variable and the addition of calcium, boron, pectin type and concentration were fixed explanatory variables. Initially, models were fit based on each fixed explanatory variable separately prior to fitting models looking at all of the fixed explanatory variables together as "treatment combinations". GAMs were generated using the gam function from the "mgcv" package (Wood, 2021). The Akaike information criterion (AIC) score was used when building models to select for the most optimum model. The data was log-transformed in order to improve the distribution of the data. Function gam.check was used for model checking. The statistical significance of the GAMs was analyzed using analysis of variance (ANOVA), function, with the argument "test" being set equal to "F", thereby running f-tests as opposed to t-tests. Figures of each GAM were individually created for each of the pectin solutions using function "plot.gam()", in addition to packages "mgcViz" and "rgl" (Adler & Murdoch, 2021; Fasiolo et al., 2020). Package, "devtools" was used

to download the colour palette, "inauguration_2021", which was used for the colours of each figure (Wickham et al., 2020).

ANOVA's were also utilized to analyze changes in viscosity amongst the pectin solutions within each of the main three temperatures of focus, 20ºC (included data points from 20ºC -19ºC), 12ºC (included data points from 12ºC -11ºC) and 4ºC (included data points from 4ºC -3ºC). The RStudio statistical software (Version 1.2.5033) was used to complete all of the above statistical methods.

3.2.2 Texture Analysis

3.2.2.1 Allium fistulosum

Allium fistulosum (*A. fistulosum*) seeds that had been previously collected from plants in 2014 which were growing outdoors in Saskatoon, SK (52°7'N) were germinated in the Agriculture Greenhouses at the University of Saskatchewan (45 Innovation Blvd, Saskatoon, Saskatchewan) and then repotted into 6" pots containing Sunshine No.4 (Sun Gro Horticulture Canada Ltd. Seba Beach, AB, Canada). Sunshine No. 4 is a soilless mix containing 60-70% peat moss, perlite, and limestone. This media was used for both germination and continuous growth of the plants. The plants were grown in the greenhouse at approximately 25°C /22°C (day/night) under natural light supplemented with high pressure sodium lights (17hr photoperiod, average 600 µmol $m^{-2}s^{-1}$). Watering (City of Saskatoon water) was conducted every second day during the spring/summer months and every third day during the fall/winter months. An all-purpose 20/20/20 (NPK) fertilizer with micronutrients (boron [0.02%], copper [0.05%], iron [0.1%], magnesium 0.05%], molybdenum [0.0005%] and zinc [0.05%]) was applied to the plants. The fertilizer also contains 1% EDTA as a chelating agent. Fertilizer was applied weekly during the spring/summer months and twice weekly during the fall/winter months. The bench was organized using a randomized complete block design.

3.2.2.2 Calcium Application

For plants selected to receive calcium, $CaCl_2$ (Fisher Scientific, Waltham, MA, USA) was soil drenched every second day. Irrigation or application of fertilizer was applied prior to the application of $CaCl_2$ if both occurred on the same day. Plants were treated with 100mL of a 0.05M calcium solution every second day for four weeks.

*Note: Water samples were collected from the water sources used to irrigate the plants (Agriculture Greenhouses and Agriculture and Bioresources building). ICP-MS was done on these samples to determine the concentration of calcium within the water, as additional calcium may have been added to the plants via. the water source (Table A2). ICP-MS was kindly performed by Barry Goetz from Dr. Albert Vandenberg's lab (Dept. Plant Sciences, University of Saskatchewan). See Section 4.2.4.2 for further details.

3.2.2.3 Cold Acclimation

Cold acclimation treatment was performed for a two-week period using the Conviron growth chambers at the University of Saskatchewan, College of Agriculture and Bioresources phytotron facilities. Two different cold acclimation treatments were examined: 1) 12°C/4°C (day/night) with an 8hr photoperiod (ACC12-4) and a light intensity of 80+/-10 μmol m^{-2} s^{-1}, and 2) 4°C /4°C (day/night) with a 12hr photoperiod and a light intensity of 250+/- 10 μmol m^{-2} s^{-1} (ACC4-4). For plants receiving both calcium and cold acclimation, calcium application occurred over a two-week period in the greenhouse, followed by the remainder of the calcium application occurring concurrently with cold acclimation in the Conviron chamber (Winnipeg, Manitoba, Canada).

In total there were 6 treatment groups: 1) NACC/ NCA (non-acclimated/ non-calcium treated), 2) ACC12-4/ CA (cold acclimated 12°C /4°C / calcium treated), 3) NA/ CA (non-acclimated/ calcium treated), 4) ACC12-4/ NCA (cold acclimated12°C /4°C / non-calcium treated), 5) ACC4-4/ CA (cold acclimated 4°C /4°C / calcium treated) and 6) ACC4-4/ NCA (cold acclimated 4°C /4°C /non-calcium treated).

3.2.2.4 Texture Analysis

The Allo-Kramer shear force required to shear through *A. fistulosum* sheaths with the ligule and intact epidermal cell layer was measured using the TMS-Pro Texture Press (Food Technology Corp., Sterling, Virginia, USA) (Figure A2 and Figure A3). For consistency, A. *fistulosum* sheaths were taken from the youngest *A. fistulosum* leaf with the most developed sheath. Once this leaf was selected, a 4cm cutting of the sheath was sampled, beginning at the bottom of the sheath where

it had been cut from the soil. Three 4cm sheaths were used per measurement and were laid perpendicularly across the slots in the texture analyzer cell (Figure A2).

A 10-blade Allo-Kramer shearing compression cell was used to shear the onion sheaths (Figure A3). The full-scale load was 1000N, while the crosshead speed was 500mm min^{-1}. The shear force (in Newtons) required to shear 1g of fresh sample was calculated by dividing the peak shear force (in Newtons) by the sample weight (in grams) (Willick, 2018). Shear force was measured in N g^{-1} (Willick, 2018). Shear force was measured in order to gain an understanding of how calcium application and/or cold acclimation impact the toughness of *A. fistulosum* sheaths. These results are intended to complement the results obtained from the rheological analysis of pectin solutions. The experiment was repeated three independent times, with four replicates per trial (n=12).

3.2.2.5 Statistical Analysis

Results of this 2X2 factorial experiment were analyzed using an ANOVA, $p<0.05$ was deemed significant. A Tukey test was done as a method of post-hoc analysis for the relationship between shear force and cold acclimation; calcium application was excluded from this analysis as there are less than three treatment levels within the calcium application treatment. Model checking was done through the inspection of residuals. "ggplot" and "ggplot2" were used for the construction of select figures (Wickham, 2020). The RStudio statistical software (Version 1.2.5033) was used to conduct the aforementioned analysis.

3.3 Results

3.3.1 Rheology

GAMs were initially fit based on each separate fixed explanatory variable (calcium, boron, pectin type and concentration). GAMs were then fit based on the combination of each explanatory variable. While Figure 3.2 and Figure 3.3 outline various patterns with respect to viscosity such as increasing viscosity with decreasing temperature and a general increase in viscosity with the addition of either calcium or boron, not every fixed explanatory variable had a significant ($p<0.05$) effect on viscosity (Table 3.1).

An ANOVA ran on GAMs examining each fixed explanatory variable separately found in general pectin type, concentration and boron had a significant ($p<0.05$) effect on viscosity (Table 3.1). However, the main effect of the calcium treatment was not significant ($p>0.05$) (Table 3.1). Nevertheless, when each of the aforementioned treatments is broken down to each individual level, each level of treatment was found to have a significant ($p<0.05$) effect on the viscosity when the relationship between each treatment and temperature was considered (Table 3.1). In other words, with the addition of calcium, boron, and when the type of pectin and concentration were examined individually with respect to their relationship with temperature, there was a significant ($p<0.05$) difference in viscosity for each individual treatment (Table 3.1). The empirical distribution factor (edf) for the majority of the relationships (excluding s(Temperature): Genu Beta)) was also found to be greater than one, therefore the majority of these relationships were non-linear, and the use of GAMs were justified as a means to analyze the data (Table 3.1).

Table 3.1 ANOVA ran on a generalized additive model examining pectin type, concentration, boron and calcium individually with respect to relationship with temperature and viscosity

Results from an ANOVA run on a GAM examining each treatment (pectin type, concentration, boron and calcium) separately, with respect to their effect on viscosity and relationship to temperature. This GAM is representative of the second lowest AIC value in the below table. $p<0.05$ is significant.

Data Selection	General Effect	Smoothing Effect	EDF	Ref.df	F-value	P-value
Pectin Type	Pectin Type			2	7642	<2e-16
		s(Temperature): Genu Beta	1.00	1.00	4107.841	<2e-16
		s(Temperature): High Methylated	8.547	8.938	1057.392	<2e-16
Calcium	Calcium			1	3.53	0.0603
		s(Temperature): No Calcium	1.973	2.000	4816	<2e-16
		s(Temperature): Yes Calcium	8.384	8.888	355	<2e-16
Boron	Boron			1	254.3	<2e-16
		s(Temperature): No Boron	8.724	8.976	966.3	<2e-16
		s(Temperature): Yes Boron	1.938	1.996	3789.3	<2e-16
Concentration	Concentration			1	265.6	<2e-16
		s(Temperature): Four Percent	1.988	2.001	2421	<2e-16
		s(Temperature): Eight Percent	8.649	8.962	1646	<2e-16

Since this experiment is focused on the role of all four treatments in combination, the more relevant results come from the model that was fit to examine each treatment combination together. This GAM also had the lowest AIC value (Table A3). In total, this model addressed twelve different treatment combinations outlined in Table 3.2. The results of an ANOVA for this GAM found for each of the treatment combinations, there was a significant effect ($p<0.05$) between the treatment combination and temperature in relation to viscosity (Figure 3.4 and Table 3.2). The edf for the majority of the relationships were above one, indicating when all three treatments were analyzed in combination, the relationship was non-linear, and the use of a GAM was justified to analyze the data (Table 3.2). The treatment combination, 8% Genu Beta +Ca/-B was the only exception to this

statement, as it had an edf of 1, indicating that the relationship between temperature and viscosity for this treatment combination was linear (Table 3.2).

In addition to analyzing viscosity over the entire temperature ramp, viscosity was also analyzed within each of the 3 main temperatures of interest, 20ºC, 12ºC and 4ºC using ANOVA's. While there was a significant difference ($p<0.05$) in viscosity when the various pectin solutions were compared, within each individual pectin solution there was no significant ($p>0.05$) change in viscosity during the temperature point of interest (Table A4-A6).

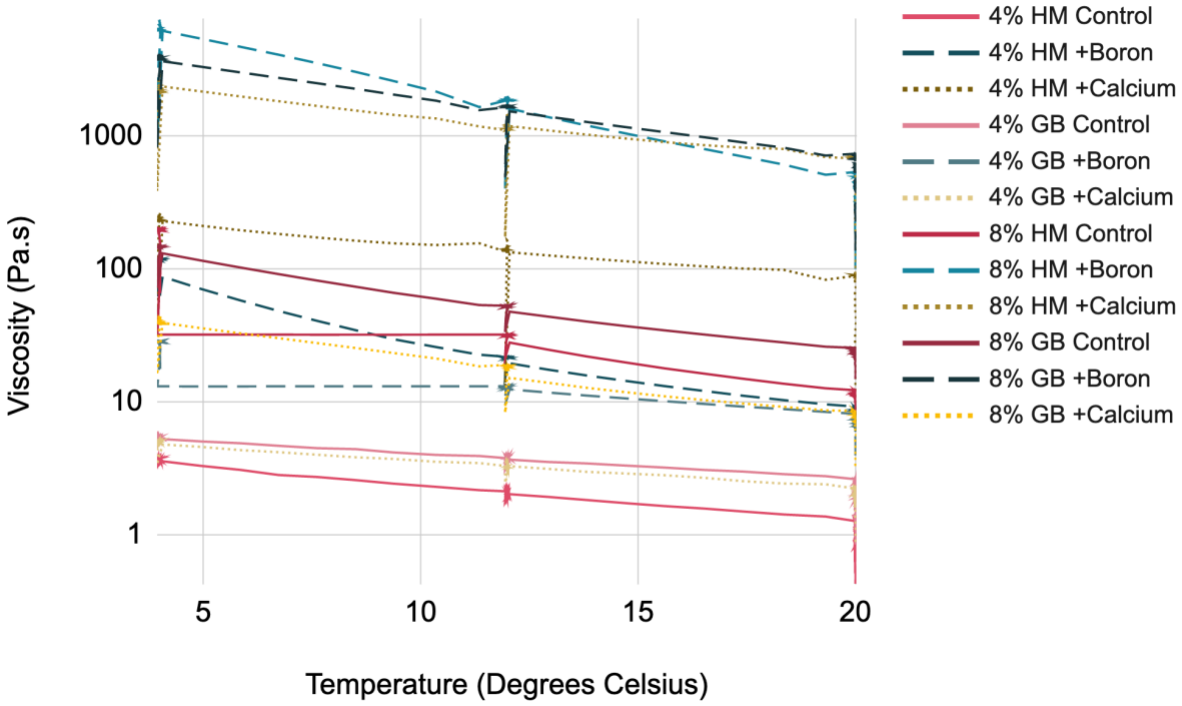

Figure 3.2 Effect of calcium, boron, pectin type and temperature on viscosity- Log scale

Log scale change in viscosity with decreasing temperature across two concentrations of pectin (4% or 8%), two types of pectin (high methylated citrus pectin or Genu Beta (sugar beet) pectin), with the addition of either calcium (0.05M $CaCl_2$), boron (0.05M H_3BO_3) or no additional element.

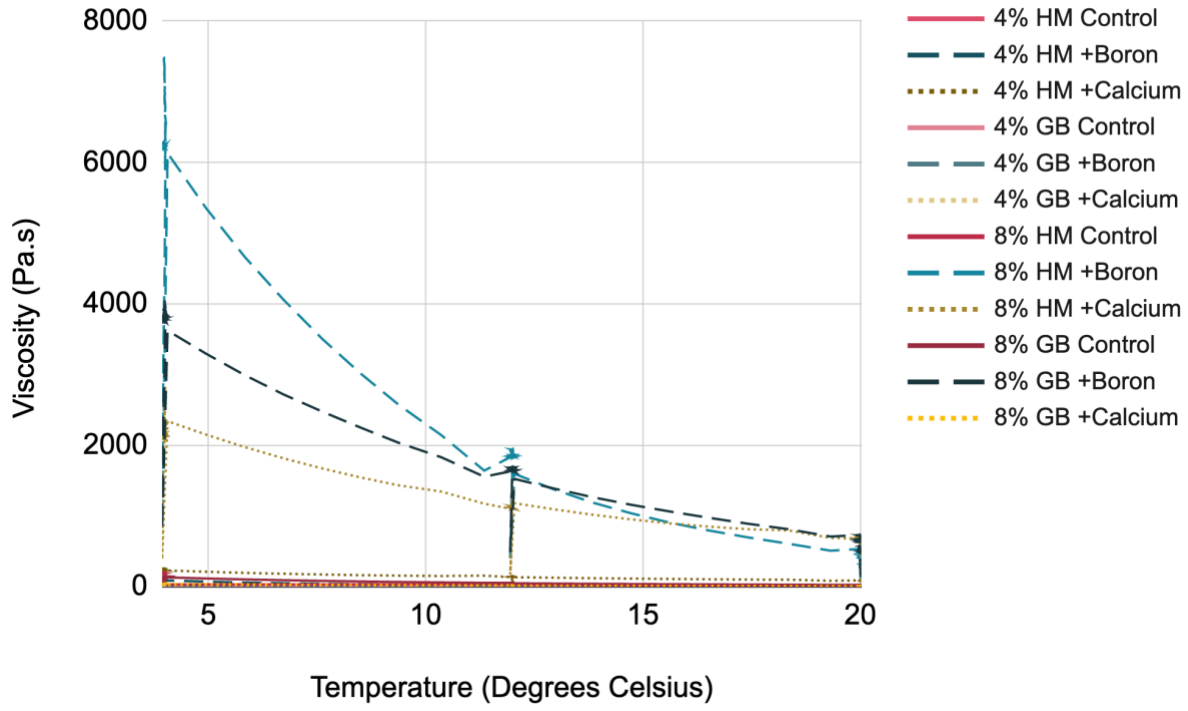

Figure 3.3 Effect of calcium, boron, pectin type and temperature on viscosity

Change in viscosity with decreasing temperature across two concentrations of pectin (4% or 8%), two types of pectin (high methylated citrus pectin or Genu Beta (sugar beet) pectin), with the addition of either calcium (0.05M $CaCl_2$), boron (0.05M H_3BO_3) or no additional element.

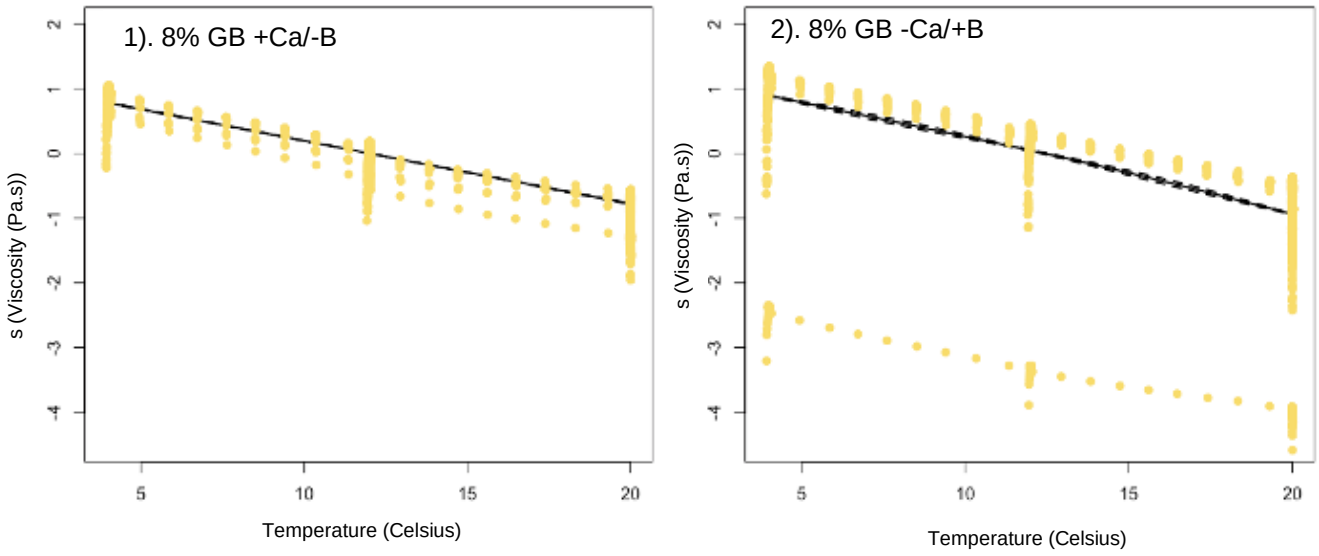

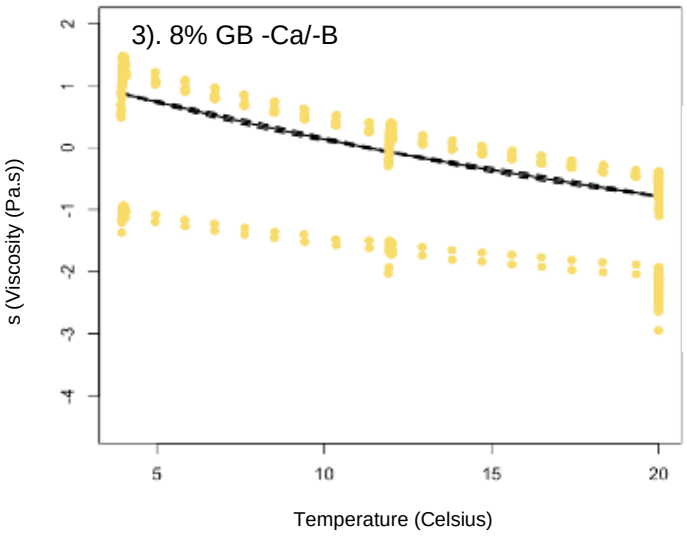
3). 8% GB -Ca/-B
s (Viscosity (Pa.s))
Temperature (Celsius)

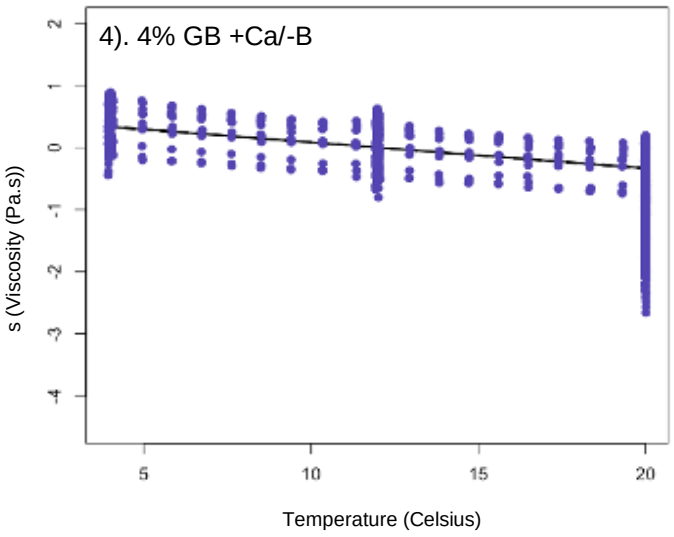
4). 4% GB +Ca/-B
s (Viscosity (Pa.s))
Temperature (Celsius)

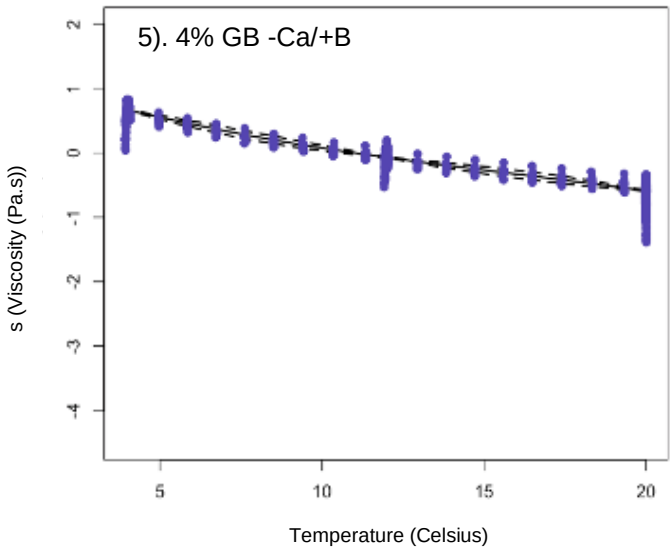
5). 4% GB -Ca/+B
s (Viscosity (Pa.s))
Temperature (Celsius)

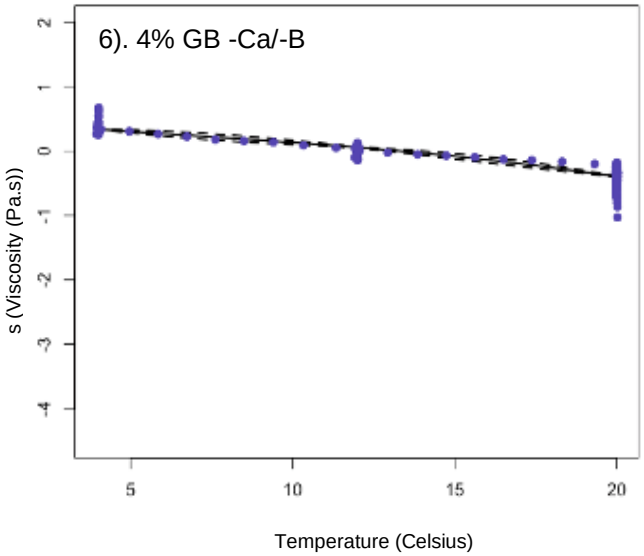
6). 4% GB -Ca/-B
s (Viscosity (Pa.s))
Temperature (Celsius)

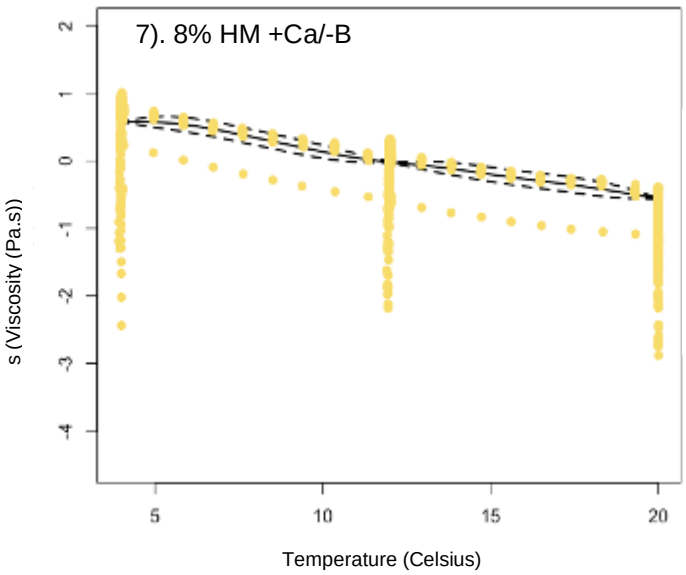
7). 8% HM +Ca/-B
s (Viscosity (Pa.s))
Temperature (Celsius)

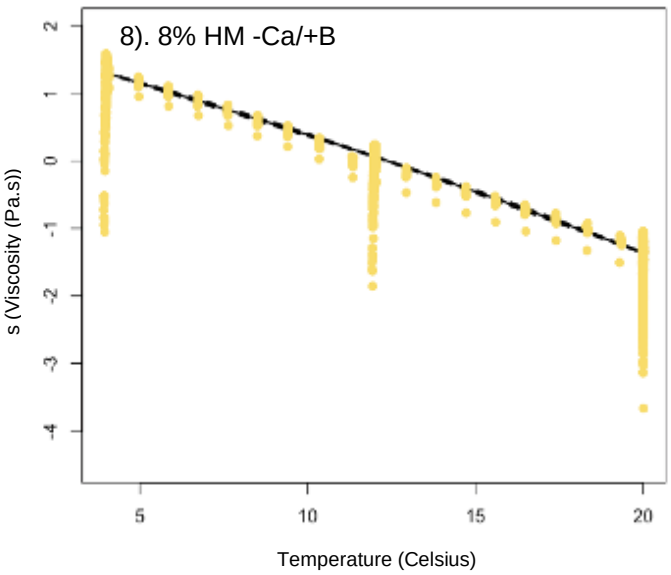
8). 8% HM -Ca/+B
s (Viscosity (Pa.s))
Temperature (Celsius)

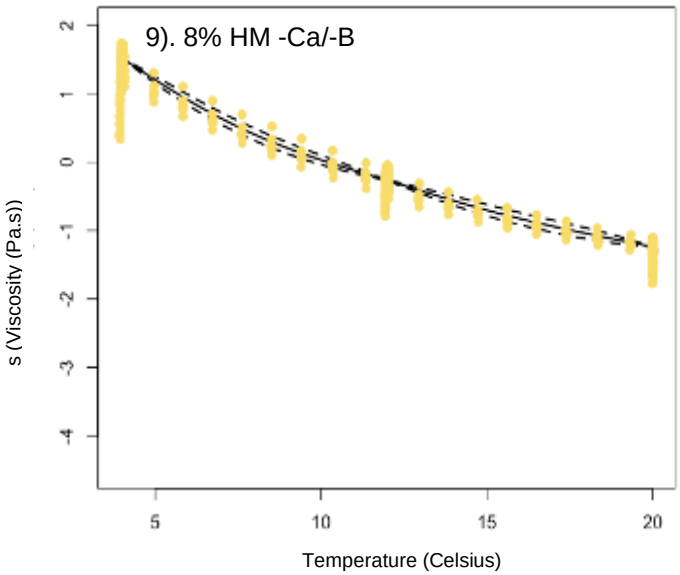
9). 8% HM -Ca/-B
s (Viscosity (Pa.s))
Temperature (Celsius)

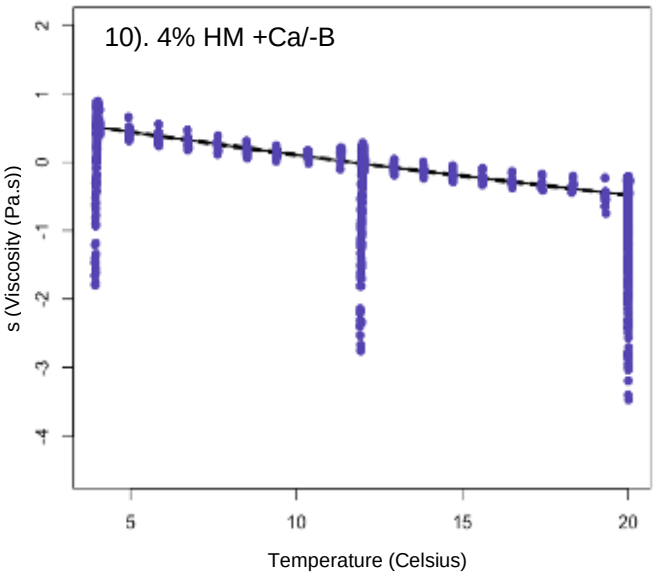
10). 4% HM +Ca/-B
s (Viscosity (Pa.s))
Temperature (Celsius)

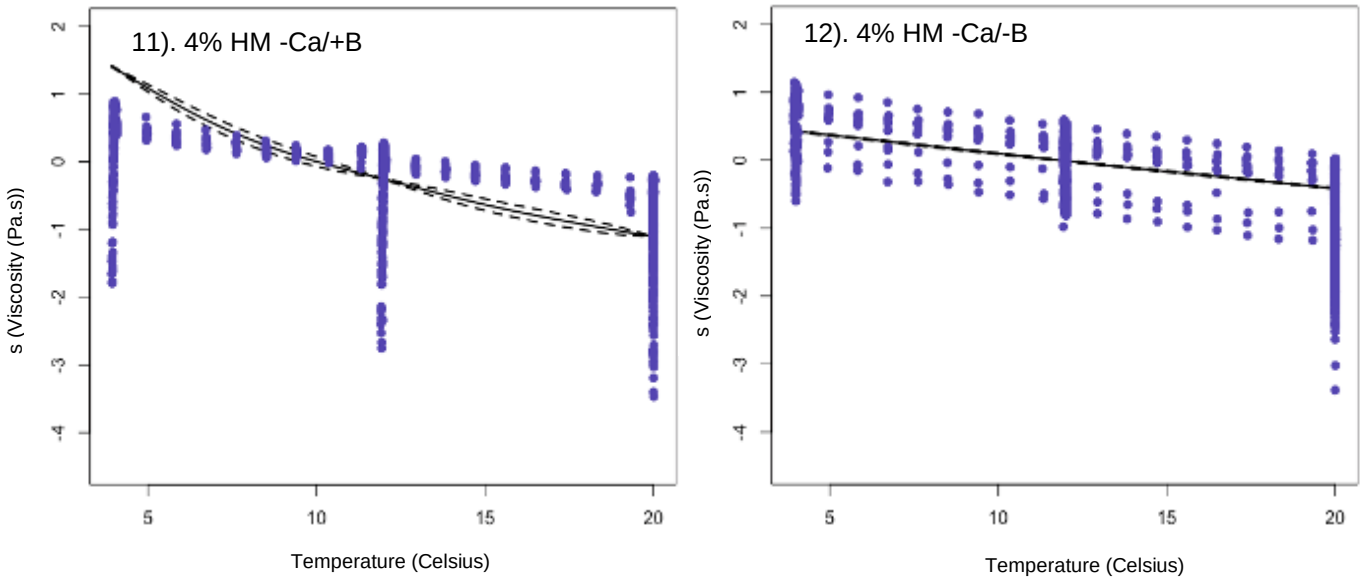

Figure 3.4 Generalized additive models showing relationship between temperature and viscosity of pectin solutions

Relationship between increasing temperature (ºC) and viscosity (Pa.s) for each of the 12 pectin solutions analyzed using a rheometer: 1) 8% GENU BETA +Calcium/-Boron, 2) 8% GENU BETA -Calcium/+Boron, 3) 8% GENUA BETA -Calcium/-Boron, 4) 4% GENU BETA +Calcium/-Boron, 5) 4% GENU BETA -Calcium/+Boron, 6) 4% GENU BETA -Calcium/-Boron, 7) 8% High methylated citrus +Calcium/-Boron, 8) 8% High methylated citrus -Calcium/+Boron, 9) 8% High methylated citrus -Calcium/-Boron, 10) 4% High methylated citrus +Calcium/-Boron, 11) 4% High methylated citrus -Calcium/+Boron, and 12) 4% High methylated citrus -Calcium/-Boron. Dark solid lines indicate the mean value for the response variable. Dotted lines indicate 95% confidence intervals around the predicted values. Individual dots are representative of single data points. Data points shown represent an average across all 12 replicates (n=12). Yellow dots were used to represent 8% pectin solutions, purple dots represent 4% pectin solutions. Values on the y-axis have been smoothed, as indicated by the "s" on the label. Statistical analysis found significant differences between all pectin solutions and viscosity ($p<0.05$). See Tables 3.2 and A4 for statistical analysis.

Table 3.2 ANOVA ran on a generalized additive model (GAM) examining pectin type, concentration, boron and calcium in combination with respect to relationship with temperature and viscosity

Results from an ANOVA run on a GAM in which all 4 treatment options (pectin type, concentration, boron [B] and calcium [Ca]) were looked at in combination with respect to their relationship with temperature and effect on pectin viscosity. Two types of pectin were analyzed, Genu Beta and High Methylated. This GAM is representative of the lowest AIC value in the above table. $p<0.05$ is significant**.**

Data Selection	**Smoothing Effect**	**EDF**	**Ref.df**	**F-value**	**P-value**
Combined Treatment Groups	s(Temperature):8% GenuBeta -Ca / -B	1.996	2.004	14329	<2e-16
	s(Temperature):8% GenuBeta +Ca / -B	1.00	1.000	28084	<2e-16
	s(Temperature):8% GenuBeta -Ca / +B	2.722	2.923	13613	<2e-16
	s(Temperature):8% HighMethylated -Ca / -B	2.858	2.981	31769	<2e-16
	s(Temperature):8% HighMethylated +Ca / -B	8.925	8.998	1449	<2e-16
	s(Temperature):8% HighMethylated -Ca / +B	1.993	2.003	40911	<2e-16
	s(Temperature):4% GenuBeta -Ca / -B	2.825	2.970	2215	<2e-16
	s(Temperature):4% GenuBeta +Ca / -B	1.062	1.121	4401	<2e-16
	s(Temperature):4% GenuBeta -Ca / +B	2.645	2.874	5594	<2e-16
	s(Temperature):4% HighMethylated -Ca / -B	1.721	1.922	3543	<2e-16
	s(Temperature):4% HighMethylated +Ca / -B	1.959	1.999	6077	<2e-16
	s(Temperature):4% HighMethylated -Ca / +B	2.880	2.987	24108	<2e-16

3.3.2 Texture Analysis

Both cold acclimation and calcium application alone and in combination significantly ($p<0.05$) increased the force required to shear through the *A. fistulosum* sheaths (Figure 3.5 and Table A7). The effect sizes for comparisons made between each of the treatment groups were also all above 0.8, with the exception of CA/NACC & CA/ACC12-4 which had an effect size of 0.2 (Table A8). Generally, an effect size above 0.8 is an acceptable indicator that the statistical difference observed

is meaningful (Lakens, 2013; Cohen, 1988). On the other hand, values below that mean that while the relationship may be statistically significant the difference is negligible (Lakens, 2013; Cohen, 1988). However, within this general trend, there was variation of the force required to shear through the *A. fistulosum* sheaths for each treatment (Figure 3.5).

While CA/ ACC12-4 and NCA/ ACC12-4 significantly ($p<0.05$) increased shear force in comparison to NCA/ NACC, only CA/ ACC4-4 did significantly ($p>0.05$) increased shear force in comparison to NCA/ NACC (Figure 3.6 and Table A9). Cold acclimation at 4°C /4°C without calcium application (NCA/ ACC4-4) did not significantly increase shear force compared to NCA/ ACC (Figure 3.6 and Table A9). Furthermore, while the addition of calcium in general increased the shear force, the effect does not appear to be additive with cold acclimation as there was a decrease in shear force for plants treated with calcium and cold acclimated at 12ºC /4°C (Figure 3.5).

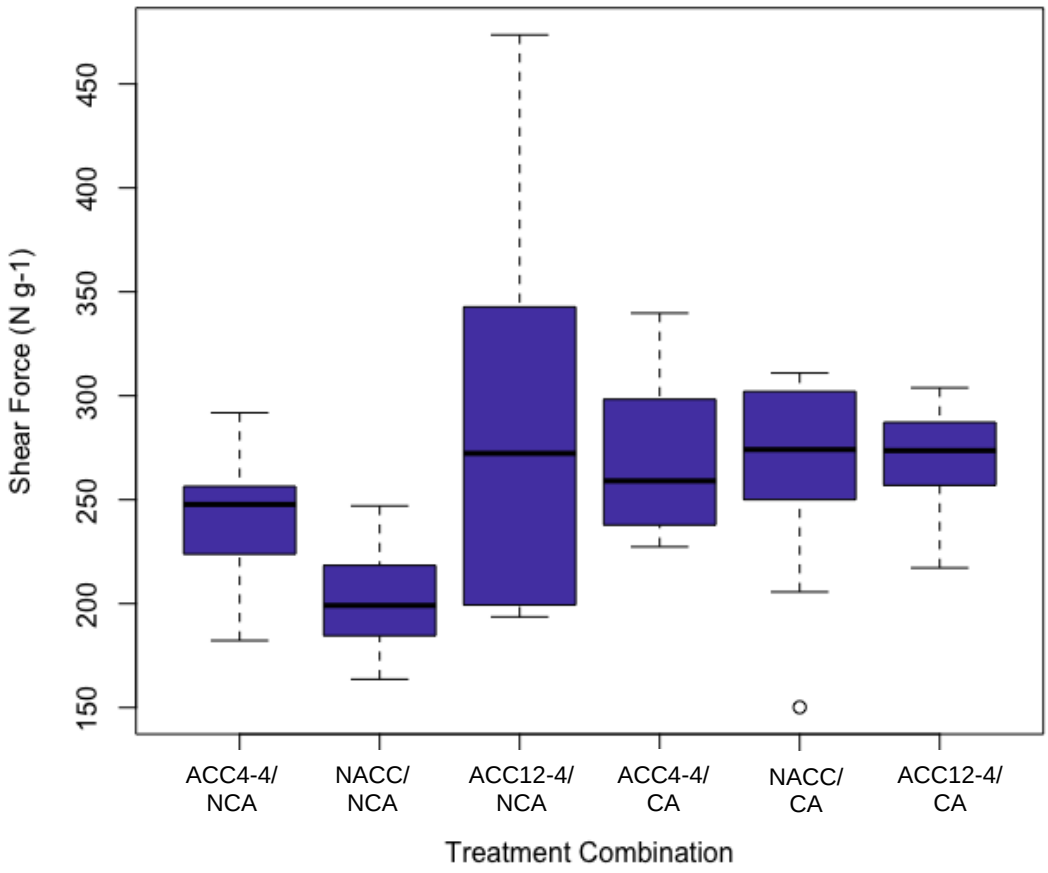

Figure 3.5 Effect of calcium application and cold acclimation on force required to shear *Allium fistulosum*

The effect of both calcium application and cold acclimation on the force required to shear *Allium fistulosum* sheaths. Six treatment groups were analyzed: 1) ACC4-4/ NCA (4°C /4°C cold acclimation, -$CaCl_2$); 2) NACC/ NCA (no cold acclimation, - $CaCl_2$); 3) ACC12-4/ NCA (12°C /4°C cold acclimation, -$CaCl_2$); 4) ACC4-4/ CA (4°C /4°C cold acclimation, + $CaCl_2$); 5) NACC/ CA (no cold acclimation, + $CaCl_2$); 6) ACC12-4/ CA (12°C /4°C cold acclimation, +$CaCl_2$). Plants acclimated at 4°C /4°C were under a 12hr photoperiod, while plants acclimated at 12°C /4°C were under an 8hr photoperiod. Cold acclimation was performed for 2 weeks. Plants treated with calcium received 0.05M of $CaCl_2$ every second day for 4 weeks. See Table 7 for statistical analysis.

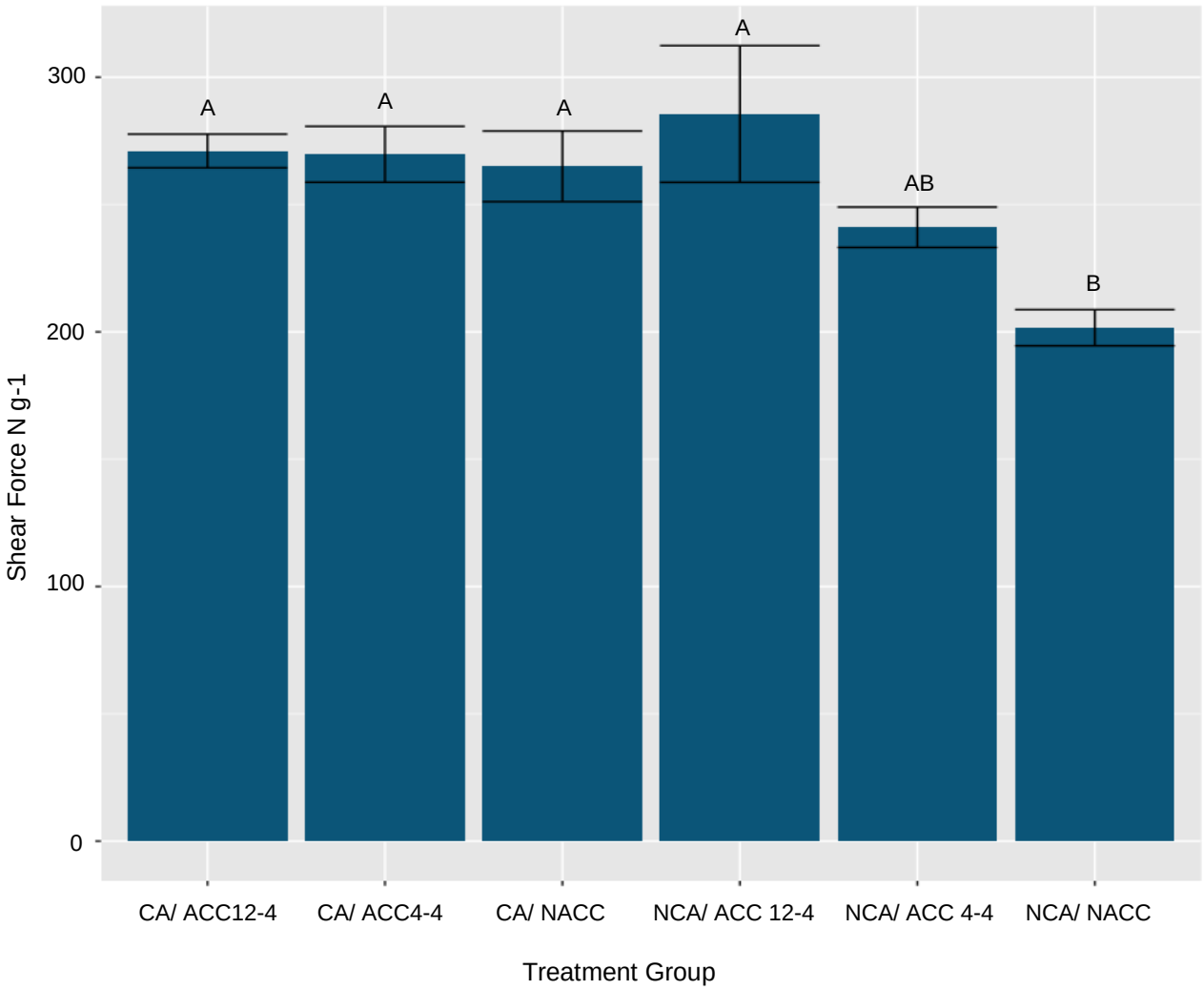

Figure 3.6 Effect of calcium application and cold acclimation on force required to shear *Allium fistulosum*- Figure for Tukey test

Force required to shear *Allium fistulosum* sheaths from various cold acclimation treatments, 1) ACC4-4 (cold acclimation at 4°C /4°C), 2) NACC (no cold acclimation), 3) ACC12-4 (cold acclimation at 12°C /4°C). Plants acclimated at 4°C /4°C were under a 12hr photoperiod, while plants acclimated at 12°C /4°C were under an 8hr photoperiod. Cold acclimation was performed for 2 weeks. Error bars represent standard error. See Table A9 for statistical analysis.

3.4 Discussion

3.4.1 Rheology

Generally, type of pectin, the addition of calcium/or boron, increasing pectin concentrations as well as decreasing temperature were all found to increase the viscosity of pectin. The addition of calcium resulted in one of the three most viscous solutions. The 8% citrus pectin with the addition of 0.05M of $CaCl_2$ resulted in a pectin solution which at its highest point, had a viscosity of just

above 2000 Pa.s. This finding is supportive of predictions made not only in this thesis but also of trends in data from the existing body of literature that investigated how the addition of calcium to HG pectin results in the formation of "egg-box" structures (Wormit & Usadel, 2018). However, while this finding does suggest that "egg-box" structures may be forming in this pectin solution, it is of interest to restate that the citrus pectin utilized in this experiment had a high level of methylation. This is an important factor to consider because "egg-box" structures are only known to form once HG is demethylesterified by PME in a block-wise manner (Wormit & Usadel, 2018; Braccini & Pé Rez, 2001). Nevertheless, as the citrus pectin utilized in this study had a degree of methylation between 69-75% (Hutton, B. pers.comm. 2019), it is likely that a proportion of the demethylesterfied HG was demethylesterfiied in a block-wise manner, thus allowing for the possible formation of "egg-box" structures.

Unexpectedly, the most viscous solution was 8% HM citrus pectin with boron. This finding is unusual because citrus pectin is primarily composed of HG and only RG-II has the ability to form cross-links with boron. In this thesis research, it appears the HM citrus pectin also contains RG-II, however, the manufacturer was unable to provide a breakdown of the pectin composition and conducting this analysis was outside of the scope of this project. Previous research however has suggested that citrus pectins are primarily composed of HG, and therefore this is likely comparable to that of the HM citrus pectin utilized here (Yapo et al., 2007). In contrast, the proposition that the high viscosity of the GENU Beta pectin with boron is likely a result of RG-II dimer formation was expected. GENU Beta pectin is made of sugar beet pectin, where rhamnose, a key component of RG-II consists of approximately 5% of the monosaccharides that comprise the pectin found in sugar beets (Zhemerichkin & Ptitchkina, 1995). Moreover, the pectin composition of dicots including sugar beets is made up of ~4% RG-II (Mohnen, 1999). The proposition that RG-II dimer formation is occurring in the 8% GB pectin with boron is supported by the finding from O'Neill et al. (1996) who observed borate cross-linking can occur with only RG-II and boric acid if the required divalent cations are present.

In addition to studying the effect of calcium and boron on pectin viscosity, the effect of decreasing temperature was also examined in this thesis. Specifically, 12ºC and 4ºC, were selected to mimic day/night temperatures of a cold acclimation regimen previously used by the Tanino lab to cold

acclimate *A. fistulosum* (Liu, 2015). While there is a body of evidence examining the role of increasing temperature (20-60ºC) on viscosity such as Muhidinov et al. (2010) who found orange and sunflower pectin viscosities decreased linearly with increasing temperature, there appears to be a lack of research analyzing pectin viscosity at low temperatures (below 20ºC). Therefore, while the effect of temperature has been analyzed on pectin viscosity, the low temperature benchmark of 20ºC for these studies puts them outside the temperature range analyzed in this experiment.

However, while there do not appear to be any studies examining pectin viscosity at low temperatures, the findings from this thesis support findings of Muhidinov et al. (2010) who found viscosity decreased with increasing temperature from 20ºC to 60ºC. Further, the results of this thesis showed at 4ºC, the three most viscous solutions had viscosities of approximately 6000 Pa.s, 3800 Pa.s and 2200 Pa.s. However as the temperature increased, viscosity decreased with the same three solutions having viscosities around 2200 Pa.s, 2000 Pa.s and 1600 Pa.s at 12ºC. Viscosity continued to decrease as temperature increased even further to 20ºC, with the same three most viscous solutions all having a viscosity around 500-700 Pa.s. While the viscosities in our experiments exceed those reported by Zhang et al. (2020) who found at 25ºC and a shear rate of $100s^{-1}$, the viscosity of citrus pectin was around 120 mPa.s (0.12 Pa.s), they are in the same order of magnitude.

On average, pectin makes up between 30-50% of primary cell walls (Cosgrove & Jarvis, 2012). However, due to limitations with the rheometer, only 4% and 8% pectin solutions were utilized in this experiment. Therefore, while it was observed that an increase in concentration did result in increased viscosity, it would be incorrect to assume that based on extrapolations from this data alone, pectin would continue to follow the same trends observed within this experiment when present at a higher concentration. However, anecdotal evidence from preliminary experiments where 35% pectin concentration solutions were made did show that at this concentration, pectin viscosity did substantially increase (data not shown). Furthermore, results from the texture analysis do provide further support for the prediction that pectin would behave in a similar manner at a concentration more similar to what is observed in the cell wall.

However, caution still should be taken when interpretating these *in vitro* results and extrapolating to biological systems. Nonetheless, biological implications in relation to pectin viscosity and shear force will be discussed in Section 3.5.

3.4.2 Texture Analysis

As hypothesized, the findings demonstrated that both calcium application and cold acclimation resulted in an increase to the force required to shear through *A. fistulosum* sheaths. This increase in shear force is indicative that both calcium application and cold acclimation increased the toughness of the sheath, and likely in turn the cell wall, possibly in part due to structural modifications in pectin. However, the original hypothesis had also stated calcium application and cold acclimation when paired together would be additive in nature; this was not necessarily the case.

While the application of calcium to ACC4-4 plants increased the force required to shear through the sheaths (+28.65 N g^{-1}), the application of calcium to ACC12-4 plants decreased the shear force (-14.51 N g^{-1}). This finding is of interest because Liu (2015) had previously demonstrated that following two weeks of cold acclimation at 12ºC/4ºC, PME activity in the *A. fistulosum* epidermal cell layer was enhanced (Liu, 2015). While an increase in PME activity following 12ºC/4ºC cold acclimation would have hypothetically decreased the level of methylation in HG allowing for the formation of "egg-box" structures and thus increased rigidity, the results from this experiment show the opposite. Potentially, PMEI's may be feeding back on PME's to alter methylation or in the case that demethylation is occurring, it may not be in a block-wise manner and therefore "egg-boxes" are unable to form (Wormit & Usadel, 2018).

Both cold acclimation and calcium application alone increased shear force as previously hypothesized. Beginning first with cold acclimation, treatments at both 12ºC/4ºC and 4ºC/4ºC increased the force required to shear through *A. fistulosum* sheaths. In addition to Liu (2015), PME activity has also been found to be enhanced by cold acclimation in both winter oil-seed rape and *A. thaliana* (Liu, 2015; Solecka et al., 2008; Lee & Lee, 2003). As PME is responsible for reducing the degree of pectin methyl esterification through demethylation, PME also affects cell wall rigidity since the more demethylation, the more sites to which calcium can form cross-bridges

resulting in the egg-box structure. Therefore, it is likely that the increase in shear force, translating to increased toughness in the sheath, observed in ACC12-4 and ACC4-4 plants is due to increased cell wall rigidity as a result from enhanced PME activity.

While the composition of pectin in the *A. fistulosum* epidermal cell wall was not analyzed in this thesis, Mankarios et al. (1980) has previously found pectin with the cell walls of *A. cepa* contain 93.7% uronic acid, indicating pectin within these cell walls is primarily composed of HG. Therefore, the pectin composition of epidermal cell walls of the *A. fistulosum* is likely primarily dominated by HG. As the pectin composition with *A. fistulosum* epidermal cell walls is likely primarily composed of HG, the increase in shear force observed as a result of calcium application is presumably the result of the formation of "egg-box" structures. Analysis of shear force found calcium application increased the force required to shear through the *A. fistulosum* sheaths by 63.385 N g^{-1}.

The results of both the texture and viscosity experiments suggest pectin within the cell wall may be behaving in a similar manner as seen in the results from the experiment which analyzed pectin *in vitro*, especially in cases where the cell wall is primarily composed of HG pectin since the composition of citrus pectin is similar to that of pectin within onion cell walls (Yapo et al., 2007). While pectin in dicots, gymnosperms and non-grass monocots is present at approximately 35% concentration in cell walls, limitations with the rheometer prevented the analysis of pectin solutions above an 8% concentration (Ridley et al., 2001; O'Neill et al., 1990). However as discussed in Section 3.3, increasing concentration significantly ($p<0.05$) influenced viscosity, as did the application of calcium when factored in with increasing concentration. Similarly, shear force also increased by 63.385 N g^{-1} as a result of calcium application.

3.5 Biological Implications

While mechanical properties relating to fluid flow such as viscosity and their relationship with other properties such as toughness are complex, the results obtained with this chapter do have the potential to have interesting biological implications. The structure of the cell wall, and in turn pectin, a major structural component of the cell wall, is essential for not only overall plant health, but also the ability for the cell wall to act as a barrier to stress (Houston et al., 2016; Cosgrove &

Jarvis, 2012). With regards to water loss, the focus of the upcoming chapter, cellular water loss can occur through both freezing stress and drought stress. Regardless of the underlying abiotic stress causing the water loss, the cell structure can become damaged beyond repair and plant death can occur. For example, during both drought and freezing stress, loss of turgor pressure can occur as the cell loses water (Arora, 2018; Moore et al., 2008; Burke et al., 1976). As the cell loses water, it may begin to undergo cytorrhysis, and while this process is beneficial to a certain extent as it prevents the plasma membrane from tearing away from the cell wall, cytorrhysis can also occur beyond a tolerable limit and cause cell death (Arora, 2018). Thus, it is critical to avoid going beyond the tolerable limit and the structure of the cell wall has been shown to play a key role in this. Oertli (1986) and Oertli et al. (1990) have found that the ability for the cell wall to resist cytorrhysis depends on the mechanical strength of the cell wall. Based on this understanding, one of the biological implications from our results is that calcium application and cold acclimation may reduce cytorrhysis through their ability to strengthen the cell wall. While not directly tested in this thesis, the findings obtained from the texture analyzer showing an increase in shear force coupled with those showing increased viscosity in pectin, a key component of the cell wall, are indicative that calcium and cold increased cell wall strength.

The implications from increased shear force and increased pectin viscosity also have the potential to stretch beyond abiotic stress and into biotic stress. The cell wall plays a key role in preventing pathogens from infecting the cell by acting as a layer of defense for the plant, therefore pathogens have developed means to penetrate the cell wall (Houston et al., 2016). One example of this is in *C. higginsianum* which has the ability to penetrate the cell wall through physical force alone (Yan et al., 2018). The ability to strengthen the cell wall may in turn reduce the rate of *C. higginsianum* infection as the cell wall is increasingly difficult to penetrate. Therefore, another biological implication of these results is the notion that calcium application and cold acclimation may reduce the rate of *C. higginsianum* and other pathogens that penetrate the cell wall by shear force alone.

3.6 Connection to Next Study

We have determined that calcium application as well as temperature, whether in the formation of cold acclimation or in decreasing temperature, have an influence on the structural properties of both pectin and *A. fistulosum* biomass. In general, the findings from this Chapter are supportive of

the initial hypotheses, with the caveats that together calcium application and cold acclimation did not have an additive effect on the force required to shear *A. fistulosum* and calcium alone did not significantly increase pectin viscosity.

Thus, given the knowledge of these structural changes based on our results and in addition to findings from the literature, the next step was to see how these structural changes may influence resistance to dehydration stress. Therefore, the next step was to determine if the changes in pectin viscosity and shear force reduced the rate of water loss in a range of species. The underlying aim is that if there is a positive link between increased pectin viscosity and shear force and dehydration stress resistance, these principles of altering structural properties of pectin, and in turn the cell wall, could be exploited to create plants with a greater resistance to dehydration and other stresses. Chapter 4 will first explore the rate of water loss in pectin *in vitro* and then moves to examine how the structural changes revealed in Chapter 3 impact dehydration stress resistance in two *Allium* species and a range of *Arabidopsis* genotypes. A range of species in addition to varying time scales of water loss will be utilized in order to gain a more comprehensive picture on how cold acclimation and calcium application can reduce water loss. Percent water loss will also be explored in *Arabidopsis* boron transporter mutants.

4.0 UNDERSTANDING THE INFLUENCE OF CALCIUM AND BORON ON THE RATE OF WATER LOSS FROM PURE PECTIN STANDARDS AND PLANT SPECIES

4.1 Introduction

As a result of climate change, the frequency and severity of drought and in turn dehydration, are predicted to increase. Given this prediction, it is critical to find an effective solution to help mitigate the damaging effects of dehydration stress on plants, which have the potential to threaten food security. Numerous papers have studied the role of calcium in mitigating drought stress across a range of species, however the majority of the research conducted has focused primarily on the role of calcium as a signaling molecule (Thor, 2019; White & Broadley, 2003; Sanders et al., 2002; White, 2000). While the role of calcium as a signaling molecule should not be undervalued, calcium also plays a critical role in the structure of the cell wall (Hepler, 2005; White & Broadley, 2003; Matoh & Kobayashi, 1998).

Previous research conducted in the Tanino lab found calcium application when paired with cold acclimation led to a 44% higher freezing stress survival through blockage of ice propagation across the cell wall in comparison to just cold acclimation alone (Liu, 2015). This finding further demonstrates the valuable role of calcium in mitigating stress. Given the potential central role the cell wall may play as both a barrier against cellular water loss and blockage of ice propagation into the cell, the role of calcium in the structure of the cell wall may also be beneficial to mitigating multiple stresses. Furthermore, given similar characteristics of drought stress and freezing stress, cold acclimation may also be beneficial to enhancing dehydration stress tolerance as Liu (2015) also found cold acclimation increased the extracellular freeze dehydration stress tolerance in *A. fistulosum* epidermal cells.

Similar to studies involving calcium and drought stress, the majority of research investigating the role of boron in mitigating the damaging effects of dehydration stress have focused on the role of boron in a range of areas such as gene expression. The role of boron in the structure of the cell wall and the possible implications of that role in mitigating dehydration stress appears to have been overlooked in the current body of research. This gap in the literature exists despite the fact that structural implications of boron in the cell are well known (Hu & Brown, 1994). One of the

mechanisms by which boron influences cell wall structure is through the formation of RG-II dimers who found these cross-linkages influence tensile strength and cell wall porosity (O'Neill et al., 2004). Given these gaps in the literature, this chapter aims to investigate the role of calcium and boron with respect to reducing water loss.

We utilized both pure pectin standards as well as a range of biological systems to explore the role of calcium, boron and to a certain extent cold acclimation on dehydration stress. The nature of biological systems is complicated, with numerous factors at play not only in basic cell functioning but also in response to dehydration stress. By first exploring percent water loss in pure pectin standards, the goal is to establish clear trends relating to impact of calcium and boron in influencing water loss. These trends will then serve as a basis to explore how calcium and boron influence water loss in the cell wall as a result of their likely interactions with pectin.

As mentioned above, a range of biological systems were utilized to explore water loss. Two *Allium* species were selected since they have contrasting ability to cold acclimate as well as survive extreme cold temperatures (Palta et al., 1977; Tanino et al., 2013). Therefore, these two species were selected as they are predicted to also have contrasting abilities to survive dehydration stress. High methylated citrus pectin was used during the initial pectin water loss experiment as a proxy for pectin within the cell walls of both *Allium* species since citrus pectin has a high proportion of HG, similar to that of pectin in *Allium* cell walls (Yapo et al., 2007; Mankarios et al., 1980). Since calcium ions are known to form cross-linkages with HG pectin, creating "egg-box" structures, calcium was used as a treatment to explore the mitigation of water loss in both *Allium* species (Ravanat & Rinaudo, 1980). The resulting "egg-box" structures influence the rigidity and stabilization of the cell (Burstrom, 1968; Jones & Lunt, 1967). Furthermore, given that Liu (2015) observed cold acclimating *A. fistulosum* reduced cell wall permeability in epidermal cells, cold acclimation was explored in relation to mitigating dehydration stress in relation to *A. fistulosum*.

In addition to investigating water loss in *A. fistulosum* and *A. cepa*, water loss was examined in various *Arabidopsis* mutant genotypes. The use of *Arabidopsis* mutants enabled exploration into the role of boron and PMEI in relation to their possible role in mitigating dehydration stress. Three boron transporters were examined: NIP5-1, NIP6-1 and BOR1. While NIP5-1 and NIP6-1 are very

similar, NIP5-1 is involved in the uptake of boric acid from the root surface under boron limiting conditions, while NIP6-1 is mainly expressed in the shoots, helping to direct boron to young developing tissues (TAIR, 2015; TAIR, 2013; Takano et al., 2008; Zimmermann et al., 2004). BOR1 is an efflux-type boron transporter responsible for xylem loading and boron translocation from roots to shoots under B limited conditions (TAIR, 2021; Miwa et al., 2006; Noguchi et al., 1997). With regards to analysis of PMEI, a PMEI over-expression mutant, specifically over-expressing PMEI5 was analyzed (Müller et al., 2013).

Both boron and PMEI play a critical role in the structure of the cell wall with respect to pectin (Wormit & Usadel, 2018; Brown et al., 2002; Power & Woods, 1997; Hu & Brown, 1994). More specifically, boron forms RG-II dimers, while PMEI inhibits PME, in turn impacting the ability for "egg-box" structures (Wormit & Usadel, 2018; Ishii et al., 1999; O'Neill et al., 1996; Hu & Brown, 1994). The large bank of mutants available for *Arabidopsis* made it an ideal model to explore these factors. GENU BETA pectin was used as a proxy for the pectin within *Arabidopsis* cell walls as GENU BETA pectin has more RG-II in comparison to citrus pectin, which better simulates *Arabidopsis* (O'Neill et al., 1996; Ishii & Matsunaga, 1996; Zhemerichkin & Ptitchkina, 1995).

In addition to studying water loss in multiple models, water loss is also examined over multiple time courses throughout the experiments to analyze how calcium, boron, PMEI and cold acclimation influence water loss over various time periods. The experiments below address the overarching hypothesis: Calcium, boron and pectin concentration all impact tolerance to dehydration stress, both in terms of percent water loss as well as limit of damage (for biological models) following the stress.

More specifically, the following hypotheses are addressed in this chapter:

1. Increasing concentration along with calcium or boron will reduce water loss over 6hr in pure pectin standards. Moreover, boron will have a greater influence on reducing water loss in GB pectin, while calcium will have a larger effect on HM pectin.

2. The exogenous application of CaCl2 localizes to the apoplast of *Allium fistulosum* (*A. fistulosum*) and reduces the rate of cellular water loss over short-term (15min) and long-term (16-18hr and 12-24hr) periods.
3. *Allium cepa (A. cepa)* has greater percent water loss compared to *Allium fistulosum*, however the addition of calcium reduces percent water loss.
4. *Arabidopsis thaliana* (*A. thaliana*) lines with mutations in boron transporters and a pectin methylesterase inhibitor (PMEI) will lose water at a faster rate over a short-term (15min) and long-term (2-10hr) compared to Col-0.

Experiments laid out within this Chapter address two sub-objectives:

1. Analyze how calcium and boron concentration, influences the rate of water loss in pure pectin solutions over 6 hr.
2. Investigate the influence of calcium on water loss in *Allium fistulosum*, *Allium cepa* and various *Arabidopsis thaliana* mutant genotypes over short (15minutes) and long periods (16hr and 24hr).

4.2 Materials and Methods

4.2.1 Water Loss in Pure Pectin Solutions

4.2.1.1 Pectin Powders and Pectin Solutions

See Section 3.2.1.1

4.2.1.2 Water Loss

Water loss of pure pectin solutions was analyzed over 0 - 6hr at hourly intervals through assessment of weight loss. This timeline was selected following preliminary experiments. Water loss was first analyzed by pipetting approximately 1g of each of the pectin solutions outlined in Section 3.2.1.1 into a petri dish (Figure A4). For consistency of evaporation, care was taken to gain an even area distribution of the various treatment solutions from the center of the plate. Throughout the course of the dehydration experiment, lids were kept off the petri dishes in order to allow for evaporation to occur. Temperature remained constant at 23°C, with a relative humidity of about 22% during the experiment. Percent water loss was calculated using Equation A1.

4.2.1.3 Statistical Analysis

Results obtained from the analysis of pectin water loss over 0 - 6hr were first analyzed using an ANOVA. The ANOVA examined each element of the pectin solution (concentration, type, presence/absence of calcium or boron) in combination as opposed to examining each explanatory variable separately in relation to water loss over time. Thus, in total 12 different pectin combinations were analyzed using an ANOVA. In addition, a Tukey test was also performed to check for differences in rate of water loss between each of the pectin solutions. Figures were created using the "ggplot" and "ggplot2" package in RStudio (Version 1.2.5033), in addition to Microsoft Excel (Version 16.32) (Wickham, 2020). All statistical analysis was preformed using the RStudio statistical software (Version 1.2.5033).

4.2.2 *Allium fistulosum* Water Loss

4.2.2.1 Plant Material (Allium fistulosum) and Experimental Design

Section 3.2.2.1

4.2.2.2 Calcium Application

Section 3.2.2.2

4.2.2.3 Cold Acclimation

Section 3.2.2.3

***Note:** After looking at water loss over both a 15min and 24hr time course, the decision was made to drop the cold acclimation portion of the project since the data outlined in (Figure 4.8 and Figure 4.12) indicates the relationship between water loss and limit of damage in cold acclimated plants is extremely complex. A dedicated project is required to solely focus on the role of cold acclimation and water loss. Thus, the focus for this project became the influence of calcium, boron and PMEI on water loss.

4.2.2.4 Short-Term Water Loss- 15min

Percent water loss over a 15 min period was analyzed by recording the weight of a single epidermal cell layer every minute using a Mettler Toledo analytical balance (Columbus, OH, United States). The epidermal cell layer was placed with the abaxial surface down on the slide. The slide was then placed on an upside-down weigh-boat as this allowed for the slide to be more easily removed from the scale (Figure A5). Percent water loss at T0 was 0% and from there water loss was calculated (Equation A1) (Arve et al., 2014).

4.2.2.5 Long-Term Water Loss 24hr (Original Method)

An analysis of water loss over a 24hr period (12, 14, 16, 18, 20, 22 and 24 hr) in the dark at 23°C and about 33% RH was performed by preparing 7 slides per replication, with a single epidermal cell layer per slide (Figure A6 [3,4]) and weighed using a Mettler Toledo balance (Columbus, OH, United States) and analyzed for percent water loss (Arve et al., 2014). The single epidermal cell layer was then wrapped in two premoistened Kimwipes™ and placed in a 50mL tube with the lid for 24hr (Figure A6 [4-6]) in the dark at 23°C. Kimwipes™ were used to rehydrate the sample in order to assess the limit of damage. Percent water loss was calculated using equation A1, with percent water loss at T0 set at 0. Limit of damage after rehydration was then observed and quantified using methods outlined in Section 4.2.2.7.

***Note:** As a result of the findings of the above analysis, the decision was made to leave the epidermal layer leaf intact on the sheath during the period of dehydration and rehydration in order to avoid applying dehydration stress artificially to the excised single cell layer since dehydration would normally occur on the intact sheath. In addition, water loss was only analyzed at 16hr and 18hr using this method as these time points were found to be of greatest interest in the experiment. This experimental designed is outlined in Section 4.2.2.6.

4.2.2.6 Long-Term Water Loss- 16hr and 18hr

Water loss over 16hr and 18hr was analyzed by first identifying and removing the youngest leaf blade with the most developed sheath. The sheath was then cut from the base into a 4cm section (Figure A7). Both ends of the sheath were then sealed with petroleum jelly and weighed to

obtain a T0 weight. Samples were then placed in the dark at a constant temperature of about 23°C. Sheaths were weighed at the 16 hr and 18 hr time points for water loss. Samples at each of the time points were then wrapped in moist Kimwipes™ and placed inside 50mL tubes with the lid on for 24hr as outlined in Section 4.2.2.5. The process was repeated at 18hr. Following the 24hr rehydration period, the epidermal cell layer was peeled and fixed to a slide and assessed for limit of damage using methods outlined in Section 4.2.2.7.

4.2.2.7 Measurements of Limit of Damage

Limit of damage was measured using two different checks: the visualization and quantification of protoplasmic streaming and staining using fluorescein diacetate (FDA) (Figure 4.1). The visualization of protoplasmic streaming was performed using a digital LEICA DM4 B microscope (Wetzlar, Germany) at 40x with a LEICA DFC7000 T camera (Wetzlar, Germany) attached. Protoplasmic streaming was quantified as a percent of the limit of damage across the epidermal cell layer (Equation A2).

FDA stain was prepared by dissolving FDA into acetone. Slides mounted with epidermal cell layers were immersed in FDA, placed in a desiccator for 5 min and then washed with PBS. Staining and subsequent washing with PBS was conducted in the dark. Cells were imaged using a digital LEICA DM4 B microscope (Wetzlar, Germany) with a LEICA DFC7000 T camera (Wetzlar, Germany) attached at the 40x objective along with the GFP filter and the fluorescence setting. Viable cells fluoresce bright green as shown in Figure 4.1 as an intact, functioning esterase integral membrane protein is required to cleave FDA in order for fluorescence to occur (Proffitt et al., 1996; Thermo Fisher Scientific, n.d.). Thus, failure to fluoresce is indicative of a non-viable cell. Non-viable cells will appear dark, non-fluorescent green as a result of FDA staining. Thus, the quantification of fluorescence by way of image analysis in ImageJ (Version 1.53) was used to further analyze differences in the limit of damage between cell layers based on FDA staining.

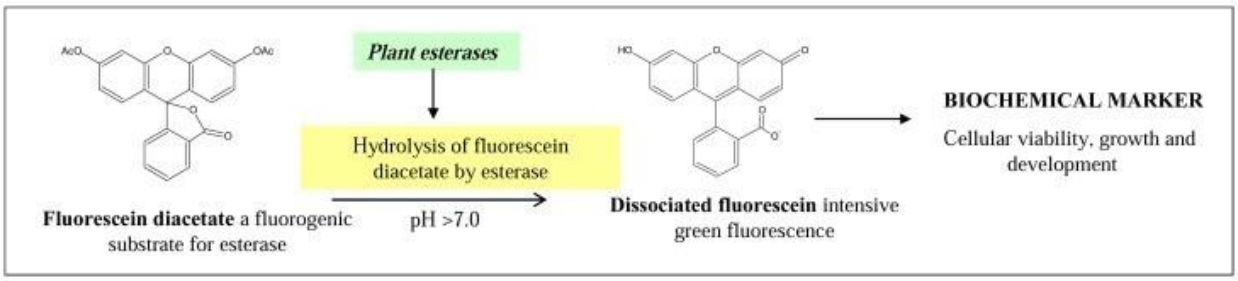

Figure 4.1 Chemical reaction for fluorescein diacetate

The chemical reaction of fluorescein diacetate to confirm the limit of damage within epidermal cells. Image from Vitecek et al. (2007). Used under Creative Commons Attribution 4.0 International (https://creativecommons.org/licenses/by/4.0/).

4.2.2.8 Determining Stomatal Aperture

Stomatal aperture was measured using the Suzuki Universal Micro-Printing (SUMP) method (Banik et al., 2016). Using SUMP discs and SUMP liquid, imprints of the stomata were taken. From there, the disc imprints were examined to determine if the stomata were open or closed using a digital LEICA DM4 B microscope (Wetzlar, Germany) at 40X with a LEICA DFC7000 T camera (Wetzlar, Germany) attached. Imprints were also taken prior to dehydration in order to ensure stomata were functional and subsequently closed during dehydration stress (Figure A8).

4.2.2.9 Statistical Analysis

The results from the analysis of water loss over 15min were analyzed using generalized additive models (GAMs). A generalized additive model is a method of statistical analysis similar to generalized linear modeling (GLM) (Crawley, 2013). Crawley (2013) further outlines that with a GAM, the shape of the relationship between y and the continuous explanatory variable x is not specified by an explicit functional form, such as a linear shape. This makes GAMs a good method of analysis for non-linear relationships. In a GAM, a non-parametric smoother replaces the typical linear function that would be used to build a GLM (Crawley, 2013; Hastie & Tibshirani, n.d.). Therefore, the GAM was a suitable method of analysis as the relationships examined in this section are non-linear. When analyzing a non-linear relationship, some methods of analysis may fail to capture certain non-linear patterns (Larsen, 2015). Larsen (2015) goes on to further outline that GAM predictor functions are generated while the model is constructed and therefore there is no need-to-know what type of functions will be required to build the model. The ability to generate

the predictor functions during the model construction allows for patterns to be discovered that may have been missed with another form of analysis (Larsen, 2015).

With respect to the creation of the GAMs, water loss was the response variable, while time was the continuous explanatory variable and the application of calcium, and cold acclimation were explanatory variables. GAMs were generated using the "mgcv" package from for RStudio (Version 1.2.5033) (Wood, 2019). The Akaike information criterion (AIC) score was used when building models to select for the most optimum model. The empirical distribution factor (edf) was used to confirm that the data modeled by the GAM was non-linear, which is indicated by an edf greater than 1. Model checking was done using the gam.check function to examine the residual vs. fitted plots. The distribution of the data was checked prior to the creation of the GAMs and while the data did not follow a normal distribution, a log-transformation did not improve the distribution of the data. Therefore, the data was not transformed. The statistical significance of the GAMs was analyzed using analysis of variance (ANOVA), function, with the argument "test" being set equal to "F", thereby running f-tests as opposed to t-tests. A Tukey test was also done to further analyze the relationship between the various cold acclimation treatments, without the influence of the variable, time. Figures of each GAM were individually created for each of the 6 possible treatment combinations using function "plot.gam()", in addition to packages "mgcViz" and "rgl". Package, "devtools" was used to download the colour palette, "inauguration_2021", which was used for the colours of each figure.

In addition, attempts were made to create GAMs in order to analyze the results from the experiment examining water loss over 24hr, however this was unsuccessful as a result of an error in attempting to build the GAM. Attempts were made to correct the error, however none of the troubleshooting methods resolved the error. Therefore, those results were analyzed using an ANOVA, where $p<0.05$ was deemed significant. Results obtained from the observing protoplasmic streaming were analyzed using the same method. A Tukey test was also conducted to further analyze the relationship between the various cold acclimation treatments and their effect on percent water loss over 24hr. Data collected from the experiment analyzing water loss over 16hr and 18hr was analyzed using an ANOVA, where $p<0.05$ was deemed significant. Figures were created using the "ggplot" and "ggplot2" package in RStudio (Version 1.2.5033), in addition to Microsoft Excel

(Version 16.32) (Wickham, 2016). All statistical analysis was preformed using the RStudio statistical software (Version 1.2.5033).

4.2.3 *Allium cepa* Water Loss

4.2.3.1 Plant Material (Allium cepa) and Experimental Design

A. cepa was planted similarly to *A. fistulosum* as outlined in Section 3.2.2.1. Yellow Sweet Spanish *A. cepa* seeds (Early's Farm & Garden Center, 2615 Lorne Ave. Saskatoon, SK) were germinated in the Agriculture Greenhouse at the University of Saskatchewan (45 Innovation Blvd, Saskatoon, Saskatchewan) and then transplanted into 6" pots after approximately 2 weeks containing Sunshine No.4 (Sun Gro Horticulture Canada Ltd. Seba Beach, AB, Canada). *A. cepa* was grown on the same bench in the greenhouse as *A. fistulosum* and therefore exposed to the same environmental and cultural conditions (Section 3.2.2.1). The bench was organized using a randomized complete block design.

4.2.3.2 Calcium Application

Calcium was applied following the method outlined in Section 3.2.2.2

4.2.3.3 Short-Term Water Loss- 15min

Analysis of water loss over 15min was performed as outlined in Section 4.2.2.4

4.2.3.4 Long-Term Water Loss- 16hr and 18hr

Analysis of water loss over 16hr and 18hr was performed as outlined in Section 4.2.2.6

4.2.3.5 Limit of Damage

Analysis of the limit of damage within cells was performed as outlined in Section 4.2.2.7

4.2.3.6 Determining Stomatal Aperture

Analysis of stomatal aperture was performed as outlined in Section 4.2.2.8

4.2.3.7 Statistical Analysis

Statistical analysis was conducted as outlined in Section 4.2.2.9, however cold-acclimation was not used as a variable as this treatment was not applied to *A. cepa*.

4.2.4 *Arabidopsis thaliana* Water Loss

4.2.4.1 Arabidopsis thaliana Genotypes

Five *A. thaliana* lines were selected and grown for this experiment, including three boron-transporter mutants (*nip5-1*, *nip6-1* and *bor1*), a pectin methylesterase inhibitor over-expression mutant (*p35S::PMEI5*) and a wild-type (Col-0) line respectively (TAIR, 2021; TAIR, 2015; Müller et al., 2013; TAIR, 2013). All three boron transporter mutants were obtained from the Arabidopsis Biological Resource Centre (ABRC) (Columbus, OH, United States), *p35S::PMEI5* was kindly sent to the Tanino lab by Kerstin Müller (Simon Fraser University, Burnaby, BC). PMEI5 over-expression in this line is under the control of the Cauliflower mosaic virus (CaMV) 35S promoter (Müller et al., 2013).

NIP5-1 (AT4G10380.1) encodes for a boric acid channel that is essential for efficient boron uptake and plant development under boron limited conditions (TAIR, 2015). Boron is taken up through the roots by the boric acid channel which is coded for by NIP5-1 and then is moved into the xylem by a boron transporter that is coded for by BOR1 (TAIR, 2015; TAIR, 2021). Similar to the protein coded for by NIP5-1, NIP6-1 encodes a protein with boron transporter activity however, this transporter helps to preferentially direct boron to young developing tissues in the shoot when under boron limited conditions (TAIR, 2015; TAIR, 2013). BOR1 (AT2G47160.2) codes for a boron transporter that is localized in the shoots and roots under conditions where boron is deficient and is subsequently degraded within hours once the level of boron is restored in the plant (TAIR, 2021). Initially, BOR2 mutant seeds were also ordered however an issue arising genotyping as a result of an error by the seed bank impeded the use of this line. The *p35S::PMEI5* line mutant selected specifically over-expresses PMEI5 (Müller et al., 2013). Müller et al. (2013) further outlines that PMEI5 codes for a pectin methylesterase inhibitor. Furthermore, they found that when compared to Col-0, this mutant has been found to show a number of phenotypic variations. The *p35S::PMEI5*

plants have been found to have decreased fertility, faster germination and larger seed size amongst other phenotypic variations (Müller et al., 2013).

These lines were kindly genotyped by Dr. Sheng Wang (University of Saskatchewan). Plants were genotyped by first preparing genomic data according to Edwards et al. (1991), with some modifications (Wang et al., 2011; Edwards et al., 1991). More specifically, 1µL of DNA sample was used for a 20µL polymerase chain reaction (PCR) (Wang et al., 2011). Instructions in the manual for Taq DNA polymerase (Invitrogen) were followed to prepare the PCR reaction mixtures. Amplifications were conducted using a T100 programmable thermal controller (Bio-Rad). Denaturing was performed at 94 °C for 1min, followed by annealing for 1min. Primer extension was then carried out at 72 °C for 1 min per kilobase of DNA. These steps were repeated for 30 cycles (Wang et al., 2011). Table A10 lists the primers used to genotype *nip5-1*, *nip6-1* and *bor1*. Primers were ordered from Integrated DNA Technologies (Coralville, IA, USA). *p35S::PMEI5* was obtained previous to these lines and thus was genotyped separately. The results of that genotyping are not shown within this thesis.

All lines were grown in a Conviron chamber (Winnipeg, Manitoba, Canada) with the following environmental conditions; 20ºC constant temperature, 50% RH, 16-8hr/light-dark period and 150 +/-10 µmol $m^{-2}s^{-1}$. Plants were watered every second day, using water from the City of Saskatoon, while fertilizer (20-20-20) was applied weekly. When preparing the fertilizer solution, 2g of 20-20-20 was added to 1L of water. Each tray containing ~12 pots received 1L of fertilizer solution. Plants were grown to two-weeks of age (Figure A7).

4.2.4.2 Inductively Coupled Plasma Mass Spectrometry (ICP-MS) Analysis of Arabidopsis Genotypes

Analysis of boron in the *A. thaliana* using ICP-MS was done using above-ground biomass samples obtained from various genotypes (*nip5-1*, *nip6-1*, *p35S::PMEI5* and Col-0). Plants were two-weeks old at the time of analysis. Section 4.2.4.1 outlines how the genotypes were grown. Samples were freeze-dried and ground with a mortar and pestle prior to analysis.

Samples were first digested in the microwave. Digestion in the microwave was done by adding 2.25mL HNO_3 + 2.25mL H_2O + 0.5mL HCl to 0.25g of sample (Khazaei & Vandenberg, 2020) (Goetz, B. pers.comm. 2021). Vials were heated to 200ºC over 15min and then held at 200 ºC for 15min according to the manufacturer's guidelines (CEM, n.d). The pressure in the microwave was held constant at 800psi, and the power was maintained at 900-1050W (CEM, n.d). The analysis was conducted after digestion using a solution of 2.25% HNO_3 and 0.5% HCl. Note, the aforementioned values were decreased by 10X for this experiment due to small sample sizes (Goetz, B. pers.comm. 2021). Citrus leaves and tomato leaves were used as certified standards.

Water samples obtained from the Environmental Stress Lab in the College of Agriculture and Bioresource Building (51 Campus Drive, Saskatoon, SK) and the Agriculture Greenhouses (45 Innovation Blvd., Saskatoon, SK) were analyzed using the same method, however samples were not digested prior to analysis.

Tissue and water samples were analyzed for B using iCAP™ RQ inductively-couples plasma mass spectrometry and the kinetic energy discrimination cell mode as described in the manufacturer's instructions (model: ICAP-RQ, S/N ICAPRQ00250, Thermo Fisher Scientific, Bremen, Germany).

Tables containing results from this experiment are presented in the Appendix as they are intended to be supplementary to experiments analyzing *A. thaliana* (Tables A2, A11-A14).

4.2.4.3 Short-Term Water Loss

Percent water loss over a 15 min period was analyzed by recording the weight of a single two-week-old plant that was cut off at the base of the shoot, sealed with Vaseline at the cut stem and weighed every minute for 15 minutes using a Mettler Toledo (Columbus, OH, United States) balance (Arve et al., 2014). The percent water loss at T0 was set at 0%, and Equation A1 was used to calculate percent water loss. Two models of hygrometers outlined in Section 4.2.2.4 were used to monitor the temperature and humidity of the lab. The lab was approximately 24°C with an approximate RH of 33%. The experiment was conducted under dark conditions in order to ensure

the stomata remained closed in an attempt to reduce stomatal water loss so that water loss reflected non-stomatal pathways.

***Note:** Due to unforeseen issues with seed set, the *bor1* mutant was not included in this analysis.

4.2.4.4 Long-Term Water Loss (2-24hr)

Water loss every 2hr over a 24hr period was performed on plants sampled as per the analysis of short-term water loss. An initial weight was recorded at 0hr. To rehydrate the plants, plants were carefully placed in 2mL sepia toned bottles along with 100µL of dH_2O. Caution was taken to ensure the plant was not sitting directly in the water and the lid was placed on the bottle to ensure a humid environment. This was repeated every 2hr for 24hr. Equation A1 was used to calculate percent water loss.

***Note:** Due to unforeseen issues with seed set, *bor1* was not included in the analysis taken between 12hr-24hr.

4.2.4.5 Limit of Damage

Approximately 24hr following rehydration, 1000µL of dH_2O was added to the 2mL sepia-colored bottles. Care was taken to ensure the plant made contact with the water and the bottles were then left on the shaker overnight (~19hr). Electrical conductivity was then measured using the Twin Compact Meter (Horiba, Japan).

The initial measurement of electrical conductivity was conducted after the sample had been shaken overnight. This measurement was taken used the liquid that had been used to submerge the plant. Specifically, 100µL of the water used to submerge the plant was pipetted into the conductivity meter according to instructions for the Twin Compact Meter (Horiba, Japan). Following the initial measurement and subsequent recording of the value, the water was then added back to the vial. From there, the total electrolyte conductivity (µS/cm) was measured by placing the sample in a 100ºC dry bath for 10 minutes and then vortexing the vial containing both the plant and the water. The vials were then cooled prior to taking the final measurement, which again was done by

pipetting 100µL of the water that had been used to submerge the plant into the conductivity meter for readings. Equation A3 was used to calculate limit of damage.

4.2.4.6 Determining Stomatal Aperture

Analysis of stomatal aperture was performed as outlined in Section 4.2.2.8 (Figure A10).

4.2.4.7 Statistical Analysis

Results were analyzed using the same statistical tests outlined in Section 4.2.2.9, however using "genotype" as the explanatory variable as opposed to cold acclimation and calcium application.

4.3 Results

4.3.2 General Results and Overview

In general, calcium did significantly reduce overall percent water loss in both high methylated pectin and GENU BETA pectin (Figure 4.2, Figure 4.3, Table 4.1 and Table A15). However, the effect of calcium on water loss in *A. fistulosum* and *A. cepa* was less clear. Overall, the most striking biological response was the significantly greater water loss in the stress sensitive *A. cepa* compared to the stress resistant *A. fistulosum* (Figures 4.4-4.7, Table A16 and Table A18). Sensitive *A. cepa* lost more than double the water than resistant *A. fistulosum* over a 15-minute period, although this trend narrowed over 16-18hr (Figures 4.4-4.7). *A. fistulosum* also had a significantly ($p<0.05$) lower limit of damage following long-term dehydration (16-18hr) compared to *A. cepa* (Figures 4.8-4.9 and Table A22). Furthermore, when the *A. fistulosum* epidermal cell layer (as a separated cell layer) was dehydrated for 16hrs, calcium application significantly ($p<0.05$) increased protoplasmic streaming, indicating a reduced limit of damage (Figure 4.15 and Table A27). Calcium did not reduced the limit of damage in *A. cepa* based on protoplasmic streaming (Figure 4.8 and Table A25). However, unlike *A. fistulosum*, calcium treatments significantly ($p<0.05$) reduced water loss in *A. cepa* over 15 minutes (Figure 4.5, Figure 4.16 and Table 4.2). In the stress resistant *Allium fistulosum*, over short-term water loss, surprisingly all treatments increased water loss above controls (Figure 4.17, Figure 4.18 and Table 4.3). In general, under long term water loss over 12-24hr, cold acclimation in conjunction with calcium had no significant ($p>0.05$) effect on percent water loss or percent protoplasmic streaming

(Table A26 and Table A28). The application of cold acclimation alone or in conjunction with calcium did not improve dehydration stress resistance (Figure 4.15).

Boron reduced water loss in GENU BETA pectin, which served as a proxy for *Arabidopsis* pectin (Figure 4.2, Figure 4.3, Table 4.1 and Table A15). However, in *Arabidopsis* the relationship between percent water loss and limit of damage in the case of long-term water loss showed more variation (Figure 4.21-4.24). While boron transporter mutants generally lost more water, this did not always result in a direct increase in percent electrolyte leakage which would have reflected as increased damage to the plasma membrane (Figure 4.21-4.24). Of the *Arabidopsis* mutants, the pectin methylesterase inhibitor overexpressing mutant (*pme5i-oe*) had the least water loss and lowest electrolyte leakage over time compared to the boron transporter mutants (Figure 4.21-4.25).

4.3.2 Pectin Water Loss

Over the 6hr period of water loss, all of the pectin solutions exhibited a linear water loss (Figure 4.2). However, while the majority of the pectin solutions followed a similar trajectory, losing on average between 60-70% of their total water by 6hr, the treatment of 8% high methylated pectin combined with calcium had only 48.5% water loss (Figure 4.2 and Figure 4.3). As a result of its lower percent water loss, the 8% high methylated pectin combined with calcium was significantly ($p<0.05$) different from: 8% GENU BETA pectin with calcium, 8% high methylated pectin with no elements, and 8% high methylated pectin with boron (Figure 4.3, Table 4.1 and Table A15).

Furthermore, the addition of calcium and boron (separately) to 8% GENU BETA was also found to significantly ($p<0.05$) reduce percent water loss in comparison to 8% GENU BETA without the addition of either element (Figure 4.3, Table 4.1 and Table A15). Also notable, this significant ($p<0.05$) reduction in percent water loss resulted in these two pectin solutions (8% GENU BETA pectin with calcium and 8% GENU BETA pectin with boron) having the second and third smallest overall percent water losses (Figure 4.3, Table 4.1 and Table A15). 8% high methylated pectin with calcium had the smallest percent water loss of 48.5% followed by 8% GENU BETA pectin with calcium with a percent water loss of 58.3% and 8% GENU BETA pectin with boron with an overall percent water loss of 59.7% (Figure 4.2 and Figure 4.3).

In contrast, the greatest average water loss after 6hr was found to occur in the 4% high methylated pectin with boric acid (70.19%) (Figure 4.2 and Figure 4.3). This overall percent water loss was significantly ($p<0.05$) different from: 4% high methylated pectin without added elements and 4% high methylated pectin with calcium (Figure 4.3, Table 4.1 and Table A15). Other comparisons were also significantly ($p<0.05$) different, and they are listed in Table 4.1.

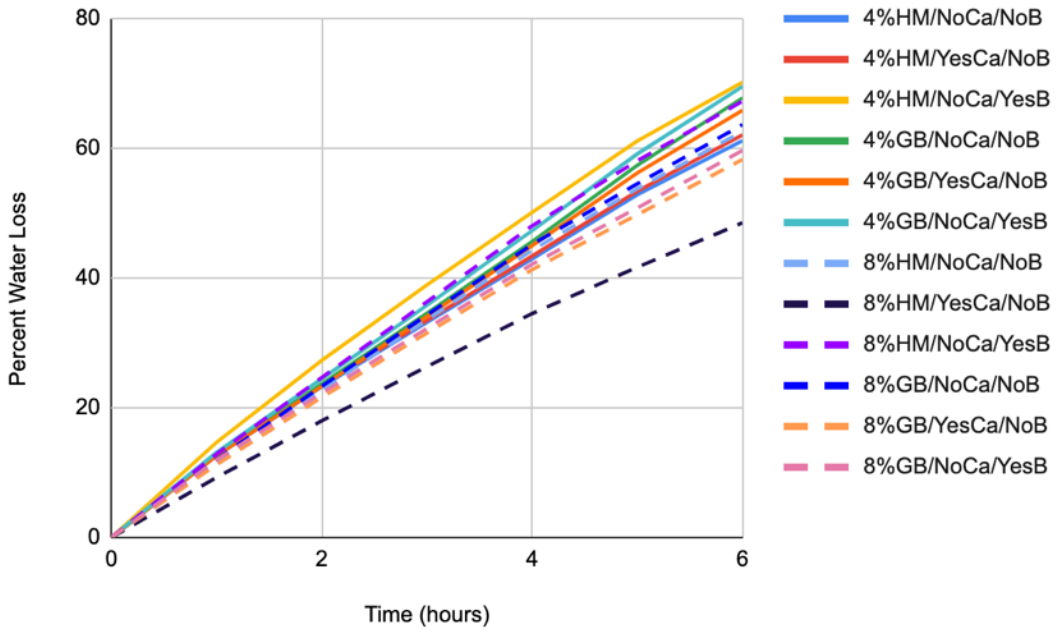

Figure 4.2 Percent water loss over 6hr in pectin solutions

Percent water loss over 6hr across two concentrations of pectin (4% or 8%), two types of pectin (high methylated (HM) citrus pectin or Genu Beta (GB) (sugar beet) pectin), with the addition of either calcium (Ca) (0.05M $CaCl_2$), boron (B) (0.05M H_3BO_3) or no additional element.

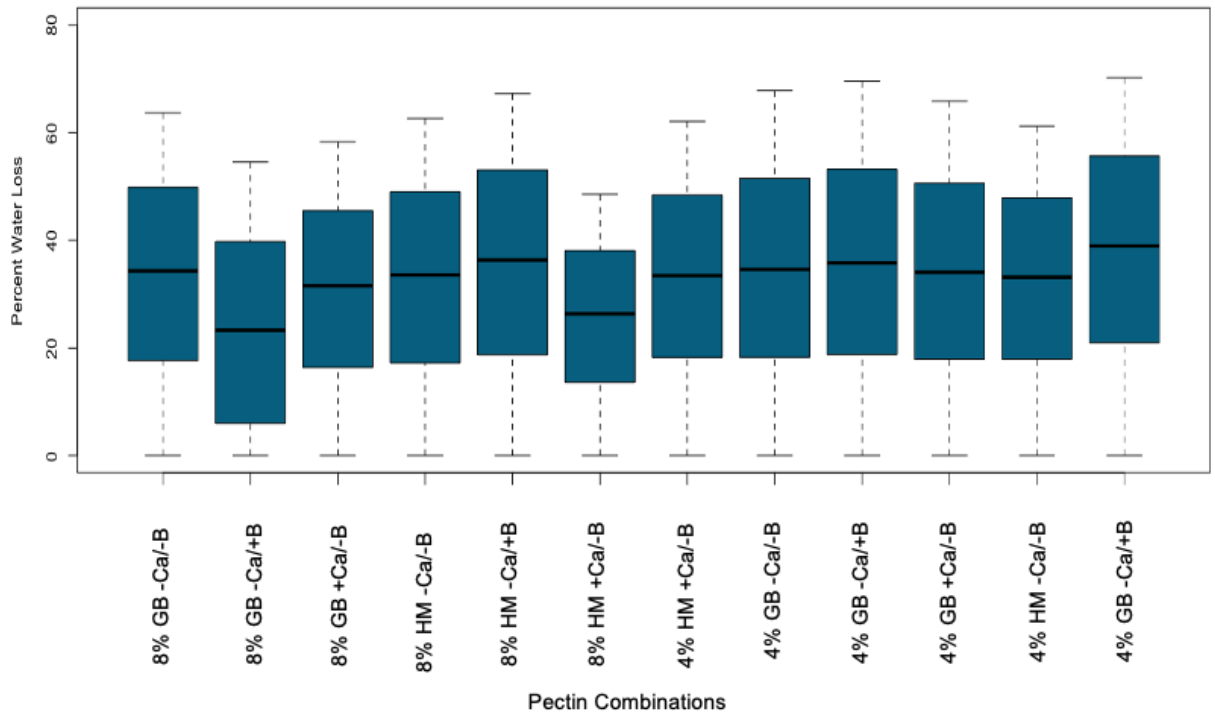

Figure 4.3 Box-pot showing average percent water loss in pectin solutions over 6hr

Boxplot showing average percent water loss over a 6hr period, across two concentrations of pectin (4% or 8%), two types of pectin (high methylated (HM) citrus pectin or Genu Beta (GB) (sugar beet) pectin), with the addition of either calcium (Ca) (0.05M $CaCl_2$), boron (B) (0.05M H_3BO_3) or no additional element. See Tables 4.1 and A15 for statistical analysis.

Table 4.1 Tukey test for results obtained from analysis of water loss in pectin solutions

Results from a Tukey test conducted to further analyze the relationship between various pectin solutions and percent water loss over 6hr. * represents $p \leq 0.05$, ** represents $p \leq 0.01$, and *** represents $p \leq 0.001$. $p<0.05$ is significant.

Treatment Combination	**P value**
EightGB/NoCa/YesB-EightGB/NoCa/NoB	0.000 ***
EightGB/YesCa/NoB-EightGB/NoCa/NoB	0.041 *
EightHM/NoCa/NoB-EightGB/NoCa/NoB	0.999
EightHM/NoCa/YesB-EightGB/NoCa/NoB	0.319
EightHM/YesCa/NoB-EightGB/NoCa/NoB	0.000 ***
FouHM/YesCa/NoB-EightGB/NoCa/NoB	0.999
FourGB/NoCa/NoB-EightGB/NoCa/NoB	0.905
FourGB/NoCa/YesB-EightGB/NoCa/NoB	0.149
FourGB/YesCa/NoB-EightGB/NoCa/NoB	0.999
FourHM/NoCa/NoB-EightGB/NoCa/NoB	0.980

FourHM/NoCa/YesB-EightGB/NoCa/NoB	0.000 ***
EightGB/YesCa/NoB-EightGB/NoCa/YesB	0.000 ***
EightHM/NoCa/NoB-EightGB/NoCa/YesB	0.000 ***
EightHM/NoCa/YesB-EightGB/NoCa/YesB	0.000 ***
EightHM/YesCa/NoB-EightGB/NoCa/YesB	0.897
FouHM/YesCa/NoB-EightGB/NoCa/YesB	0.000 ***
FourGB/NoCa/NoB-EightGB/NoCa/YesB	0.000 ***
FourGB/NoCa/YesB-EightGB/NoCa/YesB	0.000 ***
FourGB/YesCa/NoB-EightGB/NoCa/YesB	0.000 ***
FourHM/NoCa/NoB-EightGB/NoCa/YesB	0.000 ***
FourHM/NoCa/YesB-EightGB/NoCa/YesB	0.000 ***
EightHM/NoCa/NoB-EightGB/YesCa/NoB	0.256
EightHM/NoCa/YesB-EightGB/YesCa/NoB	0.000 ***
EightHM/YesCa/NoB-EightGB/YesCa/NoB	0.000 ***
FouHM/YesCa/NoB-EightGB/YesCa/NoB	0.245
FourGB/NoCa/NoB-EightGB/YesCa/NoB	0.000 ***
FourGB/NoCa/YesB-EightGB/YesCa/NoB	0.000 ***
FourGB/YesCa/NoB-EightGB/YesCa/NoB	0.005 *
FourHM/NoCa/NoB-EightGB/YesCa/NoB	0.549
FourHM/NoCa/YesB-EightGB/YesCa/NoB	0.000 ***
EightHM/NoCa/YesB-EightHM/NoCa/NoB	0.056
EightHM/YesCa/NoB-EightHM/NoCa/NoB	0.000 ***
FouHM/YesCa/NoB-EightHM/NoCa/NoB	1.000
FourGB/NoCa/NoB-EightHM/NoCa/NoB	0.437
FourGB/NoCa/YesB-EightHM/NoCa/NoB	0.019 *
FourGB/YesCa/NoB-EightHM/NoCa/NoB	0.933
FourHM/NoCa/NoB-EightHM/NoCa/NoB	0.999
FourHM/NoCa/YesB-EightHM/NoCa/NoB	0.000 ***
EightHM/YesCa/NoB-EightHM/NoCa/YesB	0.000 ***
FouHM/YesCa/NoB-EightHM/NoCa/YesB	0.059
FourGB/NoCa/NoB-EightHM/NoCa/YesB	0.997
FourGB/NoCa/YesB-EightHM/NoCa/YesB	0.999
FourGB/YesCa/NoB-EightHM/NoCa/YesB	0.783
FourHM/NoCa/NoB-EightHM/NoCa/YesB	0.014 *
FourHM/NoCa/YesB-EightHM/NoCa/YesB	0.238
FouHM/YesCa/NoB-EightHM/YesCa/NoB	0.000 ***
FourGB/NoCa/NoB-EightHM/YesCa/NoB	0.000 ***
FourGB/NoCa/YesB-EightHM/YesCa/NoB	0.000 ***
FourGB/YesCa/NoB-EightHM/YesCa/NoB	0.000 ***
FourHM/NoCa/NoB-EightHM/YesCa/NoB	0.000 ***
FourHM/NoCa/YesB-EightHM/YesCa/NoB	0.000 ***
FourGB/NoCa/NoB-FouHM/YesCa/NoB	0.452
FourGB/NoCa/YesB-FouHM/YesCa/NoB	0.020 *
FourGB/YesCa/NoB-FouHM/YesCa/NoB	0.939

FourHM/NoCa/NoB-FouHM/YesCa/NoB	0.999
FourHM/NoCa/YesB-FouHM/YesCa/NoB	0.000 ***
FourGB/NoCa/YesB-FourGB/NoCa/NoB	0.966
FourGB/YesCa/NoB-FourGB/NoCa/NoB	0.999
FourHM/NoCa/NoB-FourGB/NoCa/NoB	0.183
FourHM/NoCa/YesB-FourGB/NoCa/NoB	0.021 *
FourGB/YesCa/NoB-FourGB/NoCa/YesB	0.534
FourHM/NoCa/NoB-FourGB/NoCa/YesB	0.004 *
FourHM/NoCa/YesB-FourGB/NoCa/YesB	0.457
FourHM/NoCa/NoB-FourGB/YesCa/NoB	0.700
FourHM/NoCa/YesB-FourGB/YesCa/NoB	0.001 **
FourHM/NoCa/YesB-FourHM/NoCa/NoB	0.000 ***

4.3.3 Stress resistant *Allium fistulosum* and Stress Sensitive *Allium cepa* Water Loss

As predicted, stress resistant *A. fistulosum* lost significantly ($p<0.05$) less water compared to stress sensitive *A. cepa* over 15 minutes (Figure 4.4, Figure 4.5 and Table A16). Without factoring in the addition of calcium, *A. fistulosum* epidermal cells lost just over 20% (23.7%) of their total water in 15min, while epidermal cells obtained from *A. cepa* lost over 40% (45.4%) of their total water after 15min (Figure 4.4). Moreover, the effect size for the comparison of the relationship between *A. fistulosum* and *A. cepa* in general was above 0.8, which is considered a large effect size, and therefore also meaningful (Table A17) (Lakens, 2013; Cohen, 1988).

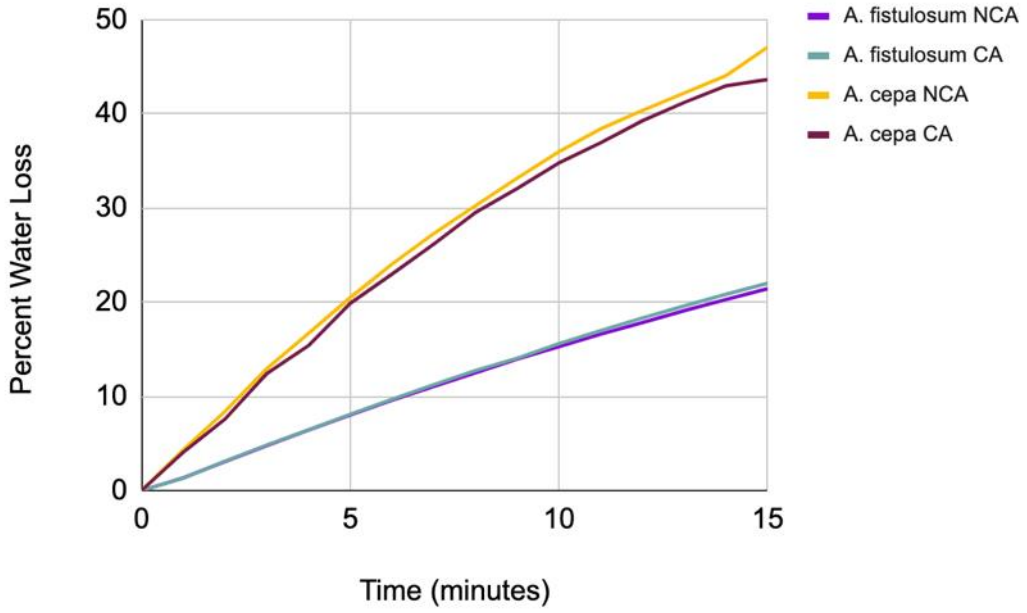

Figure 4.4 Percent water loss over 15 minutes in *Allium fistulosum* and *Allium cepa* epidermal cell layers

Percent water loss over 15 minutes in epidermal cell layers obtained from both *Allium fistulosum* and *Allium cepa*. This graph shows both treatment groups (1) NCA (-$CaCl_2$), and 2) CA (+$CaCl_2$) from both *Allium* spp. analyzed. Plants treated with calcium received 0.05M of $CaCl_2$ every second day for 4 weeks.

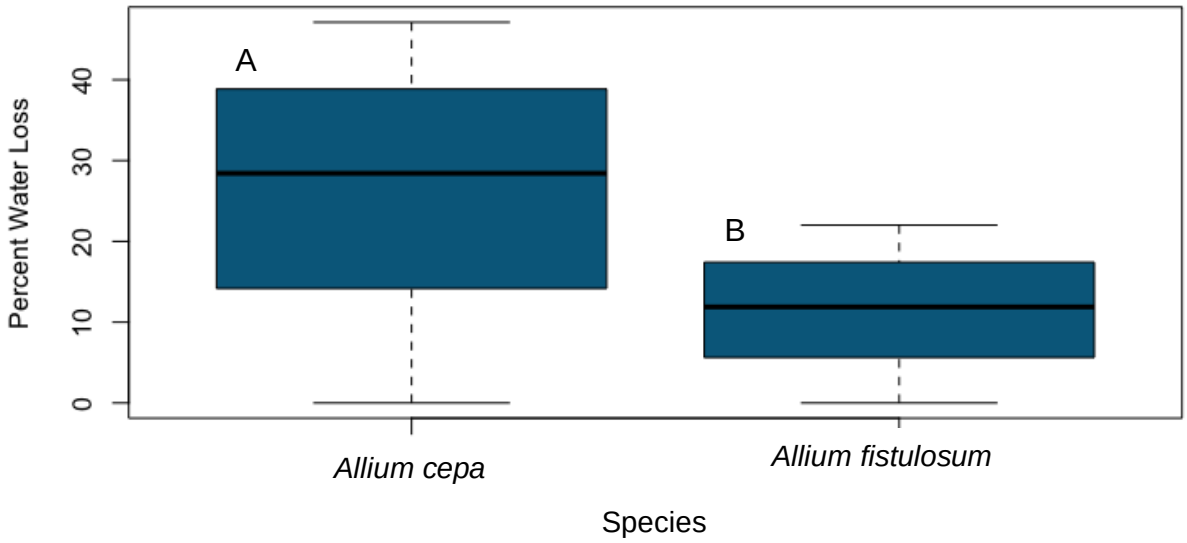

Figure 4.5 Box-pot showing average percent water loss in *Allium fistulosum* and *Allium cepa* over 15min. Treatment groups (CA and NCA) combined

Boxplot showing average percent water loss over 15min between *A. cepa* and *A. fistulosum* in general, with treatment groups (CA and NCA) combined. See Table A16 statistical analysis.

In general, when the treatment groups (calcium treated and control) were combined, *A. fistulosum* continued to show a significantly ($p<0.05$) reduced water loss when examined over 16-18hr (Figure 4.6, Figure 4.7 and Table A18). One caveat however is that while there was a significant difference in water loss between *A. cepa* and *A. fistulosum* over 16-18hr, the effect size was small (Table A19). At 16hr, *A. fistulosum* sheaths had a percent water loss of 27.1%, while *A. cepa* sheaths had a percent water loss of 33.1% (Figure 4.6). At 18hr, *A. fistulosum* sheaths had a percent water loss of 28.1% while, *A. cepa* sheaths had lost 33.3% of their water (Figure 4.6). While calcium application did slightly reduce percent water loss in *A. fistulosum*, the effect of calcium on *A. fistulosum* was not statistically significant (Figure 4.6 and Table A20). Calcium application also failed to create a statistically significant difference in water loss over 16-18hr in *A. cepa* (Table A21).

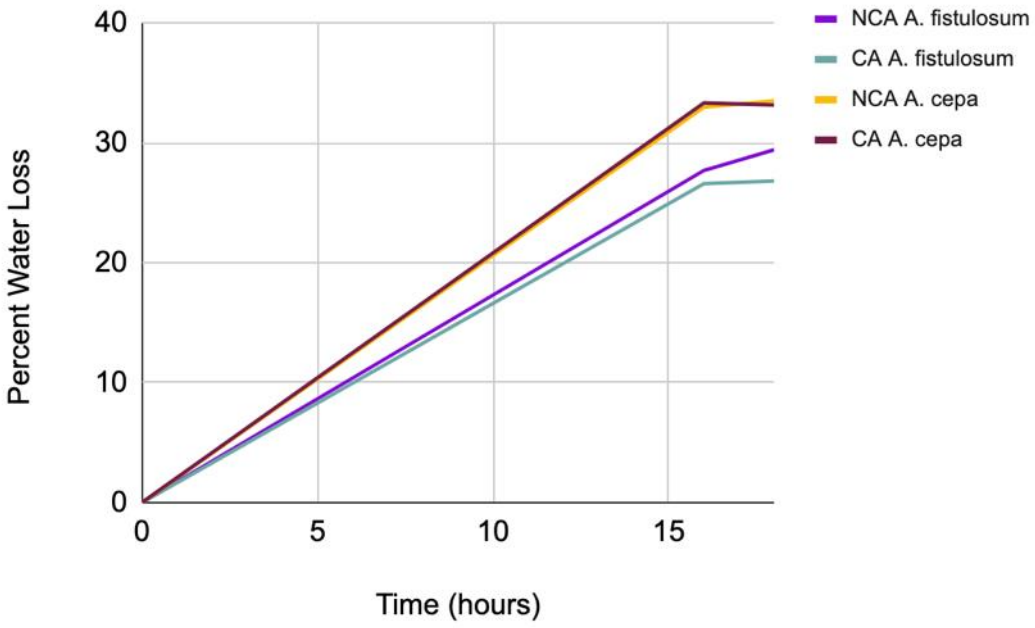

Figure 4.6 Percent water loss over 16-18hr in *Allium fistulosum* and *Allium cepa*

Percent water loss in 4cm sections Allium *fistulosum* and *Allium cepa* sheaths over 16-18hr. Epidermal cell layers were left attached to the sheath. This graph shows both treatment groups: 1) -$CaCl_2$, and 2) +$CaCl_2$) from both *Allium* spp. analyzed. Plants treated with calcium received 0.05M of $CaCl_2$ every second day for four- weeks.

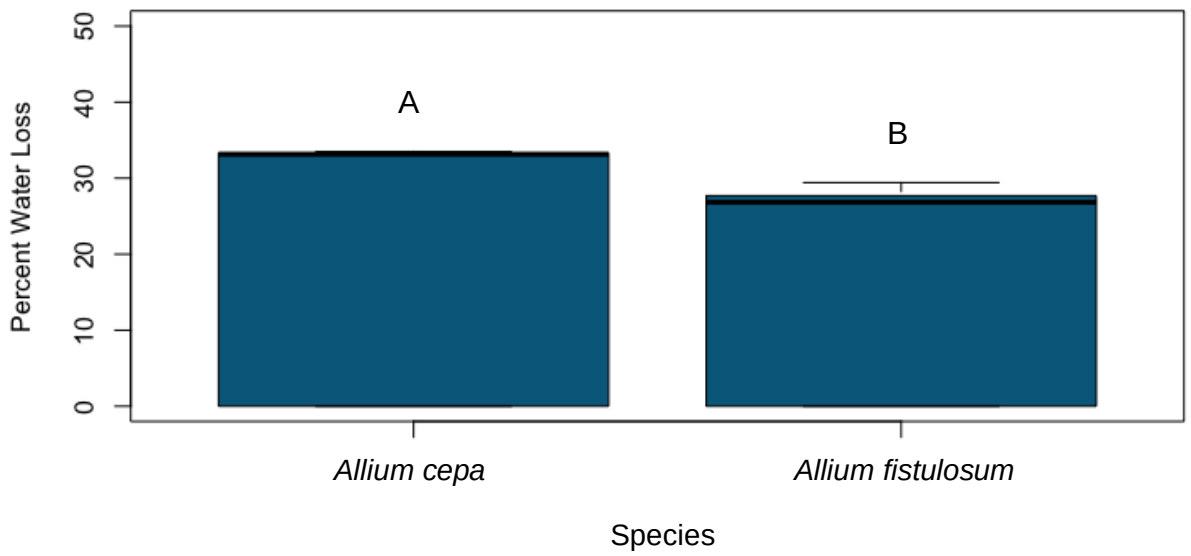

Figure 4.7 Box-pot showing average percent water loss in *Allium fistulosum* and *Allium cepa* over 16-18hr

Boxplot showing average percent water loss over 16-18hr between *A. cepa* and *A. fistulosum* in general, with treatment groups (CA and NCA) combined. See Table A18 for statistical analysis.

A. fistulosum's increased dehydration tolerance in comparison to *A. cepa* was also reflected in the significantly ($p<0.05$) higher percent protoplasmic streaming of *A. fistulosum* epidermal cells following dehydration stress in comparison to *A. cepa* (Figure 4.8, Figure 4.9 and Table A22). The effect size for the relationship between the limit of damage (based on percent protoplasmic streaming) of both species was also large (Table A23). After 16hr of water loss, in general, *A. fistulosum* epidermal cells had a percent protoplasmic streaming of 57.5%, while *A. cepa* epidermal cells had an average percent protoplasmic streaming of 7.1% (Figure 4.8). After 18hr of water loss, *A. fistulosum* epidermal cells had an average percent protoplasmic streaming of 39.2% while *A. cepa* epidermal cells had an average percent protoplasmic streaming of 2.5% (Figure 4.8). A higher level of protoplasmic streaming is indicative of a reduced limit of damage. Despite these significant ($p<0.05$) differences in interspecies percent protoplasmic streaming, when intraspecies percent protoplasmic streaming was examined with regards to the influence of calcium on limit of damage, no significant ($p>0.05$) differences were found for either *A. cepa* or *A. fistulosum* (Table A24 and Table A25). Nevertheless, calcium application did slightly improve percent protoplasmic streaming in *A. fistulosum*, however as mentioned above it was not significant ($p>0.05$) (Figure 4.8).

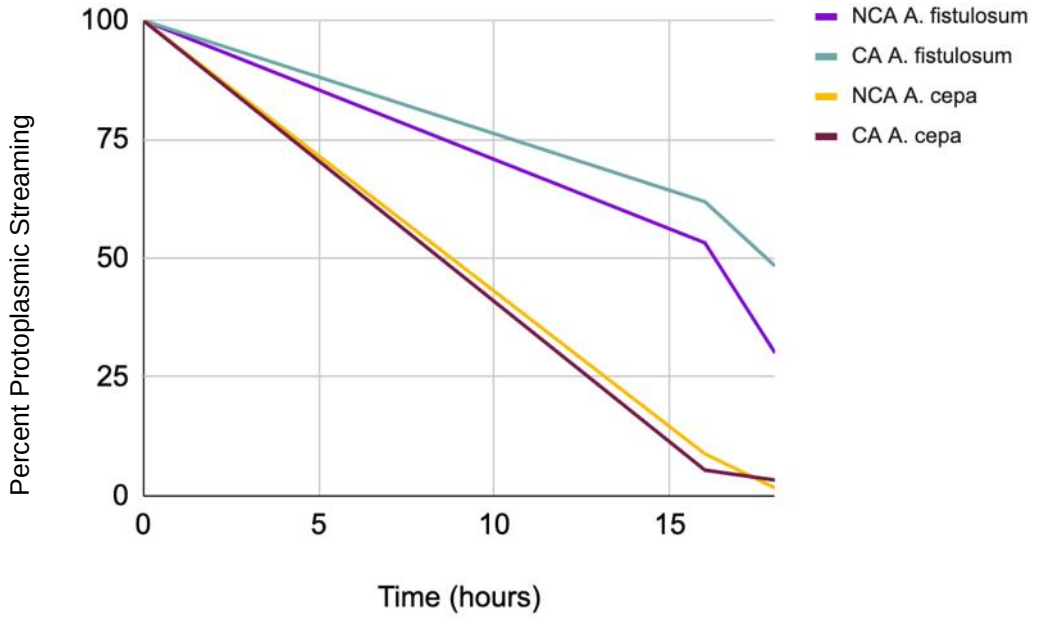

Figure 4.8 Percent protoplasmic streaming (limit of damage) of *Allium fistulosum* and *Allium cepa* epidermal cell layers after 16-18hr dehydration

Limit of damage based on protoplasmic streaming over 16hr and 18hr hours in 4cm sections of *Allium fistulosum* and *Allium cepa* sheath in which the epidermal cell layers in which the epidermal cell layers were left intact. This graph shows both treatment groups (1) -$CaCl_2$, and 2) +$CaCl_2$) from both *Allium* spp. analyzed. Plants treated with calcium received 0.05M of $CaCl_2$ every second day for 4 weeks.

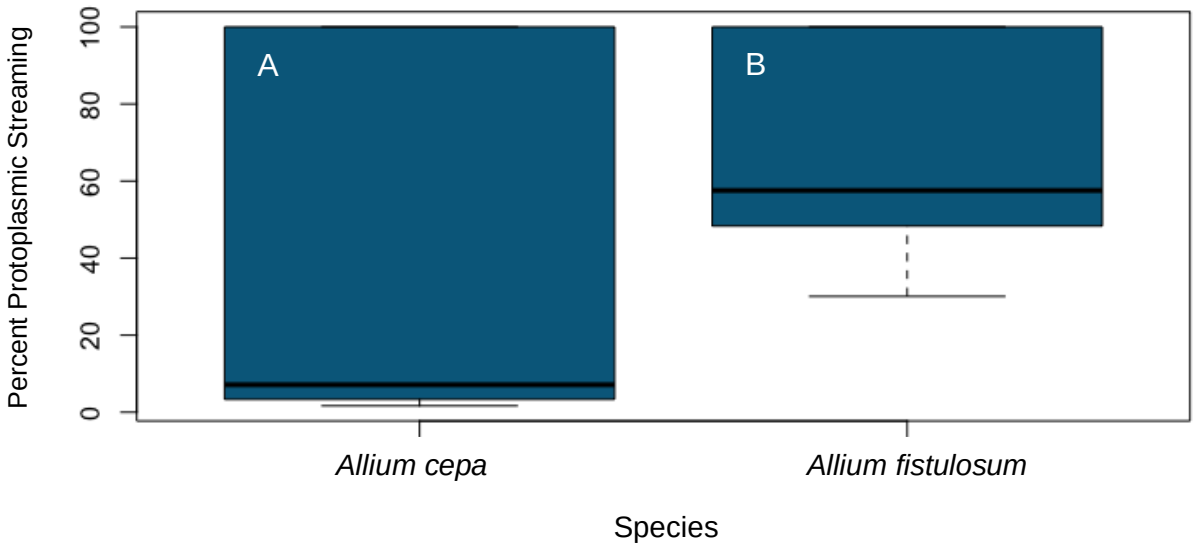

Figure 4.9 Box-pot showing average percent protoplasmic streaming (limit of damage) of *Allium fistulosum* and *Allium cepa* epidermal cell layers after 16-18hr dehydration. Treatment groups (CA and NCA) combined

Boxplot showing average limit of damage based on protoplasmic streaming following dehydration over 16-18hr and subsequent rehydration, with treatment groups (CA and NCA) combined. See Table A22 for statistical analysis.

In addition to analyzing the limit of damage using protoplasmic streaming, fluorescein diacetate was also used. Figure 4.10 provides a reference showing the visual difference between viable vs non-viable *A. fistulosum* cells. The images captured using FDA and fluorescence microscopy confirm epidermal cell layers obtained from *A. fistulosum* sheaths had a lower limit of damage following dehydration stress compared to those obtained from *A. cepa* sheaths. Figures 4.11, 4.12, A11 and A12, show a greener fluorescence in the images of the epidermal cell layers obtained from *A. fistulosum* plants compared to *A. cepa*. In particular, this is more evident after 16hr dehydration (Figure 4.11 and Figure 4.12). Analysis of those images using ImageJ also show images obtained from *A. fistulosum* sheaths had a greater number of green pixels, compared to cell layers obtained from *A. cepa* (Figure 4.13-4.14).

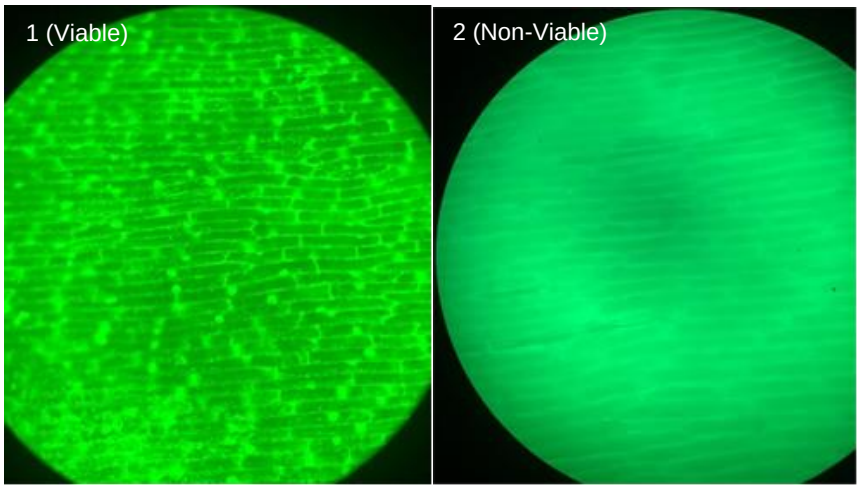

Figure 4.10 *Allium fistulosum* epidermal cells stained with fluorescein diacetate (reference photo with live and dead cells)

Images taken from an *Allium fistulosum* epidermal cell layer stained immediately after removal from the ligule (1) and from an *Allium fistulosum* cell layer that had been dehydrated to the point where no live cells remained (2). Images were taken at 20X using the GFP filter cube and a LEICA DM4 B microscope.

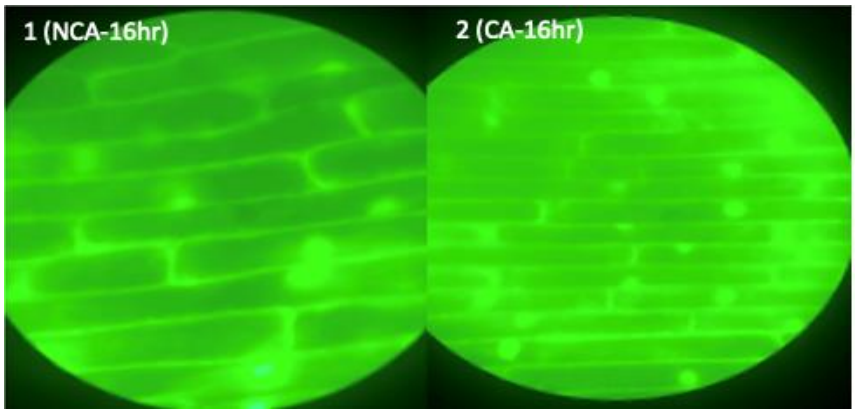

Figure 4.11 *Allium fistulosum* epidermal cells stained with fluorescein diacetate following 16hr dehydration and subsequent rehydration

Allium fistulosum epidermal cell layers stained with fluorescein diacetate. Cell layers had previously been dehydrated for 16hr, followed by rehydration (24hr). Cell layers were obtained from *Allium fistulosum* treated with a 0.05M $CaCl_2$ solution every second day for four-weeks or from non-calcium treated plants. Cells were stained for 5min followed by a wash with PBS. Images from left to right are: 1). Post-16hr dehydration, NCA (-calcium) and 2). Post 16-hr dehydration, CA (+calcium). Images were taken at 40X using the GFP filter cube and a LEICA DM4 B microscope.

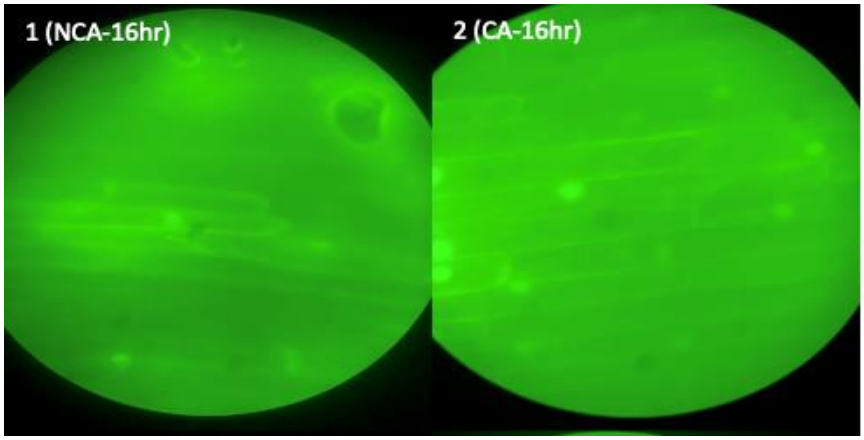

Figure 4.12 *Allium cepa* epidermal cells stained with fluorescein diacetate following dehydration 16hr and subsequent rehydration

Allium cepa epidermal cell layers stained with fluorescein diacetate. Cell layers had previously been dehydrated for 16hr, followed by rehydration (24hr). Cell layers were obtained from *Allium cepa* that had been treated with a 0.05M $CaCl_2$ solution every second day for four-weeks or from non-calcium treated plants. Cells were stained for 5min followed by a wash with PBS. Images from left to right are: 1). Post-16hr dehydration, NCA (-calcium) and 2). Post 16-hr dehydration, CA (+calcium). Images were taken at 40X using the GFP filter cube and a LEICA DM4 B microscope.

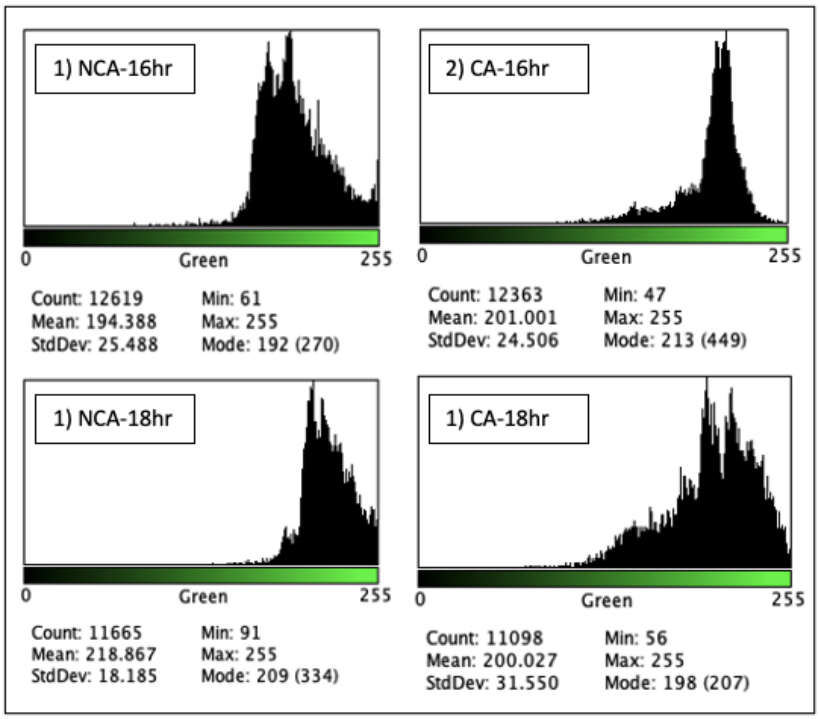

Figure 4.13 Analysis of green pixels captured in images of *Allium fistulosum* epidermal cell layers stained with fluorescein diacetate

Analysis of green pixels captured in images of *Allium fistulosum* epidermal cell layers stained with fluorescein diacetate following dehydration (16hr and 18hr) and subsequent rehydration (24hr). Graphs from left to right: 1). Post-16hr dehydration, NCA (-calcium), 2). Post 16-hr dehydration, CA (+calcium), 3). Post-18hr dehydration, NCA (- calcium), and 4). Post 18-hr dehydration, CA (+calcium). Graphs were generated using ImageJ (Version 1.53a).

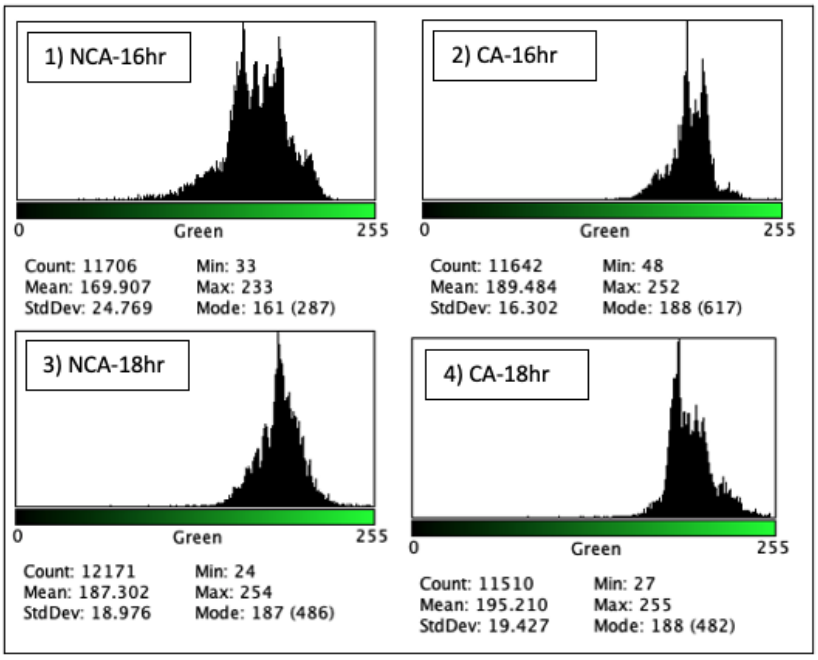

Figure 4.14 Analysis of green pixels captured in images of *Allium cepa* epidermal cell layers stained with fluorescein diacetate

Analysis of green pixels captured in images of *Allium cepa* epidermal cell layers stained with fluorescein diacetate following dehydration (16hr and 18hr) and subsequent rehydration (24hr). Graphs from left to right: 1). Post-16hr dehydration, NCA (-calcium), 2). Post 16-hr dehydration, CA (+calcium), 3). Post-18hr dehydration, NCA (- calcium), and 4). Post 18-hr dehydration, CA (+calcium). Graphs were generated using ImageJ (Version 1.53a).

In addition, when just a single layer of *A. fistulosum* epidermal cells was dehydrated, calcium application was also found to significantly ($p<0.05$) improve percent protoplasmic streaming after 16hr dehydration, thus reducing the limit of damage (Figure 4.15, Table A26 and Table A27). However, the effect of calcium on reducing water loss in a single layer of epidermal cells dehydrated over 12-24hr or more specifically at the 16hr time point was not significant ($p>0.05$) (Figure 4.15, Table A28 and Table A29). In contrast, calcium under no circumstances improved *A. cepa*'s ability to withstand long term dehydration stress (Figure 4.6, Figure 4.8, Table A21 and Table A25).

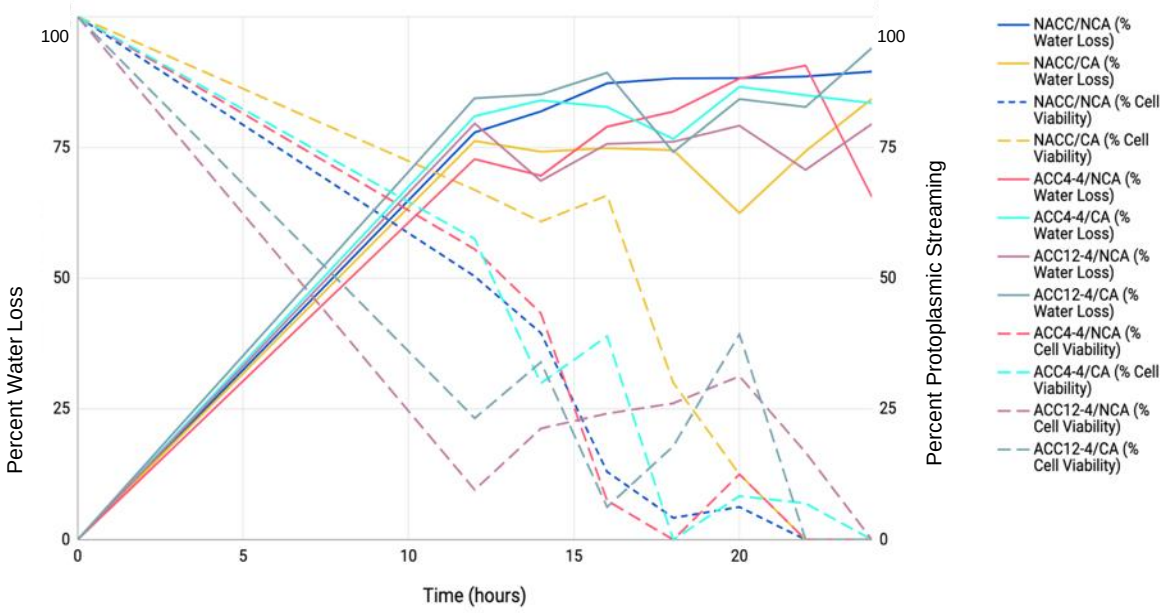

Figure 4.15 Percent water loss over 12-24hr dehydration and subsequent percent protoplasmic streaming in *Allium fistulosum* epidermal cell layers

Percent water loss and limit of damage (based on protoplasmic streaming) over 24 hours in an *Allium fistulosum* epidermal cell layer. In total, 6 treatment groups were examined: 1) 1) NACC/NCA (no cold acclimation, -$CaCl_2$), 2) NACC/CA (no cold acclimation, +$CaCl_2$), 3) ACC4-4/NCA (4°C /4°C cold acclimation, -$CaCl_2$), 4) ACC4-4/CA (4°C /4°C cold acclimation, +$CaCl_2$), 5) ACC12-4/NCA (12°C /4°C cold acclimation, -$CaCl_2$), 6) 6) ACC/CA (12°C /4°C cold acclimation, +$CaCl_2$). *Allium fistulosum* plants acclimated at 4°C /4°C had a 12hr photoperiod, while plants acclimated at 12°C /4°C had an 8hr photoperiod. Cold acclimation was performed over 2 weeks. Plants treated with calcium received 0.05M of $CaCl_2$ every second day for 4 weeks. Differences in percent water loss and percent protoplasmic streaming were non-significant ($p>0.05$), with the exception of percent protoplasmic streaming following 16hr dehydration ($p<0.05$).

However, over 15min, calcium application was found to significantly ($p<0.05$) reduce percent water loss in *A. cepa* (Figure 4.4, Figure 4.16 and Table 4.2). This was in contrast to a surprising finding in *A. fistulosum* where all treatments were found to significantly ($p<0.05$) increase percent water loss over 15min (Figure 4.17, Figure 4.18 and Table 4.3). While all of the aforementioned findings were significant ($p<0.05$), it should be noted that the effect sizes were small (Table A30 and Table A31).

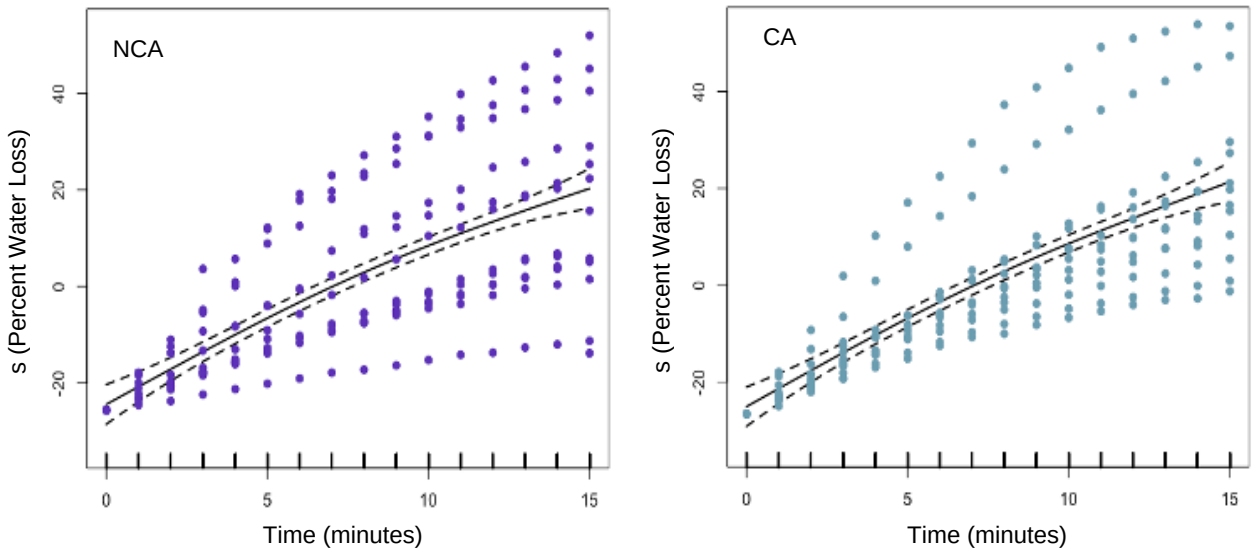

Figure 4.16 Generalized additive models showing relationship between time (15min) and percent water loss in control and calcium treated *Allium cepa* epidermal cells

Relationship between time (min) and percent water loss between NCA *Allium cepa* (non-calcium treated, control) and CA *Allium cepa* (calcium treated) over a 15-minute period. Dark solid lines indicate the mean value for the response variable. Dotted lines indicate 95% confidence intervals around the predicted values. Individual dots are representative of single data points collected in each replicate of the experiment (n=12). Values on the y-axis have been smoothed, as indicated by the "s" on the label. See Tables 4.2 and A32 for statistical analysis.

Table 4.2 ANOVA ran on a generalized additive model (GAM) examining percent water loss over 15min in *Allium cepa* (dehydration of single epidermal cell layer)

Results from an ANOVA ran on a GAM examining calcium application (CA), with respect to average water loss over 15 minutes in *Allium cepa* epidermal cells. Information in this table was obtained from the GAM with the lowest AIC. $p<0.05$ is significant.

Smoothed Effect	**General Effect**	**EDF**	**Ref.df**	**F-value**	**P-value**
	Calcium		1	127.8	7.16e-10
s(Time): NCA		5.128	6.232	7245	<2e-16
s(Time): CA		5.900	7.056	6853	<2e-16

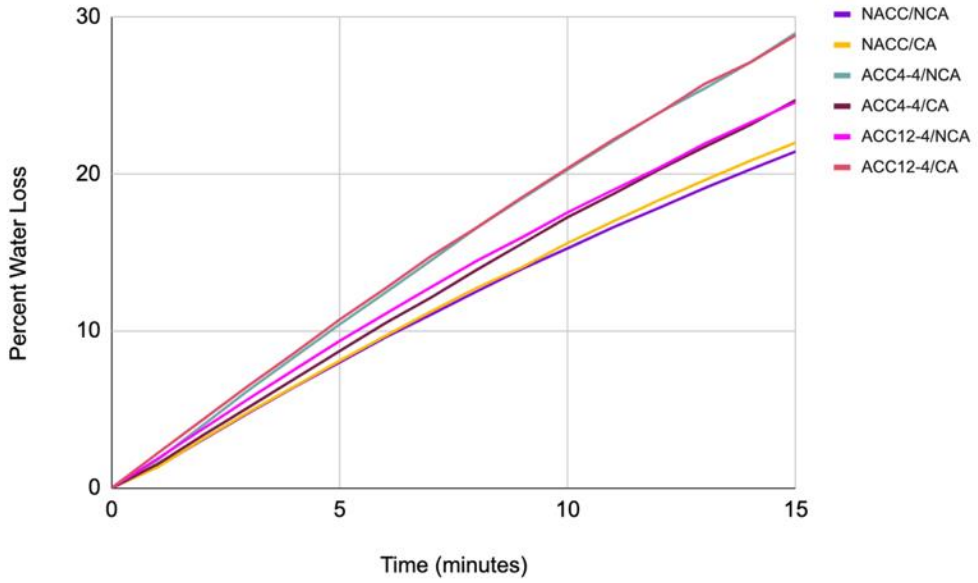

Figure 4.17 Percent water loss over 15 minutes in epidermal cell layers obtained from *Allium fistulosum* that were cold acclimated and/or calcium treated

Percent water loss over 15 minutes in the *Allium fistulosum* epidermal cell layer. In total, 6 treatment groups were examined: 1) NACC/NCA (no cold acclimation, -$CaCl_2$), 2) NACC/CA (no cold acclimation, +$CaCl_2$), 3) ACC4-4/NCA (4°C /4°C cold acclimation, -$CaCl_2$), 4) -$CaCl_2$), 4) ACC4-4/CA (4°C /4°C cold acclimation, +$CaCl_2$), 5) ACC12-4/NCA (12°C /4°C cold acclimation, -$CaCl_2$), 6) ACC/CA (12°C /4°C cold acclimation, +$CaCl_2$). *Allium fistulosum* plants acclimated at 4°C /4°C had a 12hr photoperiod, while plants acclimated at 12°C /4°C had an 8hr photoperiod. Cold acclimation was done for 2 weeks. Plants treated with calcium received 0.05M of $CaCl_2$ every second day for 4 weeks.

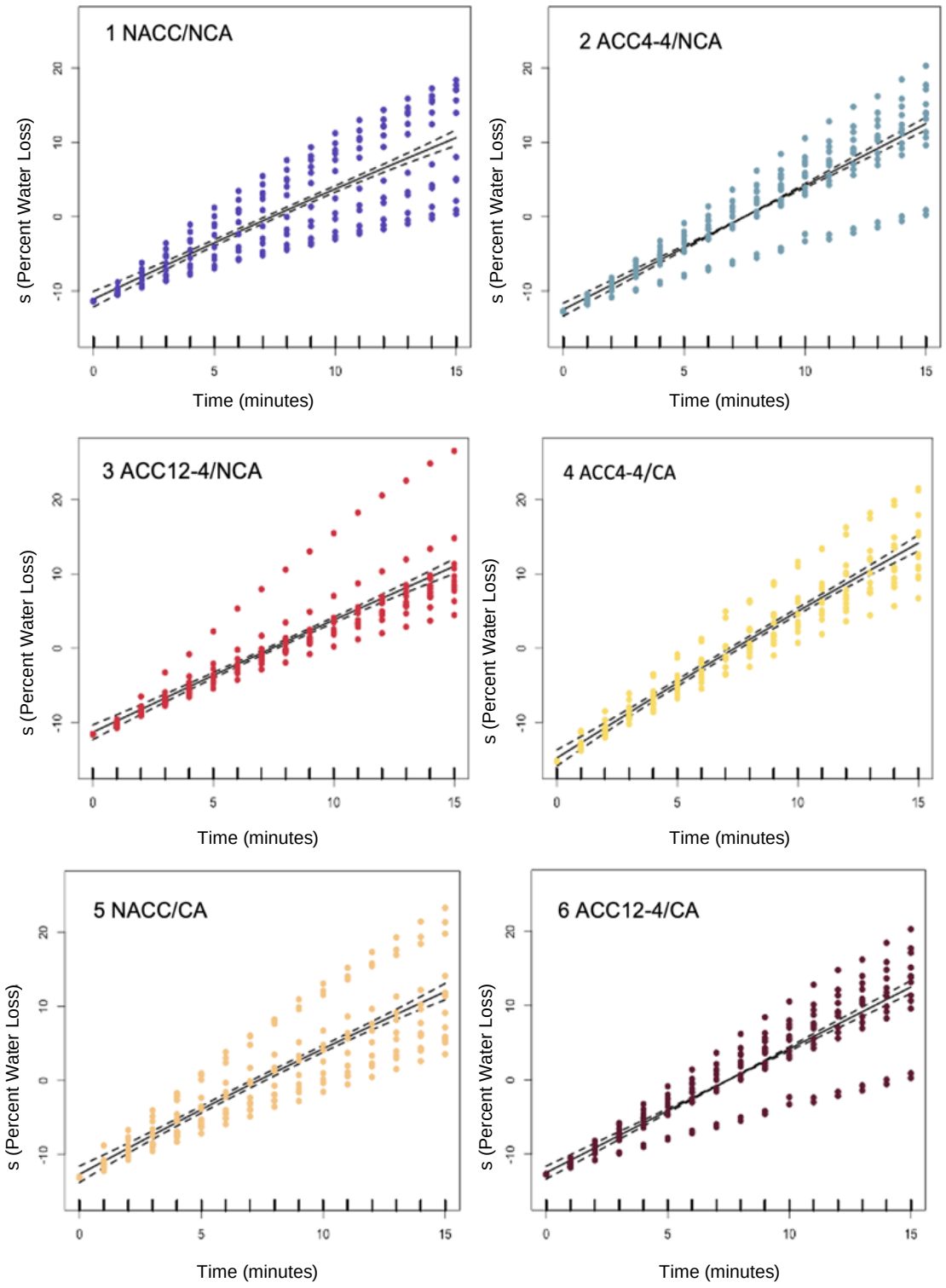

Figure 4.18 Generalized additive models showing relationship between time (15min) and percent water loss in *Allium fistulosum* epidermal cells obtained from cold acclimated and/or calcium treated plants

Relationship between time (min) and percent water loss for each of the 6 treatment combinations over a 15 minute period: 1) NACC/NCA (no cold acclimation, -$CaCl_2$), 2) ACC4-4/NCA (4°C /4°C cold acclimation, -$CaCl_2$), 3) ACC12-4/NCA (12°C /4°C cold acclimation, -$CaCl_2$), 4) ACC4-4/CA (4°C /4°C cold acclimation, +$CaCl_2$), 5) NACC/CA (no cold acclimation, +$CaCl_2$), 6) ACC12-4/CA (12°C /4°C cold acclimation, +$CaCl_2$). Dark solid lines indicate the mean value for the response variable. Dotted lines indicate 95% confidence intervals around the predicted values. Individual dots are representative of single data points collected in each replicate of the experiment (n=12). Values on the y-axis have been smoothed, as indicated by the "s" on the label. See Tables 4.3 and A33 for statistical analysis.

Table 4. 3 ANOVA ran on a generalized additive model (GAM) examining percent water loss over 15min in *Allium fistulosum* (dehydration of single epidermal cell layer)

Results from an ANOVA ran on a GAM examining calcium application (CA) and cold acclimation (ACC) along and in partnership, with respect to average water loss over 15 minutes in *Allium fistulosum* epidermal cells. Information in this table was obtained from the GAM with the lowest AIC. $p<0.05$ is significant.

Data Selection	**General Effect**	**Smoothing Effect**	**EDF**	**Ref.df**	**F-value**	**P-value**
Combined Treatments	Combined Treatment			5	15517	<2e-16
		s(Time): NACC/ NCA	6.922	8.006	31437	<2e-16
		s(Time): ACC4-4/ NCA	8.315	8.870	51402	<2e-16
		s(Time): ACC12-4/ NCA	4.130	5.088	63748	<2e-16
		s(Time): ACC4-4/ CA	6.128	7.283	45682	<2e-16
		s(Time): ACC12-4/ CA	4.630	5.671	78707	<2e-16
		s(Time): NACC/ CA	8.191	8.822	30212	<2e-16

Furthermore, when a single layer of *A. fistulosum* epidermal cells were dehydrated over 12-24hr, neither cold acclimation alone nor in conjunction with calcium application significantly increased tolerance to dehydration stress (Figure 4.15, Table A26 and Table A28). Overall, all of the treatments were found to either increase percent water loss, increase the limit of damage or do both.

4.3.3 *Arabidopsis thaliana* Water Loss

Genotypes with mutations in boron transporters consistently had the highest percent water loss over both short-term and long-term periods of water loss (Figure 4.19, Figure 4.21 and Figure 4.23). Over 15min, *nip5-1* and *nip6-1*, two genotypes with mutations in boron transporters, had the greatest overall percent water loss compared to Col-0 and *p35S::PMEI5* (Figure 4.19 and Figure 4.20). All genotypes lost a significant ($p<0.05$) amount of water over 15min (Figure 4.20 and Table 4.4). However, the effect sizes were small (Table A34).

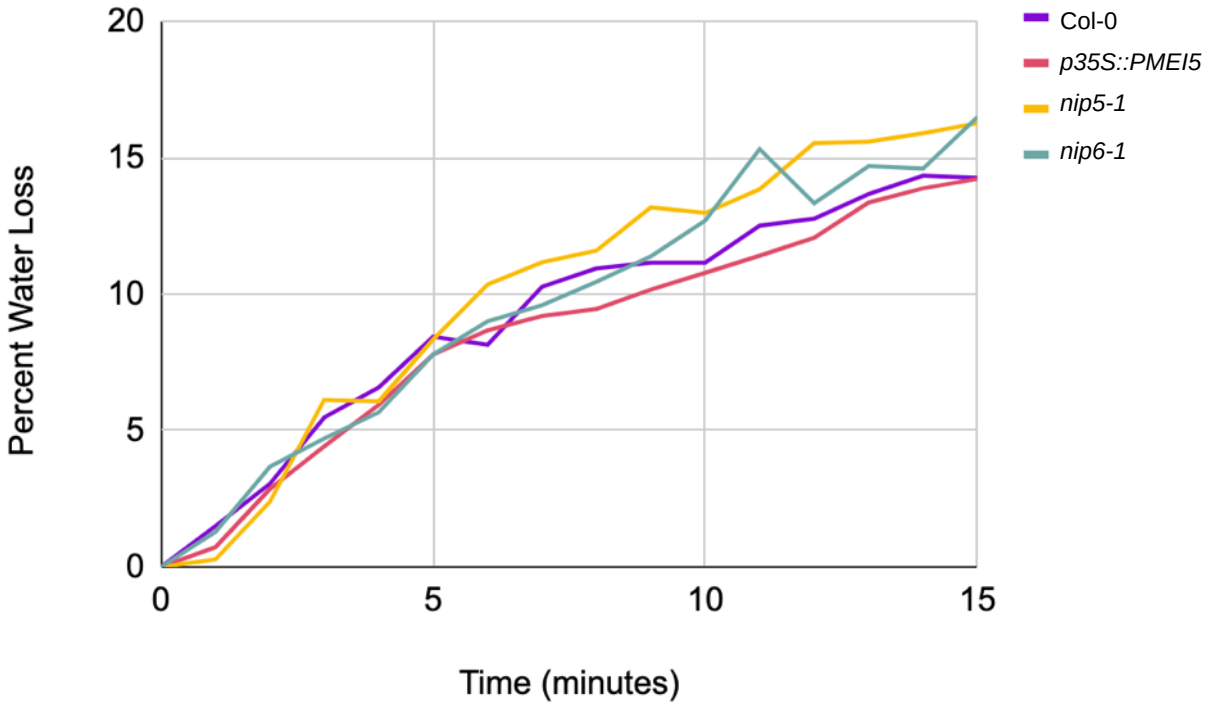

Figure 4. 19 Percent water loss over 15 minutes in various *Arabidopsis thaliana* genotypes (*nip5-1*, *nip6-1*, *p35S::PMEI5* and Col-0)

Percent water loss over 15 minutes in various *Arabidopsis thaliana* genotypes. In total, 4 genotypes were analyzed: 1) *nip5-1* (boron transporter mutant), 2) *nip6-1* (boron transporter mutant), 3) *p35S::PMEI5* (Pectin methylesterase inhibitor overexpressing mutant) and 4) Col-0 (wildtype).

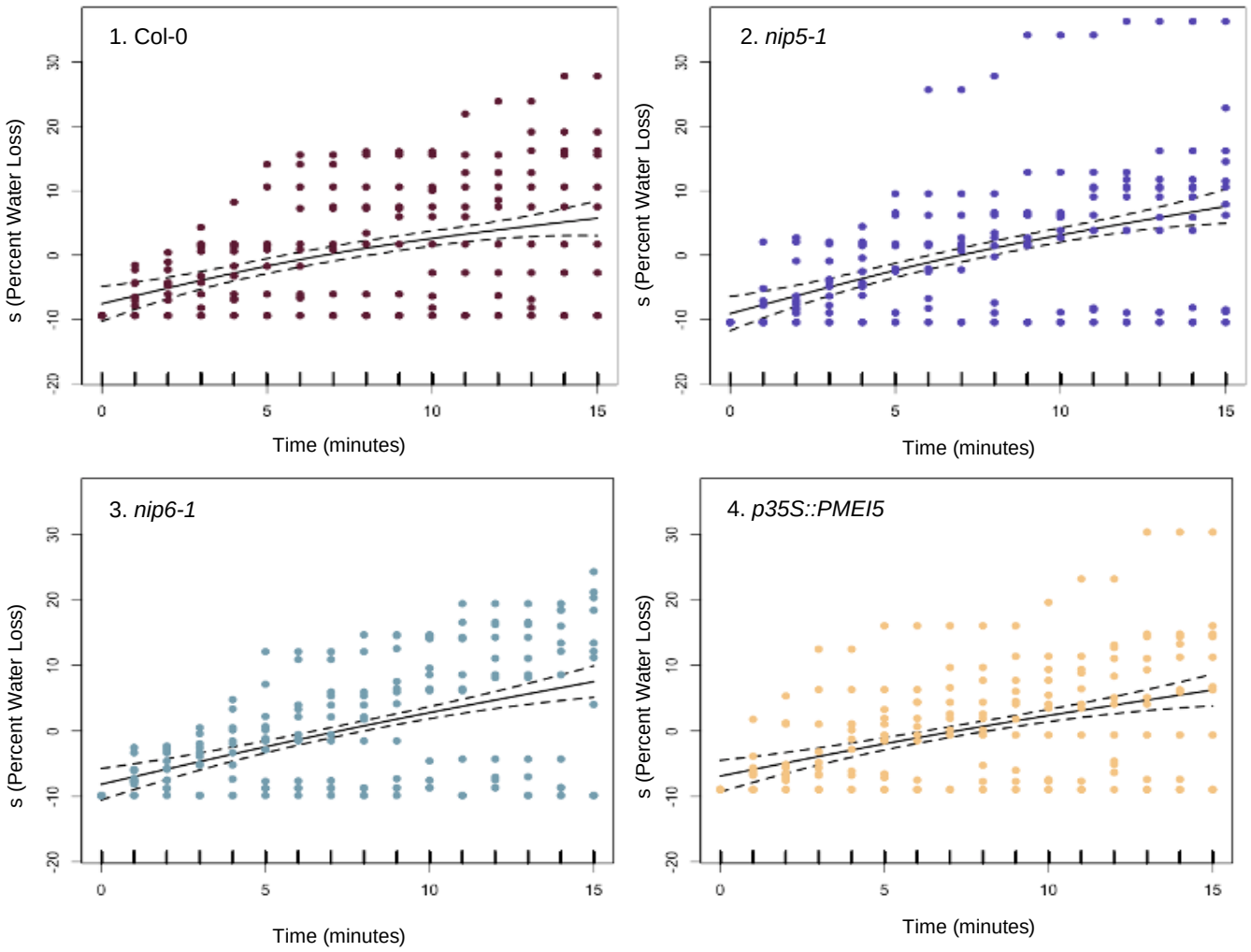

Figure 4.20 Generalized additive models showing relationship between time (15min) and percent water loss in in various *Arabidopsis thaliana* genotypes (*nip5-1*, *nip6-1*, *p35S::PMEI5* and Col-0)

Relationship between time (min) and percent water loss between *Arabidopsis thaliana* genotypes of interest: 1) Col-0 (wild-type), 2) *nip5-1*, 3) *nip6-1* and 4) *p35S::PMEI5*. Dark solid lines indicate the mean value for the response variable. Dotted lines indicate 95% confidence intervals around the predicted values. Individual dots are representative of single data points collected in each replicate of the experiment (n=12). Values on the y-axis have been smoothed, as indicated by the "s" on the label. See Tables 4.4 and A35 for statistical analysis.

Table 4.4 ANOVA ran on a generalized additive model (GAM) examining percent water loss over 15min in *Arabidopsis* genotypes

Results from an ANOVA ran on a GAM examining various *Arabidopsis thaliana* genotypes, with respect to average water loss over 15 minutes. Information in this table was obtained from the GAM with the lowest AIC. $p<0.05$ is significant.

General Effect	**Smoothing Effect**	**EDF**	**Ref.df**	**F-value**	**P-value**
Genotype			3	20.8	9.79e-09
	s(Time): *nip5-1*	3.203	3.976	349.2	<2e-16
	s(Time): *nip6-1*	2.786	3.465	345.6	<2e-16
	s(Time): *p35S::PMEI5*	3.597	4.452	207.9	<2e-16
	s(Time): Col-0	3.147	3.907	241.3	<2e-16

When the duration of water loss was extended beyond 15min to 2-10hr, no significant ($p>0.05$) differences amongst the genotypes in either percent water loss or percent electrolyte leakage were observed (Figure 4.21, Figure 4.22, Table A36 and A37). However, genotypes with mutations in boron transporters continued to have amongst the highest values of percent water loss and percent electrolyte leakage (Figure 4.21 and Figure 4.22). On the other hand, the *p35S::PMEI5* genotype continued to appear to be more dehydration tolerant compared to the other genotypes (Figure 4.21 and Figure 4.22). *p35S::PMEI5* had amongst the lowest percent water loss values and the lowest percent electrolyte leakage (Figure 4.21 and Figure 4.22).

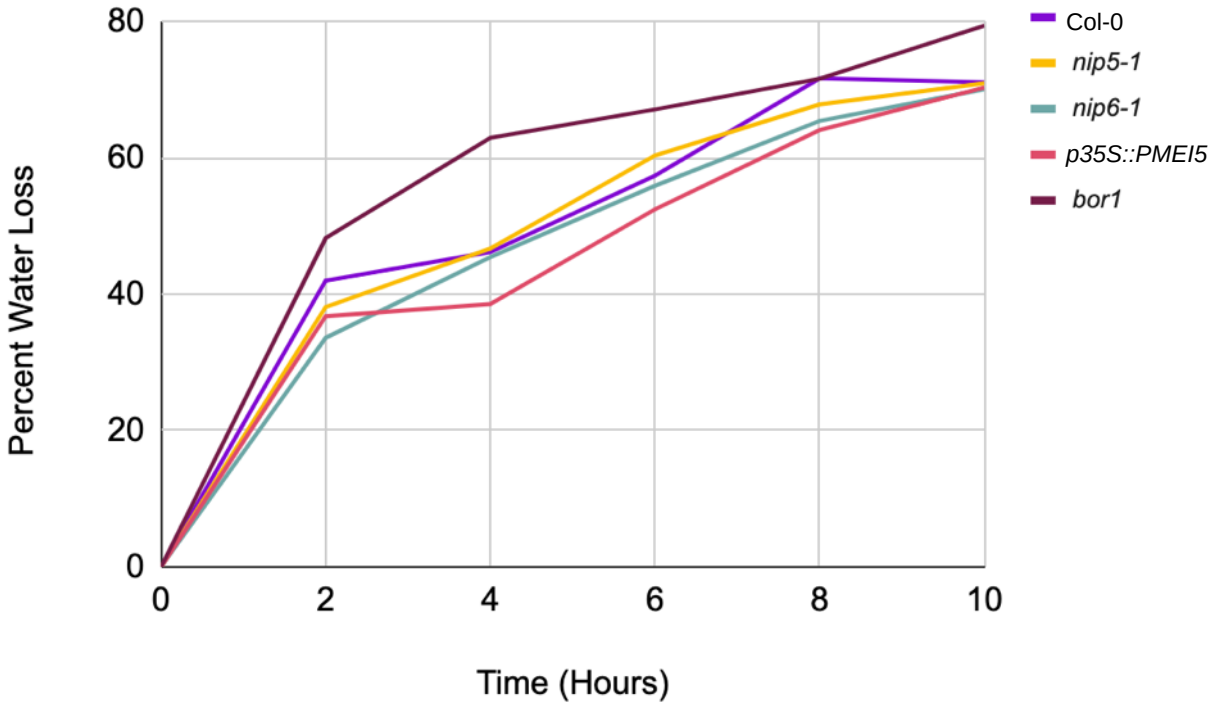

Figure 4.21 Percent water loss over 2-10hr in various *Arabidopsis thaliana* genotypes (*nip5-1*, *nip6-1*, *bor1*, *p35S::PMEI5* and Col-0)

Percent water loss over 2-10hr in various *Arabidopsis thaliana* genotypes. In total, four genotypes were analyzed: 1) *nip5-1* (boron transporter mutant), 2) *nip6-1* (boron transporter mutant), 3) *p35S::PMEI5* (PMEI mutant) and 4) Col-0 (wildtype). Differences in percent water loss between genotypes were non-significant ($p>0.05$).

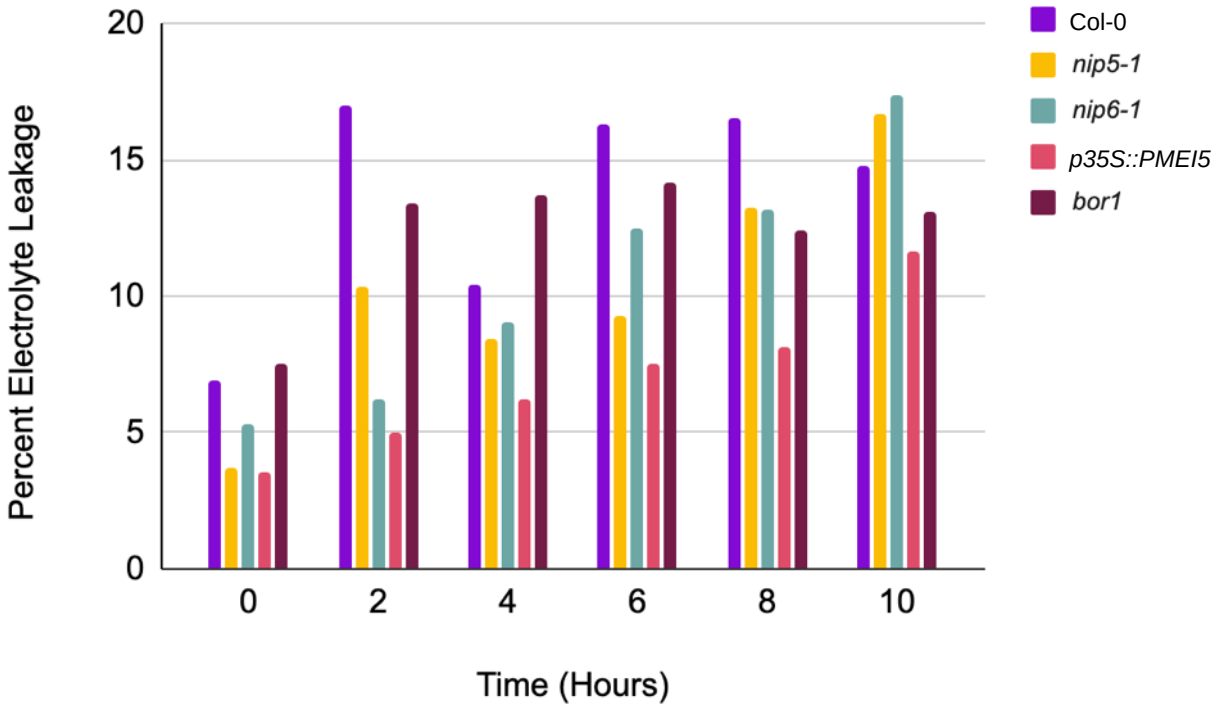

Figure 4.22 Average percent electrolyte leakage from various *Arabidopsis thaliana* genotypes (*nip5-1*, *nip6-1*, *bor1*, *p35S::PMEI5* and Col-0) after 2-10hr dehydration and subsequent rehydration

Percent electrolyte leakage from various *Arabidopsis thaliana* genotypes (*bor1* [boron transporter mutant], *nip5-1* [boron transporter mutant], *nip6-1* [boron transporter mutant], *p35S::PMEI5* [PMEI mutant] and Col-0 [wildtype]) after a period of dehydration between 2-10hr and subsequent rehydration. Differences in percent electrolyte leakage between genotypes were non-significant ($p>0.05$).

When the duration of water loss was further extended from 2-10hr to 12-24hr, these trends continued. While again, there were no significant ($p>0.05$) differences in percent water loss amongst the genotypes, both boron transporters mutants (*nip5-1* and *nip6-1*) had the highest percent water loss (Figure 4.23 and Table A38). *p35S::PMEI5* continued to have a higher tolerance to dehydration, having a significantly ($p<0.05$) lower overall percent electrolyte leakage (indicating a decrease in the limit of damage) compared to the other genotypes (Figure 4.24, Figure 4.25, Table A39 and Table A40). Following a 24hr period of water loss, *p35S::PMEI5* had a percent electrolyte leakage of 17.0%, while Col-0, *nip5-1* and *nip6-1* collectively had a percent electrolyte leakage greater than 30% (Figure 4.24). Furthermore, while the effect size for the majority of the relationships between the genotypes was less than 0.8, the relationship between

Col-0 & *p35S::PMEI5 and nip5-1* & *p35S::PMEI5* had an effect size above 0.8 (Table A41). An effect size of 0.8 is considered large and acceptable (Lakens, 2013; Cohen, 1988).

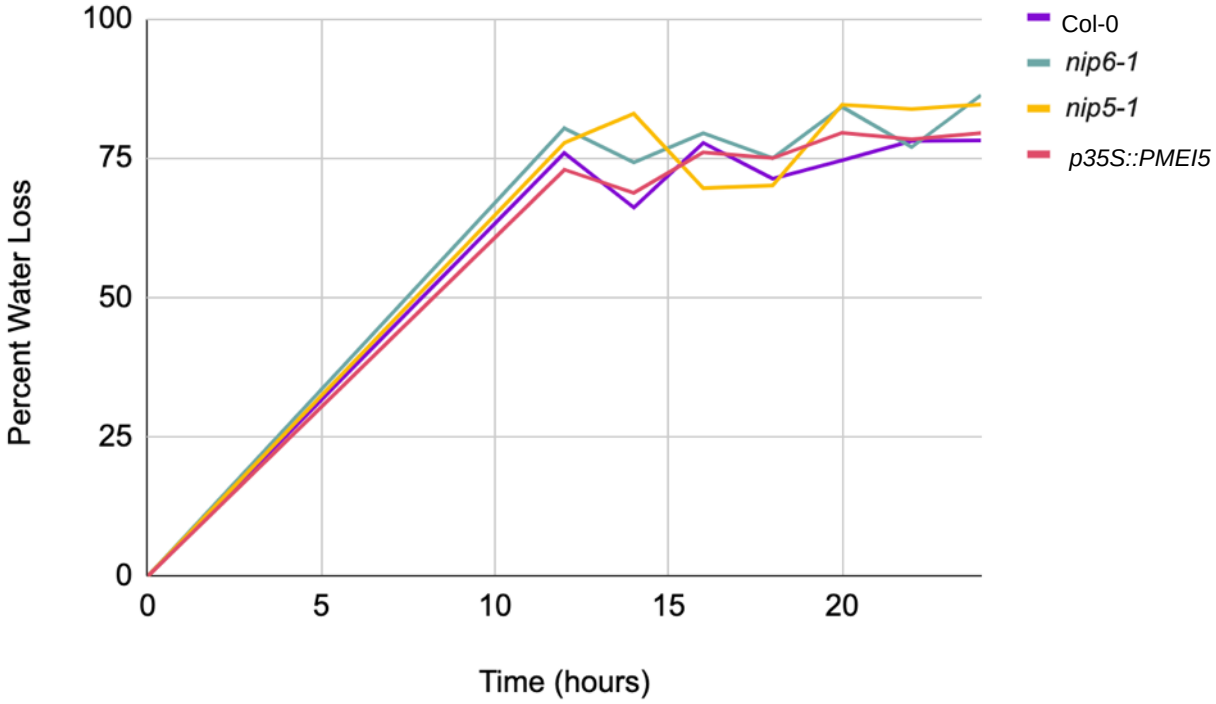

Figure 4.23 Percent water loss over 12-24hr in various *Arabidopsis thaliana* genotypes (*nip5-1*, *nip6-1*, *p35S::PMEI5* and Col-0)

Percent water loss over 12-24hr in various *Arabidopsis thaliana* genotypes. In total, four genotypes were analyzed: 1) *bor1* [boron transporter mutant], 2) *nip5-1* [boron transporter mutant], 3) *nip6-1* [boron transporter mutant], 4) *p35S::PMEI5* [PMEI mutant] and 5) Col-0 [wildtype]). Differences in percent water loss between genotypes were non-significant ($p>0.05$).

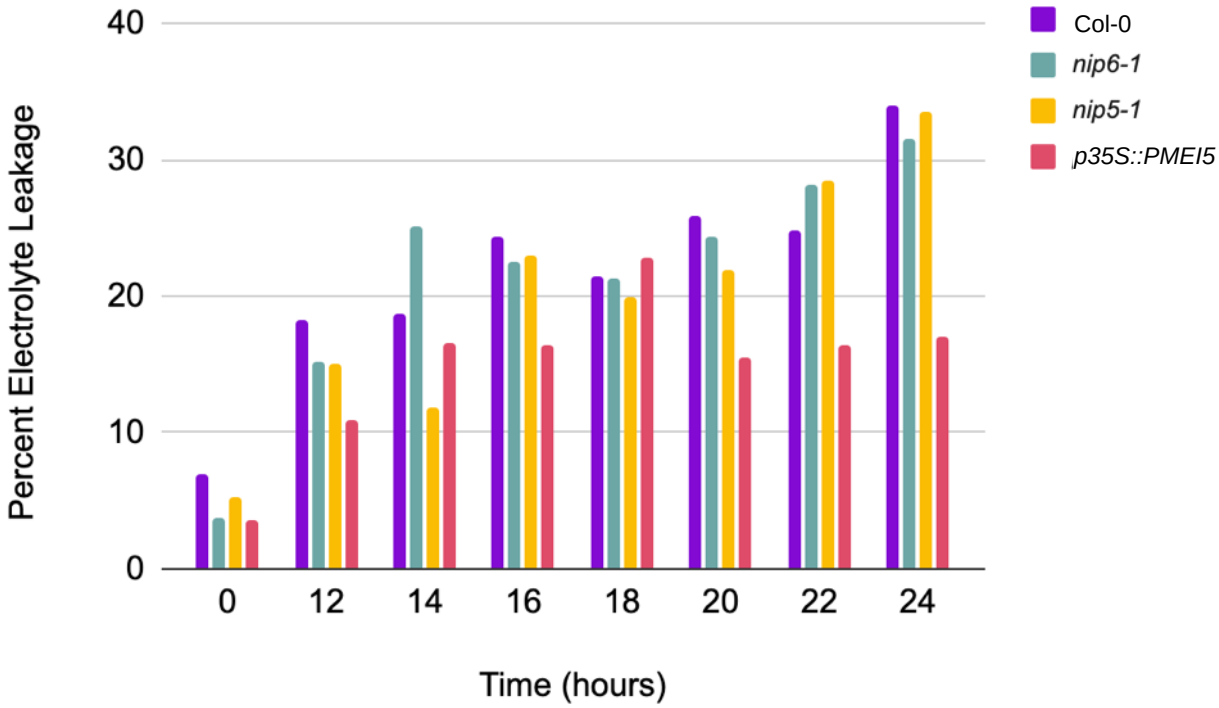

Figure 4. 24 Average percent electrolyte leakage from various *Arabidopsis thaliana* genotypes (*nip5-1*, *nip6-1*, *p35S::PMEI5* and Col-0) after 12-24hr dehydration and subsequent rehydration

Average percent electrolyte leakage from various *Arabidopsis thaliana* genotypes (*nip5-1* [boron transporter mutant], *nip6-1* [boron transporter mutant], *p35S::PMEI5* [PMEI mutant] and Col-0 [wildtype]) after a period of dehydration between 12-24hr and subsequent rehydration.

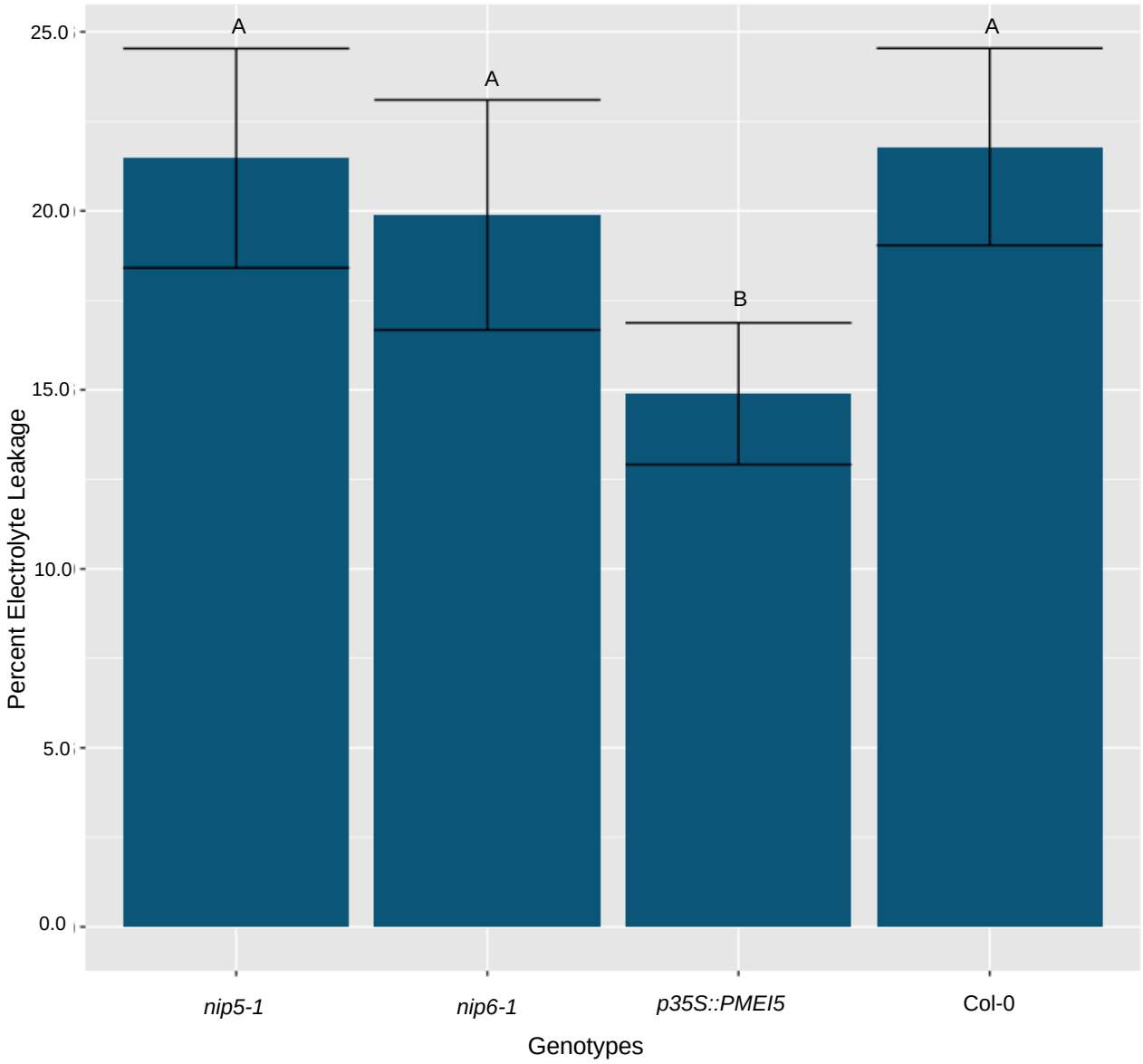

Figure 4. 25 Average percent electrolyte leakage from various *Arabidopsis thaliana* genotypes after 12-24hr dehydration and subsequent rehydration- Figure for Tukey test

Average percent electrolyte leakage from various *Arabidopsis thaliana* genotypes (*nip5-1* [boron transporter mutant], *nip6-1* [boron transporter mutant], *p35S::PMEI5* [PMEI mutant] and Col-0 following dehydration over a 12-24hr period and subsequent rehydration. Error bars represent standard error. See Table A40 for statistical analysis.

4.4 Discussion

4.4.1 Pectin Water Loss

Given the mechanical changes noted in Chapter 3 in pectin viscosity or strength, the first step in this chapter was to analyze water loss in pure pectin. The goal of this experiment was to establish

clear relationships between pectin type, concentration and the presence/ absence of boron or calcium and with that goal in mind, results from this experiment do clearly show certain trends.

Since calcium application was found to increase viscosity as concentration increased presumably as a result of the formation of "egg-box" structures, calcium application was found to have the same effect on percent water loss in pectin. The more pronounced impact of calcium on 8% high methylated pectin in comparison to GENU BETA pectin at the same concentration is likely due to the difference in overall pectin composition between the two. As previously mentioned, the high methylated pectin standard comes from citrus pectin, while the GENU BETA pectin is derived from sugar beets. Naturally, citrus pectin contains more HG, while sugar beet pectin contains more RG-II (Yapo et al., 2007; Zhemerichkin & Ptitchkina, 1995). Thus, despite the fact the citrus pectin is highly methylated, and "egg-box" structures can only form on demethylated HG, the high methylated (69-75% methylation) pectin is still likely more conducive to the formation of "egg-box" structures (Wormit & Usadel, 2018; Braccini & Pé Rez, 2001; Ravanat & Rinaudo, 1980). Ravant and Rinaudo (1980) noted, the gelatinization of pectin has been found to occur as a result of interactions between calcium ions and blocks of galacturonic acid. Therefore, it is plausible that increased gelatinization occurred in these pectin solutions led to a reduction in percent water loss across the period of dehydration.

While boric acid is also known to influence the structure of the cell wall by way of the formation of RG-II dimers, the impact of boric acid on reducing water loss was lower in comparison to calcium and less consistent (O'Neill et al., 2004; Ishii et al., 2001; Matoh, 1997). The addition of boron was only found to reduce percent water loss in 8% GENU BETA pectin by 4.0%. This is a smaller reduction in water loss in comparison to that observed following the addition of calcium (5.4%) to the same pectin, despite GENU BETA pectin presumably having more RG-II in comparison to the high methylated citrus pectin. This finding suggests that the formation of RG-II dimers is likely not as effective as "egg-box" structures in holding water within the pectin matrix. While there do not appear to be any studies of this nature within the current body of the literature, it is well known that HG is the most common form of pectin, while RG-II is the third-most common (Mohnen, 2008). Therefore, it is plausible that "egg-box" structures are more abundant within

pectin in comparison to RG-II dimers and as a result have a greater influence on the ability for the pectin matrix to withhold water.

Furthermore, the addition of boron was found to increase overall percent water loss in other pectin solutions (4% high methylated pectin, 4% GENUA BETA pectin and 8% high methylated pectin). This increase in overall percent water loss was most notable in 8% high methylated pectin, as the addition of boric acid increased overall percent water loss by 4.6%. This finding is of particular interest because 8% high methylated pectin with boron was found to have the highest viscosity of all pectin solutions in Chapter 3. Therefore, this calls into question whether there is a direct link between pectin viscosity and the ability for the pectin matrix to hold onto water.

While pectin makes up between 30-50 % of the cell wall and this experiment explored 4% and 8% pectin, the general trend of reduced water loss with increasing concentration does suggest that at a 35% concentration, pectin would have an even greater ability to hold onto water (Cosgrove & Jarvis, 2012). Furthermore, the impact of calcium on reducing water loss as pectin concentration increased is also suggestive that at a higher pectin concentration, calcium would likely have an even greater influence on reducing water loss. At a 4% concentration, calcium application increased water loss by 0.9% after 6hr, however at an 8% concentration, calcium application reduced water loss by 14.1%. Therefore, hypothetically at a concentration of 35%, the addition of calcium would result in a greater than a 30% reduction in percent water loss after 6hr. However, the cell wall and biological systems as a whole are more complex than pure pectin standards. Therefore, we are not able to make concrete predictions as to the role of pectin within the cell wall during dehydration stress based on extrapolations from this data. Nevertheless, the findings from this experiment suggest the addition of calcium and to a lesser extent boron, would reduce water loss in plants during dehydration stress as a result of their likely interactions with HG and RG-II and the resulting changes within the cell wall.

4.4.2 *Allium* Water Loss

The connection between the observations in dehydration stress tolerance in *A. fistulosum* and *A. cepa* and the abilities for these species to tolerate cold stress is an extremely valuable finding and one of great interest that should be further explored. As previously mentioned, *A. cepa* is known

to be a stress sensitive species, in comparison to *A. fistulosum*, as *A. cepa* lacks the ability to cold acclimate and has a low tolerance to cold stress (Tanino et al., 2013; Palta et al., 1977). In comparison, *A. fistulosum* is able to tolerate extreme freezing conditions, and also has been shown to have the ability to cold acclimate (Tanino et al., 2013). Previous research from the Tanino lab has demonstrated when *A. fistulosum* was cold acclimated for two-weeks at 12ºC/4ºC (day/night), freezing resistance increased from an LT50 of -12ºC to -27ºC (Liu, 2015). A similar pattern was observed in tolerance of water loss over 16-18hr. In general, *A. fistulosum* not only lost significantly ($p<0.05$) less water after 18hr in comparison to *A. cepa*, but *A. fistulosum* epidermal cells showed a significantly ($p<0.05$) higher percent protoplasmic streaming (reduced limit of damage) following water loss. More specifically without taking into account treatment, after 16hr of water loss, percent protoplasmic streaming in *A. cepa* had plummeted to 7.1%, while the general percent protoplasmic streaming of *A. fistulosum* epidermal cells was much greater (57.5%). While at first glance the importance of the connection between tolerance to water loss and cold stress may seem unclear, the ability for a plant to withstand both of these stresses is critical.

First of all, during cold stress, formation of ice in the extracellular space can result in dehydration stress (Burke et al., 1976). While this dehydration stress may be tolerable to a certain extent, dehydration beyond the tolerable limit may cause cell collapse, resulting in irreversible cellular damage and death (Arora, 2018; Burke et al., 1976). Therefore, the ability for a plant to not only tolerate extreme freezing but dehydration as well may increase the tolerable limit for dehydration stress during extracellular ice formation. The potential for a plant to tolerate both cold stress and dehydration stress is also valuable through the lens of climate change. While increased warming is consistently associated with climate change, the risk of frost damage to plants is also predicted to increase (Gu et al., 2008). Thus, this potential link between resistance to these two stresses may be of great value in the race to find effective solutions for plants against multiple stresses.

While there appears to be a link between dehydration stress and freezing stress tolerance as demonstrated by *A. fistulosum* and contrasting *A. cepa*, the connection between the effect of calcium on enhancing resistance to dehydration stress is less clear. Despite the fact that calcium application influenced mechanical properties of pectin and *A. fistulosum* sheaths, as demonstrated in Chapter 3, for the most part there was a lack of significant ($p>0.05$) differences in the effect of

calcium application on percent water loss. Calcium only significantly ($p<0.05$) decreased water loss over 15min in *A. cepa*, however in *A. fistulosum* calcium application increased water loss. While these results were significant ($p<0.05$), the effect size was small, thus calling into question the true significance of the effect.

However, as periods of dehydration are typically long and drawn out, the findings from the analysis of water loss over 16-18hr provide a better insight into the effect of calcium in enhancing dehydration stress tolerance. A range of studies have previously found results supporting the efficacy of calcium application in enhancing tolerance to drought stress. Hosseini et al. (2019) explored the role of calcium application on enhancing drought stress tolerance in sugar beet, ultimately discovering calcium application increased plant biomass, sucrose transport and in turn concentration, as well as mitigating oxidative stress. Calcium application also enhanced drought stress tolerance in *Nicotiana tabacum* (Hu et al, 2018). Hu et al. (2018) found calcium application was beneficial in a multitude of ways including stabilizing the structure and function of organelles within the mesophyll cells and maintaining normal leaf net photosynthetic rate and gas exchange. Wheat has also been found to have enhanced drought stress tolerance as a result of calcium application (Khushboo et a., 2018).

Despite calcium application enhancing drought stress tolerance in a wide range of species, resistance to dehydration stress, a component of drought stress, was not improved in *A. cepa* or *A. fistulosum* following calcium application. Over 16-18hr, calcium application had a non-significant ($p>0.05$) effect on percent water loss and percent protoplasmic streaming in *A. cepa*. While in *A. fistulosum*, calcium application did slightly improve percent water loss and percent protoplasmic streaming when the entire sheath was dehydrated, the only significant ($p<0.05$) effect of calcium was on percent protoplasmic streaming at 16hr when a single epidermal cell layer was dehydrated. This may have been the result of a masking of treatment effect due to the larger volume of water stored in the whole sheath. Future experiments should be conducted analyzing other processes involved in dehydration stress to further confirm the efficacy or lack thereof in calcium's ability to reduce water loss in *Allium* species.

Our lab has previously used the 12ºC/4ºC (day/night) cold acclimation regime to acclimate *A. fistulosum* and found that in cold acclimated plants, the LT50 increased to -27ºC in comparison to -12ºC for control plants (Liu, 2015). In addition, Liu (2015) observed a decrease in apoplastic permeability in cold acclimated *A. fistulosum* epidermal cells. Fluorescein diffused across the apoplast at a rate 70 times faster in epidermal cells obtained from non-cold acclimated plants in comparison to those obtained from cold acclimated plants (Liu, 2015).

While this thesis worked on the basis that cold acclimation would reduce percent water loss given that it reduced apoplastic permeability (Liu, 2015), experiments conducted analyzing cold acclimation and water loss found the opposite. Epidermal cells obtained from *A. fistulosum* plants cold acclimated at 12ºC/4ºC (day/night) in conjunction with calcium application, had the greatest overall percent water loss and the most rapid increase in the limit of damage based on percent protoplasmic streaming. While epidermal cells obtained from cold acclimated (12ºC/4ºC (day/night)) *A. fistulosum* plants had the second lowest overall percent water loss, this treatment group had the most rapid increase in the limit of damage based on percent protoplasmic streaming. This finding suggests that while 12ºC/4ºC (day/night) cold acclimation may have slightly reduced water loss, it did not equate to a greater ability to withstand dehydration. In addition, while 12ºC/4ºC had been previously identified by the Tanino lab as the optimal temperature to cold acclimate *A. fistulosum* as opposed to 4ºC/4ºC, this treatment was not found to have a significant ($p>0.05$) difference in percent water loss. There was also no significant ($p>0.05$) difference in percent protoplasmic streaming. This further suggests while differences in freezing tolerance between *A. fistulosum* and *A. cepa* may be linked to reduced water loss, the connection between changes in cell wall permeability during cold acclimation in *A. fistulosum* and dehydration stress are less clear. The seemingly contradictory results obtained in this chapter may be the result of a couple of factors.

Firstly, while Liu (2015) observed that cold acclimation at 12ºC/4ºC decreased the diameter of pores within epidermal cells to less than 1.3nm, the diameter of a water molecule at 25ºC is ~0.27nm (2.7Å) (Schatzberg, 1967). Therefore, while reduced permeability as a result of cold acclimation was successful in reducing the diffusion of fluorescein, the small diameter of a water molecule may have allowed it to diffuse out of the cell without obstruction. In addition, a study by

Rahman et al. (2020) found that in *Arabidopsis*, cold acclimation resulted in an upregulation of PIP1-4 and PIP2-5 aquaporin expression. While this study was conducted using *Arabidopsis*, the possibility of something similar occurring in cold acclimated *A. fistulosum* may explain why cold acclimation not only did not significantly ($p>0.05$) improve dehydration stress tolerance but in some instances it increased percent water loss. Finally, cold acclimation was only incorporated into the initial analysis of long-term water loss at the point when the epidermal cell layer was separated from the sheath prior to dehydration. As previously mentioned, a shift in method was made in order to try and mimic conditions that are more likely to occur in a natural setting, where the epidermal cell layer would never be separated from the sheath. Thus, results pertaining to long-term percent water loss and subsequent limit of damage (based on percent protoplasmic streaming) which include cold acclimated plants may be skewed.

4.4.3 *Arabidopsis* Water Loss

In contrast to the more inconsistent trends observed when analyzing calcium and dehydration stress resistance, analysis of boron and dehydration stress resistance produced more consistent trends. Generally, genotypes with mutations in boron transporters consistently showed the highest rate of water loss, in addition to some of the highest values of percent electrolyte leakage.

While genotypes *nip5-1* and *nip6-1*, appeared to be more susceptible to water loss after 15min and 12-24hr, this trend was not observed in the analysis of water loss over 2-10hr. In comparison, analysis of water loss over 2-10hr found that *nip5-1* and *nip6-1* overall had the same percent water loss as Col-0 and *p35S::PMEI5*, which were more tolerant to water loss over 15min. Instead, the *bor1* genotype showed the greatest overall percent water loss over 2-10hr. While like the genotypes *nip5-1* and *nip6-1*, the *bor1* genotype is a boron-transporter mutant, the targeted boron transporter is different (TAIR, 2021). Genotypes *nip5-1* and *nip6-1* have mutations in the NIP boron transporters NIP5-1 and NIP6-1 and which are expressed in fewer locations at the cellular level and are involved in less biological processes compared to the BOR1 transporter (TAIR, 2021; TAIR, 2015; TAIR, 2013).

Collectively, NIP5-1 and NIP6-1 expressed in the plasma membrane, and are characterized as being involved in borate transport (TAIR, 2021; TAIR, 2015; TAIR, 2013). NIP5-1 is also

involved in biological processes related to arsenite transport and responses to arsenic-containing substances (TAIR, 2015; TAIR, 2013). In contrast, the BOR1 transporter is located in the cytoplasm, endosome and vacuole in addition to the locations of NIP5-1 and NIP6-1 (TAIR, 2021; TAIR, 2015; TAIR, 2013). The BOR1 transporter is also involved in a range of other biological processes including detection of nutrients, ion homeostasis and transmembrane transport, as well as borate transport and response to boron-containing substances as seen in NIP5-1 and NIP6-1 transporter (TAIR, 2021; TAIR, 2015; TAIR, 2013). Therefore, differences in overall water loss over 2-10hr between these two classes of boron transporter mutants may be attributable to far reaching consequences of the BOR1 transporters. Anecdotal evidence collected during the process of growing the various *A. thaliana* genotypes also found that *bor1* plants were smaller and more sensitive in comparison to *nip5-1* and *nip6-1*, further suggesting a mutation in the BOR1 transporter has wider reaching consequences as opposed to mutations in NIP5-1 or NIP6-1 transporter.

Despite the findings from this experiment, there is a lack of additional research to back up these findings, with no previous papers appearing to analyze NIP, BOR or other similar boron transporters in relation to dehydration stress tolerance. However, as previously mentioned *nip5-1* and *nip6-1* had a significantly ($p<0.05$) higher proportion of boron in comparison to Col-0 and *p35S::PMEI5* based on the results from an ICP-MS analysis (Col-0=25.4ppm, *p35S::PMEI5* =28.2ppm, *nip5-1*=30.0ppm and *nip6-1*=34.9ppm) (Table A11-A14). Based on this, the observation that over 15min and 12-24hr, both of these genotypes had the highest overall percent water loss contradicts previous research in relation to boron application and drought stress tolerance. A range of species including maize, winter wheat and tomatoes have been found to have enhanced drought stress tolerance as a result of boron application, primarily by way of foliar application (Aydin et al., 2019; Naeem et al., 2018; Abdel-Motagally & El-Zohri, 2018; Karim et al., 2012). These studies applied boron at various concentrations including 4mg L^{-1}, 50µm and 50ppm. In addition, unforeseen delays in the acquisition of the mutant lines in addition to delays in seed set of the *bor1* mutant, resulted in the exclusion of *bor1* from the analysis of water loss over 15min or 12-24hr. The exclusion of *bor1* from these experiments makes it impossible to know if the trends would have occurred over 15min and throughout the more extended 12-24hr water loss time period. Therefore, questions remain regarding if *nip5-1* and *nip6-1* are truly the more

dehydration susceptible solely based on their higher overall percent water loss after 12-24hr compared to Col-0 and *p35S::PMEI5* or if *bor1* would have experienced an even greater overall percent water loss after 24hr.

While percent water loss serves as a measurement of a plant's ability to withstand dehydration stress, another arguably more important factor is the level of damage to the cell(s) following dehydration. Our analysis of long-term water loss was followed up by an assessment of the limit of damage which was based on percent electrolyte leakage, where a lower percent electrolyte leakage indicated a decreased limit of damage. Percent electrolyte leakage serves as a measurement for damage as the leakage of ions such as K^+ out of the cell is indicative of damage to the cell membrane (Demidchik et al., 2014). While our results found genotypes with mutations in boron transporters (BOR1, NIP5-1 and NIP6-1) had the highest overall percent water loss, with *bor1* having the highest over 2-10hr and *nip5-1* and *nip6-1* having the greatest over 12-24hr, percent electrolyte leakage did not follow these trends. For example, while following 24hrs of water loss, *nip5-1* and nip6-1 had the greatest overall percent water loss, analysis of percent electrolyte leakage found Col-0 had the highest percent electrolyte leakage. Similar contradictions were also observed in the data collected from analysis of electrolyte leakage following 2-10hr. While *bor1* consistently had a higher percent water loss, compared to other genotypes over 2-10hr, over the same time period the *bor1* genotype never showed the highest percent electrolyte leakage with the exception of at 0hr. This trend is of interest because while *bor1* appeared to be the least tolerant to dehydration in comparison to the other genotypes when percent water loss was the sole focus, percent electrolyte leakage results suggest that *bor1* may actually have a higher dehydration tolerance in comparison to the other genotypes with the exception of *p35S::PMEI5*.

In comparison, the *p35S::PMEI5* genotype in general appeared to be the most dehydration tolerant line amongst the other lines of interest. This finding is in contrast to the initial hypothesis put forth which predicted *p35S::PMEI5* would have decreased dehydration stress tolerance comparison to Col-0. With the exception of water loss over 12-24hr, where *p35S::PMEI5* had a slightly higher percent water loss, the *p35S::PMEI5* line had the lowest overall percent water loss following analysis of water loss both over 15min and 2-10hr. In addition, the *p35S::PMEI5* line had the lowest percent electrolyte leakage following both periods of long-term water loss (2-10hr and 12-

24hr) when compared to the other lines with the exception of dehydration following 14hr, and 18hr. The general trend of enhanced dehydration resistance in the *p35S::PMEI5* genotype falls in line with research from An et al. (2008) who found the over-expression of CaPMEI1, a PMEI from peppers, enhanced tolerance to drought stress. Reduced dehydration stress as a result of PMEI over-expression may the result of changes in cell wall permeability and porosity, which are closely tied to the level of methylation in pectin and the pattern of that methylation (Peaucelle et al., 2012; Wolf et al., 2009).

4.5 Connection to the Next Study

Calcium application, cold acclimation, alterations in boron via. mutations in transporters, in addition to enhanced expression of PMEI all produced differential results in tolerance to dehydration stress depending on the length of the water loss. However, when the rate of water loss over 1-6hr was examined using pure pectin standards, calcium chloride and boric acid reduced overall percent water loss in certain cases. This was likely a result of the formation of "egg-box" structures and RG-II dimers. Therefore, while there was a lot of noise in the biological system results obtained, the clear results obtained from the analysis of water loss in pectin is indicative that calcium chloride, and to a lesser extent boric acid, do play a role in influencing percent water loss. While this finding was not as clear in the trends produced by the data analyzing water loss in the *Allium* spp. and *Arabidopsis* and there are likely other biological mechanisms outside the realm of this thesis at work, calcium and boron still hold potential in enhancing tolerance to dehydration stress.

Overall, the results from this chapter fully support two of the sub-hypotheses associated with this chapter; "Increasing concentration along with calcium or boron will reduce water loss over 6hr in pure pectin standards. Moreover, boron will have a greater influence on reducing water loss in GB pectin, while calcium will have a larger effect on HM pectin". In addition, data collected within this chapter also found that *A. fistulosum* had a lower percent water loss compared to *A. cepa*, allowing for the support of hypothesis six. The other hypotheses are rejected by data collected within this chapter.

While investigating the role of the cell wall as a barrier to dehydration stress is critical in the face of climate change and the increased prevalence of dehydration stress, plants are exposed to multiple stresses at once. Thus, it is critical to find solutions that allow plants to mitigate a range of stresses. Based on that assumption, Chapter 5 explores how pectin modifications influence resistance to fungal pathogens. In particular, the role of boron and PMEI-5. Chapter 5 utilizes *Arabidopsis* genotypes analyzed in Chapter 4 to explore biotic stress given the close genetic relationship between *Arabidopsis* and rapeseed, a crop of large economic value.

5.0 INVESTIGATING THE ROLE OF BORON AND PECTIN METHYLESTERASE INHIBITORS ON BIOTIC STRESS

5.1 Introduction

Botrytis cinerea (*B. cinerea*) is known to infect over 200 plant species and as a result causes annual loss of between $10 billion to $100 billion (USD) annually (Boddy, 2016). Boddy (2016) further outlines that the necrotrophic nature of *B. cinerea* means that it does not rely on its host being alive in order to replicate. They go on to explain that once *B. cinerea* breaches the cell wall through the use pectinolytic machinery it has a large arsenal of lethal chemicals that it releases to kill the infected cells. Given the reliance on pectinolytic machinery in order to circumvent the cell wall, cell walls with low pectin contents pose more of a challenge to *B. cinerea's* abilities to overcome the cell wall (Boddy, 2016). Section 2.6.1 further outlines how *B. cinerea* infects its host plant.

In contrast, Yan et al. (2018) outline that *C. higginsianum* does not rely on pectinolytic machinery in order to overcome the cell wall. The structure of the appressoria in *C. higginsianum* allows for the pathogen to penetrate the cell wall by shear force alone, *B. cinerea* is not capable of this (Yan et al., 2018; Boddy, 2016). In addition, unlike *B. cinerea* which is a necrotroph, *C. higginsianum* is a hemibiotroph (Yan et al., 2018). The hemibiotrophic nature of *C. higginsianum* means that initially the lifecycle of the pathogen is dependent on keeping it's host alive. However, as it exits the biotrophic stage and transitions into the nectrotrophic stage, it becomes like *B. cinerea* in the sense that it then seeks to kill the cells of the host plant in order to complete its lifecycle. (Yan et al., 2018). Section 2.6.2 provides further information on how *C. higginsianum* infects cells within the host plant. Nevertheless, *C. higginsianum* is similar to *B. cinerea* in its abilities to cause economic devastation (Dowling et al., 2020). *C. higginsianum* is capable of infecting a range of agricultural and horticultural crops including *Brassica napus* which contributes approximately $26.7 billion dollars to the Canadian economy each year (Dowling et al., 2020; Industry Overview-Canola Council of Canada, n.d.).

As outlined in Chapter 2, boron and PMEI's not only play a critical role in the structure of the cell wall but have also been associated with both *B. cinerea* and *C. higginsianum* infections through a range of studies. Therefore, genotypes with mutations in boron transporters (*nip5-1*, *nip6-1* and *bor1*) and PMEI5 (*p35S::PMEI5*) were selected to investigate how boron and *p35S::PMEI5*

influence the rate of *B. cinerea* and *C. higginsianum* infections. The experiments below address the hypotheses:

a. *A. thaliana* plants with mutations in boron transporters (NIP5-1, NIP6l-1 and BOR1) and a pectin methyl esterase inhibitor overexpressing line (*p35S::PMEI5*) will show an increased rate of *B. cinerea* infection based on lesion size.
b. *A. thaliana* plants with mutations in boron transporters (NIP5-1, NIP6l-1 and BOR1) and a pectin methyl esterase inhibitor overexpressing line (*p35S::PMEI5*) will show an increased rate of *C. higginsianum* infection based on lesion size.

The objective for experiments within this Chapter was to investigate the influence of boron transporters and *p35S::PMEI5* mutations on *Botrytis cinerea* and *Colletotrichum higginsianum* infections in *Arabidopsis thaliana* by assessing lesion sizes.

5.2 Materials and Methods

5.2.1 *Botrytis cinerea*

5.2.1.1 Arabidopsis thaliana Genotypes

A. thaliana genotypes outlined in Section 4.2.4.1 which were genotyped, were utilized for the following experiment. All genotypes were grown in a Conviron chamber (Winnipeg, Manitoba, Canada) with the following environmental conditions; 20ºC, 50%RH, 16-8/light-dark period and 150 +/-10 µmol $m^{-2}s^{-1}$. Watering was conducted every second day, using water from the City of Saskatoon, while fertilizer (20-20-20) was applied weekly. When preparing the fertilizer solution, 2g of 20-20-20 was added to 1L of water. Each tray containing ~12 pots received 1L of fertilizing solution. Plants were grown to four-weeks of age (Figure A13).

5.2.1.2 Inoculation and Measuring Rate of Infection

B. cinerea was grown on a potato dextrose agar (PDA) plate for 7 days at 22°C (Wang et al., 2020). The oldest leaves from four-week-old *A. thaliana* genotypes were placed on 2 damp filter in a Petri dish. Leaves were then inoculated by placing a small piece (~0.1cm^2) of agar containing mycelium obtained from the culture top-down in the center of the leaf. A small drop of ddH_2O was placed on and around the piece of agar to help promote inoculation. The petri dishes were then sealed using parafilm and placed in a dark area with a constant temperature of approximately 23°C for

the period of the experiment. Photos were taken of the petri dish beginning at 0hr for every 24hr up until 96hr, and ImageJ was used to measure the area of the lesion over the time course (Figure A14). Equation A4 was used to calculate the size of the lesion.

5.2.1.3 Statistical Analysis

Results were analyzed using an ANOVA, at a level of significance of $p<0.05$. A Tukey test analyzed the relationship between each genotype and lesion growth. Figures were created using the "ggplot" and "ggplot2" package in RStudio (Version 1.2.5033), in addition to Microsoft Excel (Version 16.32) (Wickham, 2020). All statistical analyses were preformed using the RStudio statistical software (Version 1.2.5033).

5.2.2 *Colletotrichum higginsianum*

5.2.2.1 Arabidopsis thaliana Genotypes

See Section 4.2.4.1 and Section 5.2.1.1

5.2.2.2 Inoculation and Rate of Infection

A culture containing spores from a *C. higginsianum* Sacc culture, isolate IMI349061, originating from *Brassica rapa* (obtained from CABI Bioscience) was kindly prepared by Dr. Li Qin (University of Saskatchewan). The culture was prepared as outlined by Liu et al. (2010) and Liu et al. (2007). Spores were then suspended by first washing the surface of the DPA medium with 3mL ddH_2O and then centrifuging the solution for 1min at 5000rpm (8236 m/s^2) at 23°C. The supernatant was then extracted, and the spores were resuspended in 1mL of ddH_20 and centrifuged for 1min at 5000rpm. This process was repeated 3 times to promote germination. Spores were then counted using a hemocytometer and Equation A5 was used to produce a solution containing 10^6 spores/mL.

Following the preparation of the spores from the *C. higginsianum*, the oldest leaf from each of the four-week-old *A. thaliana* genotypes were placed in a petri dish containing moist filter paper and six 1µL droplets of the spore solution were placed on the leaf, with caution taken to avoid the leaf midvein. The petri dishes were then kept in the following environmental conditions: Day 1-2) 16-8hr/light-dark period and 150 +/-10 µmol $m^{-2}s^{-1}$; Day 3) Complete darkness; and Day 4-5) 16-

8hr/light-dark period and 150 +/-10 µmol $m^{-2}s^{-1}$. Complete darkness was used on day 3 to promote germination of the appressorium while the leaves were transferred back to a day/night light cycle on days 4-5 to prevent chlorosis. The temperature was approximately 20°C.

Photos were taken of the leaves beginning at 0hr for every 24hr up until 120hr, and ImageJ was used to measure the area of the lesion over the time course (Figure A15). While the diameter of the agar was subtracted from the total lesion size with respect to *B. cinerea*, this was not done here as the culture was applied in liquid drops which were not visible throughout the entire time course.

5.2.2.3 Statistical Analysis

Statistical analysis was done as outlined in Section 5.2.1.3

5.3 Results

5.3.1 Rate of Infection- *Botrytis cinerea*

While *bor1* appeared to have the lowest rate of infection, unlike the other genotypes, *bor1* leaves were extremely small and the *Botrytis* gel took up most of the leaf area, thereby creating an apparent lack of growth (Figure A14, Figure 5.1 and Figure 5.2). Thus, the *Botrytis* infection should be considered an artifact of *bor1*'s small leaf size (0.109cm^2 compared to 0.164cm^2 for the other genotypes) and alternative methodology will be required in future. As a result, while Table A42 shows a statistically significant ($p<0.05$) difference between genotypes and lesion growth, this result is skewed.

However, the leaves of the other genotypes (Col-0, *nip5-1*, *nip6*-1 and *p35S::PMEI5*) were of the same larger size and were more comparable (Figure A13). The rate of *B. cinerea* infection progressed steadily until 72hr, with the boron transporter mutant *nip5-1* initially showed the largest lesion size at 24hr, followed by *nip6-1* at 48hr and Col-0 at 72hr (Figure 5.1). While *nip5-1* initially showed the largest lesion size, from 48hr to 96hr it consistently had the smallest lesion size (Figure 5.1), however, there were no significant ($p>0.05$) differences between these 4 genotypes (Figure 5.2 and Table A43). The growth in lesion size continued to increase for all

mutant genotypes over the 96hr observation period but plateaued for Col-0 between 72-96hr (Figure 5.1).

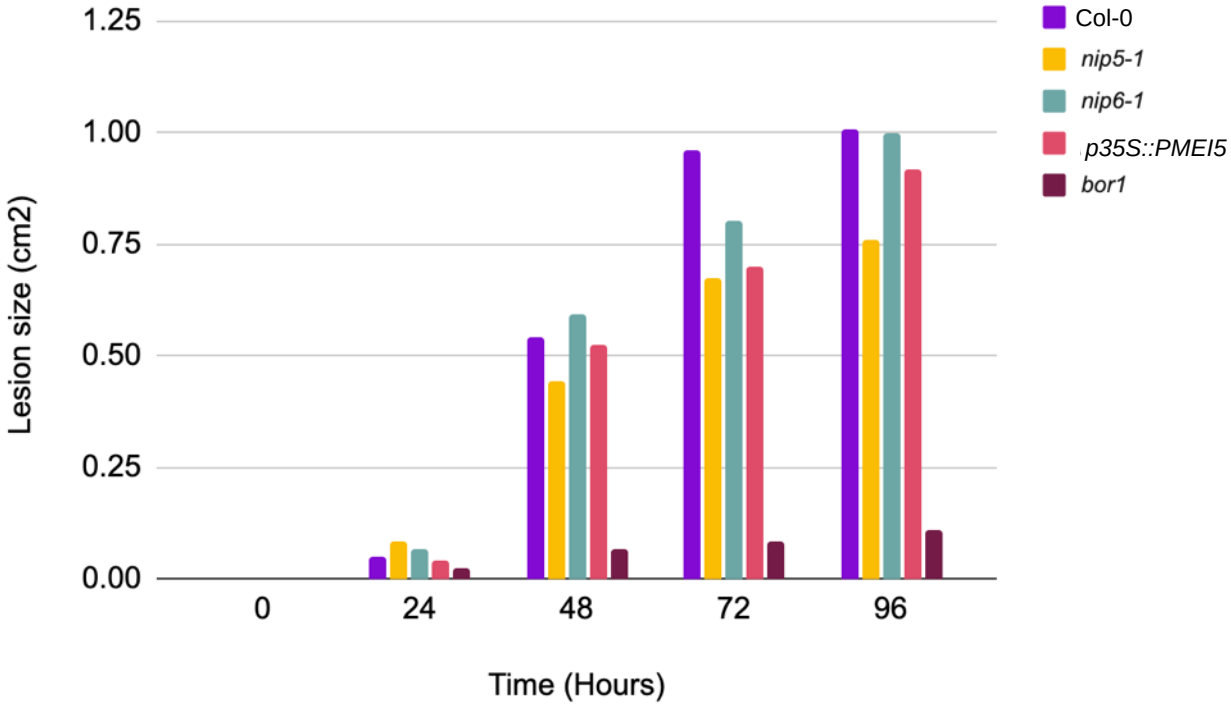

Figure 5.1 Size of lesion caused by *Botrytis cinerea* infection in leaves from various *Arabidopsis thaliana* genotypes (*nip5-1*, *nip6-1*, *bor1*, *p35S::PMEI5* and Col-0)

Size of lesion caused by *Botrytis cinerea* infection in leaves from various *Arabidopsis thaliana* genotypes (Col-0, *nip5*-1 [boron transporter mutant], *nip6-1* [boron transporter mutant], *p35S::PMEI5* [PMEI mutant] and *bor1* [boron transporter mutant]) between 0-96hr post-inoculation.

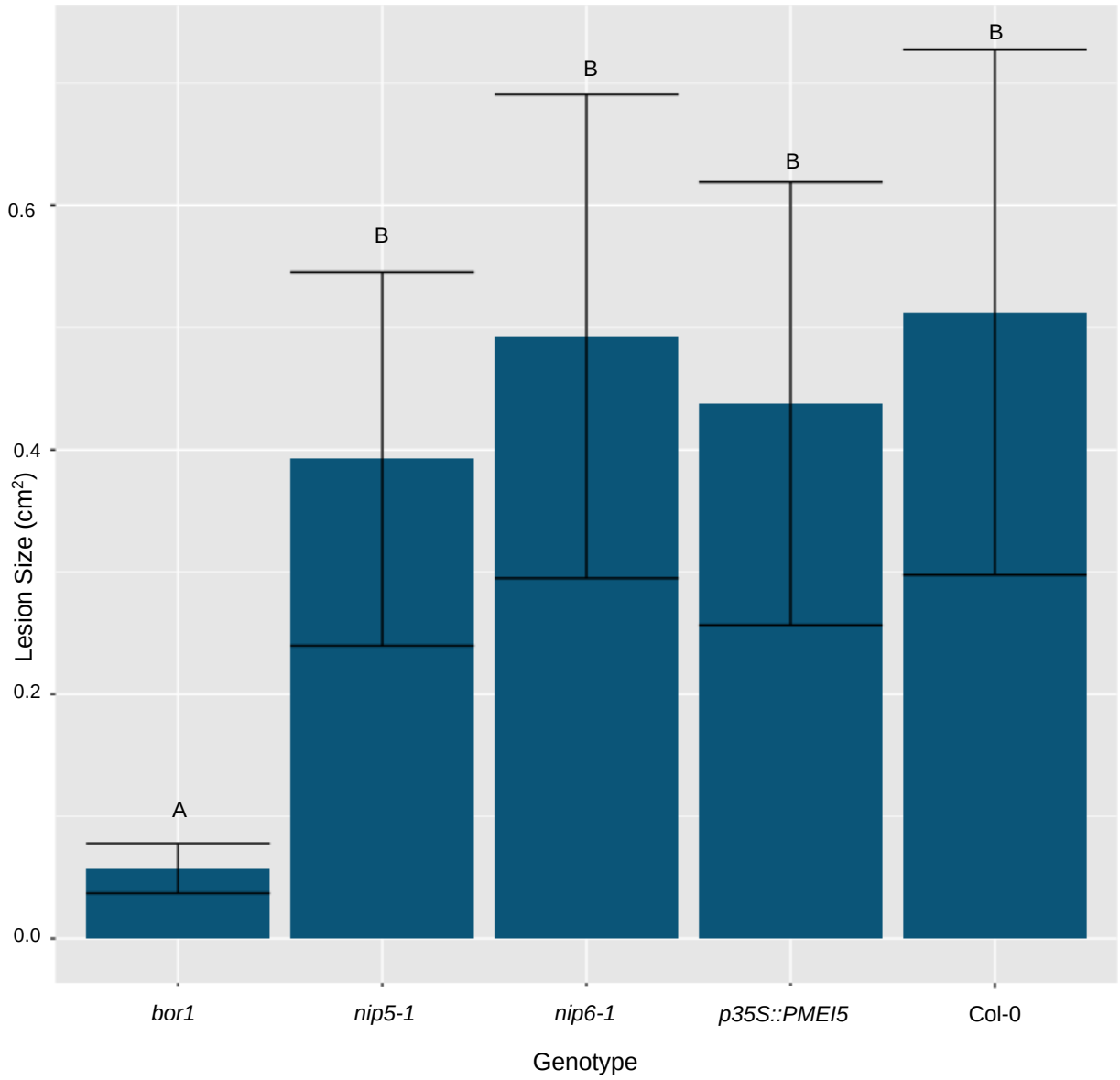

Figure 5.2 Average *Botrytis cinerea* lesion size from the leaves of various *Arabidopsis thaliana* genotypes (*nip5-1*, *nip6-1*, *bor1*, *p35S::PMEI5* and Col-0) - Figure for Tukey test

Average *Botrytis cinerea* lesion size from the leaves of various *Arabidopsis thaliana* genotypes (*bor1* [boron transporter mutant], *nip5-1* [boron transporter mutant], *nip6-1* [boron transporter mutant], *p35S::PMEI5* [PMEI mutant], and Col-0 [wild type]) over a 0-96hr period post-inoculation. Error bars represent standard error. See Table A43 for statistical analysis.

5.3.2 Rate of Infection- *Colletotrichum higginsianum*

While data collected on the rate of *B. cinerea* growth did not allow for *bor1* to be included amongst the comparison of other *A. thaliana* genotypes of interest, this was not an issue for C. *higginsianum*

since inoculation method of this pathogen used small (1µL) drops of ddH_2O with spores suspended in the liquid and did not interfere with measurement of lesion size (Figure A15).

The *bor1* mutant not only had the most rapid onset of *C. higginsianum* infection based on a visual observation, but this genotype also continued to show the largest lesion size up until 96hr (Figure 5.3). Overall, the lesion size present on leaves from the *bor1* genotype were significantly ($p<0.05$) larger in comparison to *nip5-1*, *nip6-1* and Col-0 (Figure 5.4, Table A44 and Table A45). While *bor1* also initially outpaced *p35S::PMEI5* in lesion size, the lesion size in *p35S::PMEI5* leaves grew rapidly between 96-120hr, ultimately resulting in a non-significant ($p>0.05$) difference between *bor1* and *p35S::PMEI5* (Figure 5.3, Figure 5.4 and Table A45). Moreover, the effect sizes for some of the relationships between genotypes was above 0.8 (Table A46). This is considered a large effect size (Lakens, 2013; Cohen, 1988).

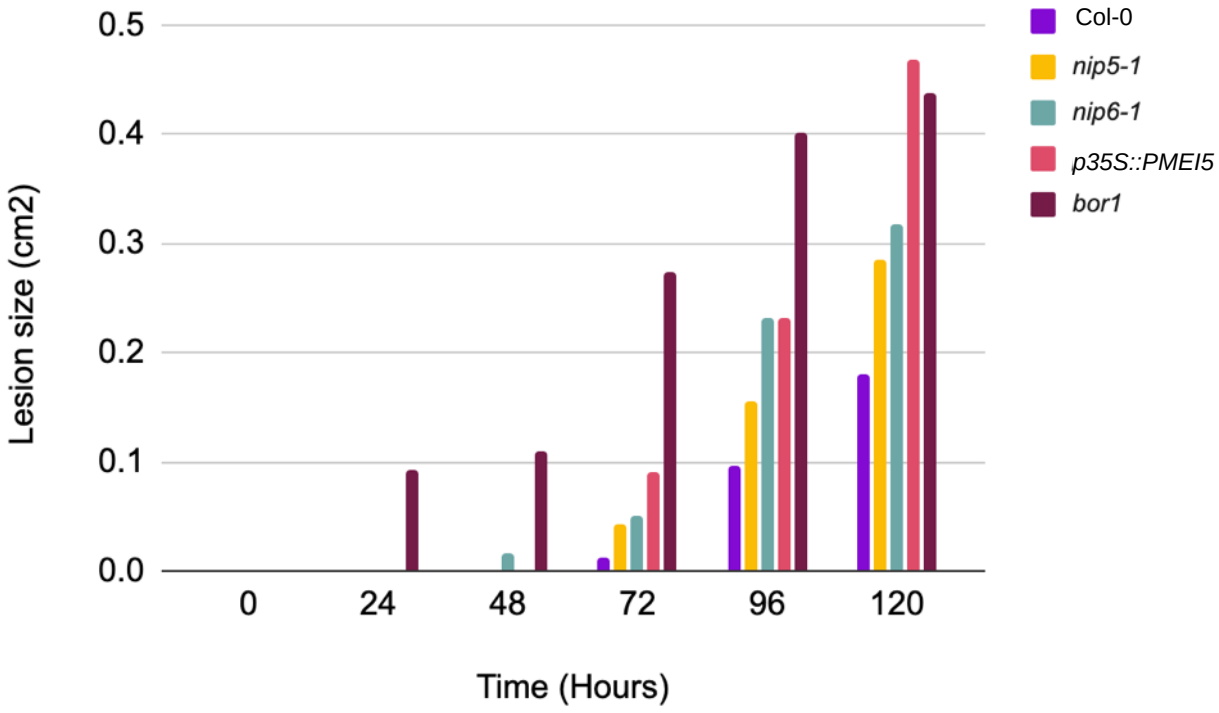

Figure 5.3 Size of lesion caused by *Colletotrichum higginsianum* infection in leaves from various *Arabidopsis thaliana* genotypes (*nip5-1*, *nip6-1*, *bor1*, *p35S::PMEI5* and Col-0)

Size of lesion caused by *Colletotrichum higginsianum* infection in four-week-old leaves from various *Arabidopsis thaliana* genotypes (Col-0 [wild type], *nip5-1* [boron transporter mutant], *nip6-1* [boron transporter mutant], *p35S::PMEI5* [PMEI mutant] and *bor1* [boron transporter mutant) between 0-120hr post-inoculation.

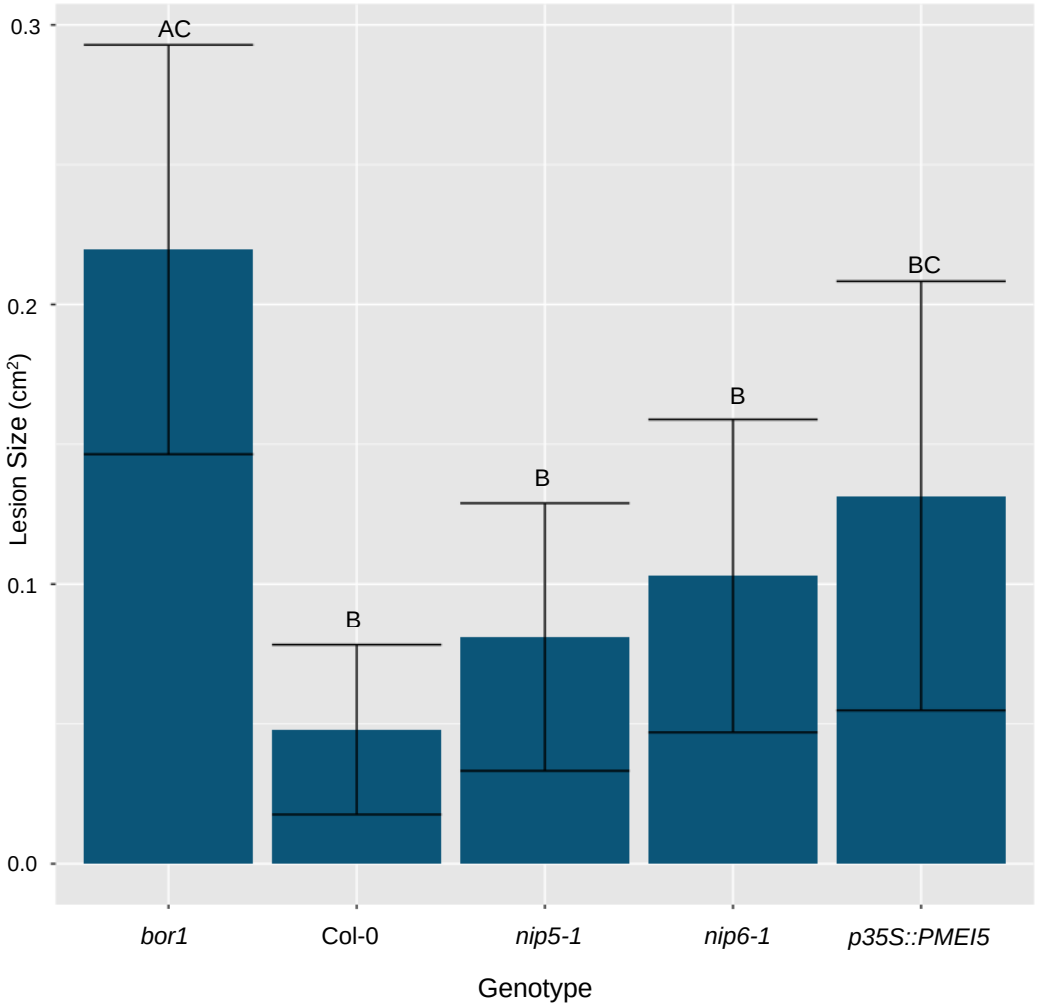

Figure 5.4 Size of lesion caused by *Colletotrichum higginsianum* infection in leaves from various *Arabidopsis thaliana* genotypes (*nip5-1*, *nip6-1*, *bor1*, *p35S::PMEI5* and Col-0) - Figure for Tukey test

Average *Colletotrichum higginsianum* lesion size from four-week-old leaves of various *Arabidopsis thaliana* genotypes (*bor1* [boron transporter mutant], *nip5-1* [boron transporter mutant], *nip6-1* [boron transporter mutant], *p35S::PMEI5* [PMEI mutant], and Col-0 [wildtype]) over a 0-120hr period post-inoculation. Error bars represent standard error. See Table A45 for statistical analysis.

5.4 Discussion

5.4.1 *Botrytis cinerea*

The method of inoculation of *B. cinerea* as outlined in Section 5.2.1.2 and the small leaf area of *bor1* compared to the other genotypes created an artefact and skewed the data. Thus, the *Botrytis cinerea* results on *bor1* are inconclusive at this time.

Nevertheless, after four weeks of growth, the remaining four genotypes had relatively larger leaves of roughly the same size and could be compared. There was no significant difference ($p>0.05$) in lesion size across these genotypes compared to Col-0. It is not clear if the lack of difference between the Col-0 and the remaining three *Arabidopsis* mutants is due to inoculation method/experimental method or if there is in fact, no significant ($p>0.05$) difference among the four remaining *Arabidopsis* mutants to *Botrytis* infection. Unfortunately, there is a lack of current research exploring the role of boron transporters such as members of the NIP or BOR family in *B. cinerea* or other similar fungal infections. Despite this, there is a small body of research that has examined the role of exogenously applied boron on *B. cinerea* and similar fungal pathogens.

Qin et al. (2010) found boron application decreased the rate of decay typically seen in table grapes as a result of *B. cinerea.* Boron is believed to have mitigated *B. cinerea* in table grapes by disrupting the cell membrane of the pathogen, leading to the breakdown of the cell membrane and the loss of cytoplasmic material from the hyphae (Qin et al., 2010). Boron in partnership with iron was also found to mitigate the effects of *Fusarium oxysporum* (*F. oxysporum*) in banana by decreasing both the conidial germination rate and overall fungal growth (Dong et al., 2016). Both *B. cinerea* and *F. oxysporum* are necrotrophic pathogens (Frontiers, n.d.). Necrotrophic pathogens kill the cells of the host plant and use the contents of these cells to support their own growth in order to complete their lifecycle (Frontiers, n.d.). The classification of fungi as biotrophic, hemibiotrophic or necrotrophic is critical to understanding the lifecycle of the fungi inside the cells of the host plant. While the genotype *nip6-1* is a boron-transporter mutant, ICP-MS results showed the concentration of boron was significantly ($p<0.05$) higher in this genotype compared to Col-0 and *nip5-1*. Nevertheless, despite having more boron, *nip6-1* had the fastest rate of *B. cinerea* infection based on lesion size compared to Col-0 and *nip5*-1.

By contrast, numerous studies have explored *B. cinerea* infections in relation to mutations in PMEI's since the pectin matrix is the main cell wall target of *B. cinerea* (Lionetti et al., 2017). According to Lionetti et al. (2017), over-expression of PMEI10, PMEI11 and PMEI12 all helped maintain the integrity of the cell wall in *A. thaliana* plants infected with *B. cinerea.* In addition, this group of researchers also found *A. thaliana* plants under-expressing these PMEI's were

compromised in their immunity to *B. cinerea.* While these three PMEI's were identified to play key roles in mitigating *B. cinerea* infection, none of these PMEI's belong to Group 3, the group of PMEI's that includes PMEI5, the PMEI mutated in the *p35S::PMEI5* genotype (Lionetti et al., 2017).

Lionetti et al. (2017) states that Group 1 includes PMEI's involved in fruit development amongst other functions. Group 2 comprises CaPMEI1, an inhibitor involved in resistance to abiotic and biotic stress, amongst other PMEI's such as PMEI4, found in *A. thaliana* roots (Lionetti et al., 2017; An et al., 2008). Group 3 includes a range of PMEI's in addition to related invertase inhibitors (RIH's) (Lionetti et al., 2017). This group also previously showed transformed *A. thaliana* plants over-expressing PMEI1 and PMEI2 were more resistant to *B. cinerea*, with the reduction in symptoms tied to *B. cinerea*'s reduced ability to grow on methylesterified pectin. While an over-expression of PMEI appears to reduce susceptibility to *B. cinerea*, Raiola et al. (2011) also confirmed the important role of pectin methylesterification in *B. cinerea* infection. They found rapid expression of PME3 is critical for the initial colonization of *B. cinerea* into the host tissue, further supporting the concept that the degree of pectin methylesterification influences susceptibility to *B. cinerea*.

5.4.2 *Colletotrichum higginsianum*

Contrary to the results obtained from the experiment outlined in Section 5.3.1, a difference in the method used for the inoculation of *C. higginsianum* avoided the challenges outlined in Section 5.3.1.

The *bor1* mutant continuously showed the fastest rate of *C. higginsianum* infection in comparison to the other genotypes. 24hr post-inoculation, *bor1* was the only genotype of interest to have developed a lesion. The majority of the other genotypes with the exclusion of *nip6-1* only developed a lesion 72hr post-inoculation. While *bor1* showed a larger lesion size throughout the period of the infection, in general the other genotypes between 72hr-96hr had lesions similar in size. However, the *p35S::PMEI5* genotype's lesion size more than doubled by 120 hrs, resulting in the lesion size equivalence between *p35S::PMEI5* and the *bor1* genotype. Overall, while *bor1*

had a significantly larger lesion size compared to Col-0, *nip5-1* and *nip6-1*, *p35S::PMEI5* was not statistically different ($p>0.05$) from any of the genotypes.

The larger lesion size of the *p35S::PMEI5* genotype is in contrast to a previous study that found the higher degree of pectin methylation (an increase in the level of methylation), in *Colletotrichum lindemuthianum* resistant bean cultivars compared to susceptible genotypes (Boudart et al., 1998). However, Engelsdorf et al. (2016) found susceptibility to *C. higginsianum* was unaffected in mutants under-expressing PME3 and PME35-1. As outlined in Chapter 2, PME is responsible for the demethylesterification of HG, while PMEI inhibits PME, presumably increasing the level of methylation (Wormit & Usadel, 2018). Contrasting evidence may be the result of variation between various PME's and PMEI's. As outlined in Section 5.4.1, PMEI's are divided into three groups with PMEI5, the PMEI of interest in this study, falling into Group 3 (Lionetti et al., 2017). In addition, there have been 27 PME genes and 71 putative PMEI genes identified in *A. thaliana* (Wormit & Usadel, 2018; Xue et al., 2020). While the general function of both PME and PMEI is well understood, there appears to be a lack of literature examining specific differences in the physiological functions of the various PME's and PMEI's. Therefore, it is plausible that the contrasting results from this thesis in comparison to those from Boudart et al. (1998) and others may be the result of unknown differences between the various PME's and PMEI's. Future research should focus on examining the physiological differences between these various enzymes, in addition to specifically exploring PMEI5 since there does not appear to be any research examining this PMEI with respect to any fungal pathogens.

Despite the lack of characterization of the majority of PMEI genes in *A. thaliana*, differences in the various boron transporters are well documented. However, there appears to be a significant gap in the literature exploring how boron transporters or the application of boron through foliar application influences the susceptibility of plants to *C. higginsianum*. The differences in biological processes between NIP5-1 and NIP6-1, both members of the same family, and BOR1, may be responsible for the differences observed between these genotypes and the *C. higginsianum* lesion size (TAIR 2021; TAIR 2015; TAIR 2013). More specifically, the rapid appearance of lesions on *bor1* leaves in contrast to *nip5-1* and *nip6-1*, coupled with the significantly ($p<0.05$) larger lesion

size observed on leaves of *bor1* mutants in comparison to *nip5-1* and *nip6-1* provides a basis for future research.

Another possible scenario which may explain the rapid development of the lesions in *bor1* leaves in comparison to the other genotypes is the process by which *C. higginsianum* infects host plants. *C. higginsianum* has the ability to penetrate the cell wall through the use of physical pressure alone (Yan et al., 2018). This paper explains the ability to penetrate the cell wall physically without the use of enzymes is the result of the ability for high turgor pressure to build in the appressoria, something that is not seen in *B. cinerea* infections. Furthermore, since *C. higginsianum* is a hemibiotroph, it goes through a biotrophic phase first, following the breach of the cell wall, prior to switching to the necrotrophic phase. The necrotrophic phase is partially characterized by the appearance of "water-soaked" necrotic lesions (Münch et al., 2008). While this phase typically begins around 84hr post-infection, the appearance of lesions in *bor1* began 24hr post infection. The early appearance of lesions at 24hr in *bor1* may be indicative that cell walls within the *bor1* genotype are extremely weak. In *bor1*, *C. higginsianum* may have had the ability to penetrate the cell walls with much less pressure, speeding up the process of infection and in turn making the switch from the biotrophic to necrotrophic phase more rapid.

Despite this general trend in the results, there do not appear to be any studies examining NIP, BOR, or any other boron-transporters in relation to *C. higginsianum*. However, there are studies examining how boron applied as a foliar spray acts as an antifungal agent for a range of species infected with *Colletotrichum graminicola* (Shi et al., 2012; Shi et al., 2011). These studies are of interest as they suggest boron has a protective role in reducing susceptibility to *Colletotrichum graminicola*. However, this is contradictory to our findings from *nip5-1* and *nip6-1* since although these genotypes are boron-transporter mutants, these genotypes had a significantly ($p<0.05$) higher concentration of boron in comparison to Col-0 according to ICP-MS analysis. Unfortunately, *bor1* was not included in that study. The differences may lie in the modifications in the cell wall integrity of the *bor1* genotype.

5.4 Connection to Next Study

Throughout Chapter 5 as well as Chapter 4, we explored the role of both calcium and boron on resistance to dehydration stress and fungal pathogens in various species. However, challenges with the method used to inoculate leaves with *B. cinerea* made it challenging to accept the portion of the hypothesis associated with that pathogen. Nevertheless, results obtained from leaves inoculated with *C. higginsianum* clearly showed mutations in boron transporters and PMEI, most notably BOR1 and PMEI5, resulted in a more rapid rate of infection compared to Col-0. Thus, the second half of the original sub-hypothesis related to *C. higginsianum* is accepted. The accepted sub-hypothesis stated, " *A. thaliana* plants with mutations in boron transporters (NIP5-1, NIP6l-1 and BOR1) and a pectin methyl esterase inhibitor overexpressing line (*p35S::PMEI5*) will show an increased rate of *C. higginsianum* infection based on lesion size". These experiments were performed under the assumption that calcium localized to the cell wall following exogenous calcium application. In addition, as various *A. thaliana* genotypes were utilized with mutations in various boron transporters, it was assumed there would be variation amongst the genotypes, *nip5-1*, *nip6-1* and *bor1*, and in comparison, to Col-0 and *p35S::PMEI5*. Thus, it was critical for us to perform analyses that would explore these assumptions. In Chapter 6 we utilize both synchrotron sciences and microscopy to investigate a range of topics including calcium localization, boron speciation and semi-quantification.

6.0 UTILIZING SYNCHROTRON SCIENCES AND MICROSCOPY TO ANALYZE CALCIUM AND BORON IN ALLIUM SPECIES AND ARABIDOPSIS THALIANA

6.1 Introduction

Calcium and boron are both known to play key roles in the structure of the cell wall through modifications (Matoh & Kobayashi, 1998). Most notably, these structural changes are the result of cross-linkages with various forms of pectin (HG and RG-II) (Braccini & Pé Rez, 2001; O'Neill et al., 1996). While these concepts are generally well understood, the role of boron within plant cells remains less clear than that of calcium. It is well understood that calcium is taken up by Ca^{2+} permeable channels in root cells and within the plant calcium continues to exist as ions (White & Broadley, 2003). These ions are also responsible for the creation of "egg-box" structures, a key mechanism in which calcium influences the structure of the cell wall (Lara-Espinoza et al., 2018; Braccini & Pé Rez, 2001; Ravanat & Rinaudo, 1980).

However, boron is a unique element, as it is the only non-metal in Group 13 (XIII) of the periodic table (Kot, 2009). Properties of boron include its nature to form covalent bonds as opposed to ionic bonds (National Center for Biotechnology Information, 2021; Kot, 2009; Bassett, 1980). B^{3+} ions have a high oxidation potential and because of the incomplete octet of BX3 compounds, they behave as acceptors in order to complete their full octet, therefore within compounds they are covalently bonded to other elements (Ball & Key, 2014). In addition, in nature boron is not found on its own, rather it occurs in nature as oxo-compounds (Kot, 2009). Oxo-compounds are compounds containing an oxygen atom doubly bonded to carbon or another element, in this case boron (Nic et al., 2014). Thus, boron is believed to exist only in nature as borates ie. boric acid, sodium borate and boric oxide (Kot, 2009). While boron is also able to form covalent bonds with nitrogen (N) atoms, the stability of B-N compounds in nature has not yet been confirmed (Kot, 2009; Goldbach & Wimmer, 2007). Within plants, boron is known to be taken up by the roots as boric acid and then remains as boric acid within the plant (Kot, 2009; Power & Woods, 1997; Hu et al., 1996). Boric acid is also known to be responsible for the formation of RG-II dimers (Funakawa & Miwa 2015; Kobayashi et al., 1996; O'Neill et al., 1996). The formation of these dimers plays a critical role in the structure of the cell wall (Matsunaga et al., 2004; Ishii et al., 2001; Fleischer et al., 1999; O'Neill et al., 1996). However, information on the roles of other B

species in plants is not well understood as evidenced by the lack of literature regarding this topic. In addition, the majority of papers discussing the role of boron within plants refer to it as boron and occasionally boric acid, there do not appear to be any references to other species of boron being present in plant tissues (Brown et al., 2002; Blevins & Lukaszewski, 1998; Matoh & Kobayashi, 1998; Matoh, 1997).

Therefore, this chapter focuses on the two elements, calcium and boron. The first set of experiments outlined in this chapter focus on the speciation and semi-quantification of boron. Boron will be analyzed in a range of *Arabidopsis* genotypes including boron-transporter mutants in order to compare the differences in boron between genotypes with mutations in boron transporters (*nip5-1* and *nip6-1*) and *p35S::PMEI5*, a PMEI mutant, and Col-0 (TAIR, 2021; TAIR, 2015; Müller, 2013; TAIR, 2013). The analysis of a range of genotypes will help to further the understanding of boron species within *Arabidopsis* in general as well as help to identify more specific differences resulting from these mutations. Furthermore, analysis of boron in both calcium treated and non-calcium treated *A. fistulosum* will be conducted in order to not only gain a further understanding of boron in *Arabidopsis*, but also to identify any differences in boron as a result of calcium. For example, understanding whether or not the addition of calcium will result in different boron species, given that boron can form bonds with calcium creating compounds such as calcium borate. Furthermore, while the method used to analyze the species of boron is only semi-quantitative, calcium is thought to influence the uptake of boron (Tanaka, 1967a). Tanaka (1967a) found that boron uptake in radish decreased with increasing calcium, thus it was of interest to see if these changes are also seen in *A. fistulosum*. In addition to speciation and semi-quantification, this chapter uses curcumin to localize boron within *Arabidopsis* leaves. While the use of curcumin to identify boron has been done before, primarily in health sciences, the application of this method in plants is novel.

The focus of this chapter is centered on the localization of calcium. As outlined above, calcium plays a key role in the structure of the cell wall through the formation of cross-linkages to HG creating “egg-box” structures (Lara-Espinoza et al., 2018; White & Broadley, 2003; Braccini & Pé Rez, 2001; Ravanat & Rinaudo, 1980). Again, pectin is only found within the cell wall (Keegstra, 2010; O’Neill et al., 1990). This thesis was based on the assumption that the structural

changes observed in Chapter 3 are the result of "egg-box" structures. In addition, differences observed in dehydration stress tolerance are based on the assumption that structural changes in the cell wall resulting from calcium application may be partially responsible. Therefore, it was critical to confirm spatial localization of calcium to the apoplast. This chapter addressed that task using both synchrotron sciences and microscopy. Furthermore, pectin as a whole was also semi-quantified using microscopy in order to detect changes to the quantity of pectin within the cell wall as a result of calcium application.

Specifically, this chapter addresses the following hypotheses:

1. Species and quantity of boron present in the above ground biomass of *Arabidopsis thaliana* will vary based on genotype.
2. Species of boron present with the epidermal cell layer of *A. fistulosum* will not vary as a result of calcium application.
3. *A. fistulosum* treated with $CaCl_2$ accumulates more calcium localized to the cell wall of the epidermal cell layer than controls and will have no influence on the quantity of pectin within the cell layer.

6.2 Materials and Methods

6.2.1 Speciation and Semi-Quantification of Boron

6.2.1.1 Arabidopsis thaliana

Bulk analysis and speciation of boron was completed on the aboveground biomass and soil samples from the respective pots of four *A. thaliana* genotypes (Col-0, *nip5-1*, *nip6-1* and *p35S::PMEI5*). Plants were grown in a Conviron chamber (Winnipeg, Manitoba, Canada) with the following environmental conditions; 20ºC constant temperature, 50% RH, 16-8hr/light-dark period and 150 +/-10 µmol $m^{-2}s^{-1}$. Watering was done every second day, using water from the City of Saskatoon. Fertilizer (20-20-20) was applied weekly. Section 4.2.4.1 provides further details relating to the genotypes and how the fertilizer solution was prepared.

Six biomass samples and six soil samples were analyzed per each individual genotype. Above ground biomass samples, consisting of the leaves and shoots were freeze dried, while soil samples were dried by manually pressing water out of the soil using a paper towel. Both the biomass

samples and the soil samples were then ground using a mortar and pestle until homogenous. Samples were then mounted onto the sample holder using carbon tape (Figure A16). Boron nitride (BN) and sodium tetraborate ($Na_2[B_4O_5(OH)_4]\cdot 8H_2O$) were used as standards and were loaded onto the sample holders in the same manner describe above. Compressed air was used to remove any loose sample prior to loading the sample holders into the beamline.

Data was collected using the Variable Line Spacing Plane Grating Monochromator (VLS-PGM) beamline at the Canadian Light Source (44 Innovation Blvd, Saskatoon, SK). More specifically, this beamline was used to collect boron K-edge XAS (track s electron transitions) data. The incident energy of the beamline was approximately 185eV and the slit size (both entrance and exit slits) was 100µm. The vacuum in the chamber was maintained at a value close to or greater than $1x10^7$ torr, while the energy range was between 185eV to 210eV with a dwell time of 1 second. Step Scan was originally used in order to ensure that boron was detectable within the samples, prior to switching to Fast (on-the-Fly) Scan. Step Scan differs from Fast Scan, as during Step Scan, each measurement taken occurs after the motors have stopped. Step Scan is also slower and therefore was only done to initially confirm that boron was detectable in the plant and soil samples. Three scans were completed per sample.

6.2.1.2 Allium fistulosum

The bulk analysis and speciation of boron in *A. fistulosum* was completed through the analysis of epidermal cell layers. Plants were grown and treated with calcium as outlined in Section 3.2.2.2. Prior to analysis, epidermal cell layers were air dried for ~10 days. Cell layers were then ground using a mortar and pestle and mounted on the slide holder shown in Figure A16 using the method outlined in Section 6.2.1.1.

Data was then collected using the VLS-PGM beamline (Canadian Light Source, Saskatoon, SK). The parameters were the same as outlined above in Section 6.2.1.1. Three samples were analyzed per treatment group (control and calcium treated). This experiment was kindly completed by Dongniu (David) Wang and Lucia Zuin from the Canadian Light Source (Saskatoon, SK).

6.2.2 Data Analysis

Normalized FLY (FLY/I0) was used to create the Y-axis for the plots in the Origin software by OriginLab. Repeats were averaged prior to the creation of the graphs. The background in the pre-edge was removed to make the pre-edge flat, while post-edge was normalized to an edge jump of 1 to ensure similar heights allowing for better comparison. Analysis was kindly performed by Dongniu (David) Wang from the Canadian Light Source (Saskatoon, SK).

6.2.3 Spatial Localization of $CaCl_2$ in *Allium fistulosum*

6.2.3.1 Plant Material (Allium fistulosum) and Experimental Design

See Section 3.2.2.1

6.2.3.3 Calcium Spatial Localization

Confocal X-ray microscopy was used to spatially localize calcium within the epidermal cell layer of *A. fistulosum*. *A. fistulosum* plants were grown and treated with calcium as outlined in Sections 3.2.2.1 and 3.2.2.2, respectively. Calcium treated plants received 100mL of a 0.05M $CaCl_2$ (Fisher Scientific, Waltham, MA, USA) solution every second day for one month.

Data was then collected at the CLS and Advanced Photon Source (APS) beamline (20-ID: Section 20- Insertion Device Beamline (Lemont, IL, USA). The following parameters were used: incident energy of 10keV, a map size of 160x160µm, step size of 1µm and a dwell time of 10 milliseconds. A total of 10 maps were collected at a depth of every 2µm in the sample (Stobbs, J. pers.comm. 2021). The experiment was kindly conducted by Dr. Zou Finfrock from the Advanced Photon Source (Lemont, IL, USA).

6.2.3.4 Image Processing

All data was preprocessed and normalized in OriginPro 2020. 2D images were then processed by first using PyMCA in Python to fit the average spectra of all of the points of the map generated at the APS, Origin was then used to increase image quality. 3D images were processed using the 2D tiff images previously created with PyMCA and Python. A stack of 16-tiff images was created using a custom Python script, which were then used to create a volume rendering in Avizo. False colour maps were produced with a physics colour map where blue and red show low and high

relative calcium concentration distributions in the sample (Stobbs, J. pers. comm. 2021). Image processing was completed by Jarvis Stobbs and Miranda Lavier (Canadian Light Source, Saskatoon, SK).

In addition to the aforementioned image processing, the "analyze particles" tool in ImageJ (Version 1.53a) was used to analyze the intensity in the colour of the pixels within the images created along with individual red, green and blue colored pixels. Analysis conducted in ImageJ focused on the apoplast, using the selection tool to select only this region. Values obtained from these image analyses (mean weighted intensity, mean blue pixel count, mean green pixel count and mean red pixel count) were analyzed using two-tailed t-tests (RStudio Version 1.3).

6.2.4 Staining and Microscopy

6.2.4.1 Allium fistulosum

See Section 3.2.2.1

6.2.4.2 Calcium Application

See Section 3.2.2.2

6.2.4.3 Alizarin Red S

Slides mounted with a single layer of *A. fistulosum* epidermal cells were immersed in Alizarin red S (Sigma-Aldrich Canada Co., Oakville, ON, Canada), stain for 5 minutes and then washed with PBS. Alizarin red S was prepared according to the Histology Procedure Manuals published by Pathology Laboratory for Medical Education at The University of Utah (Dahl, 1952). Alizarin red S is a very sensitive method of detecting calcium, with the ability to detect calcium that is above a surface density of 0.02-0.002 $\mu g/mm^2$ (Paul et al., 1983; Dahl, 1952). Imaging was performed using a digital LEICA DM4 B microscope with a LEICA DFC7000 T camera. Six replicates were done per treatment group (control and calcium treated).

6.2.4.4 Ruthenium Red

Ruthenium red (Sigma-Aldrich Canada Co., Oakville, ON, Canada) staining was based on protocols outlined in Section 6.2.4.3. Ruthenium red stain was prepared according Hornatowska (2005). Six replicates were conducted per treatment group (control and calcium treated).

6.2.4.4.1 Ruthenium Red Image and Statistical Analysis

ImageJ (Version 1.53a) was used to analyze the intensity and RGB pixels within the images obtained. The selection tool was used to trace around the apoplast in order to specifically analyze this area. Values obtained were analyzed for statistical significance using T-tests in RStudio (Version .2.5033).

6.2.4.5 Arabidopsis thaliana

Section 4.2.3.1

6.2.4.6 Curcumin

Slides mounted with above ground biomass from two-week old *A. thaliana* plants were immersed in a curcumin stain (Sigma-Aldrich Canada Co., Oakville, ON, Canada) for 10 minutes while being held in a desiccator and then washed with PBS. Curcumin is highly sensitive to boron and has been found to detect small amounts of boron, including detection18-58µg of boron in various plant parts (roots, stems and leaves) (Wimmer & Goldbach, 1999). However, the range of detection appears variable based on the medium in which boron is being detected. To the best of our knowledge, curcumin has never been previously used to detect boron in plant cells. Imaging was performed using a digital LEICA DM4 B microscope with a LEICA DFC7000 T camera attached at 20x using bright field microscopy. Six replicates were done per genotype (Col-0, *nip5-1*, *nip6-1*, *p35S::PMEI5* and *bor1*).

6.2.4.6.1 Curcumin Image Analysis

ImageJ (Version 1.53a) was used to measure the areas of the curcumin complexes observed in the images obtained from the LEICA DM4 B microscope. This analysis was performed using the polygon selection tool to select the area of interest, and then using the “measure” tool under the

"analyze" drop-down menu. Values obtained were analyzed for statistical significance using T-tests in RStudio (Version .2.5033).

6.3 Results

6.3.1 Speciation and Semi-Quantification of Boron in *Arabidopsis thaliana*

6.3.1.1 Leaf Samples

As shown in Figure 6.1, while differences exist within the level of intensity in the spectra collected for each genotype, all of the genotypes exhibit spectra matching that of the boron nitride (BN) standard. Each genotype also had spectra matching sodium tetraborate ($NaBO_4$) but of much lower intensity than BN (Figure 6.1). Furthermore, *nip6-1* showed the highest intensity despite its boron transporter mutation. *nip5-1*, the counterpart to *nip6-1* had the second lowest intensity, with *p35S::PMEI5* having the lowest intensity (Figure 6.1). Since the CLS data is semi-quantitative, ICP-MS (kindly performed by Barry Goetz from Dr. Albert Vandenberg's lab in the Dept. Plant Sciences) quantified boron levels within the above ground biomass of the various *A. thaliana* lines (Table A11). Results from ICP-MS analysis found that *nip6-1* had the highest concentration of boron (34.93ppm) followed by *nip5-1* (30.04ppm), Col-0 (25.04ppm) and finally *p35S::PMEI5* (28.24ppm) (Table A11). All of the genotypes analyzed were significantly ($p<0.05$) different with regards to the proportion of B in them (Table A12-14).

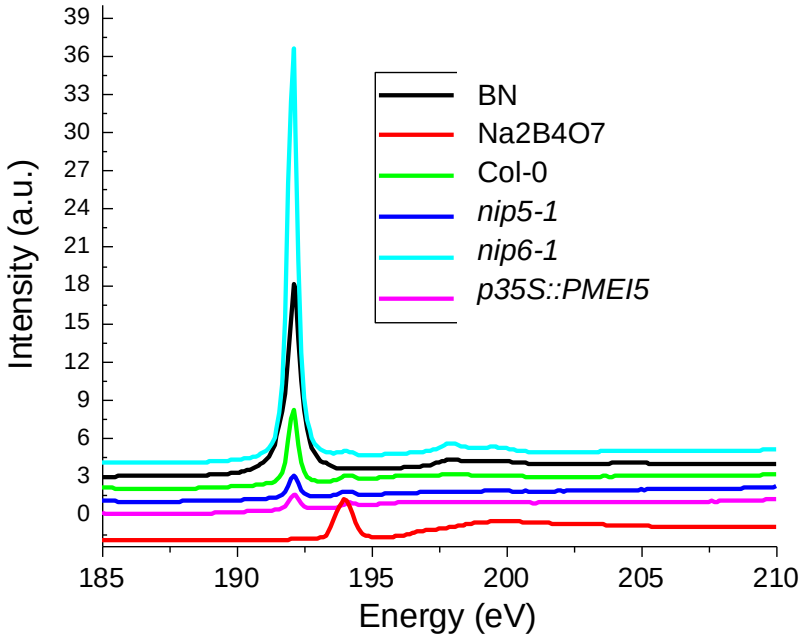

Figure 6.1 XAS (track s electron transitions) spectra from above ground biomass of various *Arabidopsis thaliana* genotypes (*nip5-1*, *nip6-1*, *p35S::PMEI5* and Col-0)

XAS (track s electron transitions) spectra of *nip5-1*, *nip6-1*, *p35S::PMEI5* and WT leaf material from lines of *Arabidopsis thaliana*. Boron nitride (BN) and sodium tetraborate ($NaBO_4$) were used as standards. Intensity, as shown on the Y axis, was normalized to the intensity of the incident beam (I_o). Six biomass samples were analyzed per each individual genotype (Col-0, *nip5-1*, *nip6-1*, *p35S::PMEI5* and *bor1*). Three scans were completed per sample. Experiment completed at the Canadian Light Source, Saskatoon, SK.

6.3.1.2 Soil Samples

In addition to analyzing the boron species in the above ground biomass of the four *A. thaliana* lines of interest (*nip5-1*, *nip6-1*, *p35S::PMEI5* and Col-0), soil samples obtained from each pot were also analyzed. While both BN and $NaBO_4$ were detected in the soil samples, the intensity of these spectra was lower than the plant biomass samples (Figure 6.2). Moreover, while Col-0, had the second highest level of intensity in the above ground biomass, soil samples obtained from these pots exhibited the lowest intensity spectra when compared to the other lines (Figures 6.1-6.2).

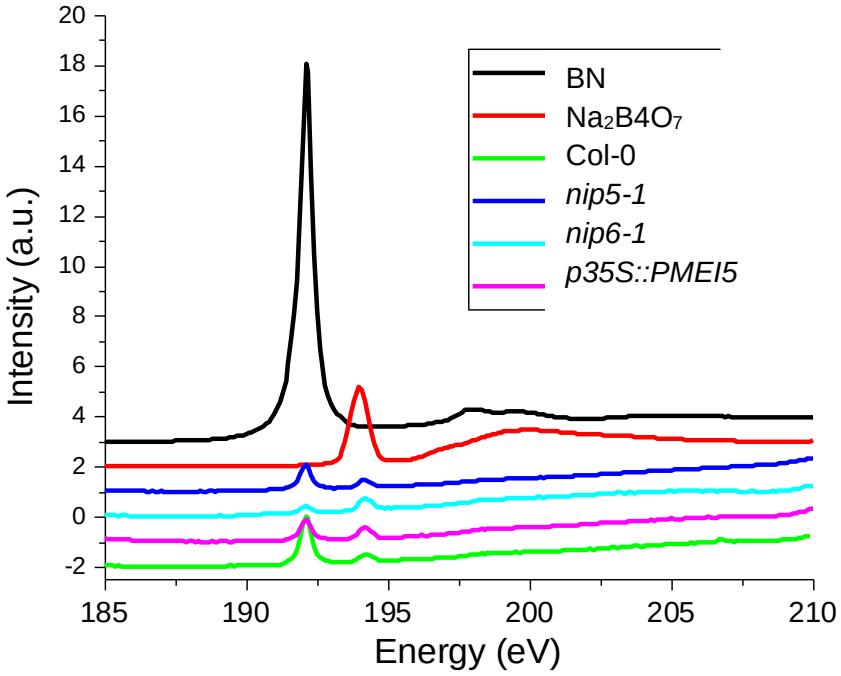

Figure 6.2 XAS (track s electron transitions) spectra from soil collected from pots of various *Arabidopsis thaliana* genotypes (*nip5-1*, *nip6-1*, *p35S::PMEI5* and Col-0*)*

XAS (track s electron transitions) spectra of soil from pots where *nip5-1*, *nip6*-1, *p35S::PMEI5* and Col-0 lines of *Arabidopsis thaliana* was grown. Boron nitride (BN) and sodium tetraborate ($NaBO_4$) were used as standards. Intensity, as shown on the Y axis, was normalized to the intensity of the incident beam (I_o). Six soil samples were analyzed per each individual genotype (*nip5-1*, *nip6*-1, *p35S::PMEI5* and Col-0). Three scans were completed per sample. Experiment completed at the Canadian Light Source, Saskatoon, SK.

6.3.2 Speciation and Semi-Quantification of Boron in *Allium fistulosum*

While the pectin within the cell walls of *A. fistulosum* consists of primarily HG, RG-II accounts for ~1% of pectin within the cell wall of monocots, which includes *Allium* species (Mohnen, 1999). Therefore, boron likely still plays an important structural role in *A. fistulosum* cell walls. Thus, the VLS-PGM beamline was also used to detect and semi-quantify boron species within epidermal cell layers obtained from both *A. fistulosum* plants treated with calcium as well as those from non-calcium treated plants. While both sets of epidermal cell layers contained boron, epidermal cell layers obtained from calcium treated plants exhibited a higher intensity boron spectrum (Figure 6.3). Both cell layers also contained BN and $NaBO_4$, however the intensity for the BN peak was greater than the $NaBO_4$ peak for both the calcium treated group and control (Figure 6.3).

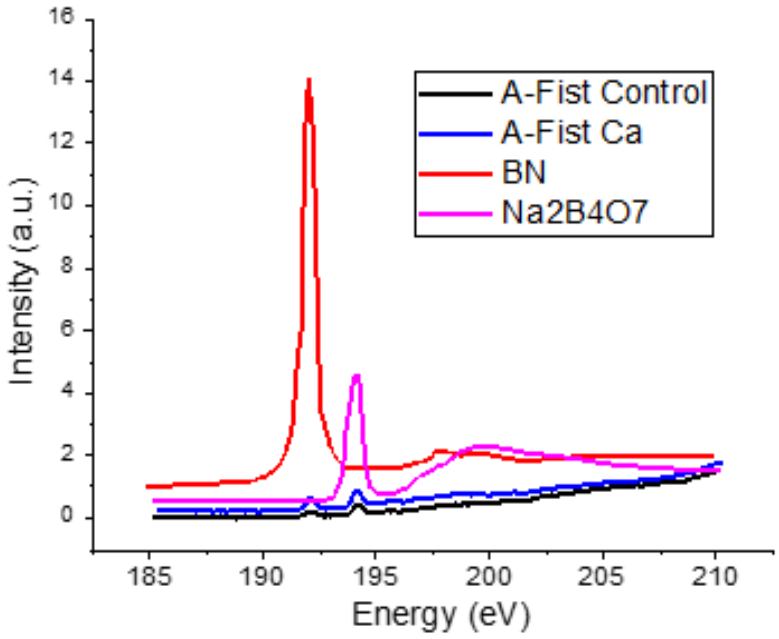

Figure 6.3 XAS (track s electron transitions) spectra from *Allium fistulosum* epidermal cell layers

XAS (track s electron transitions) spectra from epidermal cell layers obtained from *Allium fistulosum* plants that had received 0.05M of $CaCl_2$ every second day for four-weeks (A-Fist Ca), as well as *Allium fistulosum* plants that received no additional $CaCl_2$. This spectrum shows the standards (BN and $Na_2B_4O_7$) used. Three samples were analyzer per treatment group (control and calcium treated). Experiment completed at the Canadian Light Source, Saskatoon, SK.

6.3.3 Spatial Localization of $CaCl_2$ in *Allium fistulosum*

Assuming the addition of $CaCl_2$ to *A. fistulosum* results in alterations in cell wall structure, it was critical to spatially localize calcium within the epidermal cell layers of *A. fistulosum* plants. While the epidermal cell layer obtained from the non-calcium treated *A. fistulosum* plant still had calcium present, the epidermal cell layer obtained from the *A. fistulosum* plant treated with calcium had a visually higher level of calcium (Figure 6.4 and Figure 6.5). However, quantitative analysis of the apoplast (based on the 2D maps) using ImageJ found no significant differences in the mean colour intensity or the mean green or red pixel count (Figure 6.6 and Table A47).

In addition, in non-calcium treated plants, calcium was more randomly distributed within the cell walls (Figure 6.5). In contrast, in calcium treated plants, calcium appears to be primarily

distributed to the radial cell walls (Figure 6.4). The epidermal cell layer of the calcium treated plants also shows numerous hot spots of calcium (Figure 6.4). While these hot spots are also present in the epidermal cell layer obtained from the non-calcium treated plant, there are fewer of them (Figure 6.5).

Unfortunately, issues with the calcium treated epidermal cell layer for the 3D image did not yield a clear photo that could provide further details regarding calcium distribution; however, it still clearly shows greater calcium accumulation localized to the cell wall compared to the control (Figure 6.7 and Figure 6.8).

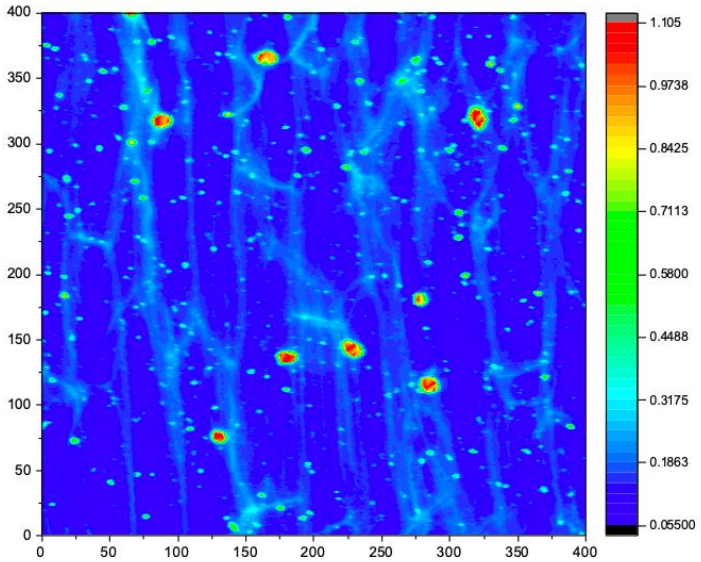

Figure 6.4 2D Calcium map from *Allium fistulosum* epidermal cell layer obtained from a calcium treated plant

2D Calcium map from a single *Allium fistulosum* epidermal cell layer obtained from a plant treated with 0.05M of $CaCl_2$ every second day for four-weeks. The map was obtained using the 20-ID beamline and the X-ray microprobe technique (Advanced Photon Source, Lemont, IL).

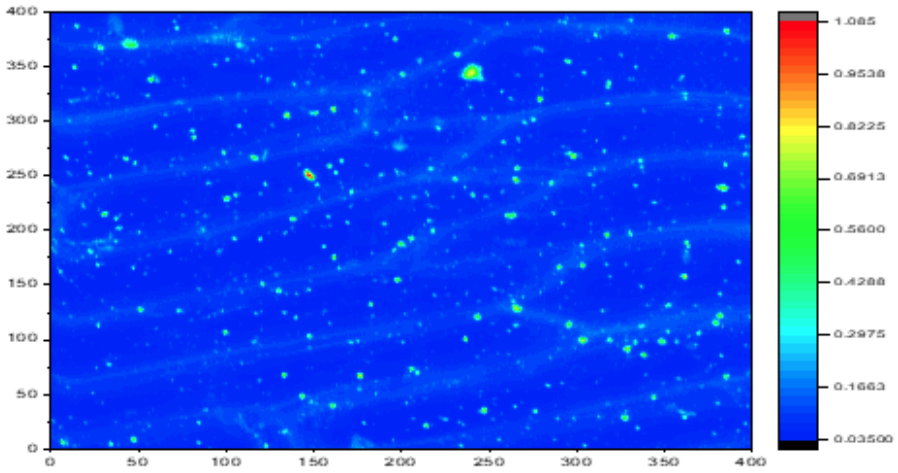

Figure 6.5 2D Calcium map from *Allium fistulosum* epidermal cell layer obtained from a non-calcium treated plant

2D Calcium map from a single *Allium fistulosum* epidermal cell layer obtained from a non-calcium treated plant (control). The map was obtained using the 20-ID beamline and the X-ray microprobe technique (Advanced Photon Source, Lemont, IL).

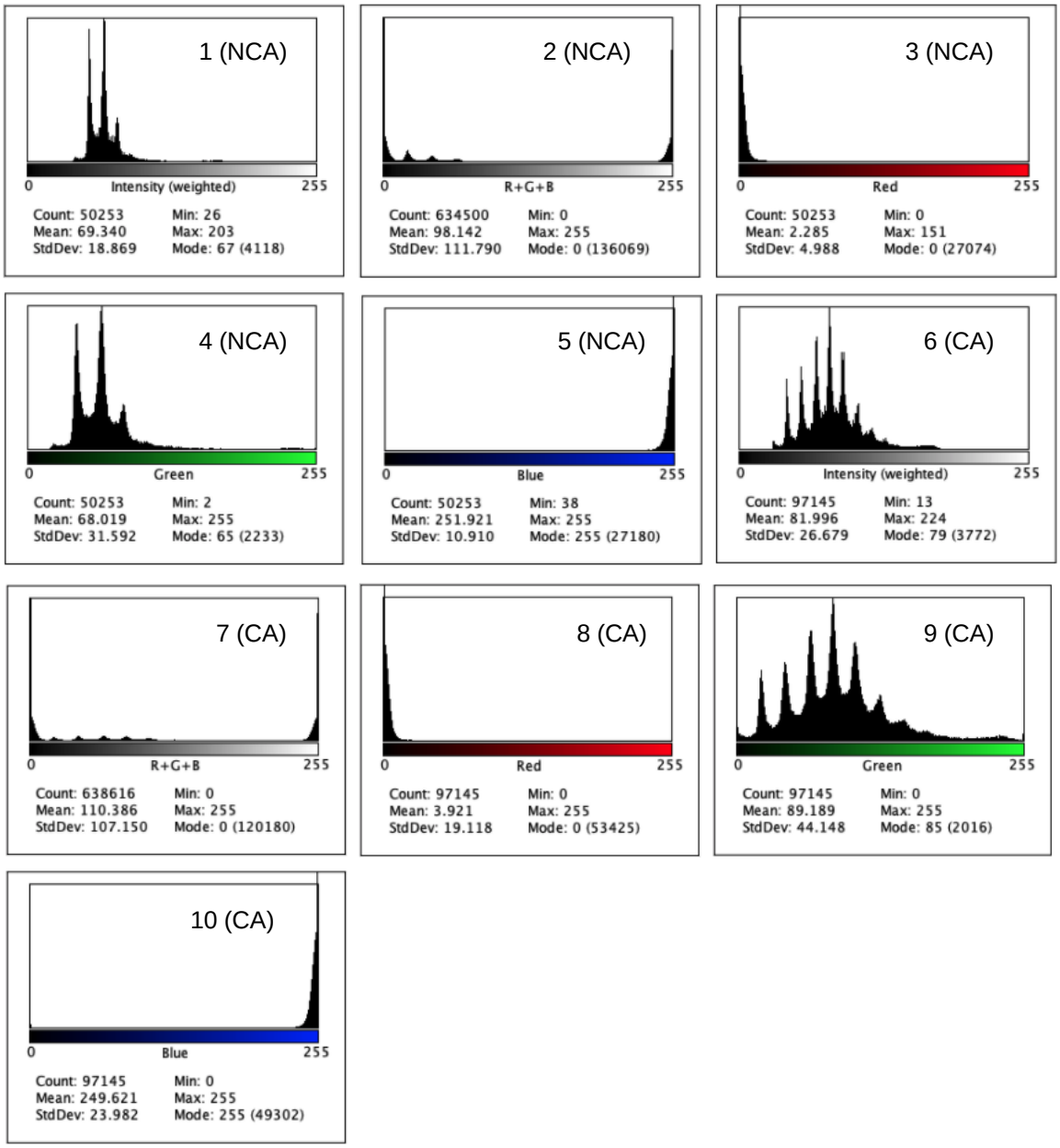

Figure 6.6 Analysis of 2D images of calcium treated and non-calcium treated *Allium fistulosum* epidermal cell layers

Analysis of 2D images of calcium treated (CA) and non-calcium (NCA) treated *Allium fistulosum* epidermal cell layers obtained from 20-ID beamline and the X-ray microprobe technique (Advanced Photon Source, Lemont, IL). Calcium treated plants received 100mL of a 0.05M of $CaCl_2$ solution every second day for four-weeks. Graphs from left to right: 1) weighted intensity of pixel colours (NCA), 2) red, green and blue pixels added together (NCA), 3) green pixels (NCA), 4) red pixels (NCA), 5) blue pixels (NCA), 6) weighted intensity of pixel colours (CA), 7) red, green and blue pixels added together (CA), 8) green pixels (CA), 9) red pixels (CA) and 10) blue pixels (CA). Graphs were generated using ImageJ (Version 1.53a)

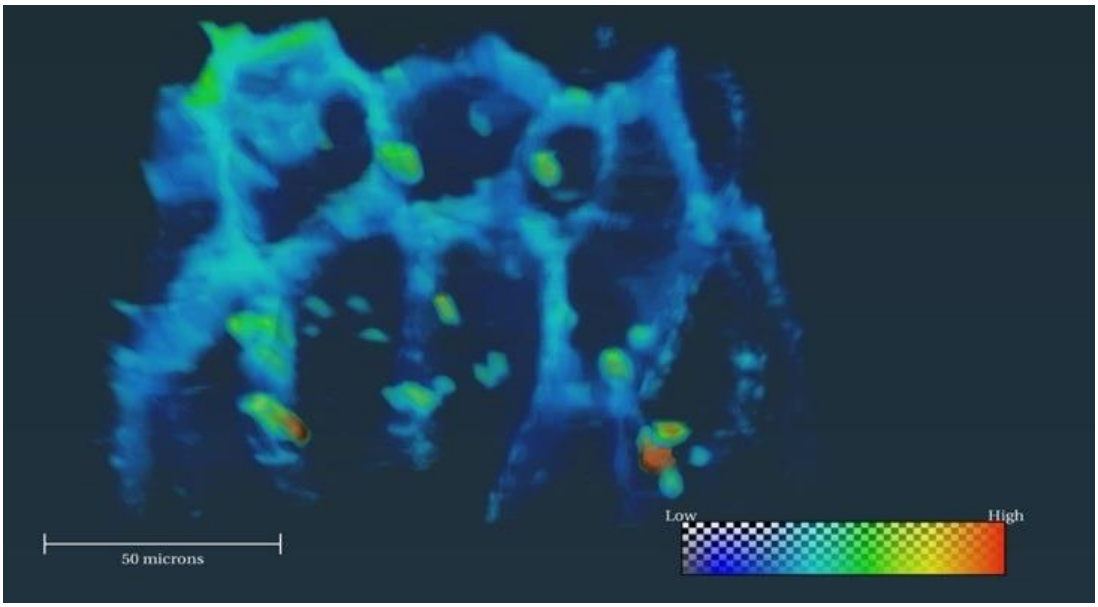

Figure 6.7 3D Calcium map from *Allium fistulosum* epidermal cell layer obtained from a non-calcium treated plant

3D Calcium map from a single *Allium fistulosum* epidermal cell layer obtained from a non-calcium treated plant (control). The map was obtained using the 20-ID beamline and the X-ray microprobe technique (Advanced Photon Source, Lemont, IL).

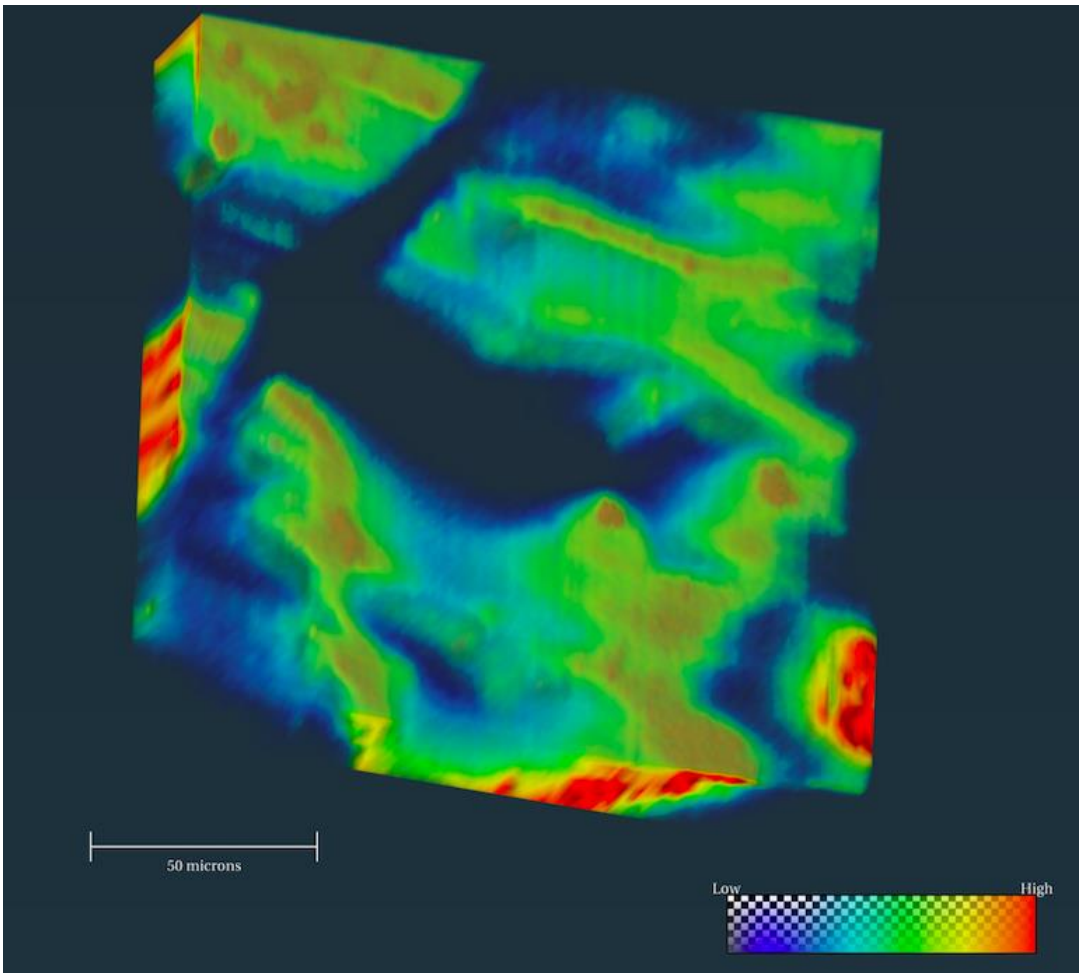

Figure 6.8 3D Calcium map from *Allium fistulosum* epidermal cell layer obtained from a calcium treated plant

3D Calcium map from a single *Allium fistulosum* epidermal cell layer obtained from a calcium treated plant. Plants treated with calcium received 100mL of a 0.05M $CaCl_2$ solution every second day for four-weeks. The map was obtained using the 20-ID beamline and the X-ray microprobe technique (Advanced Photon Source, Lemont, IL).

6.3.4 Staining and Microscopy

6.3.4.1 Alizarin Red S

Staining and microscopy techniques were also utilized to spatially localize $CaCl_2$ within the epidermal cell layer in order to confirm the CLS results. Despite the overall yellow hue across the epidermal cell layer obtained from a non-calcium treated plant, the epidermal cell layer with calcium treatment appears to have a higher level of calcium based on the darker red staining of the apoplast (Figure 6.9). The presence of this colour around the borders of the cells indicates that calcium primarily localizes within and around the cell wall (Figure 6.9). In addition, while the

calcium maps obtained using synchrotron technology showed the distribution of calcium was more random in the epidermal cell layer obtained from the control plant, the distribution appears less random in Figure 6.9. In both cell layers, calcium appears to be distributed primarily around the transverse cell walls, further contrasting observations made from the synchrotron-based calcium maps presented above.

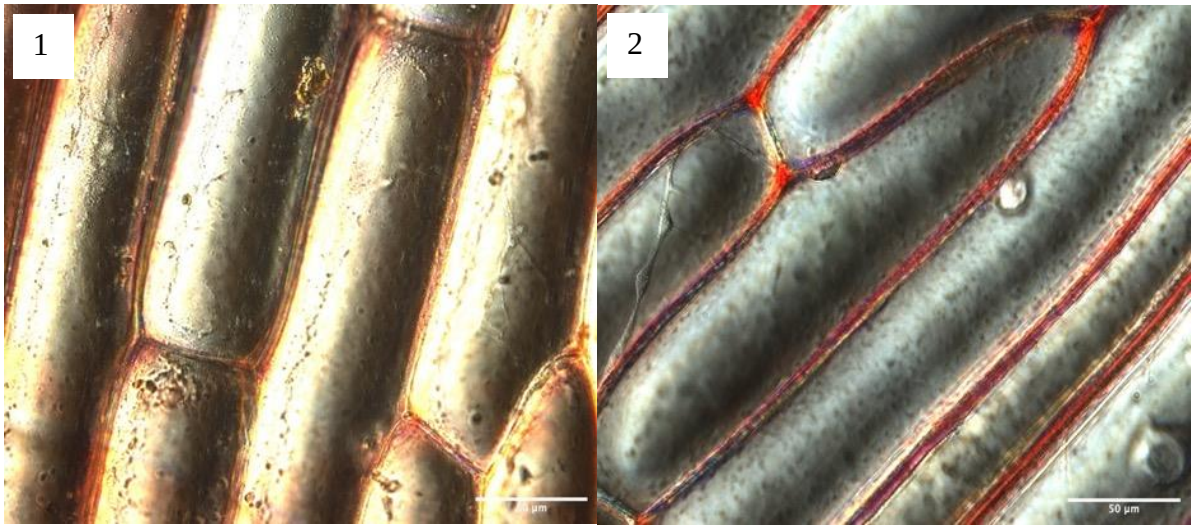

Figure 6.9 *Allium fistulosum* epidermal cell layers (obtained from a non-calcium treated [1] and calcium treated plants [2]) stained with Alizarin red S

Allium fistulosum epidermal cell layers obtained from non-calcium treated *Allium fistulosum* (left) and calcium treated *Allium fistulosum* (right) stained with Alizarin red S for 4min followed by a wash with PBS. Plants treated with calcium received 0.05M of a 100mL $CaCl_2$ solution every second day for four-weeks. Six replicates were done per treatment group (control and calcium treated). Images were taken at 40X on polarized light using a LEICA DM4 B microscope with a LEICA DFC7000 T camera.

6.5.4.2 Ruthenium Red

While visually it is difficult to detect difference between NCA and CA epidermal cell layers stained with Ruthenium red, the analysis of these images using ImageJ shows cell layers obtained from NCA plants had a significantly ($p<0.05$) greater mean number of red, green and blue pixels (Figure 6.10, Figure 6.11 and Table A48). Ruthenium red is a non-specific dye that binds to negative charges including the acidic polysaccharides that make up pectin, thus it can be used to detect pectin (McFarlane, 2014).

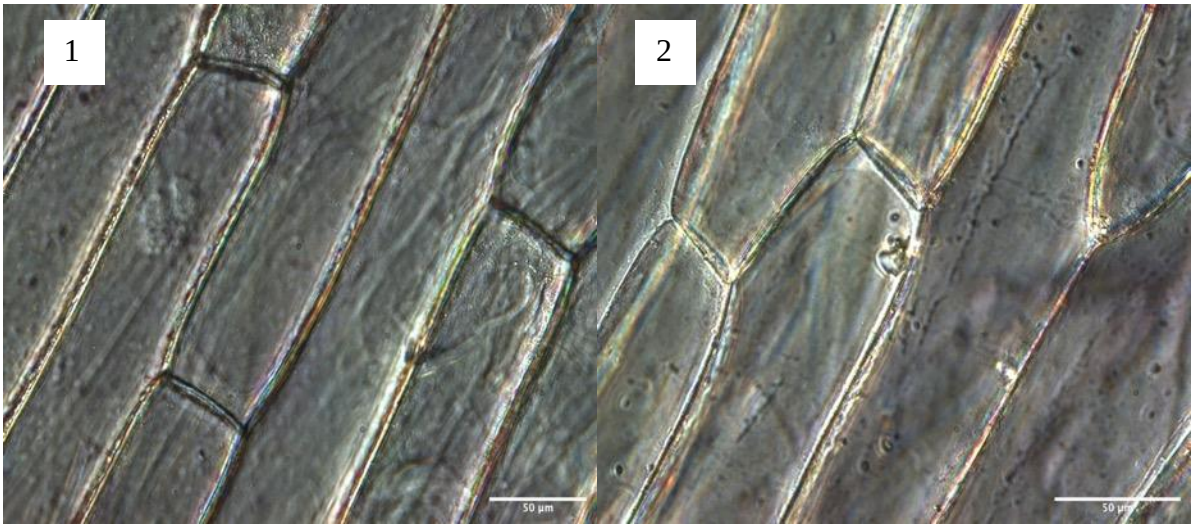

Figure 6.10 *Allium fistulosum* epidermal cell layers (obtained from a non-calcium treated [1] and a calcium treated [2] plants) stained with Ruthenium red

Allium fistulosum epidermal cell layers obtained from non-calcium treated *Allium fistulosum* (right) and calcium treated *Allium fistulosum* (left) stained with Ruthenium red for 4min followed by a wash with PBS. Plants treated with calcium received 0.05M of a 100mL $CaCl_2$ solution every second day for four-weeks. Six replicates were conducted per treatment group (control and calcium treated). Images were taken at 40X on polarized light using a LEICA DM4 B microscope with a LEICA DFC7000 T camera.

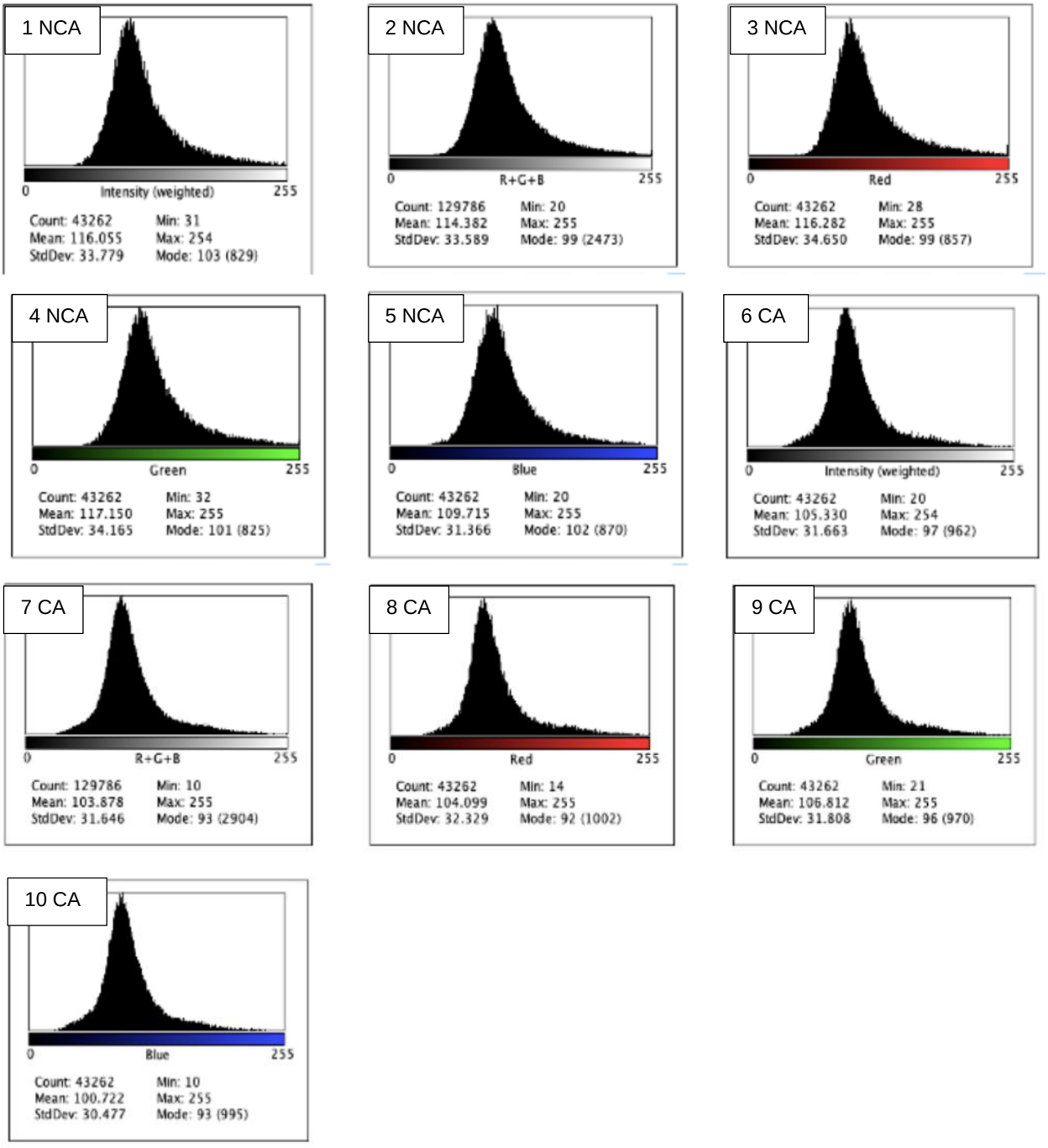

Figure 6.11 Analysis of images obtained from staining with Ruthenium red

Analysis of images obtained from staining of single *A. fistulosum* epidermal cells with Ruthenium red. Graphs from left to right: 1) weighted intensity of pixel colours (NCA), 2) red, green and blue pixels added together (NCA), 3) green pixels (NCA), 4) red pixels (NCA), 5) blue pixels (NCA), 6) weighted intensity of pixel colours (CA), 7) red, green and blue pixels added together (CA), 8) green pixels (CA), 9) red pixels (CA) and 10) blue pixels (CA). Graphs were generated using ImageJ (Version 1.53a).

6.5.4.2 Curcumin

Boron was also stained using curcumin. While curcumin is known to bind to boron, creating a curcumin-boron complex that can be visualized, using it as a stain in plant species is novel, with applications in the literature only describing its use for thin-layer chromatography (TLC) staining and staining of mammalian cells. Analysis of various *A. thaliana* genotypes (*nip5-1, nip6-1*, *p35S::PMEI5*, *bor1* and Col-0) using curcumin stain was able to support some of the results obtained from the VLS-PGM beamline. For example, staining showed that *p35S::PMEI5* had the lowest quantity of orange particulates compared to the other genotypes (Col-0, *nip5-1*, *nip6-1* and *bor1*), supporting results from both the VLS-PGM beamline and ICP-MS (Figure 6.1, Figure 6.12, Figure A17 and Table A11). In addition, staining on leaves showed greater accumulation of orange particulates on Col-0 leaves compared to *nip5-1* (6105 pixels/mm difference), confirming the VLS-PGM results (Figure 6.1, Figure 6.12 and Figure A17).

However, despite comparisons that can be drawn between data obtained from ICP-MS, the VLS-PGM beamline and curcumin staining, amongst the various genotypes there were no significant differences in the pixels/mm area of curcumin complexes found on the leaf tissue (Table A49). Moreover, while some findings obtained from the staining did support data obtained from the VLS-PGM beamline, this was not the case for all genotypes. The remaining contradictory findings between curcumin staining and the VLS-PGM beamline may be reflective of the novelty for curcumin staining in plants and thus the efficacy is unknown. Also, intensity of the spectra obtained from the VLS-PGM beamline may not be a direct indicator of concentration as intensity can be influenced by multiple factors.

In addition, distribution of boron based on the accumulation of orange particulates appears to show uneven distribution in some of the genotypes of interest (Figure 6.12 and Figure A17). This uneven distribution appears to be the most pronounced in *nip5-1*, *p35S::PMEI5* and *bor1* (Figure 6.12 and Figure A17). While this may be indicative of uneven distribution of boron within the leaves of these genotypes, it may also be artifact of variable uptake. As mentioned above, the use of curcumin staining in plants is novel and therefore the differences in distribution may be a reflection

of that. Additional research should be done to find the optimal method of curcumin staining in plants in order to understand if boron distribution is truly uneven in those genotypes.

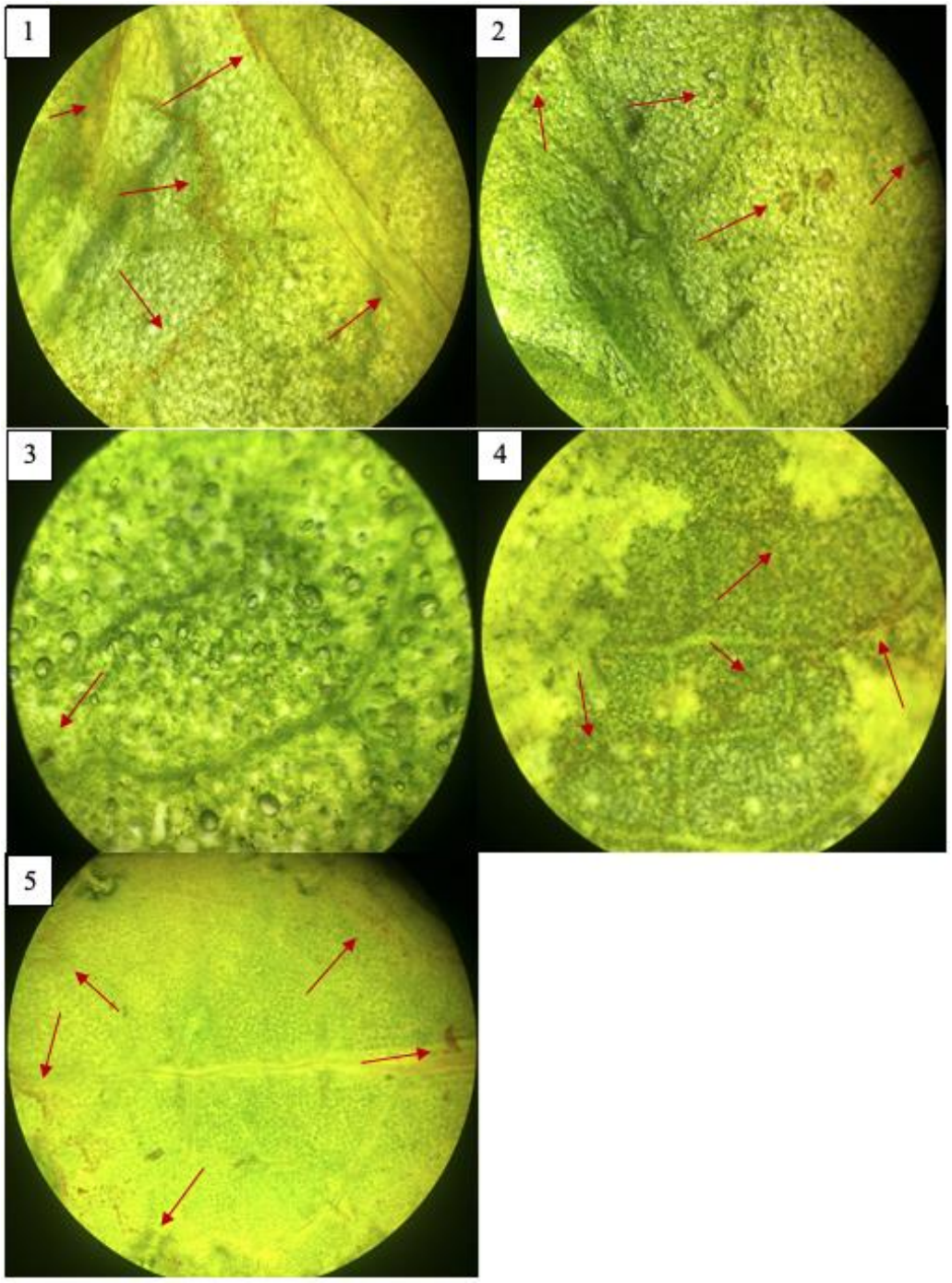

Figure 6.12 Leaves from various *Arabidopsis thaliana* genotypes (*nip5-1*, *nip6-1*, *bor1*, *p35S::PMEI5* and Col-0) stained with curcumin

Leaves from various *Arabidopsis thaliana* genotypes stained with curcumin for 10min followed by a wash with PBS. Leaves from the following lines were stained; 1). Col-0, 2). *nip5-1*, 3). *p35S::PMEI5*, 4). *nip6-1*, and 5). *bor1*. Red arrows point to areas where curcumin-boron complexes appear to have formed. Six replicates were conducted per genotype. Images were taken at 20X on bright field light using a LEICA DM4 B microscope.

6.4 Discussion

6.4.1 Calcium and Pectin

The localization of calcium to the apoplast was critical to supporting the hypothesis that structural changes observed in relation to the strength required to shear through *A. fistulosum* and changes in dehydration stress resistance was due to calcium which results in the formation of pectin "egg-box" structures in the cell wall and middle lamella. As previously outlined, while calcium plays numerous important roles within the cell as a signalling molecule, it is also critical in maintaining the structure of the cell wall (Thor, 2019; Hepler, 2005; White, 2000; Matoh & Kobayashi, 1998). One of the ways in which calcium influences the structure of the cell wall is through the formation of "egg-box" structures (Braccini & Pé Rez, 2001; Matoh & Kobayashi, 1998; Ravanat & Rinaudo, 1980). "Egg-box" structures are the result of the formation of calcium ion cross-linkages to carboxylate ions in galacturonic acid residues of HG that have been demethylesterified in a block-wise manner (Wormit & Usadel, 2018; Braccini & Pé Rez, 2001).

As pectin is only found within the apoplast of plants (cell wall + middle lamella), these structures are exclusive to this region (Keegstra, 2010; O'Neill et al., 1990). Although this thesis did not specifically identify "egg-box" structures, the localization of calcium to the apoplast as seen in both the calcium maps and microscopic imaging is a strong indicator these structures have likely formed within the pectin. Moreover, staining of pectin using Ruthenium red provided additional potential evidence supporting the notion that the addition of calcium increased the formation of "egg-box" structures. As previously mentioned, the demethylesterification of HG creates negative carboxyl groups on the GalA chain, which are subsequently able to form cross-linkages with Ca^{2+} ions, creating "egg-box" structures (Wormit & Usadel, 2018; Braccini & Pé Rez, 2001). Results obtained from staining *A. fistulosum* epidermal cells found non-calcium treated epidermal cell layers had a significantly ($p<0.05$) greater proportion of RGB pixels as a result of the stain. As the mechanism of action for Ruthenium red involves binding to negative charges and thus staining acidic polysaccharides composing pectin, the greater abundance of RGB pixels in the control is suggestive that pectin within this cell layer had more negatively charged carboxyl groups (McFarlane, 2014). A larger proportion of negative charged carboxyl groups is likely indicative of fewer calcium cross-linkages within the pectin matrix. Therefore, these results further support the

notion that the addition of calcium to *A. fistulosum* resulted in the formation of additional "egg-box" structures.

6.4.2 Boron

Since boron is also known to play a critical role in the structure of the cell wall, boron was also analyzed, using a range of techniques to perform speciation and semi-quantification. This analysis included above ground biomass samples from the *A. thaliana* mutant genotypes used throughout this thesis (Col-0 [wild-type], *nip5-1* [boron transporter mutant], *nip6*-1 [boron transporter mutant], *bor1* [boron transporter mutant] and *p35S::PMEI5* [PMEI mutant]) (TAIR, 2021; TAIR, 2015; Müller et al., 2013; TAIR 2013). Epidermal cell layers obtained from non-calcium treated and calcium treated *A. fistulosum* plants were also analyzed for differences in B.

As three of these genotypes (*nip5-1*, *nip6-1* and *bor1*) had mutations in boron transporters, it was hypothesized these mutants would show differences in their boron concentrations both between the other boron transporter mutants and Col-0 and *p35S::PMEI5* (TAIR, 2021; TAIR, 2015; TAIR, 2013). Given the nature of these mutants, the assumption was that *nip5-1*, *nip6-1* and *bor1* would have lower boron concentrations compared to Col-0 and *p35S::PMEI5*. However, this was not the case. Both the semi-quantitative results obtained from the VLS-PGM beamline at the Canadian Light Source (Saskatoon, SK, Canada) and those gathered from an ICP-MS analysis found the concentration of boron was significantly higher in the genotypes with mutations in the NIP transporters compared to Col-0 and *p35S::PMEI5*. More specifically, the semi-quantitative results from the VLS-PGM beamline found *nip6-1* had the highest concentration of boron followed by Col-0, while results from the ICP-MS found *nip6-1* followed by *nip5-1* had the highest concentration of boron. All of the genotypes were found to be significantly different from each other with regards to the quantity of boron detected. This finding is of great importance as all of the previous chapters that had utilized these mutants were conducted under the assumption the boron-transporter mutants had a lower quantity of boron.

Despite the significant variation in the quantity of boron within each genotype detected by ICP-MS, all of the of the genotypes fell within the normal boron concentration range which is between 20-100ppm depending on the species (Table A11) (Plank, 1999). Variation between species with

respect to the required amount of boron has been closely tied to quantity of pectin within the cell wall of higher plants (Hu et al., 1996; Loomis & Durst, 1992; Tanaka, 1967b). For example, the primary cell walls in dicots have a higher pectin content in comparison to gramineous monocots and therefore dicots also have a higher tissue-B requirement (20-30 μg B g^{-1} dry weight vs. 3-10μg B g^{-1} dry weight) (Darvill et al., 1992; Jones et al., 1991). This presumably allows for an increase in the dimerization of RG-II monomers which plays a key role in the mechanical strength of the cell wall amongst other things. However, while the importance of RG-II dimers in maintaining the structure of the cell wall should not be underscored, the complete absence of RG-II dimers will not inhibit the gelling of pectin (Chormova et al., 2014). Chormova et al. (2014) successfully cultured *Rosa* sp. cells in boron-free medium and found pectin within the cell wall contained RG-II monomers but no dimers, suggesting that pectin with RG-II domains can be held together in pectin by other means then boron bridges. This may be due to the structural nature of pectin, as RG-II domains are attached to HG chains which have the ability to cross-link other HG chains via. Ca^{2+} ions (Mohnen, 2008; Ravanat & Rinaudo, 1980).

The limitation of these results is that *bor1* was not included in these analyses due to previous issues discussed regarding the genotype. Thus, the concentration of boron in *bor1* is unknown. While this trend does not follow our previous assumption, one plausible hypothesis which may explain why lines with mutations in boron-transporters have higher levels of boron is that in the NIP mutant lines, other boron-transporters may be over-compensating. This hypothesis is supported by the concept of genetic redundancy, meaning more than one gene performs the same function with an organism and therefore inactivating one of these genes has little to no effect on phenotype (Ascencio & DeLuna, 2013; Nowak et al., 1997). This theory may also explain why *nip5-1* and *nip6-1* did not appear phenotypically different from Col-0.

However, curcumin staining did appear to show *bor1* has a lower concentration of boron compared to *nip6-1* and Col-0. Furthermore, *bor1* is also phenotypically very different from the other genotypes. Figures A9 and A11, capture some of those differences showing that *bor1* is much smaller than the other lines at both two-weeks and four-weeks and at two-week old *bor1* also appears more yellow in colour. On the other hand, both of the genotypes with mutations in NIP transporters (*nip5-1* and *nip6-1*) did not appear phenotypically different from Col-0. Therefore,

there may be genetic redundancy in the NIP transporters, while it appears as though the loss of BOR1 is more detrimental. Unfortunately, there is a lack of additional research available done on these genotypes in general and therefore this remains a hypothesis that should be further investigated.

In addition to using curcumin to analyze boron in *bor1*, curcumin was also used to stain the leaves of the other genotypes as well. The ability for curcumin to detect boron is a direct result of curcumin being a β-diketone ligand, allowing it to act as a chelating ligand towards a number of metals including boron (Hope-Roberts & Horobin, 2017; Hardcastle, 1960). These papers go on to describe that the chelation of curcumin and boric acid produces a cationic 2:1 complex where boron is the central atom with curcumin anions attached in a tetrahedral fashion. This complex is known as rosocyanine (Hope-Roberts & Horobin, 2017; Hardcastle, 1960). This method of boron detection has been used in various health sciences fields, including pharmacology and cancer research. However, to our knowledge, curcumin has not yet been used to stain boron in plant tissue.

Therefore, while our results should be approached with caution given the novelty of the method, the results obtained are supportive of those obtained from the VLS-PGM beamline, and to a lesser extent those obtained from ICP-MS. Curcumin staining visually appears to *show nip6-1* has the highest concentration of boron, supporting results from both the VLS-PGM beamline and ICP-MS. Col-0 followed by *nip5-1*, *bor1* and finally *p35S::PMEI5* appeared to visually have the lowest concentrations of boron in that order, based on results from staining. While this method did not allow for the localization of boron, interestingly, there appears to be variation in the curcumin stain across the leaf, both within a single leaf and when comparing leaves of different genotypes. This uneven distribution may be indicative that boron is not evenly distributed throughout the leaves, however alternatively this could also simply be the result of the novelty of this method. For example, the uptake of curcumin by the leaves may be variable, and therefore while distribution of boron may appear uneven it may be the result of the uptake of curcumin. Furthermore, while we believe the particulates within the leaves are the result of boron-curcumin complexes based on the use of this stain in primarily health sciences fields, the confirmation of this was outside the scope of this thesis. Therefore, the notion that distribution of boron within the leaves is uneven

based on this experiment should be approached with caution given that further exploration into the efficacy of this staining method in plants is required.

Even so, the detection of boric acid using curcumin is significant as boric acid is the form of boron responsible for the formation of RG-II dimers (O'Neill et al., 1996). As *Arabidopsis* is a dicot, RG-II likely makes up approximately 5% of pectin within the cell wall (Mohnen, 1999). The detection of boric acid through the use of curcumin therefore supports the notation that RG-II dimers are likely forming. While the exact proportion of these dimers is unknown, in boron sufficient conditions, more than 90% of RG-II exists in dimers (Funakawa & Miwa, 2015; O'Neill et al., 1996). Therefore, the proportion of RG-II dimers may be around 90% in these genotypes of interest. The formation of these dimers in the *Arabidopsis* leaves likely play a key role in the overall structure of the cells, as RG-II dimers formed by RG-II and boric acid have been well implicated for their role in maintaining the structure of cells.

However, despite the detection of boric acid by way of curcumin staining, analysis of the various boron species with both above ground biomass samples and soil samples obtained from the pots used to grow the lines did not detect any boric acid. Speciation performed at the VLS-PGM beamline detected boron nitride and to a lesser extent sodium tetraborate. The identification of these two boron species within these samples is interesting given what is known regarding the role of boron in plants. As previously mentioned, RG-II dimers are formed by a single borate diester cross link between the apiosyl residues on side chain A of an RG-II monomer (O'Neill et al., 2004). O'Neill et al. (1996) demonstrated RG-II dimers can only occur with boric acid. Outside of RG-II dimer formation, boron has a hand in numerous key biological processes including ion fluxes across membranes, cell division and elongation, etc. (Goldbach & Wimmer, 2007; Blevins & Lukaszewski, 1998; Cakmak & Römheld, 1997). Despite its role in these key processes, a thorough review of the literature does not reveal any studies investigating whether or not boron is present in any other species outside of boric acid. The majority of studies mentioning boron in relation to plants commonly refer to it simply as boron, and occasionally boric acid (Brown et al., 2002; Matoh & Kobayashi, 1998; Blevins & Lukaszewski, 1998; Matoh, 1997). This suggests that boron is not present in any other forms within plant tissues. While in the soil, boron is found in the form of boric acid and is also taken up by plants as boric.

Thus, results obtained from the VLS-PGM beamline are interesting in their finding of both boron nitride and sodium tetraborate. Boron nitride, the most predominant form of boron identified in both the plant biomass and the soil samples via. speciation using the VLS-PGM is of keen interest given that boron nitride does not appear to have been identified in other plant tissues within the literature. In contrast, boron nitride has been used in a range of other commercial applications including cosmetics, pencil lead and space applications (Khan, 2016). While additional analysis is outside of the scope of this project, further studies should be conducted to better understand the presence of boron nitride in plant biomass and soil. In addition, while a literature review also did not reveal any studies describing the presence of sodium tetraborate in plant tissues, sodium tetraborate is commonly used as fertilizer (Borax). Therefore, its presence may be the result of fertilizers used for culture and care.

Overall, the findings from this Chapter do not support the hypothesis which stated different species of boron would be present within the above-ground biomass of various Arabidopsis genotypes and the soil obtained from the pots used to grow them. However, the results from this Chapter show the application of calcium to *A. fistulosum* does result in an increase in calcium around the apoplast, thus supporting that hypothesis.

7.0 GENERAL DISCUSSION

The effects of climate change pose an insurmountable threat to agriculture industries across the world as the frequency and severity of abiotic and biotic stresses continue to rise as a result. The consequences of these stresses which include drought stress, cold stress and pathogens will continue to not only threaten global food supplies but also large economies, many of which rely heavily on the Agriculture and Agri-Food industry. For example, in Canada the Agriculture and Agri-Food industry generated $143 billion (CAD) in 2018, accounting for 7.4% of the GDP (Government of Canada, 2020). The success of this industry and in turn many other factors in society are at the mercy of climate change, which has the potential to reduce crop yields up to 100%. Thus, it is critical to find mechanisms within plants that provide defence against a range of stresses.

This thesis narrowed in on the potential for the cell wall to act as a physical barrier against dehydration stress and fungal pathogens, namely as a result of pectin and the influence of its structural modifications on the cell wall. Despite the structural changes observed both *in vitro* and in *A. fistulosum* sheaths as a result of calcium application and the benefit it had in reducing percent water loss in pure pectin, its effect on *Allium* species was far more complicated. While calcium improved tolerance to dehydration stress in some instances, it was also found to increase percent water loss, most notably over 15min in *A. fistulosum* (Figures 4.4). In general, findings showing calcium did not significantly ($p>0.05$) improve tolerance to dehydration stress stand in contrast to other previous findings which found calcium improved tolerance to drought stress (Table 4.3) (He at al., 2018; Ma et al., 2005). Nevertheless, the variation in the results observed with respect to calcium and dehydration stress serve as a valuable reminder as to the complexity of the response to dehydration stress and the complex role of calcium in plants.

While the threat of drought stress is increasing as a result of climate change and thus putting plants at greater risk of dehydration stress, the risk of damage to crops as a result of cold stress is also predicted to rise (Gu et al., 2008). Although drought stress and cold stress are associated with opposite weather patterns, they share the overlapping theme of dehydration stress. During cold stress as temperatures fall, plants face a risk of freezing. During freezing, ice begins to form in the

extracellular space, resulting in the occurrence of extracellular freeze dehydration stress as water leaves the cells (Burke et al., 1976). As Liu (2015) found that cold acclimation not only improved tolerance to cold stress but also decreased cell wall permeability, it was hypothesized that cold acclimation would also reduce percent water loss. However surprisingly, in most instances cold acclimation increased percent water loss in *A. fistulosum* (Figure 4.15 and Figure 4.17).

Despite the seeming disconnect between cold acclimation and percent water loss, cold hardy *A. fistulosum* which has been shown to tolerate temperatures hovering around -40ºC, was far more tolerant to dehydration stress compared to *A. cepa*, which lacks the ability to tolerate cold (Tanino et al., 2013, Palta et al., 1977). *A. fistulosum* lost significantly ($p<0.05$) less water and had a significantly ($p<0.05$) lower limit of damage based on protoplasmic streaming compared to *A. cepa* (Table A18 and Table A22). This finding indicates that while cold acclimation did not improve tolerance to dehydration stress as it does to cold stress, there is likely still a link between tolerance to cold stress and tolerance to dehydration stress. This connection may lie within the cell wall and the structural role of pectin.

Equally important to plant survival in nature and agricultural fields is resistance to both abiotic and biotic stresses. Like dehydration stress, the risk of damage to plants as a result of fungal pathogens is on the rise as factors associated with climate change are increasing the frequency of these pathogens. Thus, it is also critical to understand the role that pectin, and in turn the cell wall, may play in mitigating both stresses.

While not specifically investigated within this thesis, the boron transporter BOR1 appears to influence the integrity of the cell wall and in turn impact tolerance to dehydration stress and tolerance to *C. higginsianum*. Over 2-10hr of dehydration stress, *bor1* was amongst the least dehydration tolerant *Arabidopsis* genotypes explored, having the highest percent water loss and amongst the highest values of percent electrolyte leakage, indicating an increase in the limit of damage (Figure 4.21 and Figure 4.22). *bor1* was also one of the most susceptible genotypes to *C. higginsianum* (Figures 5.3 and 5.4). While the lesion associated with a *C. higginsianum* infection does not typically show up until ~84hr post-infection (Münch et al., 2008), leaves from *bor1* plants begun to develop lesions at 24hr (Figure 5.3). Given that *C. higginsianum* has the capability of

penetrating the host plant with shear force alone, the rapid appearance of the lesion is indicative that as a result of the mutation in *bor1*, the cell walls are much weaker (Yan et al., 2018). This may be indicative of a lack of RG-II dimers, which are known to play a critical role in the structure of the cell wall (O'Neill et al., 2004; Hu & Brown, 1994). Given that RG-II dimers have also been shown to reduce porosity, increased water loss in *bor1* during dehydration stress may further be indicative of structural changes to the cell walls in *bor1* plants (Fleischer et al., 1999; Ryden et al., 2003; O'Neill et al., 2004). These findings further demonstrate the critical nature of the cell wall as a barrier to both stresses and the role of RG-II in the structure of the cell wall.

Moreover, the over-expression of PMEI5 also appeared to enhance tolerance to dehydration stress and *B. cinerea* (Figure 4.19, Figures 4.21-4.25, Figure 5.1 and Figure 5.2). While initially the over-expression of PMEI5 was hypothesized to reduce tolerance to both stresses as the activity of PME is critical in the formation of "egg-box" structures, the results from this thesis reject the original hypothesis. *p35S::PMEI5* consistently lost amongst the lowest amounts of water during periods of dehydration and had a significantly ($p<0.05$) lower overall percent electrolyte leakage following 12-24hrs of dehydration (Figure 4.19, Figures 4.21-4.25, Table A39 and Table A40). *p35S::PMEI5* also had a smaller *B. cinerea* lesion size in comparison to other genotypes (Figure 5.1 and Figure 5.2). Increased tolerance to *B. cinerea* in *p35S::PMEI5* in comparison to *C. higginsianum* is demonstrative of the different mechanisms used by the pathogens to penetrate the cell wall. Unlike *C. higginsianum*, *B. cinerea* uses pectinolytic machinery amongst other lethal enzymes to cross the cell wall (Boddy, 2016). Demethylesterified pectin is more frequently the target of pectinolytic enzymes and therefore the inhibition of PME's such as by PMEI's has also been shown in multiple other studies to enhance tolerance to *B. cinerea* (Lionetti et al., 2017, Müller et al., 2013; Curvers et al., 2010; Lionetti et al., 2007). This difference is also demonstrative of the variation not only between abiotic and biotic stresses, but within both of those categories as well.

Therefore, while this thesis focused on the role of pectin within the cell wall and the potential to exploit pectin modifications in order to enhance the role of the cell wall as a physical barrier, it is highly likely that a single mechanism may not be effective against all stresses. Nevertheless, it is still critical to identify mechanisms which help to mitigate multiple stresses as single stresses are

never found in nature and certain combinations of stress are likely to occur more often in tandem compared to others.

While this thesis provided strong evidence suggesting that pectin modifications within the cell wall are partly responsible for changes to abiotic and biotic stress tolerance, it did not specifically eliminate the possibility that other elements within the cell wall may be also influencing stress tolerance. Therefore, one of the next steps forward in this research should further focus in on pectin within the cell wall while eliminating possible influence from other components within the cell wall. In a similar vein, future research based on this thesis should specifically identify the formation of "egg-box" structures and RG-II dimers. Furthermore, while this thesis identified mechanical changes associated with the addition of calcium and boron, analysis of shear force was performed using whole sheaths. While the epidermal cell layer was attached, it is possible other structures within the sheath may have been responsible for increased toughness. Subsequent studies should seek to further narrow in on the cell wall and identify specific structural and mechanical changes occurring within it such as permeability and toughness. Finally, abiotic and biotic stress should be applied together. Application of these stresses together would not only fill a current gap in the literature but would also provide critical insight into the potential role of the cell wall and pectin in stress defense outside of a controlled lab environment, since in nature plants experience multiple stresses at once.

8.0 GENERAL CONCLUSIONS

In conclusion, while calcium, boron, cold temperatures and cold acclimation, were all found to affect mechanical characteristics of pure pectin and A. fistulosum sheaths, as a result of modifications presumed to occur within pectin, these changes did not directly translate to enhanced tolerance to stress.

While the addition of calcium and boron to pure pectin solutions had a significant effect in reducing percent water loss, the effect of these elements in biological systems was less clear. Although calcium enhanced dehydration stress tolerance, its effect was often not significant, and variable in its efficacy. In general, *Arabidopsis* genotypes with mutations in boron transporters had reduced dehydration stress tolerance, while the over-expression of PMEI5 appeared to enhance tolerance to dehydration stress.

Moreover, we found that *A. fistulosum* which has the ability to cold acclimate and has a high freezing tolerance is also more tolerant to dehydration stress loss in comparison to *A. cepa* which lacks the ability to cold acclimate and is freezing sensitive. However, in general, we did not find that cold acclimation enhanced dehydration stress tolerance in *A. fistulosum.*

Furthermore, given that outside of a controlled environment plants are subjected to a multitude of stresses at once this thesis also explored the role of the cell wall and pectin modifications in tolerance to biotic stress. One key finding from Chapter 5 was the rapid rate of *C. higginsianum* infection in *bor1*. In Chapter 4, *bor1* was also found to be susceptible to dehydration tolerance.

Finally, while we were able to localize calcium to the cell wall, further advancements outside of our control are required to localize boron within the cell. Nevertheless, findings from Chapter 6 further supported the belief that calcium application would increase the formation of “egg-box structures”.

Thus, the general all-encompassing hypothesis, “the application of calcium and/or boron results in cell wall structural changes which translate into increased resistance to both abiotic and biotic

stress in *Allium* species and *Arabidopsis thaliana*" is rejected. However, several sub-hypotheses were fully supported. The underlined sections of the following sub-hypothesis were supported by data from this thesis:

1. Increasing concentrations of pectins and calcium/boron will reduce water loss over 6hr in pure pectin standards. Furthermore, boron will have a greater influence on reducing water loss in GB pectin, while calcium will have a larger effect on HG pectin.
2. The exogenous application of $CaCl_2$ localizes to the apoplast of *Allium fistulosum* (*A. fistulosum)*
3. The stress sensitive *Allium cepa has* greater percent water loss compared to stress resistant *Allium fistulosum.*
4. Calcium and boron independently increase the viscosity of pectin, in a dose- and temperature- dependent manner. *The caveat to this is that boron significantly increased pectin concentration independent of temperature, however calcium did not.
5. Calcium application and cold acclimation will increase the force required to shear through *Allium fistulosum*, and a combined application will further increase resistance to shear force in an additive manner.
6. *Arabidopsis thaliana* lines with mutations in boron transporters and pectin methylesterase inhibitor 5 (*p35S::PMEI5*) will have a faster rate of *Botrytis cinerea* and *Colletotrichum higginsianum* infection.

In conclusion, while response to abiotic and biotic stress by plants is highly complex and the ability for plants to withstand stress goes far beyond one mechanism, this thesis gives further insight into the key role of pectin in the cell wall and the influence of pectin modifications.

9.0 REFERENCES

Abdel-Motagally, F. M. F., & El-Zohri, M. (2018). Improvement of wheat yield grown under drought stress by boron foliar application at different growth stages. *Journal of the Saudi Society of Agricultural Sciences*, *17*(2). https://doi.org/10.1016/j.jssas.2016.03.005

Abraham, J., Sharika, T., Mishra, R. K., & Thomas, S. (2017). Rheological characteristics of nanomaterials and nanocomposites. In *Micro and Nano Fibrillar Composites (MFCs and NFCs) from Polymer Blends*. https://doi.org/10.1016/B978-0-08-101991-7.00014-5

Achary, V. M., Jena, S., Panda, K. K., & Panda, B. B. (2008). Aluminium induced oxidative stress and DNA damage in root cells of Allium cepa L. *Ecotoxicology and Environmental Safety*, *70*(2). https://doi.org/10.1016/j.ecoenv.2007.10.022

Ademe, A. (2013). Evaluation of Antifungal Activity of Plant Extracts against Papaya Anthracnose (Colletotrichum gloeosporioides). *Journal of Plant Pathology & Microbiology*, *04*(10). https://doi.org/10.4172/2157-7471.1000207

Adler, D., & Murdoch, D. (2021, March 4). rgl: 3D Visualization Using OpenGL. CRAN.

Albersheim, P., Darvill, A. G., O'Neill, M. A., Schols, H. A., & Voragen, A. G. J. (1996). An hypothesis: The same six polysaccharides are components of the primary cell walls of all higher plants. *Progress in Biotechnology*, *14*(C). https://doi.org/10.1016/S0921-0423(96)80245-0

Alberts, B., Johnson, A., & Lewis, J. (2002). Molecular Biology of the Cell (4th ed.). New York, NY: Garland Science. Retrieved from https://www.ncbi.nlm.nih.gov/books/NBK26928/

Alberts, B., Johnson, A., Lewis, J., Raff, M., Roberts, K., & Walter, P. (2002). The Plant Cell Wall. Retrieved from https://www.ncbi.nlm.nih.gov/books/NBK26928/

Alizadeh, V., Shokri, V., Soltani, A., & Yousefi, M. A. (2014). Effects of Climate Change and Drought-Stress on Plant Physiology. *International journal of Advanced Biological and Biomedical Research* (Vol. 2). Retrieved from http://www.ijabbr.com

Amsbury, S., Hunt, L., Elhaddad, N., Baillie, A., Lundgren, M., Verhertbruggen, Y., … Gray, J. E. (2016). Stomatal Function Requires Pectin De-methyl-esterification of the Guard Cell Wall. *Current Biology*, *26*(21). https://doi.org/10.1016/j.cub.2016.08.021

An, S. H., Sohn, K. H., Choi, H. W., Hwang, I. S., Lee, S. C., & Hwang, B. K. (2008). Pepper pectin methylesterase inhibitor protein CaPMEI1 is required for antifungal activity, basal disease resistance and abiotic stress tolerance. *Planta*, *228*(1). https://doi.org/10.1007/s00425-008-0719-z

Arora, R. (2018). Mechanism of freeze-thaw injury and recovery: A cool retrospective and warming up to new ideas. *Plant Science*, *270*, 301–313. https://doi.org/10.1016/J.PLANTSCI.2018.03.002

Arora, R., & Palta, J. (1988). In Vivo Perturbation of Membrane-Associated Calcium by Freeze-Thaw Stress in Onion Bulb Cells: Simulation of This Perturbation in Extracellular KCl and Alleviation by Calcium. *Plant Physiology*, *87*(3). https://doi.org/10.1104/pp.87.3.622

Arve, L. E., Carvalho, D. R., Olsen, J. E., & Torre, S. (2014). Plant Signaling & Behavior ABA induces H2O2 production in guard cells, but does not close the stomata on Vicia faba leaves developed at high air humidity. https://doi.org/10.4161/psb.29192

Ascencio, D., & DeLuna, A. (2013). Genetic Redundancy. In W. Dubitzky, O. Wolkenhauer, C. Kwang-Hyun, & Y. Hiroki (Eds.), *Encyclopedia of Systems Biology*.

Aydin, M., Tombuloglu, G., Sakcali, M. S., Hakeem, K. R., & Tombuloglu, H. (2019). Boron Alleviates Drought Stress by Enhancing Gene Expression and Antioxidant Enzyme Activity. *Journal of Soil Science and Plant Nutrition*, *19*(3). https://doi.org/10.1007/s42729-019-00053-8

Ball, W. D., & Key, A. J. (2014). Chemical Bonds. In *Introduction Chemistry- 1st Canadian Edition* (1st ed.). OpenEd.

Banik, P., Zeng, W., Tai, H., Bizimungu, B., & Tanino, K. (2016). Effects of drought acclimation on drought stress resistance in potato (Solanum tuberosum L.) genotypes. *Environmental and Experimental Botany*, *126*. https://doi.org/10.1016/j.envexpbot.2016.01.008

Bao, Y., & Ertbjerg, P. (2015). Relationship between oxygen concentration, shear force and protein oxidation in modified atmosphere packaged pork. *Meat Science*, *110*. https://doi.org/10.1016/j.meatsci.2015.07.022

Bassett, R. L. (1980). A critical evaluation of the thermodynamic data for boron ions, ion pairs, complexes, and polyanions in aqueous solution at 298.15 K and 1 bar. *Geochimica et Cosmochimica Acta*, *44*(8). https://doi.org/10.1016/0016-7037(80)90069-1

Bender, K. W., & Snedden, W. A. (2013). Calmodulin-related proteins step out from the shadow of their namesake. *Plant Physiology*. https://doi.org/10.1104/pp.113.221069

Berta, G., Altamura, M. M., Fusconi, A., Cerruti, F., Capitani, F., & Bagni, N. (1997). The plant cell wall is altered by inhibition of polyamine biosynthesis. *New Phytologist*, *137*(4). https://doi.org/10.1046/j.1469-8137.1997.00868.x

Blevins, D. G., & Lukaszewski, K. M. (1998). Boron in Plant Structure and Function. *Annual Review of Plant Physiology and Plant Molecular Biology*, *49*(1), 481–500. https://doi.org/10.1146/annurev.arplant.49.1.481

Boddy, L. (2016). Pathogens of Autotrophs. In *The Fungi: Third Edition* (pp. 245–292). Elsevier Inc. https://doi.org/10.1016/B978-0-12-382034-1.00008-6

Bonsal, B. R., Wheaton, E. E., Chipanshi, A. C., Lin, C., Sauchyn, D. J., & Wen, L. (2011). Drought research in Canada: A review. *Atmosphere - Ocean*. https://doi.org/10.1080/07055900.2011.555103

Bosch, M., Cheung, A. Y., & Hepler, P. K. (2005). Pectin methylesterase, a regulator of pollen tube growth. *Plant Physiology*, *138*(3). https://doi.org/10.1104/pp.105.059865

Boudart, G., Lafitte, C., Barthe, J. P., Frasez, D., & Esquerré-Tugayé, M. T. (1998). Differential elicitation of defense responses by pectic fragments in bean seedlings. *Planta*, *206*(1). https://doi.org/10.1007/s004250050377

Braccini, I., & Pé Rez, S. (2001). Molecular Basis of Ca 2+-Induced Gelation in Alginates and Pectins: The Egg-Box Model Revisited. https://doi.org/10.1021/bm010008g

Breydo, L. (2013). Boron, Biologically Active Compounds. In *Encyclopedia of Metalloproteins* (pp. 295–299). New York, NY: Springer New York. https://doi.org/10.1007/978-1-4614-1533-6_483

Brown, P. H., Bellaloui, N., Wimmer, M. A., Bassil, E. S., Ruiz, J., Hu, H., … Römheld, V. (2002). Boron in plant biology. *Plant Biology*. https://doi.org/10.1055/s-2002-25740

Burke, M. J., Gusto, L. V, Quamme, H. A., Weiser, C. J., & Li, P. H. (1976). Freezing and Injury in Plants. *Ann. Rev. Plant Physiol* (Vol. 27). Retrieved from www.annualreviews.org

Burstrom, H. (1968). Calcium and Plant Growth. *Biological Reviews*, *43*(3), 287–316. https://doi.org/10.1111/j.1469-185X.1968.tb00962.x

Cakmak, I., & Römheld, V. (1997). Boron deficiency-induced impairments of cellular functions in plants. In *Plant and Soil* (Vol. 193). https://doi.org/10.1007/978-94-011-5580-9_6

Carpita, N. C., Defernez, M., Findlay, K., Wells, B., Shoue, D. A., Catchpole, G., … McCann, M. C. (2001). Cell wall architecture of the elongating maize coleoptile. *Plant Physiology*, *127*(2). https://doi.org/10.1104/pp.010146

Cavitt, L. C., Youm, G. W., Meullenet, J. F., Owens, C. M., & Xiong, R. (2004). Prediction of Poultry Meat Tenderness Using Razor Blade Shear, Allo-Kramer Shear, and Sarcomere Length. *Journal of Food Science*, *69*(1). https://doi.org/10.1111/j.1365-2621.2004.tb17879.x

CEM. (n.d.). MARS 6th Method Note. Microwave Digestion of Feed Grains.

Chakraborty, A. (2015). Histological study of the interactions between Cucumber - powdery mildew, Podosphaera xanthii and Potato - Botrytis cinerea. Wageningen University and Research Centre, Wageningen.

Cheng, S. H., Willmann, M. R., Chen, H. C., & Sheen, J. (2002). Calcium signaling through protein kinases. The Arabidopsis calcium-dependent protein kinase gene family. *Plant Physiology*. https://doi.org/10.1104/pp.005645

Choquer, M., Fournier, E., Kunz, C., Levis, C., Pradier, J. M., Simon, A., & Viaud, M. (2007). Botrytis cinerea virulence factors: New insights into a necrotrophic and polyphageous pathogen. *FEMS Microbiology Letters*. https://doi.org/10.1111/j.1574-6968.2007.00930.x

Chormova, D., Messenger, D. J., & Fry, S. C. (2014). Boron bridging of rhamnogalacturonan-II, monitored by gel electrophoresis, occurs during polysaccharide synthesis and secretion but not post-secretion. *Plant Journal*, *77*(4), 534–546. https://doi.org/10.1111/tpj.12403

Coenen, G. J., Bakx, E. J., Verhoef, R. P., Schols, H. A., & Voragen, A. G. J. (2007). Identification of the connecting linkage between homo- or xylogalacturonan and rhamnogalacturonan type I. *Carbohydrate Polymers*, *70*(2). https://doi.org/10.1016/j.carbpol.2007.04.007

Cohen, J. (1988). Statistical Power Analysis for the Behavioural Science (2nd Edition). *Statistical Power Analysis for the Behavioral Sciences* (Vol. 3).

Cosgrove, D. J., & Jarvis, M. C. (2012). Comparative structure and biomechanics of plant primary and secondary cell walls. *Frontiers in Plant Science*, *3*, 204. https://doi.org/10.3389/fpls.2012.00204

Craufurd, P. Q., & Peacock, J. M. (1993). Effect of heat and drought stress on sorghum (Sorghum bicolor). II. Grain yield. *Experimenal Agriculture*, *29*(1). https://doi.org/10.1017/S0014479700020421

Crawley, M. (2013). *The R Book* (2nd ed.). West Sussex: John Wiley & Sons, Ltd.

Curvers, K., Seifi, H., Mouille, G., de Rycke, R., Asselbergh, B., Van Hecke, A., … Hofte, M. (2010). Abscisic Acid Deficiency Causes Changes in Cuticle Permeability and Pectin Composition That Influence Tomato Resistance to Botrytis cinerea. *Plant Physiology*, *154*, 847–860.

Dahl, L. K. (1952). A simple and sensitive histochemical method for calcium. *Proc Soc Exp Biol Med*, *80*(3), 474–479.

Dai, A. (2013). Increasing drought under global warming in observations and models. *Nature Climate Change*, *3*(1), 52–58. https://doi.org/10.1038/nclimate1633

Darvill, A., Mcneil, M., Albersheim, P., & Delmer, D. P. (1980). The Primary Cell Walls of Flowering Plants. In N. E. Tolbert (Ed.), *The Biochemistry of Plants*. Academic Press. https://doi.org/10.1016/b978-0-12-675401-8.50009-9

Day, I. S., Reddy, V. S., Shad Ali, G., & Reddy, A. S. (2002). Analysis of EF-hand-containing proteins in Arabidopsis. *Genome Biology*, *3*(10). https://doi.org/10.1186/gb-2002-3-10-research0056

De Jong, J. C., McCormack, B. J., Smirnoff, N., & Talbot, N. J. (1997). Glycerol generates turgor in rice blast. *Nature*. https://doi.org/10.1038/38418

De Silva, D. D., Crous, P. W., Ades, P. K., Hyde, K. D., & Taylor, P. W. J. (2017). Life styles of Colletotrichum species and implications for plant biosecurity. *Fungal Biology Reviews*. https://doi.org/10.1016/j.fbr.2017.05.001

Del Corpo, D., Fullone, M. R., Miele, R., Lafond, M., Pontiggia, D., Grisel, S., … Lionetti, V. (2020). AtPME17 is a functional Arabidopsis thaliana pectin methylesterase regulated by its PRO region that triggers PME activity in the resistance to Botrytis cinerea. *Molecular Plant Pathology*, *21*(12). https://doi.org/10.1111/mpp.13002

Dell, B., & Huang, L. (1997). Physiological response of plants to low boron. *Plant and Soil*, *193*(1–2). https://doi.org/10.1023/A:1004264009230

Demidchik, V., Straltsova, D., Medvedev, S. S., Pozhvanov, G. A., Sokolik, A., & Yurin, V. (2014). Stress-induced electrolyte leakage: The role of K+-permeable channels and involvement in programmed cell death and metabolic adjustment. *Journal of Experimental Botany*. https://doi.org/10.1093/jxb/eru004

Dong, X., Wang, M., Ling, N., Shen, Q., & Guo, S. (2016). Effects of iron and boron combinations on the suppression of Fusarium wilt in banana. *Scientific Reports*, *6*. https://doi.org/10.1038/srep38944

Dotto, L., Duchesne, L., Etkin, D., Jaffit, E., Joe, P., Jones, B., … Stocks, B. (2010). *Canadians at risk: Our exposure to natural hazards*. Toronto.

Dowling, M., Peres, N., Villani, S., & Schnabel, G. (2020). Managing colletotrichum on fruit crops: A "complex" Challenge. *Plant Disease*, *104*(9). https://doi.org/10.1094/PDIS-11-19-2378-FE

Edwards, K., Johnstone, C., & Thompson, C. (1991). A simple and rapid method for the preparation of plant genomic DNA for PCR analysis. *Nucleic Acids Research*. https://doi.org/10.1093/nar/19.6.1349

El Balla, M. M. A., Hamid, A. A., & Abdelmageed, A. H. A. (2013). Effects of time of water stress on flowering, seed yield and seed quality of common onion (Allium cepa L.) under the arid tropical conditions of Sudan. *Agricultural Water Management*, *121*. https://doi.org/10.1016/j.agwat.2013.02.002

Engelsdorf, T., Will, C., Hofmann, J., Schmitt, C., Merritt, B. B., Rieger, L., … Voll, L. M. (2017). Cell wall composition and penetration resistance against the fungal pathogen Colletotrichum higginsianum are affected by impaired starch turnover in Arabidopsis mutants. *Journal of Experimental Botany*, *68*(3), 701–713. https://doi.org/10.1093/jxb/erw434

Etehadnia, E., Waterer, D. R., & Tanino, K. K. (2008). Calcium amendment and NaCl salt pre-treatment improves salinity tolerance in potato genotypes. University of Saskatchewan.

Etehadnia, M., Schoenau, J., Waterer, D., & Karen, T. (2010). The effect of CaCl2 and NaCl salt acclimation in stress tolerance and its potential role in ABA and scion/rootstock-mediated salt stress responses. *Plant Stress*, *4*.

Fasiolo, M., Nedellec, R., Goude, Y., Capezza, C., & Wood, S. (2020). mgcViz: Visualisations for Generalized Additive Models. CRAN.

Feng, W., Kita, D., Peaucelle, A., Cartwright, H. N., Doan, V., Duan, Q., … Dinneny, J. R. (2018). The FERONIA Receptor Kinase Maintains Cell-Wall Integrity during Salt Stress through Ca2+ Signaling. *Current Biology*, *28*(5). https://doi.org/10.1016/j.cub.2018.01.023

Fleischer, A., O'Neill, M. A., & Ehwald, R. (1999). The Pore Size of Non-Graminaceous Plant Cell Walls Is Rapidly Decreased by Borate Ester Cross-Linking of the Pectic Polysaccharide Rhamnogalacturonan II. *Plant Physiology*, *121*(3), 829–838. https://doi.org/10.1104/pp.121.3.829

Food and Agriculture Organization of the United Nations. (2009). How to Feed the World in 2050. Retrieved from http://www.fao.org/fileadmin/templates/wsfs/docs/expert_paper/How_to_Feed_the_World_in_2050.pdf

Friesen, N., Pollner, S., Bachmann, K., & Blattner, F. R. (1999). RAPDs and noncoding chloroplast DNA reveal a single origin of the cultivated Allium fistulosum from A. altaicum (Alliaceae). *American Journal of Botany*, *86*(4), 554–562. https://doi.org/10.2307/2656817

Frontiers. (n.d.). Research Topic- Necrotrophic Fungal Plant Pathogens.

Fu, S., Thacker, A., Sperger, D. M., Boni, R. L., Buckner, I. S., Velankar, S., … Block, L. H. (2011). Relevance of rheological properties of sodium alginate in solution to calcium alginate gel properties. *AAPS PharmSciTech*, *12*(2). https://doi.org/10.1208/s12249-011-9587-0

Funakawa, H., & Miwa, K. (2015). Synthesis of borate cross-linked rhamnogalacturonan II. *Frontiers in Plant Science*, *6*(APR). https://doi.org/10.3389/fpls.2015.00223

Geitmann, A. (1999). The Rheological Properties of the Pollen Tube Cell Wall. In M. Cresti, G. Cai, & A. Moscatelli (Eds.), *Fertilization in Higher Plants*. Springer, Berlin, Heidelberg. https://doi.org/10.1007/978-3-642-59969-9_20

Ghodke, P., Khandagale, K., Thangasamy, A., Kulkarni, A., Narwade, N., Shirsat, D., … Singh, M. (2020). Comparative transcriptome analyses in contrasting onion (Allium cepa L.) genotypes for drought stress. *PLoS ONE*, *15*(8 August). https://doi.org/10.1371/journal.pone.0237457

Gibeaut, D. M., Pauly, M., Bacic, A., & Fincher, G. B. (2005). Changes in cell wall polysaccharides in developing barley (Hordeum vulgare) coleoptiles. *Planta*, *221*(5). https://doi.org/10.1007/s00425-005-1481-0

Gimenez, E., Salinas, M., & Manzano-Agugliaro, F. (2018). Worldwide research on plant defense against biotic stresses as improvement for sustainable agriculture. *Sustainability (Switzerland)*. https://doi.org/10.3390/su10020391

Gleason, M. ., & Helland, S. . (2003). Disease| Botrytis. In *Encyclopedia of Rose Science* (pp. 144–148).

Goldbach, H. E., & Wimmer, M. A. (2007). Boron in plants and animals: Is there a role beyond cell-wall structure? *Journal of Plant Nutrition and Soil Science*, *170*(1), 39–48. https://doi.org/10.1002/jpln.200625161

Government of Canada. (2020). Overview of the Canadian agriculture and agri-food sector 2018.

Gu, L., Hanson, P. J., Post, W. Mac, Kaiser, D. P., Yang, B., Nemani, R., … Meyers, T. (2008). The 2007 Eastern US Spring Freeze: Increased Cold Damage in a Warming World? *BioScience*, *58*(3), 253–262. https://doi.org/10.1641/B580311

Guillemin, F., Guillon, F., Bonnin, E., Devaux, M. F., Chevalier, T., Knox, J. P., … Thibault, J. F. (2005). Distribution of pectic epitopes in cell walls of the sugar beet root. *Planta*, *222*(2). https://doi.org/10.1007/s00425-005-1535-3

Ha, M. A., Apperley, D. C., & Jarvis, M. C. (1997). Molecular rigidity in dry and hydrated onion cell walls. *Plant Physiology*, *115*(2). https://doi.org/10.1104/pp.115.2.593

Hamant, O., & Traas, J. (2010). The mechanics behind plant development. *New Phytologist*. https://doi.org/10.1111/j.1469-8137.2009.03100.x

Hanesiak, J. M., Stewart, R. E., Bonsal, B. R., Harder, P., Lawford, R., Aider, R., … Zha, T. (2011). Characterization and summary of the 1999-2005 Canadian prairie drought. *Atmosphere - Ocean*, *49*(4). https://doi.org/10.1080/07055900.2011.626757

Hardcastle, J. (1960). A Study of the Curcumin Method for Boron Determination. University of Richmond.

Hastie, T. J., & Tibshirani, R. J. (n.d.). Generalized Additive Models. Retrieved May 23, 2020, from https://books.google.ca/books?hl=en&lr=&id=qa29r1Ze1coC&oi=fnd&pg=IA1&dq=generalized+additive+models&ots=j44NhqvXpQ&sig=ZPMfTSp3qF_zxdTqVwVessUAalY&redir_esc=y#v=onepage&q=generalized additive models&f=false

Hegedus, D. D., & Rimmer, S. R. (2005). Sclerotinia sclerotiorum: When "to be or not to be" a pathogen? *FEMS Microbiology Letters*. https://doi.org/10.1016/j.femsle.2005.07.040

Hegedus, D. D., & Rimmer, S. R. (2005). Sclerotinia sclerotiorum: When "to be or not to be" a pathogen? *FEMS Microbiology Letters*. https://doi.org/10.1016/j.femsle.2005.07.040

Hepler, P. K. (2005). Calcium: A central regulator of plant growth and development. *Plant Cell*. https://doi.org/10.1105/tpc.105.032508

Herburger, K., Xin, A., & Holzinger, A. (2019). Homogalacturonan accumulation in cell walls of the green alga Zygnema sp. (charophyta) increases desiccation resistance. *Frontiers in Plant Science*, *10*. https://doi.org/10.3389/fpls.2019.00540

Heredia, A., Jiménez, A., & Guillén, R. (1995). Composition of plant cell walls. *Zeitschrift Für Lebensmittel-Untersuchung Und - Forschung*. https://doi.org/10.1007/BF01192903

Heyne, E. G., & Brunson, A. M. (1940). Genetic Studies of Heat and Drought Tolerance in Maize. *AgronomyJournal*, *32*(10). https://doi.org/10.2134/agronj1940.00021962003200100009x

Hohl, M., & Schopfer, P. (1995). Rheological analysis of viscoelastic cell wall changes in maize coleoptiles as affected by auxin and osmotic stress. *Physiologia Plantarum*, *94*(3). https://doi.org/10.1034/j.1399-3054.1995.940319.x

Hong, M. J., Kim, D. Y., Lee, T. G., Jeon, W. B., & Seo, Y. W. (2010). Functional characterization of pectin methylesterase inhibitor (PMEI) in wheat. *Genes & Genetic Systems*, *85*(2), 97–106. https://doi.org/10.1266/ggs.85.97

Hope-Roberts, M., & Horobin, R. W. (2017). A review of curcumin as a biological stain and as a self-visualizing pharmaceutical agent. *Biotechnic and Histochemistry*, *92*(5). https://doi.org/10.1080/10520295.2017.1310925

Hosseini, S. A., Réthoré, E., Pluchon, S., Ali, N., Billiot, B., & Yvin, J. C. (2019). Calcium application enhances drought stress tolerance in sugar beet and promotes plant biomass and beetroot sucrose concentration. *International Journal of Molecular Sciences*, *20*(15). https://doi.org/10.3390/ijms20153777

Houston, K., Tucker, M. R., Chowdhury, J., Shirley, N., & Little, A. (2016). The Plant Cell Wall: A Complex and Dynamic Structure As Revealed by the Responses of Genes under Stress Conditions. *Frontiers in Plant Science*, *7*, 984. https://doi.org/10.3389/fpls.2016.00984

Hu, H., & Brown, P. H. (1994). Localization of boron in cell walls of squash and tobacco and its association with pectin. Evidence for a structural role of boron in the cell wall. *Plant Physiology*, *105*(2). https://doi.org/10.1104/pp.105.2.681

Hu, H., Brown, P. H., & Labavitch, J. M. (1996). Species variability in boron requirement is correlated with cell wall pectin. *Journal of Experimental Botany*, *47*(295). https://doi.org/10.1093/jxb/47.2.227

Hu, W., Tian, S. B., Di, Q., Duan, S. H., & Dai, K. (2018). Effects of exogenous calcium on mesophyll cell ultrastructure, gas exchange, and photosystem II in tobacco (Nicotiana tabacum Linn.) under drought stress. *Photosynthetica*, *56*(4). https://doi.org/10.1007/s11099-018-0822-8

Industry Overview - Canola Council of Canada. (n.d.). Retrieved August 10, 2019, from https://www.canolacouncil.org/markets-stats/industry-overview/

Ishii, T., & Matsunaga, T. (2001). Pectic polysaccharide rhamnogalacturonan II is covalently linked to homogalacturonan. *Phytochemistry*, *57*(6). https://doi.org/10.1016/S0031-9422(01)00047-4

Ishii, T., Matsunaga, T., & Hayashi, N. (2001). Formation of rhamnogalacturonan II-borate dimer in pectin determines cell wall thickness of pumpkin tissue. *Plant Physiology*, *126*(4). https://doi.org/10.1104/pp.126.4.1698

Ishii, T., Matsunaga, T., Pellerin, P., O'Neill, M. A., Darvill, A., & Albersheim, P. (1999). The plant cell wall polysaccharide rhamnogalacturonan II self-assembles into a covalently cross-linked dimer. *Journal of Biological Chemistry*, *274*(19). https://doi.org/10.1074/jbc.274.19.13098

Jackson, C. L., Dreaden, T. M., Theobald, L. K., Tran, N. M., Beal, T. L., Eid, M., … Mohnen, D. (2007). Pectin induces apoptosis in human prostate cancer cells: Correlation of apoptotic function with pectin structure. *Glycobiology*, *17*(8). https://doi.org/10.1093/glycob/cwm054

Jagtap, V., Bhargava, S., Streb, P., & Feierabend, J. (1998). Comparative effect of water, heat and light stresses on photosynthetic reactions in Sorghum bicolor (L.) Moench. *Journal of Experimental Botany*, *49*(327). https://doi.org/10.1093/jxb/49.327.1715

Jayawardena, R., Bhunjun, C., Hyde, K., Gentekaki, E., & Itthayakorn, P. (2021). Colletotrichum: lifestyles, biology, morpho-species, species complexes and accepted species. *Mycosphere*, *12*(1). https://doi.org/10.5943/mycosphere/12/1/7

Jones, J. J., Wolf, B., & Mills, H. (1991). *Plant analysis handbook. A practical sampling, preparation, analysis and interpretation guide*. Athens, Georgia: Micro-Macro Publishing Inc.

Jones, R. G. W., & Lunt, O. R. (1967). The function of calcium in plants. *The Botanical Review*, *33*(4), 407–426. https://doi.org/10.1007/BF02858743

Juge, N. (2006). Plant protein inhibitors of cell wall degrading enzymes. *Trends in Plant Science*. https://doi.org/10.1016/j.tplants.2006.05.006

Karim, M. R., Zhang, Y. Q., Zhao, R. R., Chen, X. P., Zhang, F. S., & Zou, C. Q. (2012). Alleviation of drought stress in winter wheat by late foliar application of zinc, boron, and

manganese. *Journal of Plant Nutrition and Soil Science*, *175*(1). https://doi.org/10.1002/jpln.201100141

Keegstra, K. (2010). Plant Cell Walls. *Plant Physiology*. https://doi.org/10.1104/pp.110.161240

Khan, M. H. (2016). Synthesis and application of few-layered hexagonal boron nitrade. University of Wollongong.

Khazaei, H., & Vandenberg, A. (2020). Seed Mineral Composition and Protein Content of Faba Beans (Vicia faba L.) with Contrasting Tannin Contents. *Agronomy*, *10*(511).

Khushboo, Bhardwaj, K., Singh, P., Raina, M., Sharma, V., & Kumar, D. (2018). Exogenous application of calcium chloride in wheat genotypes alleviates negative effect of drought stress by modulating antioxidant machinery and enhanced osmolyte accumulation. *In Vitro Cellular and Developmental Biology - Plant*, *54*(5). https://doi.org/10.1007/s11627-018-9912-3

Knight, H., Trewavas, A. J., & Knight, M. R. (1997). Calcium signalling in Arabidopsis thaliana responding to drought and salinity. *Plant Journal*, *12*(5). https://doi.org/10.1046/j.1365-313X.1997.12051067.x

Kobayashi, M., Matoh, T., & Azuma, J. I. (1996). Two chains of rhamnogalacturonan II are cross-linked by borate-diol ester bonds in higher plant cell walls. *Plant Physiology*, *110*(3). https://doi.org/10.1104/pp.110.3.1017

Koch, G. W., Stillet, S. C., Jennings, G. M., & Davis, S. D. (2004). The limits to tree height. *Nature*, *428*(6985). https://doi.org/10.1038/nature02417

Konno, H., Yamasaki, Y., Sugimoto, M., & Takeda, K. (2008). Differential changes in cell wall matrix polysaccharides and glycoside-hydrolyzing enzymes in developing wheat seedlings differing in drought tolerance. *Journal of Plant Physiology*, *165*(7). https://doi.org/10.1016/j.jplph.2007.07.007

Kot, F. S. (2009). Boron sources, speciation and its potential impact on health. *Reviews in Environmental Science and Biotechnology*. Springer. https://doi.org/10.1007/s11157-008-9140-0

Kroeger, J. H., & Geitmann, A. (2012). Pollen tube growth: Getting a grip on cell biology through modeling. *Mechanics Research Communications*, *42*. https://doi.org/10.1016/j.mechrescom.2011.11.005

Krolikowski, K. A., Victor, J. L., Wagler, T. N., Lolle, S. J., & Pruitt, R. E. (2003). Isolation and characterization of the Arabidopsis organ fusion gene HOTHEAD. *The Plant Journal*, *35*(4), 501–511. https://doi.org/10.1046/j.1365-313X.2003.01824.x

Kunz, C., Vandelle, E., Rolland, S., Poinssot, B., Bruel, C., Cimerman, A., … Boccara, M. (2006). Characterization of a new, nonpathogenic mutant of Botrytis cinerea with impaired plant colonization capacity. *New Phytologist*, *170*(3). https://doi.org/10.1111/j.1469-8137.2006.01682.x

Lakens, D. (2013). Calculating and reporting effect sizes to facilitate cumulative science: A practical primer for t-tests and ANOVAs. *Frontiers in Psychology*, *4*(NOV). https://doi.org/10.3389/fpsyg.2013.00863

Lara-Espinoza, C., Carvajal-Millán, E., Balandrán-Quintana, R., López-Franco, Y., & Rascón-Chu, A. (2018). Pectin and pectin-based composite materials: Beyond food texture. *Molecules*. https://doi.org/10.3390/molecules23040942

Larsen, K. (2015). GAM: The Predictive Modeling Silver Bullet.

Lawrence, K., Bhalla, P., & Misra, P. C. (1995). Changes in NAD(P)H-Dependent Redox Activities in Plasmalemma-Enriched Vesicles Isolated from Boron- and Zinc-Deficient Chick Pea Roots. *Journal of Plant Physiology*, *146*(5–6). https://doi.org/10.1016/S0176-1617(11)81928-0

Le Gall, H., Philippe, F., Domon, J.-M., Gillet, F., Pelloux, J., & Rayon, C. (2015). Cell Wall Metabolism in Response to Abiotic Stress. *Plants (Basel, Switzerland)*, *4*(1), 112–166. https://doi.org/10.3390/plants4010112

Leclere, L., Cutsem, P. Van, & Michiels, C. (2013). Anti-cancer activities of pH- or heat-modified pectin. *Frontiers in Pharmacology*, *4*, 128. https://doi.org/10.3389/fphar.2013.00128

Lee, J. Y., & Lee, D. H. (2003). Use of serial analysis of gene expression technology to reveal changes in gene expression in Arabidopsis pollen undergoing cold stress. *Plant Physiology*, *132*(2). https://doi.org/10.1104/pp.103.020511

Leucci, M. R., Lenucci, M. S., Piro, G., & Dalessandro, G. (2008). Water stress and cell wall polysaccharides in the apical root zone of wheat cultivars varying in drought tolerance. *Journal of Plant Physiology*, *165*(11). https://doi.org/10.1016/j.jplph.2007.09.006

Levesque-Tremblay, G., Pelloux, J., Braybrook, S. A., & Müller, K. (2015). Tuning of pectin methylesterification: consequences for cell wall biomechanics and development. *Planta*. https://doi.org/10.1007/s00425-015-2358-5

Lionetti, V., Cervone, F., & Bellincampi, D. (2012). Methyl esterification of pectin plays a role during plant-pathogen interactions and affects plant resistance to diseases. *Journal of Plant Physiology*, *169*(16). https://doi.org/10.1016/j.jplph.2012.05.006

Lionetti, V., Fabri, E., De Caroli, M., Hansen, A. R., Willats, W. G. T., Piro, G., & Bellincampi, D. (2017). Three pectin methylesterase inhibitors protect cell wall integrity for Arabidopsis immunity to Botrytis. *Plant Physiology*, *173*(3). https://doi.org/10.1104/pp.16.01185

Lionetti, V., Raiola, A., Camardella, L., Giovane, A., Obel, N., Pauly, M., … Bellincampi, D. (2007). Overexpression of pectin methylesterase inhibitors in Arabidopsis restricts fungal infection by Botrytis cinerea. *Plant Physiology*, *143*(4). https://doi.org/10.1104/pp.106.090803

Liu, G., Ji, Y., Bhuiyan, N. H., Pilot, G., Selvaraj, G., Zou, J., & Wei, Y. (2010). Amino acid homeostasis modulates salicylic acid-associated redox status and defense responses in Arabidopsis. *Plant Cell*, *22*(11). https://doi.org/10.1105/tpc.110.079392

Liu, G., Kennedy, R., Greenshields, D. L., Peng, G., Forseille, L., Selvaraj, G., & Wei, Y. (2007). Detached and attached Arabidopsis leaf assays reveal distinctive defense responses against hemibiotrophic Colletotrichum spp. *Molecular Plant-Microbe Interactions*, *20*(10). https://doi.org/10.1094/MPMI-20-10-1308

Liu, J. (2015). Temperature-Mediated Alterations of the Plant Apoplast as a Mechanism of Intracellular Freezing Stress Avoidance. University of Saskatchewan. Retrieved from https://harvest.usask.ca/handle/10388/ETD-2015-10-2290

Loix, C., Huybrechts, M., Vangronsveld, J., Gielen, M., Keunen, E., & Cuypers, A. (2017). Reciprocal Interactions between Cadmium-Induced Cell Wall Responses and Oxidative Stress in Plants. *Frontiers in Plant Science*, *8*. https://doi.org/10.3389/fpls.2017.01867

Loomis, W. D., & Durst, R. W. (1992). Chemistry and biology of boron. *BioFactors (Oxford, England)*, *3*(4), 229–239. https://doi.org/10.1093/oxfordjournals.aob.a089871

Luan, S. (2009). The CBL-CIPK network in plant calcium signaling. *Trends in Plant Science*. https://doi.org/10.1016/j.tplants.2008.10.005

Ma, R., Zhang, M., Li, B., Du, G., Wang, J., & Chen, J. (2005). The effects of exogenous Ca2+ on endogenous polyamine levels and drought-resistant traits of spring wheat grown under arid conditions. *Journal of Arid Environments*, *63*(1). https://doi.org/10.1016/j.jaridenv.2005.01.021

Machado, L. P., Matsumoto, S. T., Jamal, C. M., da Silva, M. B., da Cruz Centeno, D., Neto, P. C., … Yokoya, N. S. (2014). Chemical analysis and toxicity of seaweed extracts with inhibitory activity against tropical fruit anthracnose fungi. *Journal of the Science of Food and Agriculture*, *94*(9). https://doi.org/10.1002/jsfa.6483

MacKinnon, I. M., Gordon Jardine, W., O'Kennedy, N., Renard, C. M. G. C., & Jarvis, M. C. (2002). Pectic methyl and nonmethyl esters in potato cell walls. *Journal of Agricultural and Food Chemistry*, *50*(2). https://doi.org/10.1021/jf010597h

MacRobbie, E. (1992). Calcium and ABA-induced stomatal closure. *Philosophical Transactions of the Royal Society of London. Series B: Biological Sciences*, *338*(1283). https://doi.org/10.1098/rstb.1992.0124

Mankarios, A. T., Hall, M. A., Jarvis, M. C., Threlfall, D. R., & Friend, J. (1980). Cell wall polysaccharides from onions. *Phytochemistry*, *19*(8), 1731–1733. https://doi.org/10.1016/S0031-9422(00)83803-0

Marrelli, M., Amodeo, V., Statti, G., & Conforti, F. (2018). Biological Properties and Bioactive Components of Allium cepa L.: Focus on Potential Benefits in the Treatment of Obesity and Related Comorbidities. *Molecules (Basel, Switzerland)*, *24*(1). https://doi.org/10.3390/molecules24010119

Marschner, H. (1995). Mineral Nutrition of Higher Plants. Mineral Nutrition of Higher Plants. https://doi.org/10.1016/b978-0-12-473542-2.x5000-7

Matoh, T. (1997). Boron in plant cell walls. Plant and Soil (Vol. 193). Kluwer Academic Publishers. Retrieved from https://link.springer.com/content/pdf/10.1023%2FA%3A1004207824251.pdf

Matoh, T., & Kobayashi, M. (1998). Boron and calcium, essential inorganic constituents of pectic polysaccharides in higher plant cell walls. *Journal of Plant Research*, *111*(1), 179–190. https://doi.org/10.1007/bf02507164

Matsunaga, T., Ishii, T., Matsumoto, S., Higuchi, M., Darvill, A., Albersheim, P., & O'Neill, M. A. (2004). Occurrence of the Primary Cell Wall Polysaccharide Rhamnogalacturonan II in Pteridophytes, Lycophytes, and Bryophytes. Implications for the Evolution of Vascular Plants. *Plant Physiology*, *134*(1). https://doi.org/10.1104/pp.103.030072

McFarlane, H., Gendre, D., & Western, T. (2014). Seed Coat Ruthenium Red Staining Assay. *BIO-PROTOCOL*, *4*(7). https://doi.org/10.21769/bioprotoc.1096

Mikshina, P. V., Petrova, A. A., & Gorshkova, T. A. (2015). Functional diversity of rhamnogalacturonans i. *Russian Chemical Bulletin*, *64*(5). https://doi.org/10.1007/s11172-015-0970-y

Mishra, A. K., & Singh, V. P. (2010). A review of drought concepts. *Journal of Hydrology*, *391*(1–2), 202–216. https://doi.org/10.1016/J.JHYDROL.2010.07.012

Mittler, R. (2006). Abiotic stress, the field environment and stress combination. *Trends in Plant Science*, *11*(1), 15–19. https://doi.org/10.1016/J.TPLANTS.2005.11.002

Miwa, K., Takano, J., & Fujiwara, T. (2006). Improvement of seed yields under boron-limiting conditions through overexpression of BOR1, a boron transporter for xylem loading, in Arabidopsis thaliana. *Plant Journal*, *46*(6). https://doi.org/10.1111/j.1365-313X.2006.02763.x

Mohnen, D. (1999). Carbohydrates and Their Derivatives Including Tannins, Cellulose, and Related Lignings. In D. Barton, K. Nakanishi, & O. Meth-Cohn (Eds.), *Comprehensive Natural Products Chemistry*. Elsevier.

Mohnen, D. (2008). Pectin structure and biosynthesis. *Current Opinion in Plant Biology*, *11*(3), 266–277. https://doi.org/10.1016/J.PBI.2008.03.006

Moore, J. P., Vicré-Gibouin, M., Farrant, J. M., & Driouich, A. (2008). Adaptations of higher plant cell walls to water loss: drought vs desiccation. *Physiologia Plantarum*, *134*(2), 237–245. https://doi.org/10.1111/j.1399-3054.2008.01134.x

Muhidinov, Z. K., Fishman, M. L., Avloev, K. K., Norova, M. T., Nasriddinov, A. S., & Khalikov, D. K. (2010). Effect of temperature on the intrinsic viscosity and conformation

of different pectins. *Polymer Science - Series A*, *52*(12). https://doi.org/10.1134/S0965545X10120035

Müller, K., Levesque-Tremblay, G., Bartels, S., Weitbrecht, K., Wormit, A., Usadel, B., … Kermode, A. R. (2013). Demethylesterification of Cell Wall Pectins in Arabidopsis Plays a Role in Seed Germination. *Plant Physiology*, *161*(1), 305–316. https://doi.org/10.1104/PP.112.205724

Münch, S., Lingner, U., Floss, D. S., Ludwig, N., Sauer, N., & Deising, H. B. (2008). The hemibiotrophic lifestyle of Colletotrichum species. *Journal of Plant Physiology*, *165*(1). https://doi.org/10.1016/j.jplph.2007.06.008

Naeem, M., Naeem, M. S., Ahmad, R., Ahmad, R., Ashraf, M. Y., Ihsan, M. Z., … Abdullah, M. (2018). Improving drought tolerance in maize by foliar application of boron: water status, antioxidative defense and photosynthetic capacity. *Archives of Agronomy and Soil Science*, *64*(5). https://doi.org/10.1080/03650340.2017.1370541

Nakamura, A., Furuta, H., Maeda, H., Takao, T., & Nagamatsu, Y. (2002). Structural studies by stepwise enzymatic degradation of the main backbone of soybean soluble polysaccharides consisting of galacturonan and rhamnogalacturonan. *Bioscience, Biotechnology and Biochemistry*, *66*(6). https://doi.org/10.1271/bbb.66.1301

National Center for Biotechnology Information. (2021). PubChem Compound Summary for CID 5462311, Boron.

Nebenführ, A., & Staehelin, L. A. (2001). Mobile factories: Golgi dynamics in plant cells. *TRENDS in Plant Science* (Vol. 6). Retrieved from http://plants.trends.com1360

Nebenführ, A., Gallagher, L. A., Dunahay, T. G., Frohlick, J. A., Mazurkiewicz, A. M., Meehl, J. B., & Staehelin, L. A. (1999). Stop-and-Go Movements of Plant Golgi Stacks Are Mediated by the Acto-Myosin System. *Plant Physiology*, *121*(4), 1127–1141. https://doi.org/10.1104/pp.121.4.1127

Nic, M., Jirat, J., & Kosata, B. (2014). Compendium of Chemical Terminology Gold Book. *IUPAC Compendium of Chemical Terminology*.

Noguchi, K., Yasumori, M., Imai, T., Naito, S., Matsunaga, T., Oda, H., … Fujiwara, T. (1997). bor1-1, an Arabidopsis thaliana mutant that requires a high level of boron. *Plant Physiology*, *115*(3). https://doi.org/10.1104/pp.115.3.901

Nowak, M. A., Boerlijst, M. C., Cooke, J., & Smith, J. M. (1997). Evolution of genetic redundancy. *Nature*, *388*(6638). https://doi.org/10.1038/40618

Nyombi, K. (2019). Diagnosis and management of nutrient constraints in bananas (Musa spp.). In *Fruit Crops: Diagnosis and Management of Nutrient Constraints*. https://doi.org/10.1016/B978-0-12-818732-6.00044-7

O'Neill, M. A., Eberhard, S., Albersheim, P., & Darvill, A. G. (2001). Requirement of borate cross-linking of cell wall rhamnogalacturonan II for Arabidopsis growth. *Science*, *294*(5543). https://doi.org/10.1126/science.1062319

O'Neill, M. A., Ishii, T., Albersheim, P., & Darvill, A. G. (2004). Rhamnogalacturonan II: Structure and Function of a Borate Cross-Linked Cell Wall Pectic Polysaccharide. *Annu. Rev. Plant Biol*, *55*, 109–148. https://doi.org/10.1146/annurev.arplant.55.031903.141750

O'Neill, M. A., Warrenfeltz, D., Kates, K., Pellerin, P., Doco, T., Darvill, A. G., & Albersheim, P. (1996). Rhamnogalacturonan-II, a pectic polysaccharide in the walls of growing plant cell, forms a dimer that is covalently cross-linked by a borate ester. In vitro conditions for the formation and hydrolysis of the dimer. *Journal of Biological Chemistry*, *271*(37). https://doi.org/10.1074/jbc.271.37.22923

O'Neill, M., Albersheim, P., & Darvill, A. (1990). The Pectic Polysaccharides of Primary Cell Walls. https://doi.org/10.1016/b978-0-12-461012-5.50018-5

Oertli, J. J. (1986). Negative Turgor Pressures in Plant Cells. *Zeitschrift Für Pflanzenernährung Und Bodenkunde*, *149*(1). https://doi.org/10.1002/jpln.19861490108

Oertli, J. J., Lips, S. H., & Agami, M. (1990). The strength of sclerophyllous cells to resist collapse due to negative turgor pressure. *Acta Oecologica*, *11*(2).

Palta, J. P., Levitt, J., & Stadelmann, E. J. (1977). Freezing Injury in Onion Bulb Cells. *Plant Physiology*, *60*(3), 393–397. https://doi.org/10.1104/pp.60.3.393

Panter, P. E., Kent, O., Dale, M., Smith, S. J., Skipsey, M., Thorlby, G., … Knight, H. (2019). MUR1-mediated cell-wall fucosylation is required for freezing tolerance in Arabidopsis thaliana. *New Phytologist*, *224*(4). https://doi.org/10.1111/nph.16209

Parre, E., & Geitmann, A. (2005). Pectin and the role of the physical properties of the cell wall in pollen tube growth of Solanum chacoense. *Planta*, *220*(4). https://doi.org/10.1007/s00425-004-1368-5

Paul, H., Reginato, A. J., & Schumacher, H. R. (1983). Alizarin red s staining as a screening test to detect calcium compounds in synovial fluid. *Arthritis & Rheumatism*, *26*(2), 191–200.

Peaucelle, A., Braybrook, S., & Höfte, H. (2012). Cell wall mechanics and growth control in plants: The role of pectins revisited. *Frontiers in Plant Science*. https://doi.org/10.3389/fpls.2012.00121

Pelloux, J., Rusterucci, C., & Mellerowicz, E. (2007). New insights into pectin methylesterase structure and function. *Trends in Plant Science*, *12*(6), 267–277. https://doi.org/10.1016/j.tplants.2007.04.001

Peters, M. (2015). Identification of S-genes associated with Botrytis cinerea susceptibility in Solanum lycopersicum. Wageningen University, Wageningen.

Petrasch, S., Silva, C. J., Mesquida-Pesci, S. D., Gallegos, K., van den Abeele, C., Papin, V., … Blanco-Ulate, B. (2019). Infection strategies deployed by Botrytis cinerea, Fusarium acuminatum, and Rhizopus stolonifer as a function of tomato fruit ripening stage. *Frontiers in Plant Science*, *10*. https://doi.org/10.3389/fpls.2019.00223

Piro, G., Leucci, M. R., Waldron, K., & Dalessandro, G. (2003). Exposure to water stress causes changes in the biosynthesis of cell wall polysaccharides in roots of wheat cultivars varying in drought tolerance. *Plant Science*, *165*(3). https://doi.org/10.1016/S0168-9452(03)00215-2

Plank, O. (1999). Plant Analysis HandBook for Georgia. College of Agriculture and Environmental Science.

Plant Cell Wall Basics. (n.d.). Retrieved August 10, 2019, from https://www.ccrc.uga.edu/~mao/intro/ouline.htm

Polymer Solutions News Team. (2015). Metal Properties: Hardness, Toughness, & Strength.

Power, P. P., & Woods, W. G. (1997). The chemistry of boron and its speciation in plants. *Plant and Soil*, *193*(2), 1–13. https://doi.org/10.1023/A:1004231922434

Proffitt, R. T., Tran, J. V., & Reynolds, C. P. (1996). A fluorescence digital image microscopy system for quantifying relative cell numbers in tissue culture plates. *Cytometry*, *24*(3). https://doi.org/10.1002/(SICI)1097-0320(19960701)24:3<204::AID-CYTO3>3.0.CO;2-H

Qin, G., Zong, Y., Chen, Q., Hua, D., & Tian, S. (2010). Inhibitory effect of boron against Botrytis cinerea on table grapes and its possible mechanisms of action. *International Journal of Food Microbiology*, *138*(1–2). https://doi.org/10.1016/j.ijfoodmicro.2009.12.018

Qin, Z., Liu, H. M., Lv, T. T., & Wang, X. De. (2020). Structure, rheological, thermal and antioxidant properties of cell wall polysaccharides from Chinese quince fruits. *International Journal of Biological Macromolecules*, *147*. https://doi.org/10.1016/j.ijbiomac.2019.10.083

Qin, Z., Liu, H. M., Lv, T. T., & Wang, X. De. (2020). Structure, rheological, thermal and antioxidant properties of cell wall polysaccharides from Chinese quince fruits. *International Journal of Biological Macromolecules*, *147*. https://doi.org/10.1016/j.ijbiomac.2019.10.083

Rahman, A., Kawamura, Y., Maeshima, M., Rahman, A., & Uemura, M. (2020). Plasma Membrane Aquaporin Members PIPs Act in Concert to Regulate Cold Acclimation and Freezing Tolerance Responses in Arabidopsis thaliana. *Plant and Cell Physiology*, *61*(4), 787–802. https://doi.org/10.1093/pcp/pcaa005

Rahman, T., Shao, M., Pahari, S., Venglat, P., Soolanayakanahally, R., Qiu, X., … Tanino, K. (2021). Dissecting the roles of cuticular wax in plant resistance to shoot dehydration and low-temperature stress in arabidopsis. *International Journal of Molecular Sciences*, *22*(4). https://doi.org/10.3390/ijms22041554

Raiola, A., Lionetti, V., Elmaghraby, I., Immerzeel, P., Mellerowicz, E. J., Salvi, G., … Bellincampi, D. (2011). Pectin Methylesterase Is Induced in Arabidopsis upon Infection and Is Necessary for a Successful Colonization by Necrotrophic Pathogens. *Molecular Plant-Microbe Interactions*, *24*(4), 432–440. https://doi.org/10.1094/MPMI-07-10-0157

Ravanat, G., & Rinaudo, M. (1980). Investigation on oligo- and polygalacturonic acids by potentiometry and circular dichroism. *Biopolymers*, *19*(12), 2209–2222. https://doi.org/10.1002/bip.1980.360191206

Reiter, W. D., Chapple, C. S., & Somerville, C. R. (1993). Altered Growth and Cell Walls in a Fucose-Deficient Mutant of Arabidopsis. *Science*, *261*, 1032–1035.

Reuhs, B. L., Glenn, J., Stephens, S. B., Kim, J. S., Christie, D. B., Glushka, J. G., … O'Neill, M. A. (2004). L-galactose replaces L-fucose in the pectic polysaccharide rhamnogalacturonan II synthesized by the L-fucose-deficient mur1 Arabidopsis mutant. *Planta*, *219*(1). https://doi.org/10.1007/s00425-004-1205-x

Ridley, B. L., O'Neill, M. A., & Mohnen, D. (2001). Pectins: Structure, biosynthesis, and oligogalacturonide-related signaling. *Phytochemistry*. https://doi.org/10.1016/S0031-9422(01)00113-3

Ritchie, R. O. (2011). The conflicts between strength and toughness. *Nature Materials*, *10*(11). https://doi.org/10.1038/nmat3115

Rizhsky, L., Liang, H., Shuman, J., Shulaev, V., Davletova, S., & Mittler, R. (2004). When Defense Pathways Collide. The Response of Arabidopsis to a Combination of Drought and Heat Stress. *Plant Physiology*, *134*(4), 1683–1696. https://doi.org/10.1104/PP.103.033431

Robertson, G. A., & Loughman, B. C. (1973). Rubidium uptake and boron deficiency in vicia faba l. *Journal of Experimental Botany*, *24*(6). https://doi.org/10.1093/jxb/24.6.1046

Romanazzi, G., & Feliziani, E. (2014). Botrytis cinerea (Gray Mold). In *Postharvest Decay: Control Strategies*. https://doi.org/10.1016/B978-0-12-411552-1.00004-1

Ryden, P., Sugimoto-Shirasu, K., Smith, A. C., Findlay, K., Reiter, W. D., & McCann, M. C. (2003). Tensile properties of Arabidopsis cell walls depend on both a xyloglucan cross-linked microfibrillar network and rhamnogalacturonan II-borate complexes. *Plant Physiology*, *132*(2). https://doi.org/10.1104/pp.103.021873

Sahaf, M., & Sharon, E. (2016). The rheology of a growing leaf: Stress-induced changes in the mechanical properties of leaves. *Journal of Experimental Botany*, *67*(18). https://doi.org/10.1093/jxb/erw316

Sanders, D., Pelloux, J., Brownlee, C., & Harper, J. F. (2002). Calcium at the crossroads of signaling. *Plant Cell*, *14*(SUPPL.). https://doi.org/10.1105/tpc.002899

Sasidharan, R., Voesenek, L. A., & Pierik, R. (2011). Cell Wall Modifying Proteins Mediate Plant Acclimatization to Biotic and Abiotic Stresses. *Critical Reviews in Plant Sciences*, *30*(6), 548–562. https://doi.org/10.1080/07352689.2011.615706

Savin, R., & Nicolas, M. E. (1996). Effects of short periods of drought and high temperature on grain growth and starch accumulation of two malting barley cultivars. *Australian Journal of Plant Physiology*, *23*(2). https://doi.org/10.1071/PP9960201

Schatzberg, P. (1967). On the molecular diameter of water from solubility and diffusion measurements. *Journal of Physical Chemistry*. https://doi.org/10.1021/j100872a075

Schreiber, L., Hartmann, K., Skrabs, M., & Zeier, J. (1999). Apoplastic barriers in roots: Chemical composition of endodermal and hypodermal cell walls. *Journal of Experimental Botany*. https://doi.org/10.1093/jxb/50.337.1267

Sechet, J., Htwe, S., Urbanowicz, B., Agyeman, A., Feng, W., Ishikawa, T., … Mortimer, J. C. (2018). Suppression of Arabidopsis GGLT1 affects growth by reducing the L-galactose content and borate cross-linking of rhamnogalacturonan-II. *Plant Journal*, *96*(5). https://doi.org/10.1111/tpj.14088

Sénéchal, F., Wattier, C., Rustérucci, C., & Pelloux, J. (2014). Homogalacturonan-modifying enzymes: Structure, expression, and roles in plants. *Journal of Experimental Botany*, *65*(18). https://doi.org/10.1093/jxb/eru272

Shaterian, J., Georges, F., Hussain, A., Waterer, D., De Jong, H., & Tanino, K. K. (2005). Root to shoot communication and abscisic acid in calreticulin (CR) gene expression and salt-stress tolerance in grafted diploid potato clones. *Environmental and Experimental Botany*, *53*(3). https://doi.org/10.1016/j.envexpbot.2004.04.008

Shi, X. Q., Li, B. Q., Qin, G. Z., & Tian, S. P. (2011). Antifungal activity and possible mode of action of borate against Colletotrichum gloeosporioides on mango. *Plant Disease*, *95*(1). https://doi.org/10.1094/PDIS-06-10-0437

Shi, X., Li, B., Qin, G., & Tian, S. (2012). Mechanism of antifungal action of borate against Colletotrichum gloeosporioides related to mitochondrial degradation in spores. *Postharvest Biology and Technology*, *67*. https://doi.org/10.1016/j.postharvbio.2012.01.003

Shireen, F., Nawaz, M. A., Chen, C., Zhang, Q., Zheng, Z., Sohail, H., … Bie, Z. (2018). Boron: Functions and approaches to enhance its availability in plants for sustainable agriculture. *International Journal of Molecular Sciences*. https://doi.org/10.3390/ijms19071856

Solecka, D., Zebrowski, J., & Kacperska, A. (2008). Are pectins involved in cold acclimation and de-acclimation of winter oil-seed rape plants? *Annals of Botany*, *101*(4). https://doi.org/10.1093/aob/mcm329

Speck, T., & Burgert, I. (2011). Plant stems: Functional design and mechanics. *Annual Review of Materials Research*, *41*. https://doi.org/10.1146/annurev-matsci-062910-100425

Suzuki, N., Rivero, R. M., Shulaev, V., Blumwald, E., & Mittler, R. (2014). Abiotic and biotic stress combinations. *New Phytologist*, *203*(1), 32–43. https://doi.org/10.1111/nph.12797

TAIR - About Arabidopsis. (n.d.). Retrieved August 10, 2019, from https://www.arabidopsis.org/portals/education/aboutarabidopsis.jsp

TAIR. (2013). Locus: AT1G80760.

TAIR. (2015). Locus: AT4G10380.

TAIR. (2021). Locus: AT2G47160.

Takano, J., Miwa, K., & Fujiwara, T. (2008). Boron transport mechanisms: collaboration of channels and transporters. *Trends in Plant Science*. Elsevier Current Trends. https://doi.org/10.1016/j.tplants.2008.05.007

Tan, C., Liu, Z., Huang, S., Li, C., Ren, J., Tang, X., … Feng, H. (2018). Pectin methylesterase inhibitor (PMEI) family can be related to male sterility in Chinese cabbage (Brassica rapa ssp. pekinensis). *Molecular Genetics and Genomics*, *293*(2), 343–357. https://doi.org/10.1007/s00438-017-1391-4

Tan, L., Eberhard, S., Pattathil, S., Warder, C., Glushka, J., Yuan, C., … Mohnen, D. (2013). An Arabidopsis cell wall proteoglycan consists of pectin and arabinoxylan covalently linked to an arabinogalactan protein. *The Plant Cell*, *25*(1), 270–287. https://doi.org/10.1105/tpc.112.107334

Tanaka, H. (1967a). Boron absorption by crop plants as affected by other nutrients of the medium. *Soil Science and Plant Nutrition*, *13*(2). https://doi.org/10.1080/00380768.1967.10431972

Tanaka, H. (1967b). Boron adsorption by plant roots. *Plant and Soil*, *27*(2). https://doi.org/10.1007/BF01373400

Tanino, K. K., Kobayashi, S., Hyett, C., Hamilton, K., Liu, J., Li, B., … Uemura, M. (2013). Allium fistulosum as a novel system to investigate mechanisms of freezing resistance. *Physiologia Plantarum*, *147*(1), 101–111. https://doi.org/10.1111/j.1399-3054.2012.01716.x

Thermo Fisher Scientific. (n.d.). Fluorescein Diacetate (FDA).

Thimm, J. C., Burritt, D. J., Sims, I. M., Newman, R. H., Ducker, W. A., & Melton, L. D. (2002). Celery (Apium graveolens) parenchyma cell walls: Cell walls with minimal xyloglucan. *Physiologia Plantarum*, *116*(2). https://doi.org/10.1034/j.1399-3054.2002.1160205.x

Thor, K. (2019). Calcium—nutrient and messenger. *Frontiers in Plant Science*. https://doi.org/10.3389/fpls.2019.00440

Underwood, W. (2012). The Plant Cell Wall: A Dynamic Barrier Against Pathogen Invasion. *Frontiers in Plant Science*, *3*, 85. https://doi.org/10.3389/fpls.2012.00085

van Kan, J. A. L. (2006). Licensed to kill: the lifestyle of a necrotrophic plant pathogen. *Trends in Plant Science*. https://doi.org/10.1016/j.tplants.2006.03.005

Vitecek, J., Petrlova, J., Adam, V., Havel, L., Kramer, K., Babula, P., & Kizek, R. (2007). A Fluorimetric Sensor for Detection of One Living Cell. *Sensors*, *7*(3), 222–238. https://doi.org/10.3390/s7030222

Voiniciuc, C., Dean, G. H., Griffiths, J. S., Kirchsteiger, K., Hwang, Y. T., Gillett, A., … Haughn, G. W. (2013). Flying saucer1 is a transmembrane RING E3 ubiquitin ligase that regulates the degree of pectin methylesterification in Arabidopsis seed mucilage. *Plant Cell*, *25*(3). https://doi.org/10.1105/tpc.112.107888

Voxeur, A., & Fry, S. C. (2014). Glycosylinositol phosphorylceramides from Rosa cell cultures are boron-bridged in the plasma membrane and form complexes with rhamnogalacturonan II. *Plant Journal*, *79*(1). https://doi.org/10.1111/tpj.12547

Voxeur, A., Soubigou-Taconnat, L., Legée, F., Sakai, K., Antelme, S., Durand-Tardif, M., … Sibout, R. (2017). Altered lignification in mur1-1 a mutant deficient in GDP-L-fucose synthesis with reduced RG-II cross linking. *PLoS ONE*, *12*(9). https://doi.org/10.1371/journal.pone.0184820

Wang, J. P., Munyampundu, J. P., Xu, Y. P., & Cai, X. Z. (2015). Phylogeny of plant calcium and calmodulin-dependent protein kinases (CcaMKs) and functional analyses of tomato CCaMK in disease resistance. *Frontiers in Plant Science*, *6*(DEC). https://doi.org/10.3389/fpls.2015.01075

Wang, M., Yuan, D., Gao, W., Li, Y., Tan, J., & Zhang, X. (2013). A comparative genome analysis of PME and PMEI families reveals the evolution of pectin metabolism in plant cell walls. *PloS One*, *8*(8), e72082. https://doi.org/10.1371/journal.pone.0072082

Wang, S., Li, Q., Zhao, L., Fu, S., Qin, L., Wei, Y., … Wang, H. (2020). Arabidopsis UBC22, an E2 able to catalyze lysine-11 specific ubiquitin linkage formation, has multiple functions in plant growth and immunity. *Plant Science*, *297*. https://doi.org/10.1016/j.plantsci.2020.110520

Wang, S., Wen, R., Shi, X., Lambrecht, A., Wang, H., & Xiao, W. (2011). RAD5a and REV3 function in two alternative pathways of DNA-damage tolerance in Arabidopsis. *DNA Repair*, *10*(6). https://doi.org/10.1016/j.dnarep.2011.04.009

White, P. B., Wang, T., Park, Y. B., Cosgrove, D. J., & Hong, M. (2014). Water-polysaccharide interactions in the primary cell wall of arabidopsis thaliana from polarization transfer solid-

state NMR. *Journal of the American Chemical Society*, *136*(29). https://doi.org/10.1021/ja504108h

White, P. J. (2001). The pathways of calcium movement to the xylem. *Journal of Experimental Botany*. https://doi.org/10.1093/jexbot/52.358.891

White, P. J., & Broadley, M. R. (2003). Calcium in plants. *Annals of Botany*. https://doi.org/10.1093/aob/mcg164

Wickham, H., Hester, J., & Chang, W. (2020, September 18). devtools: Tools to Make Developing R Packages Easier. CRAN.

Willats, W. G. T., Mccartney, L., Mackie, W., & Knox, J. P. (2001a). Pectin: Cell biology and prospects for functional analysis. *Plant Molecular Biology*. https://doi.org/10.1023/A:1010662911148

Willats, W. G. T., Orfila, C., Limberg, G., Buchholt, H. C., Van Alebeek, G. J. W. M., Voragen, A. G. J., … Knox, J. P. (2001b). Modulation of the degree and pattern of methyl-esterification of pectic homogalacturonan in plant cell walls: Implications for pectin methyl esterase action, matrix properties, and cell adhesion. *Journal of Biological Chemistry*, *276*(22). https://doi.org/10.1074/jbc.M011242200

Williamson, B., Tudzynski, B., Tudzynski, P., & Van Kan, J. A. L. (2007). Botrytis cinerea: The cause of grey mould disease. *Molecular Plant Pathology*. https://doi.org/10.1111/j.1364-3703.2007.00417.x

Willick, I. R. (2018). The Mechanism of Freezing Resistance in Cold-Acclimated Winter Wheat and Rye Crowns. The University of Saskatchewan.

Wimmer, A., & Goldbach, H. (1999). A miniaturized curcumin method for the determination of boron insolutions and biological samples. *J. Plant Nutr. Soil Sci.*, *162*, 15–18.

Wittrock, V., Wheaton, E., & Research Council, S. (2002). *The 2001 Drought in Saskatchewan, Canada*. Retrieved from https://www.parc.ca/mcri/pdfs/2001DroughtSK11182-6D02.pdf

Wójcik, P., & Lewandowski, M. (2003). Effect of calcium and boron sprays on yield and quality of "Elsanta" strawberry. *Journal of Plant Nutrition*, *26*(3). https://doi.org/10.1081/PLN-120017674

Wolf, S., Mouille, G., & Pelloux, J. (2009). Homogalacturonan methyl-esterification and plant development. *Molecular Plant*, *2*(5). https://doi.org/10.1093/mp/ssp066

Wood, S. (2019). Mixed GAM Computation Vehicle with Automatic Smoothness Estimation. https://doi.org/10.1201/9781315370279

Wood, S. (2021). Package 'mgcv.' CRAN.

Wormit, A., & Usadel, B. (2018). The Multifaceted Role of Pectin Methylesterase Inhibitors (PMEIs). *International Journal of Molecular Sciences*, *19*(10), 2878. https://doi.org/10.3390/ijms19102878

Wu, H.-C., Bulgakov, V. P., & Jinn, T.-L. (2018). Pectin Methylesterases: Cell Wall Remodeling Proteins Are Required for Plant Response to Heat Stress. *Frontiers in Plant Science*, *9*, 1612. https://doi.org/10.3389/fpls.2018.01612

Xue, C., Guan, S. C., Chen, J. Q., Wen, C. J., Cai, J. F., & Chen, X. (2020). Genome wide identification and functional characterization of strawberry pectin methylesterases related to fruit softening. *BMC Plant Biology*, *20*(1). https://doi.org/10.1186/s12870-019-2225-9

Yan, Y., Yuan, Q., Tang, J., Huang, J., Hsiang, T., Wei, Y., & Zheng, L. (2018). Colletotrichum higginsianum as a model for understanding host–pathogen interactions: A review. *International Journal of Molecular Sciences*. https://doi.org/10.3390/ijms19072142

Yang, T., & Poovaiah, B. W. (2003). Calcium/calmodulin-mediated signal network in plants. *Trends in Plant Science*. https://doi.org/10.1016/j.tplants.2003.09.004

Yang, W., Ruan, M., Xiang, M., Deng, A., Du, J., & Xiao, C. (2020). Overexpression of a pectin methylesterase gene PtoPME35 from Populus tomentosa influences stomatal function and drought tolerance in Arabidopsis thaliana. *Biochemical and Biophysical Research Communications*, *523*(2). https://doi.org/10.1016/j.bbrc.2019.12.073

Yapo, B. M., Lerouge, P., Thibault, J.-F., & Ralet, M.-C. (2007). Pectins from citrus peel cell walls contain homogalacturonans homogenous with respect to molar mass, rhamnogalacturonan I and rhamnogalacturonan II. *Carbohydrate Polymers*, *69*(3), 426–435. https://doi.org/10.1016/J.CARBPOL.2006.12.024

Zandleven, J., Beldman, G., Bosveld, M., Schols, H. A., & Voragen, A. G. J. (2006). Enzymatic degradation studies of xylogalacturonans from apple and potato, using xylogalacturonan hydrolase. https://doi.org/10.1016/j.carbpol.2006.02.015

Zhang, C., Zhu, X., Zhang, F., Yang, X., Ni, L., Zhang, W., … Zhang, Y. (2020). Improving viscosity and gelling properties of leaf pectin by comparing five pectin extraction methods using green tea leaf as a model material. *Food Hydrocolloids*, *98*. https://doi.org/10.1016/j.foodhyd.2019.105246

Zhemerichkin, D. A., & Ptitchkina, N. M. (1995). The composition and properties of pumpkin and sugar beet pectins. *Food Hydrocolloids*, *9*(2), 147–149. https://doi.org/10.1016/S0268-005X(09)80277-4

Zhong, R., & Ye, Z. H. (2015). Secondary cell walls: Biosynthesis, patterned deposition and transcriptional regulation. *Plant and Cell Physiology*, *56*(2). https://doi.org/10.1093/pcp/pcu140

Zhu, J.-K. (2016). Abiotic Stress Signaling and Responses in Plants. *Cell*, *167*(2), 313–324. https://doi.org/10.1016/J.CELL.2016.08.029

Zimmermann, P., Hirsch-Hoffmann, M., Hennig, L., & Gruissem, W. (2004). GENEVESTIGATOR. Arabidopsis Microarray Database and Analysis Toolbox. *Plant Physiology*, *136*(1). https://doi.org/10.1104/pp.104.046367

Zykwinska, A., Thibault, J. F., & Ralet, M. C. (2007). Organization of pectic arabinan and galactan side chains in association with cellulose microfibrils in primary cell walls and related models envisaged. *Journal of Experimental Botany*, *58*(7). https://doi.org/10.1093/jxb/erm037

10.0 APPENDIX

10.1 Appendix A

Table A1 Pectin solutions analyzed in Chapters 3 and 4

Twelve pectin solutions, comprising 2 types of pectin (HM=high methylated citrus pectin, GB=genu beta), 2 concentrations and 2 treatments were analyzed.

Type of Pectin	Calcium (0.05M)	Boron (0.05M)	Concentration
HM	+	-	4%
HM	-	+	4%
HM	-	-	4%
GB	+	-	4%
GB	-	+	4%
GB	-	-	4%
HM	+	-	8%
HM	-	+	8%
HM	-	-	8%
GB	+	-	8%
GB	-	+	8%
GB	-	-	8%

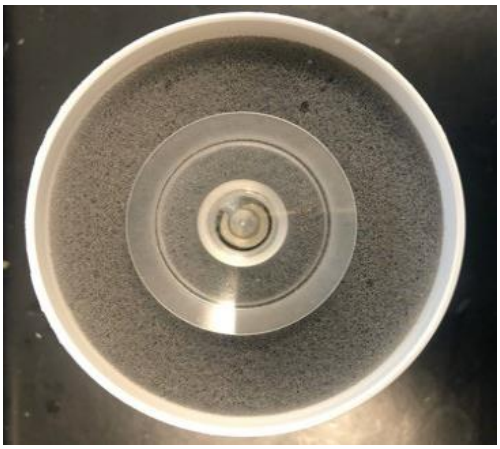

Figure A1 Geometry used for rheometer

40mm smooth acrylic geometry was used to analyze the viscosity of the pectin solutions.

Figure A2 Placement of *Allium fistulosum* sheaths in texture analyzer cell

4cm sections of *Allium fistulosum* sheaths were placed perpendicularly to the slots in the texture analyzer cell. The ligule and epidermal cell layer were left intact for this experiment. This experiment was conducted at 20°C.

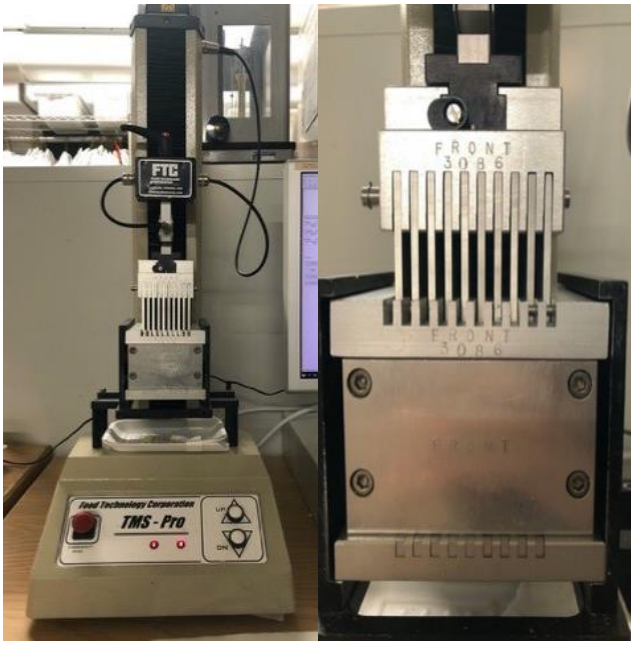

Figure A3 TMS-Pro texture analyzer with 10-blade Allo-Kramer shearing compression cell

TMS-Pro texture analyzer with the 10-blade Allo-Kramer shearing compression cell attached was used to measure shear force.

Table A2 Results from ICP-MS conducted on water samples collected throughout a calendar year

Results from an ICP-MS analysis examining calcium and boron on various water samples obtained from Lab 2C79 in the Agriculture and Bioresources Building (51 Campus Drive, Saskatoon, SK) and the Agriculture Greenhouses (45 Innovation Blvd, Saskatoon, SK) throughout a calendar year.

Sample	**Calcium (ppm)**	**Boron (ppm)**
Lab- Winter (February)	51.429	0.023
Greenhouse- Winter (February)	42.809	0.021
Lab- Spring (May)	45.535	0.026
Greenhouse- Spring (May)	45.851	0.026
Lab- Summer (June)	45.313	0.026
Greenhouse- Summer (June)	44.914	0.024
Lab- Fall (September)	44.081	0.023
Greenhouse- Fall (September)	41.381	0.027

Table A3 Atike information criteria values for GAM's constructed to analyze pectin viscosity

AIC values for the 3 GAM's built to analyze the relationship between pectin type, concentration, calcium and boron in relation to temperature and the joint effect on pectin viscosity. A lower AIC value is indicative of a better fitting model.

GAM	**AIC Value**
No smoother and no by= argument	6331.182
Smoother and no by=argument	6323.599
Smoother and by=argument	6296.639

Table A4 ANOVA analyzing viscosity in pectin solutions at 19-20ºC

ANOVA analyzing viscosity measurements of various pectin solutions taken while the temperature of the rheometer was 19-20 ºC. $p<0.05$ is significant.

	Df	Sum Sq	Mean Sq	F value	P value
Pectin solutions	11	221519258	20138114	9222.774	<2e-16
Temperature	1	4250	4250	1.947	0.163
Pectin solutions: Temperature	11	15092	1372	0.628	0.806

Table A5 ANOVA analyzing viscosity in pectin solutions at 11-12ºC

ANOVA analyzing viscosity measurements of various pectin solutions taken while the temperature of the rheometer was 11-12 ºC. $p<0.05$ is significant.

	Df	**Sum Sq**	**Mean Sq**	**F value**	**P value**
Pectin solutions	11	1.617e+09	146980193	33645.895	<2e-16
Temperature	1	4.980e+02	498	0.114	0.736
Pectin solutions: Temperature	11	9.266e+03	842	0.193	0.998

Table A6 ANOVA analyzing viscosity in pectin solutions at 3-4ºC

ANOVA analyzing viscosity measurements of various pectin solutions taken while the temperature of the rheometer was 3-4 ºC. $p<0.05$ is significant.

	Df	**Sum Sq**	**Mean Sq**	**F value**	**P value**
Pectin solutions	11	1.368e+10	1.244e+09	22979.764	<2e-16
Temperature	1	1.111e+04	1.111e+04	0.205	0.651
Pectin solutions: Temperature	11	1.422e+05	1.293e+04	0.239	0.995

Table A7 ANOVA analyzing shear force in *A. fistulosum*

Results from an ANOVA analyzing the effect of cold acclimation (ACC), calcium application (CA), and their interaction on the force required to shear *Allium fistulosum* sheaths. $p<0.05$ is significant.

Data Selection	**Degrees of Freedom**	**F-value**	**P-value**
Cold acclimation	2	5.100	0.00871
Calcium	1	5.048	0.02801
Cold acclimation: Calcium	2	3.838	0.02650

Table A8 Effect sizes for treatment groups utilized in analysis of shear force

Effect sizes for the relationships between each of the treatment groups and the force required to shear *Allium fistulosum* sheaths. NACC is indicative of no cold acclimation and ACC is cold acclimated, while NCA is non-calcium treated and CA is calcium treated. Cohen's d is reported in this table. An effect size greater than 0.8 is indicative of a meaningful difference between treatment groups.

Treatment Groups Compared	**Effect**
NACC/ NCA & NACC/ CA	2.66
NACC/ NCA & ACC4-4/ NCA	1.66
NACC/ NCA l & CA/ ACC4-4	2.86
NACC/ NCA & NCA/ ACC12-4	3.52
NACC/ NCA & CA/ ACC12-4	2.91
NACC/ CA & ACC4-4/ NCA	1.24
NACC/ CA & ACC4-4/ CA	0.2
NACC/ CA & NCA/ ACC12-4	1.01
NACC/ CA & ACC12-4/ CA	0.27
ACC4-4/ NCA & ACC4-4/ CA	1.94
ACC4-4/ NCA & ACC12-4/ NCA	3.01
ACC4-4/ NCA & ACC12-4/ CA	2.01
ACC4-4/ CA & ACC12-4/ NCA	2.34
ACC4-4/ CA & ACC12-4/ CA	0.19

Table A9 Tukey test for analysis of shear force results

Results from a Tukey test conducted to further analyze the relationship between the various treatment combinations and the force required to shear *Allium fistulosum* sheaths. NACC is indicative of no cold acclimation and ACC is cold acclimated, while NCA is non-calcium treated and CA is calcium treated. $p<0.05$ is significant.

Treatment Groups Compared	**P-value**
CA/ ACC4-4 & CA/ ACC12-4	0.999
CA/ NACC & CA/ ACC12-4	0.999
NCA/ ACC12-4 & CA/ ACC12-4	0.978
NCA/ ACC4-4 & CA/ ACC12-4	0.663
NCA/ NACC & CA/ ACC12-4	0.011
CA /NACC & CA/ ACC4-4	0.999
NCA/ ACC12-4 & CA/ ACC4-4	0.967
NCA/ ACC4-4 & CA/ ACC4-4	0.704
NCA/ NACC & CA/ ACC4-4	0.013
NCA/ ACC12-4 & CA/ NACC	0.906
NCA/ ACC4-4 & CA/ NACC	0.835
NCA/ NACC & CA/ NACC	0.026
NCA/ ACC4-4 & NCA/ ACC12-4	0.237
NCA/ NACC & NCA/ ACC12-4	0.001
NCA/ NACC & NCA/ ACC4-4	0.364

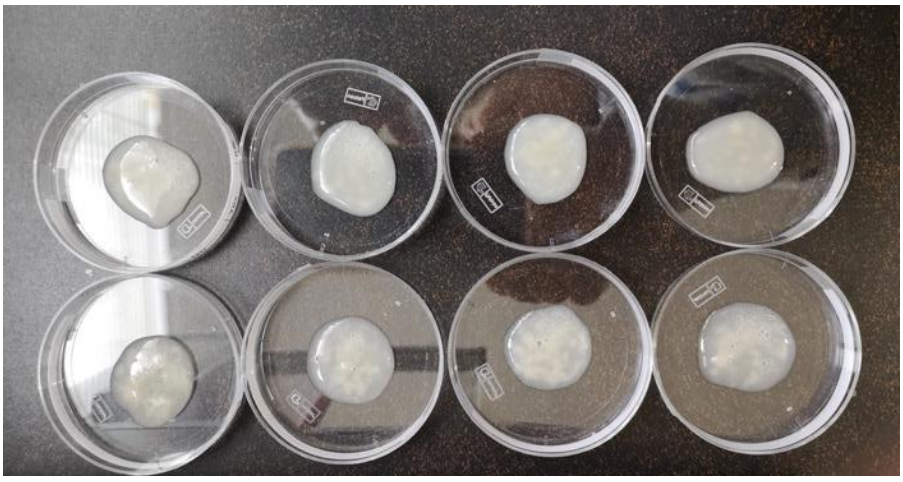

Figure A4 Method used to analyze water loss in pure pectin solutions

Water loss in pure pectin solutions was analyzed by pipetting approximately 1g of each of the pectin solutions into a petri dish.

$$Percent\ Water\ Loss = (1 - \left(\frac{T0\ weight}{T(x) weight}\right) \times 100)$$

Equation A1 Equation used to calculate percent water loss, where T is equal to the weight of the plant tissue at the time point of interest.

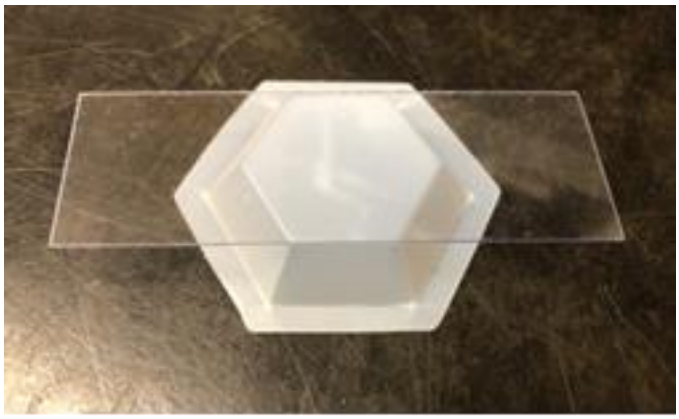

Figure A5 Placement of plastic slide on weigh boat for analysis over water loss in *Allium* epidermal cell layers over 15min

A plastic slide was placed over an upside-down weigh boat. The single layer of epidermal cells were then placed on top of the slide and placed on the analytical balance.

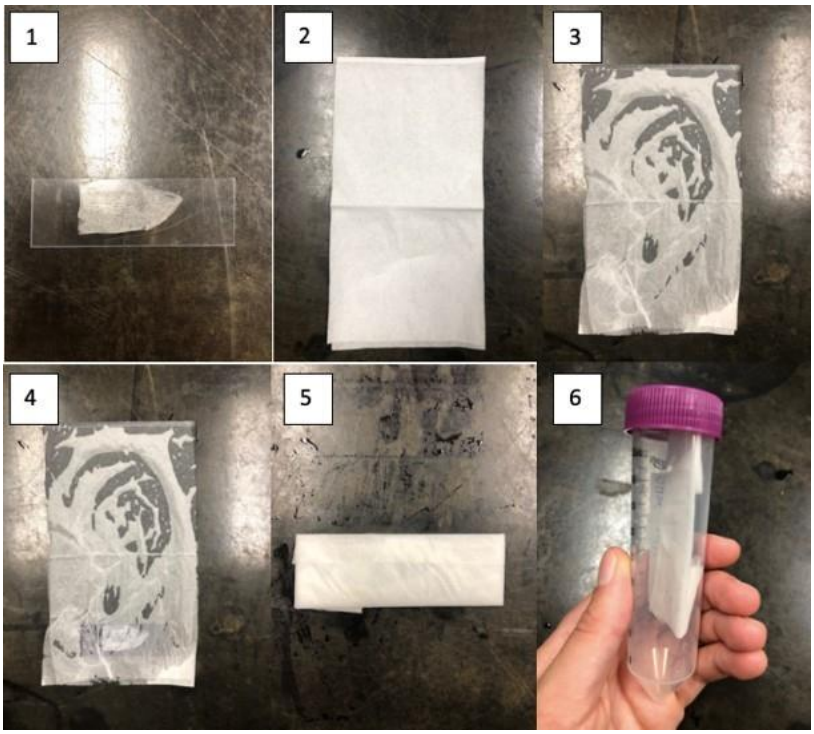

Figure A6 Method used to wrap *Allium fistulosum* epidermal cell layer for analysis of water loss between 12-24hr

A plastic slide with a single epidermal cell layer (1) was wrapped in two Kimwipes™ that had been moistened (2-4) following a period dehydration (12, 14, 16, 18, 20, 22 or 24hr). The slide wrapped in wipes was then be placed in a 50mL plastic tube with the lid on (6). Samples were kept in the dark for 24hr at ~23°C.

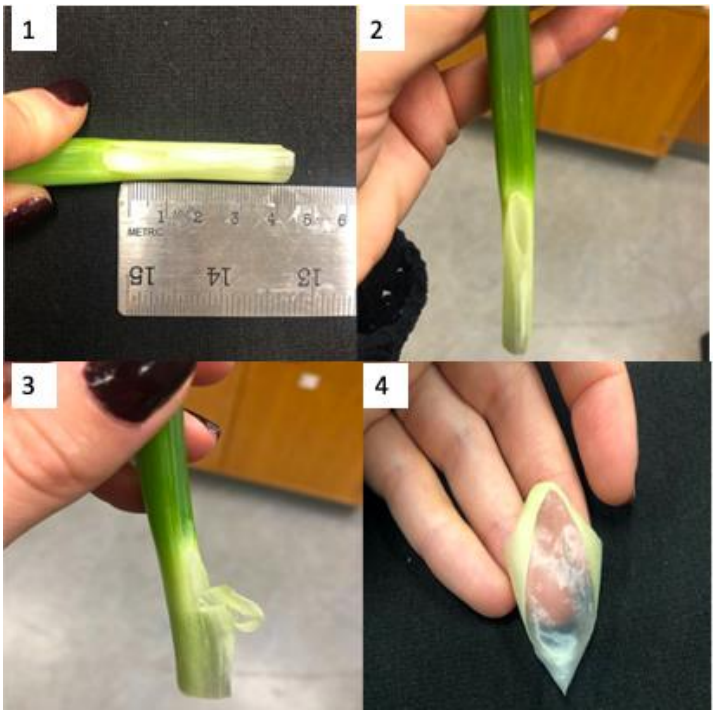

Figure A7 Method used to prepare *Allium fistulosum* sample for analysis of water loss between 16-18hr

The youngest leaf with the most developed leaf sheath was cut into a 4cm segment (a cut was also made above the leaf collar; this is not shown) (1,2). Vaseline was then applied to the areas where the cuts had been made and the segment was then stored in the dark for the period of dehydration. Following dehydration, the 4cm segment was wrapped in moist Kimwipes™ and placed in a Falcon tube in order to rehydrate (Figure 4.2). Following rehydration, the epidermal cell layer was peeled away by gently pulling down the collar (3,4).

$$Percent\ Cell\ Viability = \frac{number\ of\ cells\ with\ protoplasmic\ streaming}{total\ number\ of\ cells}$$

Equation A2 Equation used to measure the limit of damage based on percent protoplasmic streaming. Total cell count was down based on the number of cells within the frame at the 40x microscope objective.

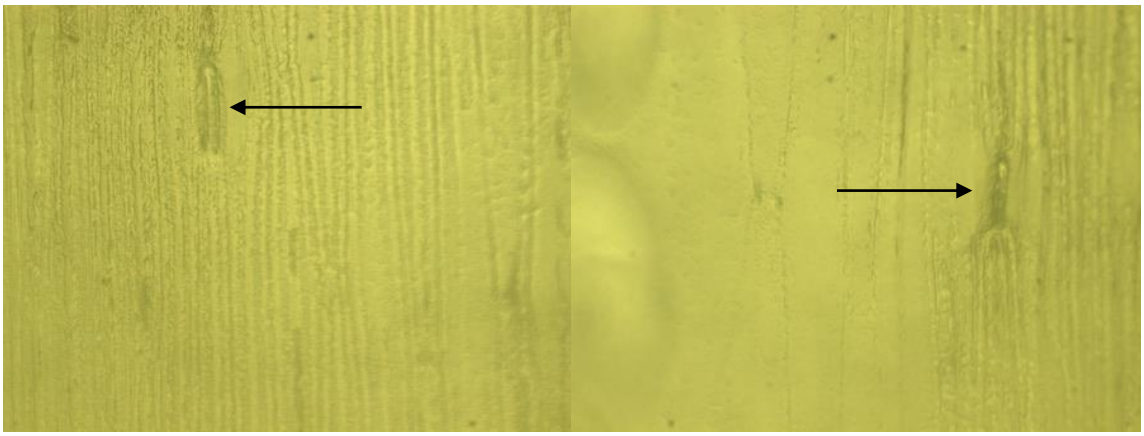

Figure A8 Leaf imprints taken from the abaxial side of *Allium fistulosum* leaves using the SUMP method and SUMP discs

Leaf imprints taken from the abaxial side of *Allium fistulosum* leaves using the SUMP method and SUMP discs. Image 1 is from a plant that was exposed to light and therefore shows a stomata that is open. Image 2 is from a plant that was kept in dark conditions and therefore the stomata is closed/ partially closed.

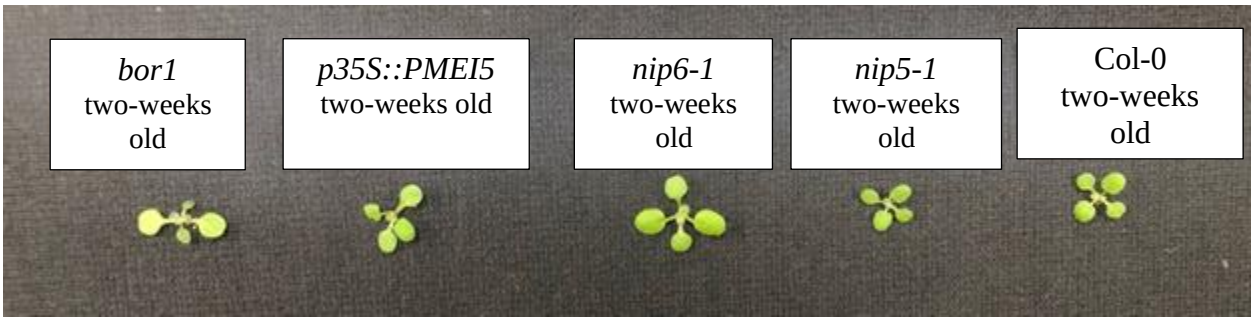

Figure A9 Two-week-old *Arabidopsis thaliana* genotypes

Two-week old *Arabidopsis thaliana* plants from each line utilized in the forementioned experiments. From left to right: *bor1* (boron transporter mutant, *p35S::PMEI5* (PMEI mutant), *nip6-1* (boron transporter mutant), *nip5-1* (boron transporter mutant), and Col-0 (wildtype).

Table A10 Primers used to genotype *nip5-1*, *nip6-1* and *bor1*

Left and right primers used to genotype *nip5-1*, *nip6-1* and *bor1*.

Line	**SALK**	**Left Primer**	**Right Primer**
AT4G10380 (*nip5-1*)	SALK_122287	TCCTAGCTCCATTTTCGTTTTC	CTCCAAGTGTGACGTAAACCC
AT1G80760 (*nip6-1*)	SALK_046323	TGTTGGGACATTGATCCTGA	TCATCTTCTGAAGCTCCTC
AT2G47160 (b*or1*)	SALK_037312	ATGCTTGATGTTCCAATCGTC	ATCCATGTGAGACCAAAGCAG

Table A11 Results from ICP-MS analyzing above-ground *Arabidopsis* biomass

Results of ICP-MS done to analyze boron quantity in various *Arabidopsis thaliana* genotypes (Col-0, *nip5-1*, *nip6-1* and *p35S::PMEI5*).

Genotype	**Boron (ppm)**
Col-0	25.41
nip5-1	30.04
nip6-1	34.93
p35S::PMEI5	28.24

Table A12 ANOVA analyzing ICP-MS results obtained from *Arabidopsis*

Results from an ANOVA analyzing data obtained from ICP-MS showing the quantity of boron in in various *Arabidopsis thaliana* genotypes (Col-0, *nip5-1*, *nip6-1* and *p35S::PMEI5*). $p<0.05$ is significant.

	Df	**Sum Sq**	**Mean Sq**	**F value**	**P value**
Genotype	3	143.83	47.94	203	6.91e-08

Table A13 Effect sizes corresponding to ICP-MS analysis of *Arabidiopsis*

Effect sizes for the relationships between each of the *Arabidopsis* genotypes of interest (Col-0, *nip5-1*, *nip6-1* and *p35S::PMEI5*). Cohen's d is reported in this table. An effect size of 0.8 is considered large.

Genotypes Compared	**Effect Size**
p35S::PMEI5 & Col-0	4.71
p35S::PMEI5 & nip5-1	3.16
p35S::PMEI5 & nip6-1	11.73
Col-0 *& nip5-1*	7.35
Col-0 *& nip6-1*	15.11
nip5-1 & nip6-1	30.56

Table A14 Tukey test for ICP-MS results obtained from *Arabidopsis*

Results from a Tukey test conducted to further analyze the relationship between the various *Arabidopsis* genotypes (Col-0, *nip5-1*, *nip6-1* and *p35S::PMEI5*) and the quantity of boron in the above ground biomass of these genotypes detected using ICP-MS. $p<0.05$ is significant.

Genotypes Compared	**P-value**
Col-0 & *nip5-1*	0.0000124
Col-0 & *nip6-1*	0.0000000
Col-0 & *p35S::PMEI5*	0.0004588
nip5-1 & *p35S::PMEI5*	0.0080708
nip6-1 & *nip5-1*	0.0000083
nip6-1 & *p35S::PMEI5*	0.0000007

$$Perecent\ Electrolyte\ Leakage = \frac{((\frac{Pre-Boil\ Conductivity\ Value}{Post-Boil\ Conductivity\ Value})*100)}{T0\ weight}$$

Equation A3 Equation used to calculate percent electrolyte leakage in *Arabidopsis thaliana* following dehydration, where T0 is the time at 0hr.

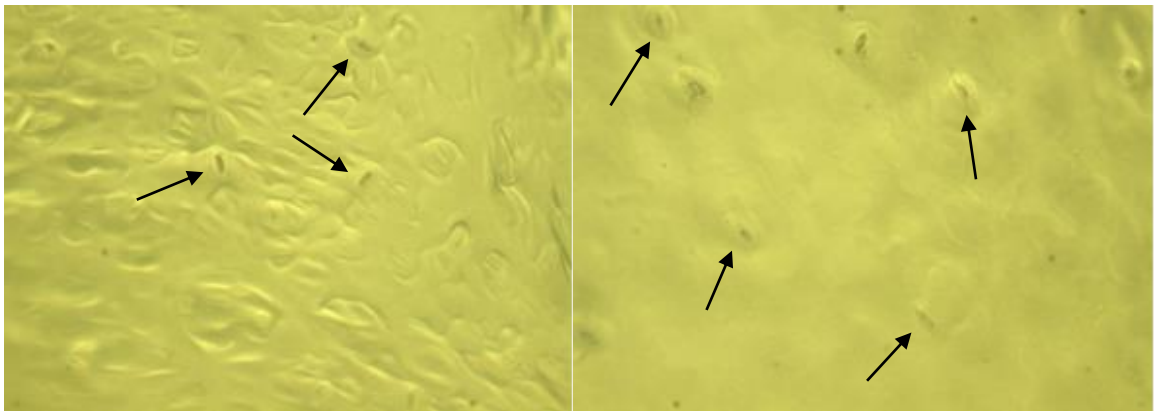

Figure A10 Leaf imprints taken from the abaxial side of *Arabidopsis thaliana* leaves using the SUMP method and SUMP discs

Leaf imprints taken from the abaxial side of *Arabidosis thaliana* leaves using the SUMP method and SUMP discs. Image 1 is from a plant that was exposed to light and therefore shows stomata that are open. Image 2 is from a plant that was kept in dark conditions and therefore the majority of the stomata are closed or partially closed.

Table A15 ANOVA analyzing percent water loss in pectin solutions

Results from an ANOVA analyzing percent water loss over 6hr in pure pectin solutions. $p<0.05$ is significant.

	Df	Sum Sq.	Mean Sq.	F value	P value
Pectin solutions	11	1199	109	49.53	< 2e-16
Time	1	36953	36953	16787.40	< 2-16
Pectin solutions: Time	11	302	27	12.46	8.4e-12

Table A16 ANOVA examining overall percent water loss over 15min in *Allium fistulosum* and *Allium cepa*

Results from an ANOVA ran on data examining average percent water loss over 15 minutes in *Allium fistulosum* and *Allium cepa* epidermal cell layers. $p<0.05$ is significant.

Data Selection	**Df**	**Sum Sq**	**Mean Sq**	**F-value**	**P-value**
Calcium	1	40	40	0.644	0.46714
Time	1	15034	15034	243.404	9.86e-05
Species	1	2803	2803	45.382	0.00253
Calcium: Time	1	24	24	0.389	0.56647
Calcium: Species	1	86	86	1.385	0.30452
Time: Species	1	1304	1304	21.113	0.01007
Calcium: Time: Species	1	45	45	0.733	0.44029

Table A17 Effect size for overall water loss after 15min in *Allium fistulosum* and *Allium cepa*

Effect sizes for the relationship between overall short term percent water loss (15min) in *Allium fistulosum* and *Allium cepa* epidermal cells. An effect size greater than 0.8 is indicative of a meaningful difference between treatment groups.

Treatments Compared	**Effect Size**
A. fistulosum (NCa & Ca) and *A. cepa* (NCa & Ca)	1.01

Table A18 ANOVA examining overall percent water loss over 16-18hr in *Allium fistulosum* and *Allium cepa* (dehydration of sheath with attached cell layer)

Results from an ANOVA ran on data examining average percent water loss in 4cm sections of *Allium fistulosum* and *Allium cepa* sheaths with intact epidermal cell layers over 16-18hr. $p<0.05$ is significant.

Data Selection	**Df**	**Sum Sq**	**Mean Sq**	**F-value**	**P-value**
Species	1	41.8	41.8	8.635	0.0425
Calcium	1	1.1	1.1	0.236	0.6527
Time	1	2452.4	2452.4	506.085	2.31e*-05
Species: Calcium	1	1.1	1.1	0.233	0.6542
Species: Time	1	20.2	20.2	4.167	0.1108
Calcium: Time	1	0.7	0.7	0.142	0.7251
Species: Calcium: Time	1	0.6	0.6	0.124	07422

Table A19 Effect size for percent water loss over 16-18hr in *Allium fistulosum* and *Allium cepa* (dehydration of sheath with attached cell layer)

Effect sizes for the relationship between overall long term percent water loss (16-18hr) in *Allium fistulosum* and *Allium cepa* sheaths with intact epidermal cell layer. Cohen's d is reported. An effect size of 0.8 is considered large.

.

Time	**Effect Size**
16hr	0.57
18hr	0.46

Table A20 ANOVA examining overall percent water loss over 16-18hr in *Allium fistulosum* (dehydration of sheath with attached cell layer)

Results from an ANOVA ran on data examining average percent water loss in 4cm sections of *Allium fistulosum* sheaths with intact epidermal cell layers over 16-18hr. $p<0.05$ is significant.

Data Selection	**Df**	**Sum Sq**	**Mean Sq**	**F-value**	**P-value**
Calcium	1	13.8	13.79	0.047	0.839
Time	1	1167.4	1167.4	710.917	0.0014
Calcium: Time	1	6.9	6.9	4.205	0.1768

Table A21 ANOVA examining overall percent water loss over 16-18hr in *Allium cepa* (dehydration of sheath with attached cell layer)

Results from an ANOVA ran on data examining average percent water loss in 4cm sections of *Allium cepa* sheaths with intact epidermal cell layers over 16-18hr. $p<0.05$ is significant.

Data Selection	**Df**	**Sum Sq**	**Mean Sq**	**F-value**	**P-value**
Calcium	1	0.0	0.0	0.0	0.99900
Time	1	1458.8	1458.8	210.5	0.00472
Calcium: Time	1	0.0	0.0	0.0	0.98963

Table A22 ANOVA examining overall limit of damage in *Allium fistulosum* and *Allium cepa* following 16-18hr dehydration of sheath

Results from an ANOVA ran on data examining average limit of damage in *Allium fistulosum* and *Allium cepa* epidermal cell layers following long term dehydration (16-18hr) of the sheath with the epidermal cell layer intact. $p<0.05$ is significant.

Data Selection	**Df**	**Sum Sq**	**Mean Sq**	**F-value**	**P-value**
Calcium	1	53	53	0.987	0.37671
Time	1	1503414617	14617	272.916	7.86e-05
Species	1	2530	2530	47.235	0.00235
Calcium: Time	1	32	32	0.594	0.48386
Calcium: Species	1	69	69	1.282	0.32080
Time: Species	1	1183	1183	22.094	0.00931
Species: Calcium: Time	1	36	36	0.670	0.45903

Table A23 Effect size for limit of damage in *Allium fistulosum* and *Allium cepa* following 16-18hr dehydration of sheath

Effect sizes for the relationship between overall limit of damage (based on protoplasmic streaming) in epidermal cell layers following long term dehydration (16-18hr) of *Allium fistulosum* and *Allium cepa* sheaths with intact epidermal cell layers. An effect size greater than 0.8 is indicative of a meaningful difference between treatment groups.

Time	**Effect Size**
16hr	4.21
18hr	8.73

Table A24 ANOVA examining overall limit of damage in *Allium fistulosum* following 16-18hr dehydration of sheath

Results from an ANOVA ran on data examining average limit of damage (based on protoplasmic streaming) in *Allium fistulosum* epidermal cell layers following long term dehydration (16-18hr) of the sheath with the epidermal cell layer intact. $p<0.05$ is significant.

Data Selection	Df	Sum Sq	Mean Sq	F-value	P-value
Calcium	1	121	121	1.468	0.3494
Time	1	3741.4	3741	45.389	0.0213
Calcium: Time	1	68	68	0.821	0.4606

Table A25 ANOVA examining overall limit of damage in *Allium cepa* following 16-18hr dehydration of sheath

Results from an ANOVA ran on data examining average limit of damage (based on protoplasmic streaming) in *Allium cepa* epidermal cell layers following long term dehydration (16-18hr) of the sheath with the epidermal cell layer intact. $p<0.05$ is significant.

Data Selection	Df	Sum Sq	Mean Sq	F-value	P-value
Calcium	1	4	4	0.021	0.89833
Time	1	12059	12059	488.377	0.00204
Calcium: Time	1	0.0	0.0	0.0	0.96485

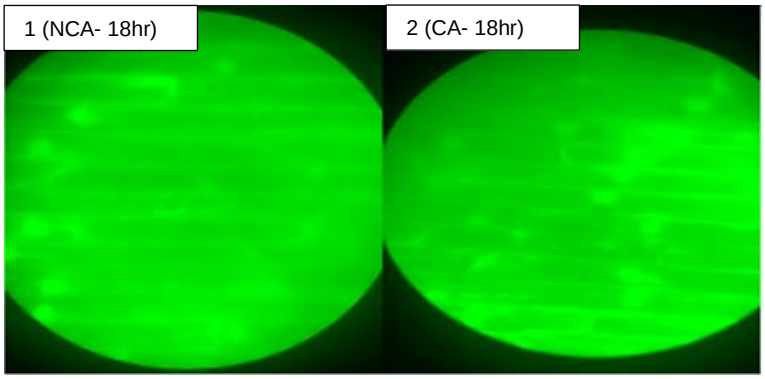

Figure A11 *Allium fistulosum* epidermal cells stained with fluorescein diacetate following 18hr dehydration and subsequent rehydration

Allium fistulosum epidermal cell layers stained with fluorescein diacetate. Cell layers had previously been dehydrated for 18hr, followed by rehydration (24hr). Cell layers were obtained from *Allium fistulosum* treated with a 0.05M $CaCl_2$ solution every second day for four-weeks or from non-calcium treated plants. Cells were stained for 5min followed by a wash with PBS. Images from left to right are: 1). Post-18hr dehydration, NCA (-calcium) and 2). Post 18-hr dehydration, CA (+calcium). Images were taken at 40X using the GFP filter cube and a LEICA DM4 B microscope.

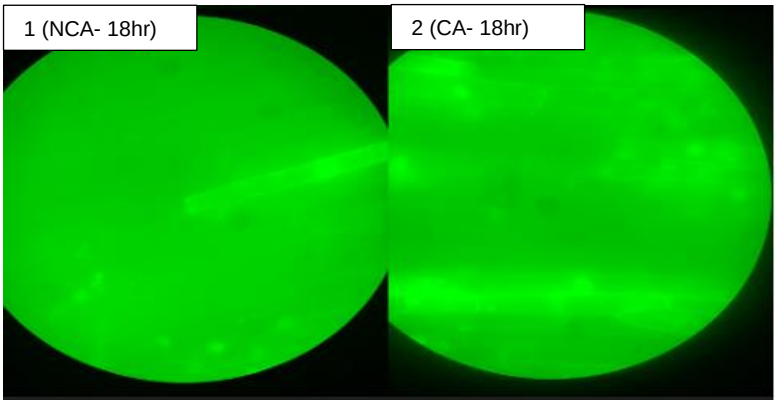

Figure A12 *Allium cepa* epidermal cells stained with fluorescein diacetate following 18hr dehydration and subsequent rehydration

Allium cepa epidermal cell layers stained with fluorescein diacetate. Cell layers had previously been dehydrated for 18hr, followed by rehydration (24hr). Cell layers were obtained from *Allium fistulosum* treated with a 0.05M $CaCl_2$ solution every second day for four-weeks or from non-calcium treated plants. Cells were stained for 5min followed by a wash with PBS. Images from left to right are: 1). Post-18hr dehydration, NCA (-calcium) and 2). Post 18-hr dehydration, CA (+calcium). Images were taken at 40X using the GFP filter cube and a LEICA DM4 B microscope.

Table A26 ANOVA examining overall limit of damage in *Allium fistulosum* following 12-24hr dehydration of single epidermal cell layer

Results from an ANOVA ran on data examining average limit of damage (based on protoplasmic streaming) following the long-term dehydration (12-24hr) of single layers of *Allium fistulosum* epidermal cells. $p<0.05$ is significant.

Data Selection	**Df**	**Sum Sq**	**Mean Sq**	**F-value**	**P-value**
Cold Acclimation	2	375	187	0.942	0.399
Calcium	1	392	392	1.971	0.169
Time	1	42192	42192	212.122	<2e-16
Cold Acclimation: Calcium	2	586	293	1.473	0.243
Cold Acclimation: Time	2	431	215	1.083	0.349
Calcium: Time	1	6	6	0.030	0.864
Cold Acclimation: Calcium: Time	2	32	16	0.081	0.922

Table A27 ANOVA examining overall limit of damage in *Allium fistulosum* following 16hr dehydration of single epidermal cell layer

Results from an ANOVA ran on data examining limit of damage (based on protoplasmic streaming) following 16hr dehydration of a single layer of *Allium fistulosum* epidermal cells. $p<0.05$ is significant.

Data Selection	**Df**	**Sum Sq**	**Mean Sq**	**F-value**	**P-value**
Cold Acclimation	2	2045	1022.4	2.059	0.1622
Calcium	1	2817	2817.3	5.673	0.0309
Cold Acclimation: Calcium	2	2717	1358.7	2.736	0.0971

Table A28 ANOVA examining overall percent water loss in *Allium fistulosum* following 12-24hr dehydration of single epidermal cell layer

Results from an ANOVA ran on data examining average water loss over 12-24hr in single layers of *Allium fistulosum* epidermal cells. $p<0.05$ is significant.

Data Selection	Df	Sum Sq	Mean Sq	F-value	P-value
Cold Acclimation	2	1	0	0.001	0.999
Calcium	1	5	5	0.020	0.887
Time	1	25950	25950	101.979	4.78e-12
Cold Acclimation: Calcium	2	727	364	1.429	0.253
Cold Acclimation: Time	2	3	1	0.006	0.994
Calcium: Time	1	1	1	0.004	0.951
Cold Acclimation: Calcium: Time	2	120	60	0.236	0.791

Table A29 ANOVA examining overall percent water loss in *Allium fistulosum* following 16hr dehydration of single epidermal cell layer

Results from an ANOVA ran on data examining percent water loss following the dehydration of a single layer of *Allium fistulosum* epidermal cells for 16hr. $p<0.05$ is significant.

Data Selection	Df	Sum Sq	Mean Sq	F-value	P-value
Cold Acclimation	2	16	8.1	0.043	0.958
Calcium	1	95	95.0	0.503	0.485
Cold Acclimation: Calcium	2	892	446.2	2.363	0.117

Table A30 Effect size for percent water loss over 15min in *Allium fistulosum* (single epidermal cell layer)

Effect sizes for the relationship between overall percent water loss in epidermal cell layers following short term dehydration (15min) of single epidermal cell layers obtained from *Allium fistulosum* treatment groups. Note, calcium application is denoted by CA and cold acclimation is referred to as ACC. Cohen's d is reported in this table. An effect size of 0.8 is considered large.

Treatments Compared	**Effect Size**
NACC/ NCA & NACC/ CA	0.03
NACC/ NCA & ACC4-4/ NCA	0.45
NACC/ NCA & ACC4-4/ CA	0.20
NACC/ NCA & ACC12-4/ NCA	0.24
NACC/ NCA & ACC12-4/ CA	0.48
NACC/ CA & ACC4-4/ NCA	0.47
NACC/ CA & ACC4-4/ CA	0.48
NACC/ CA & ACC12-4/ NCA	0.55
NACC/ CA & ACC12-4/ CA	0.48
ACC4-4 & ACC4-4/ CA	0.25
ACC4-4 & ACC12-4/ NCA	0.21
ACC4-4 & ACC12-4/ CA	0.02
ACC4-4/ CA & ACC12-4/ NCA	0.05
ACC4-4/ CA & ACC12-4/ CA	0.28

Table A31 Effect size for percent water loss over 15min in *Allium cepa* (single epidermal cell layer)

Effect sizes for the relationship between overall percent water loss in epidermal cell layers following short term dehydration (15min) of single epidermal cell layers obtained from *Allium cepa* treatment groups. Note, calcium application is denoted by CA. Cohen's d is reported in this table. An effect size of 0.8 is considered large.

Groups Compared	**Effect Size**
CA and NCA *Allium cepa*	0.071

Table A32 Atike information criteria values for GAM's constructed to analyze percent water loss over 15min in *Allium cepa*

AIC values for the 3 GAM's built to analyze the relationship between epidermal cell layers obtained *Allium cepa* treatment groups and percent water loss over 15min. A lower AIC value is indicative of a better fitting model.

GAM	**AIC Value**
No smoother and no by= argument	142.77491
Smoother and no by=argument	45.02626
Smoother and by=argument	16.32831

Table A33 Atike information criteria values for GAM's constructed to analyze percent water loss over 15min in *Allium fistulosum*

AIC values for the 3 GAM's built to analyze the relationship between epidermal cell layers obtained *Allium fistulosum* treatment groups and percent water loss over 15min. A lower AIC value is indicative of a better fitting model.

GAM	**AIC Value**
No smoother and no by= argument	6331.182
Smoother and no by=argument	6323.599
Smoother and by=argument	6296.639

Table A34 Effect size for percent water loss over 15min in *Arabidopsis* genotypes

Effect sizes for the relationship between overall percent water loss in various *Arabidopsis* genotypes following short term dehydration (15min). Cohen's d is reported in this table. An effect size of 0.8 is considered large.

Genotypes Compared	**Effect Size**
Col-0 & *p35S::PMEI5*	0.13
Col-0 & *nip5-1*	0.20
Col-0 & *nip6-1*	0.08
p35S::PMEI5 & nip5-1	0.30
p35S::PMEI5 & *nip6-1*	0.20
nip5-1 & *nip6-1*	0.10

Table A35 Atike information criteria values for GAM's constructed to analyze percent water loss over 15min in *Arabidopsis* genotypes

AIC values for the 3 GAM's built to analyze the relationship between various *Arabidopsis* genotypes and percent water loss over 15min. A lower AIC value is indicative of a better fitting model.

GAM	**AIC Value**
No smoother and no by= argument	218.56
Smoother and no by=argument	148.81
Smoother and by=argument	125.91

Table A36 ANOVA examining overall percent water loss in *Arabidopsis* genotypes over 2-10hr dehydration

Results from an ANOVA examining average percent water loss over long term dehydration (2-10hr) in various *Arabidopsis thaliana* genotypes. $p<0.05$ is significant.

Data Selection	**Df**	**Sum Sq**	**Mean Sq**	**F-value**	**P-value**
Genotype	4	448	112	0.833	0.52
Time	1	14955	14955	111.237	1.28e-09
Genotype: Time	4	4	1	0.008	1.00

Table A37 ANOVA examining overall percent electrolyte leakage in *Arabidopsis* genotypes following 2-10hr dehydration

Results from an ANOVA examining average electrolyte leakage, which was used as a measurement of the limit of damage for various *Arabidopsis thaliana* genotypes dehydrated for between 2-10hr. $p<0.05$ is significant.

Data Selection	**Df**	**Sum Sq**	**Mean Sq**	**F-value**	**P-value**
Genotype	4	32	7.9	0.039	0.9969
Time	1	1603	1603.3	7.925	0.0107
Genotype: Time	4	265	66.4	0.328	0.8558

Table A38 ANOVA examining overall percent water loss in *Arabidopsis* genotypes over 12-24hr dehydration

Results from an ANOVA examining average percent water loss over long term dehydration (12-24hr) in various *Arabidopsis thaliana* genotypes. $p<0.05$ is significant.

Data Selection	**Df**	**Sum Sq**	**Mean Sq**	**F-value**	**P-value**
Genotype	3	109	36	0.182	0.908
Time	1	16685	16685	83.199	2.872-09
Genotype: Time	3	12	4	0.021	0.996

Table A39 ANOVA examining overall percent electrolyte leakage in *Arabidopsis* genotypes following 12-24hr dehydration

Results from an ANOVA examining average percent electrolyte leakage from various *Arabidopsis thaliana* genotypes following dehydration between 12-24hr and subsequent rehydration. $p<0.05$ is significant.

Data Selection	**Df**	**Sum Sq**	**Mean Sq**	**F-value**	**P-value**
Genotype	3	224	81.3	7.668	0.00092
Time	1	1425.4	1425.4	134.392	2.55e-11
Genotype: Time	3	67.1	22.4	2.110	0.12548

Table A40 Tukey test for results obtained from analysis electrolyte leakage in *Arabidopsis* genotypes following 12-24hr dehydration

Results from a Tukey test examining the relationship between various *Arabidopsis thaliana* genotypes and average percent electrolyte leakage following dehydration between 12-24hr and subsequent rehydration. $p<0.05$ is significant.

Genotypes Compared	**P-value**
nip6-1 & *nip5-1*	0.766
p35S::PMEI5 & *nip5-1*	0.003
Col-0 & *nip5-1*	0.997
p35S::PMEI5 & nip6-1	0.025
Col-0 & *nip6-1*	0.652
Col-0 & *p35S::PMEI5*	0.001

Table A41 Effect size for percent electrolyte leakage in *Arabidopsis* genotypes following 12-24hr dehydration

Effect sizes for the relationship between overall percent electrolyte leakages in various *Arabidopsis* genotypes following long term dehydration (12-24hr). Cohen's d is reported in this table. An effect size of 0.8 is considered large.

Genotypes Compared	**Effect Size**
Col-0 & *nip5-1*	0.02
Col-0 & *nip6-1*	0.36
Col-0 & *p35S::PMEI5*	1.34
nip5-1 & *nip6-1*	0.39
nip5-1 & *p35S::PMEI5*	1.44
nip6-1 & *p35S::PMEI5*	0.73

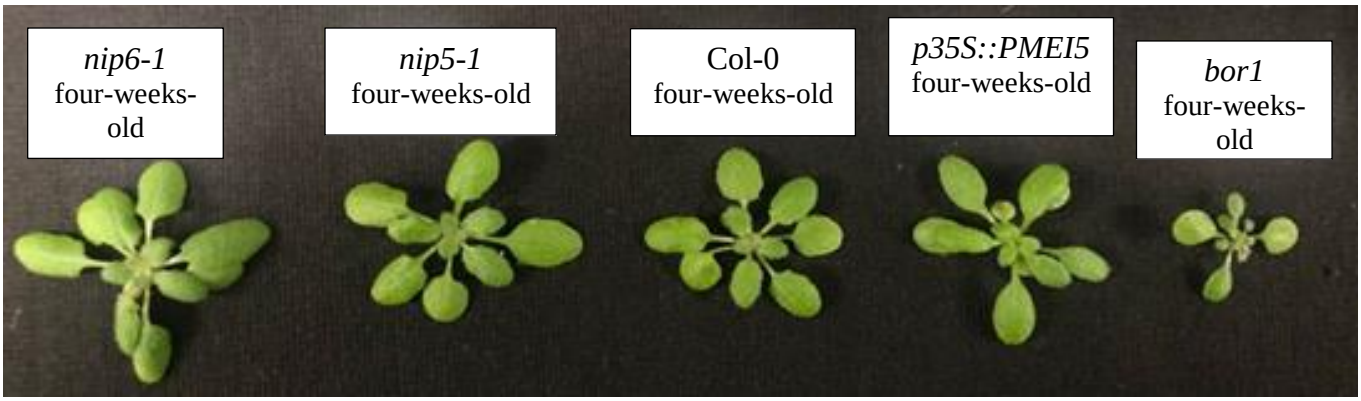

Figure A13 Four-week-old *Arabidopsis thaliana* plants

Four-week-old *Arabidopsis thaliana* plants from each genotype. From left to right: *nip6-1* (boron transporter mutant), *nip5-1*(boron transporter mutant), Col-0 (wild-type), *p35S::PMEI5* (pectin methylesterase inhibitor mutant), and b*or1* (boron transporter mutant).

$$Lesion\ size\ (cm^2) = Diamete\ of\ entire\ lesion\ including\ agar - diameter\ of\ agar\ measured\ at\ T0$$

Equation A4 Equation used to calculate lesion size following inoculation with *Botrytis cinerea*, where T0 is the time at 0hr.

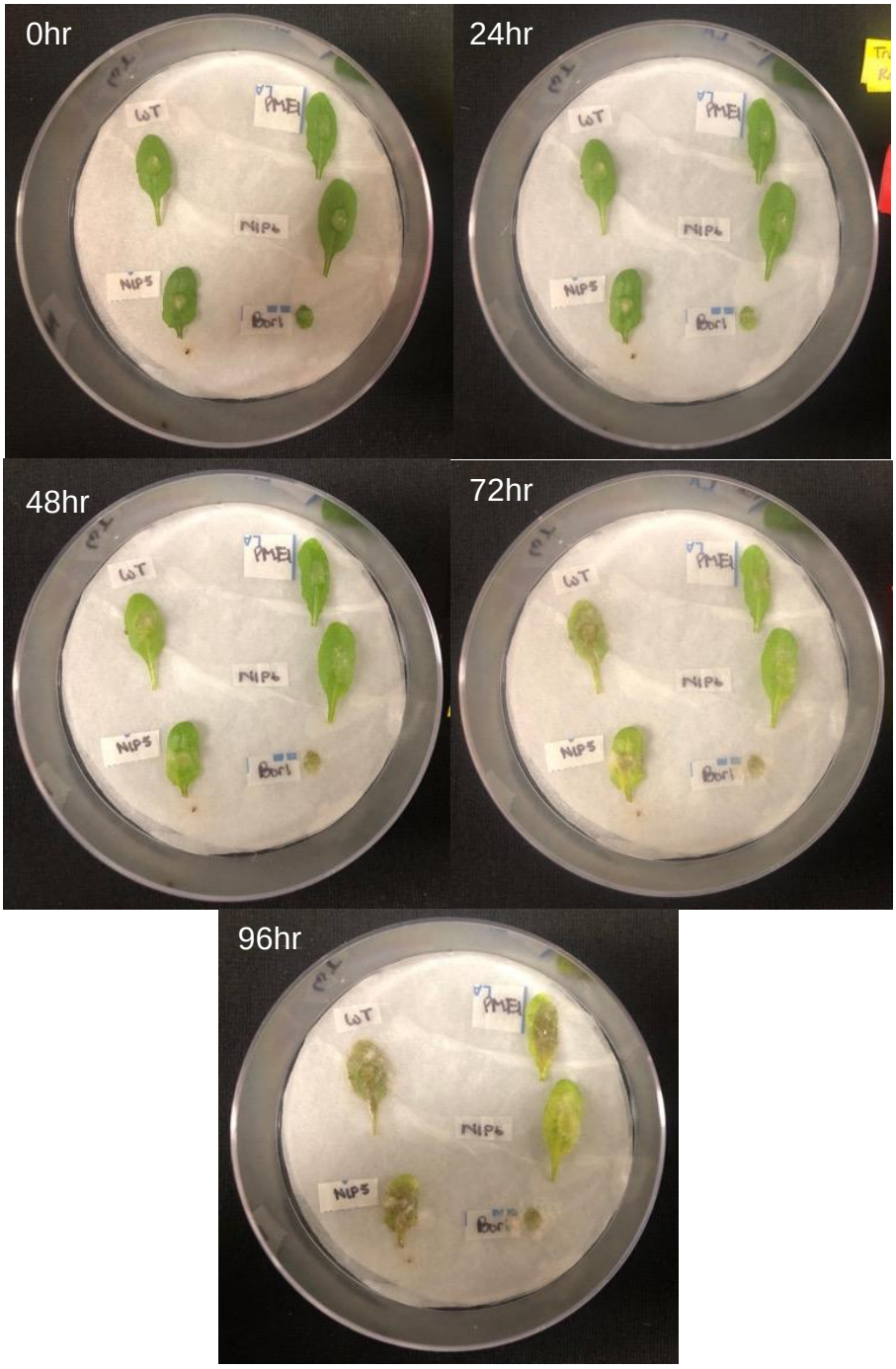

Figure A14 Progression of *Botrytis cinerea* infection on leaves from various *Arabidopsis thaliana* genotypes

Progression of *Botrytis cinerea* infection on leaves from various *Arabidopsis thaliana* genotypes over 0-96hr.

$$Inital\ volume\ of\ suspension\ from\ stock\ required = \frac{(desired\ final\ concenrtation\ \times\ total\ volume\ of\ suspension\ required)}{intial\ concentration}$$

Equation A5 Equation used to determine the volume of suspension required from the initial stock solution in order to prepare the *Colletotrichum higginsianum* spore solution.

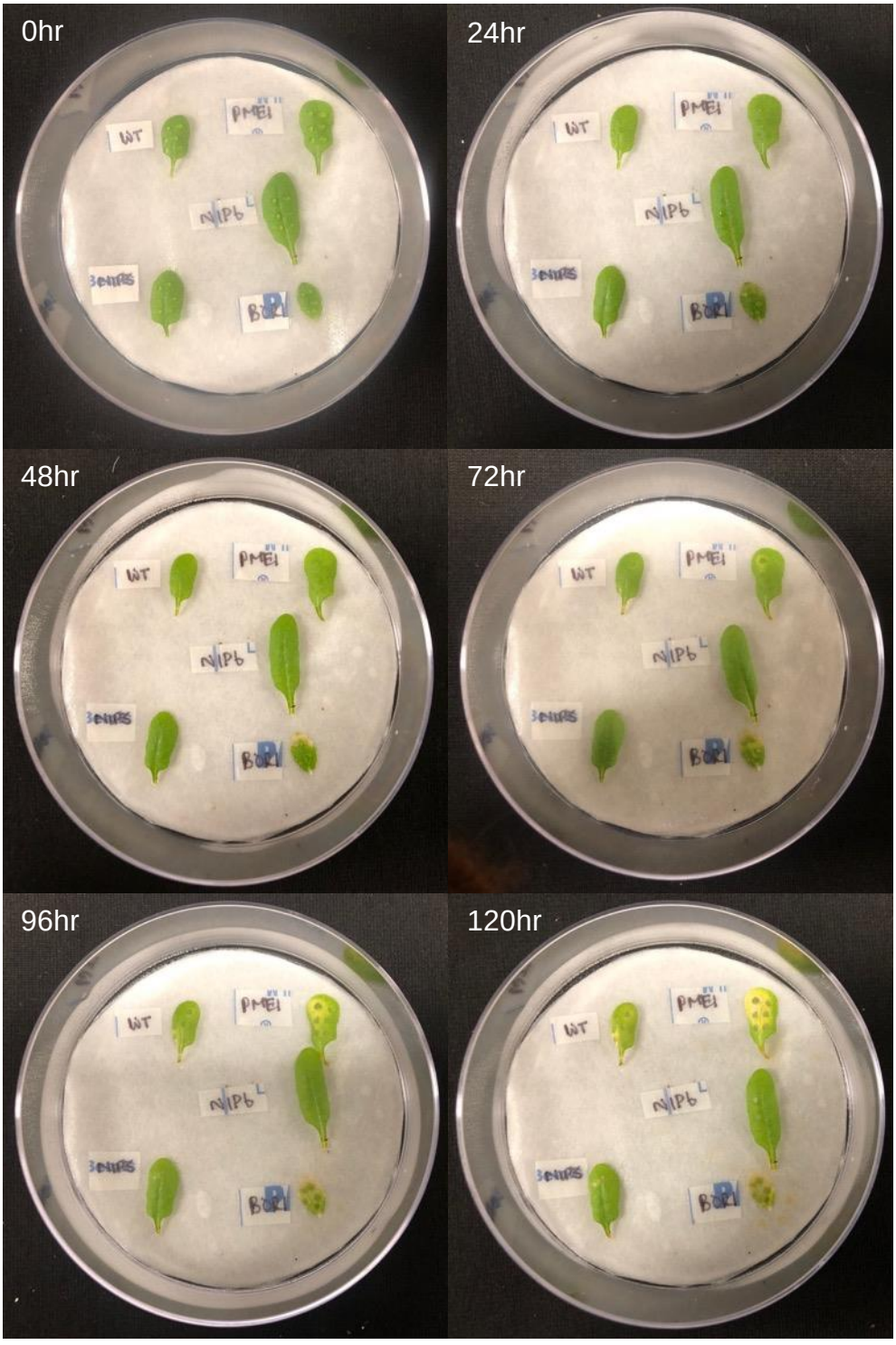

Figure A15 Progression of *Colletotrichum higginsianum* infection on leaves from various *Arabidopsis thaliana* genotypes

Progression of *Colletotrichum higginsianum* infection on leaves from various *Arabidopsis thaliana* genotypes over 0-120hr.

Table A42 ANOVA examining average lesion size following *Botrytis cinerea* inoculation in *Arabidopsis* genotypes

Results from an ANOVA examining average lesion size following *Botrytis cinerea* inoculation in various *Arabidopsis thaliana* genotypes (Col-0, *nip5-1*, *nip6-1*, *p35S::PMEI5* and *bor1*) 0-96hr post-inoculation. $p<0.05$ is significant.

Data Selection	**Df**	**Sum Sq**	**Mean Sq**	**F-value**	**P-value**
Genotype	4	0.6892	0.1723	6.307	0.000349
Time	1	2.0175	2.0175	73.850	3.53e-07
Genotype: Time	4	0.4132	0.1033	3.782	0.02551

Table A43 Tukey test for results obtained from analysis of *Botrytis cinerea* lesion size in *Arabidopsis* genotypes

Results from a Tukey test examining average lesion size following *Botrytis cinerea* inoculation in various *Arabidopsis thaliana* genotypes (Col-0, *nip5-1*, *nip6-1*, *p35S::PMEI5* and *bor1*) 0-96hr post-inoculation. $p<0.05$ is significant.

Genotypes Compared	**P-value**
nip5-1 & bor1	0.040
nip 6-1 & bor1	0.006
p35S::PMEI5 & bor1	0.018
Col-0 *& bor1*	0.004
nip6-1 & nip5-1	0.868
p35S::PMEI5 & nip5-1	0.991
Col-0 *& nip5-1*	0.779
p35S::PMEI5 & nip6-1	0.983
Col-0 *& nip6-1*	0.999
Col-0 *& p35S::PMEI5*	0.949

Table A44 ANOVA examining average lesion size following *Colletotrichum higginsianum* inoculation in *Arabidopsis* genotypes

Results from an ANOVA examining average lesion size following *Colletotrichum higginsianum* inoculation in various *Arabidopsis thaliana* genotypes (Col-0, *nip5-1*, *nip6-1*, *p35S::PMEI5* and *bor1*) 0-120hr post-inoculation. $p<0.05$ is significant.

Data Selection	**Df**	**Sum Sq**	**Mean Sq**	**F-value**	**P-value**
Genotype	4	0.1020	0.0255	6.147	0.00215
Time	1	0.4022	0.4022	96.958	4.1e-09
Genotype: Time	4	0.0424	0.0106	2.558	0.07403

Table A45 Tukey test for results obtained from analysis of *Colletotrichum higginsianum* lesion size in *Arabidopsis* genotypes

Results from a Tukey test examining average lesion size following *Colletotrichum higginsianum* inoculation in various *Arabidopsis thaliana* genotypes (Col-0, *nip5-1*, *nip6-1*, *p35S::PMEI5* and *bor1*) 0-120hr post-inoculation. $p<0.05$ is significant.

Genotypes Compared	**P-value**
nip5-1 & bor1	0.010
nip6-1 & bor1	0.037
p35S::PMEI5 & bor1	0.165
Col-0 *& bor1*	0.001
nip6-1 & nip5-1	0.975
p35S::PMEI5 & nip5-1	0.660
Col-0 *& nip5-1*	0.897
p35S::PMEI5 & nip6-1	0.936
Col-0 *& nip6-1*	0.587
Col-0 *& p35S::PMEI5*	0.202

Table A46 Effect size for *Colletotrichum higginsianum* lesion size in *Arabidopsis* genotypes

Effect sizes for the relationship between *Colletotrichum higginsianum* lesion size and various *Arabidopsis* genotypes. Cohen's d is reported in this table. An effect size of 0.8 is considered large.

Genotypes Compared	**Effect Size**
Col-0 *& nip5-1*	0.44
Col-0 *& nip6-1*	0.74
Col-0 *& p35S::PMEI5*	1.13
Col-0 *& bor1*	2.31
nip5-1 & nip6-1	0.18
nip5-1 & p35S::PMEI5	0.43
nip5-1 & bor1	0.91
nip6-1 & p35S::PMEI5	0.21
nip6-1 & bor1	0.85
p35S::PMEI5& bor1	0.47

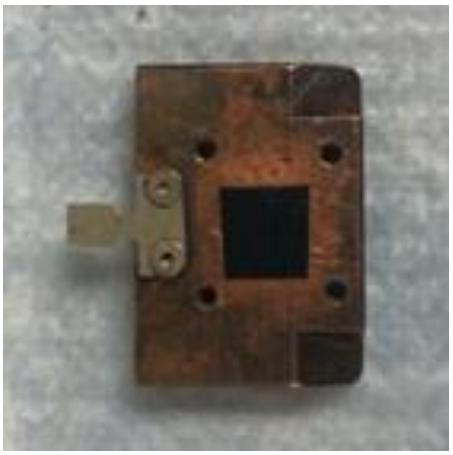

Figure A16 Sample holder used for the VLS-PGM beamline

Sample holder used for the VLS-PGM beamline. The section of black carbon tape shown on the holder is where the homogenized powder from all of the samples was mounted. The vacuum in the chamber was maintained at a value close to or greater than $1x10^{7}$ torr. The size of the entrance and exit slit was 100µm, while the energy range was between 185eV to 210eV with a dwell time of 1 second. Six samples were analyzed from each individual *A. thaliana* line: three biomass samples and three soil samples. Three scans were completed per sample.

Table A47 Statistical analysis of 2D calcium maps

Results from two-tailed T-tests used to analyze 2D calcium maps obtained from *Allium fistulosum* epidermal cell layers.

Analysis	**T**	**Df**	**P-value**
Intensity (weighted)	11.958	1	0.05312
Red pixels	3.7934	1	0.1641
Green pixels	7.426	1	0.08522
Blue pixels	218.06	1	0.002919

Table A48 Statistical analysis of images obtained from staining with Ruthenium red

Results from two-tailed T-tests used to analyze calcium treated and non-calcium treated *Allium fistulosum* epidermal cell layers stained with Ruthenium red.

Analysis	**T**	**Df**	**P-value**
Intensity (weighted)	20.642	1	0.03082
Red pixels	18.089	1	0.03516
Green pixels	21.664	1	0.02937
Blue pixels	23.4	1	0.02719

Table A49 Statistical analysis of images obtained from staining with curcumin

Results from two-tailed T-tests used to analyze leaves obtained from various *Arabidopsis* genotypes that have been stained with curcumin.

Genotypes Compared	**P-value**
Col-0 & *bor1*	0.2766
Col-0 & *nip5-1*	0.3968
Col-0 & *nip6-1*	0.07843
Col-0 & *p35S::PMEI5*	0.3608
nip5-1 & *bor1*	0.2367
nip5-1 & *nip6-1*	0.3706
nip5-1 & *p35S::PMEI5*	0.1013
nip6-1 & *p35S::PMEI5*	0.3233
p35S::PMEI5 & *bor1*	0.1528

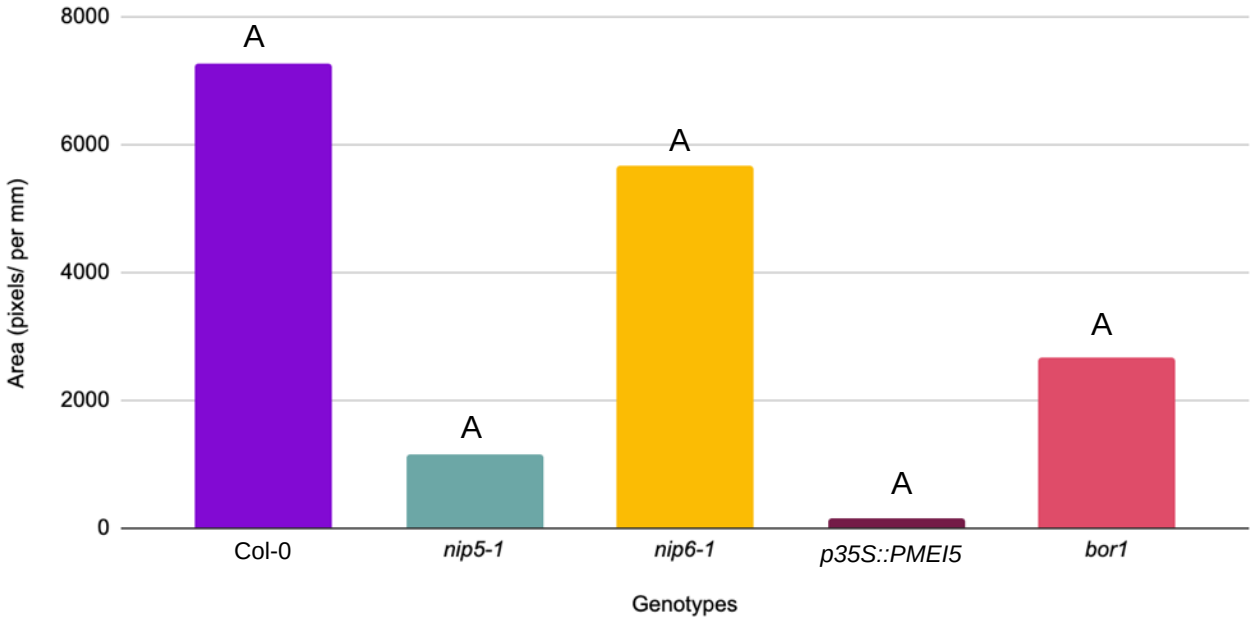

Figure A17 Area of orange particulates detected in leaves of *Arabidopsis thaliana* genotypes following staining with curcumin

Cumulative area (pixels/mm) of orange particulates detected in leaves of *Arabidopsis thaliana* mutants (Col-0, *nip5-1*, *nip6-1*, *p35S::PMEI5* and *bor1*) following staining with curcumin. Areas were measured using ImageJ (Version 1.53a). Values on this graph are directly representative of areas from the images in Figure 6.12.

10.2 Appendix B

SPRINGER NATURE LICENSE
TERMS AND CONDITIONS

May 14, 2021

This Agreement between Ms. Ariana Forand ("You") and Springer Nature ("Springer Nature") consists of your license details and the terms and conditions provided by Springer Nature and Copyright Clearance Center.

License Number	5067810251298
License date	May 14, 2021
Licensed Content Publisher	Springer Nature
Licensed Content Publication	AAPS PharmSciTech
Licensed Content Title	Relevance of Rheological Properties of Sodium Alginate in Solution to Calcium Alginate Gel Properties
Licensed Content Author	Shao Fu et al
Licensed Content Date	Mar 25, 2011
Type of Use	Thesis/Dissertation
Requestor type	academic/university or research institute
Format	print and electronic
Portion	figures/tables/illustrations
Number of	1

Figure A18 Copy of copyright license

Copyright license obtained from Springer Nature for Figure 2.4

SPRINGER NATURE LICENSE
TERMS AND CONDITIONS

May 14, 2021

This Agreement between Ms. Ariana Forand ("You") and Springer Nature ("Spri Nature") consists of your license details and the terms and conditions provided Springer Nature and Copyright Clearance Center.

License Number	5067810683540
License date	May 14, 2021
Licensed Content Publisher	Springer Nature
Licensed Content Publication	Springer eBook

Print This Page

Figure A19 Copy of copyright license

Copy of copyright license obtained from Springer Nature for Figure 2.5

JOHN WILEY AND SONS LICENSE
TERMS AND CONDITIONS

May 14, 2021

This Agreement between Ms. Ariana Forand ("You") and John Wiley and Sons ("John Wiley and Sons") consists of your license details and the terms and conditions provided by John Wiley and Sons and Copyright Clearance Center.

License Number	5067820517894
License date	May 14, 2021
Licensed Content Publisher	John Wiley and Sons
Licensed Content Publication	New Phytologist
Licensed Content Title	Abiotic and biotic stress combinations
Licensed Content Author	Nobuhiro Suzuki, Rosa M. Rivero, Vladimir Shulaev, et al
Licensed Content Date	Apr 11, 2014
Licensed Content Volume	203
Licensed Content Issue	1
Licensed Content Pages	12
Type of use	Dissertation/Thesis
Requestor type	University/Academic

Figure A20 Copy of copyright license

Copy of copyright license obtained from John Wiley and Sons for Figure 2.8